DEVELOPMENT OF AN INTEGRATED APPROACH

FOR MODELING GAS ADSORPTION

AND COAL SWELLING

By

PONGTORN CHAROENSUPPANIMIT

Bachelor of Science in Chemical Engineering
Chulalongkorn University
Bangkok, Thailand
2007

Submitted to the Faculty of the
Graduate College of the
Oklahoma State University
in partial fulfillment of
the requirements for
the Degree of
DOCTOR OF PHILOSOPHY
May, 2015

DEVELOPMENT OF AN INTEGRATED APPROACH

FOR MODELING GAS ADSORPTION

AND COAL SWELLING

Dissertation Approved:

Dr. Khaled A.M. Gasem

Dissertation Adviser

Dr. Robert L. Robinson, Jr.

Dr. Joshua Ramsey

Dr. Martin Hagan

.

ACKNOWLEDGEMENTS

I would like to express my grateful appreciation to my advisor, Dr. Khaled Gasem. He has provided me with his invaluable advice, guidance and knowledge. It is an honor that I had an opportunity to work on this project with him.

I would like to express my thanks to my co-advisor, Dr. Robert Robinson, Jr., for his continual support, suggestions and encouragement. I also would like to extend my thanks to my PhD committee members, Dr. Martin Hagan and Dr. Josh Ramsey for their time and effort in reviewing this dissertation.

I also would like to express my appreciation to my mentor, Dr. Sayeed Mohammad, for his support, encouragement and constructive comments for this work. This work would not have succeeded without his significant contributions. Also, I would like to thank Dr. Brian Neely for his advice. Last but not least, I would like to specially thank Dr. Agelia Abudor and Dr. Solomon Gebreyohannes for their encouragement, support and friendship.

I also grateful acknowledge the financial support from the U.S. Department of Energy and the Coal-Seq Consortium.

Finally, I would like to thank my parents, my brother and my sister for their support, understanding and encouragement.

Name: PONGTORN CHAROENSUPPANIMIT

Date of Degree: MAY, 2015

Title of Study: DEVELOPMENT OF AN INTEGRATED APPROACH FOR MODELING GAS ADSORPTION AND COAL SWELLING

Major Field: CHEMICAL ENGINEERING

Abstract: Accurate descriptions of gas adsorption, adsorbent swelling and permeability in coalbed reservoirs are essential for the optimal design of enhanced natural gas recovery and CO_2 sequestration processes. In practice, reservoir simulators provide a convenient way for estimating natural gas recovery rate and CO_2 injectivity for these processes. Such simulators require adsorption capacity and reservoir permeability estimates, which, in turn, require adsorption and swelling models for predicting permeability changes. As a result, a model capable of providing accurate description of adsorption behavior and adsorbent swelling is needed.

Knowledge of adsorption isotherms is essential for modeling adsorbent swelling. Further, to account carefully for gas-adsorption-induced swelling, swelling models are applied at reservoir conditions, where geothermal gradients and different types of geological formations such as coals and shales may exist. Thus, an integrated approach for modeling adsorption and swelling requires: [1] an adsorption model capable of describing the temperature-dependence of gas adsorption over the expected range of reservoir temperatures, [2] an adsorption model capable of describing adsorption behavior on a variety of coals and shales and [3] a theoretically consistent model for describing swelling. To meet these requirements, the Simplified Local-Density (SLD) model has been integrated with the Pan and Connell (PC) swelling model.

The primary objectives of this study are to: [1] modify the SLD model to describe temperature dependence of adsorption over significant temperature ranges, [2] extend the SLD model to describe adsorption behavior on shales and [3] integrate the SLD and PC models to describe the adsorption and swelling behavior of several coals and use the results obtained from the SLD-PC swelling model to calculate permeability changes and compare the results with available experimental data.

To facilitate the model development, a comprehensive database of experimental measurements was assembled for gas adsorption on activated carbons, coals and shales, as well as data for coal swelling and permeability changes. The SLD model was then modified by introducing a new temperature-dependence expression in the model. The model was tested with adsorption data on activated carbons, coals and shales. The results indicate that the SLD model can describe accurately the adsorption data on these carbonaceous adsorbents. In addition, the SLD model has better representations for gas adsorption over significant temperature ranges. Further, the SLD model was integrated with the PC model to describe coal swelling data and permeability changes. The results reveal that the integrated model is capable of describing accurately the coal swelling, thus providing useful input for permeability predictions.

TABLE OF CONTENTS

CHAPTER PAGE

CHAPTER PAGE

LIST OF TABLES

TABLE PAGE

LIST OF FIGURES

FIGURE PAGE

FIGURE PAGE

FIGURE PAGE

CHAPTER I

INTRODUCTION

1.1 Rationale

In unconventional gas reservoirs such as coalbeds and shales, the majority of the gas exists in an adsorbed state. The adsorbed molecules can cause swelling of the solid matrix, which constricts the cleat system (pore space) and eventually lead to reduction of reservoir permeability and injectivity. This, in turn, adversely affects reservoir production and sequestration operations. Thus, knowledge of adsorption capacity and reservoir permeability are crucial for two targeted applications:

A. Utilization of CO_2 in enhanced natural gas recovery: CO_2 interacts more strongly than natural gas molecules (e.g., methane and nitrogen) with carbon-based adsorbents such as coals and shales and, thus, it can "displace" pre-adsorbed natural gas. However, the injection of CO_2 may also produce adverse effects by lowering the actual rate of gas recovery due to a significant decrease in reservoir permeability [1, 2].
B. Sequestration of CO_2 in depleted or unmineable coal seams: As pressure increases during CO_2 injection, the expansion of coal and solid compression due to the injected gas pressure act as two competing factors that affect the reservoir permeability and CO_2 injectivity [1, 2] and must be accounted for.

Coalbed reservoir simulators are used to estimate CO_2 injectivity, and this calculation requires description of gas adsorption and permeability as model inputs. However, measuring these quantities

can be time-consuming and expensive. Further, reservoir operating conditions (i.e., temperature and pressure) and reservoir constituents differ by location and depth [3] and types of geological formation [4]. Thus, a need exists for an integrated adsorption-swelling model that is theoretically consistent and capable of describing accurately the whole spectrum of adsorption-related phenomena (from adsorption to permeability) on a variety of carbonaceous adsorbents over significant temperature ranges. To satisfy the need, a potentially attractive method is to combine a predictive, theory-based adsorption model such as the simplified local-density model (SLD) [5] with another theory-based model, the Pan and Connell (PC) [6] swelling model.

Developing an integrated model using the SLD approach can be divided into two main tasks:

1. Improving the SLD, which includes efforts to:
    - Modify the SLD model to improve its predictions of the temperature dependence of supercritical gas adsorption
    - Extend the SLD model to include useful descriptions of the adsorption behavior on shales
2. Integrating the PC swelling model with the SLD model

The SLD model has been used successfully in previous studies for predicting the adsorption behavior on coals based solely on the surface characterization of the adsorbent [7]. In a continuation of that work, the SLD model was extended to represent adsorption behavior on shales. Details about the extension of the SLD model for representing shale data are provided in Chapters 3 and 4. Since shale reservoirs are an increasingly important resource [8], a model capable of accurate predictions of gas adsorbed on shale should prove useful to the natural gas industry.

One aspect of the SLD model that needs improvement is the temperature dependence of adsorption over significant temperature ranges. Specifically, analysis of the current model capabilities indicated that the temperature dependence in the basic SLD model is inadequate. To remedy this

deficiency, a new temperature dependence functionality was incorporated, based on the volume expansivity approach proposed by Do [9]. This approach has been used successfully in the Ono-Kondo and the two-dimensional equation-of-state models [10, 11]. Results to date indicate that inclusion of this new term in the SLD model provides marked improvements to adsorption predictions over larger temperature ranges.

The SLD model is capable of predicting adsorption of methane, nitrogen and CO_2 based solely on adsorbent characterization [7]. This unique attribute is quite useful for extending the application of adsorption/coal swelling model proposed in this study. In particular, the SLD model can be used to provide *a priori* predictions of gas adsorption isotherms when such data are unavailable for systems of interest.

Application of the PC model involves calculation of the adsorbent surface potential - an intermediate variable for swelling calculations. Originally, the PC model employed the Langmuir adsorption model due to its simplicity [6, 12]. However, the Langmuir-PC model cannot be applied in the absence of adsorption isotherm data. Further, the Langmuir-PC model contains another simplification which involves replacing the fugacities with pressures in the surface potential calculations. Analysis has shown that this approximation can increase the errors significantly when applied to CO_2 at high pressures. In addition, a term in the equation containing a product of pressure and adsorbed-phase volume in the surface potential calculation was ignored in the Langmuir-PC model. Subsequent analysis has shown that this term can be significant, specifically at high pressures. In the present study, both these simplifying assumptions are replaced with more rigorous calculations. Thus, combining the PC and SLD models has two benefits: (1) The SLD model predicts the required inputs for the PC model, even in cases where the adsorption data are unavailable, and (2) the SLD-PC model is theoretically consistent, since fugacities are employed, and the volume term is not neglected in calculating the surface potential.

1.2 Goals and Objectives

The goal of this research is to develop and evaluate the efficacy of an integrated model for gas adsorption and swelling behaviors in unconventional reservoirs. This goal is accomplished by combining the SLD adsorption model with the PC swelling model and addressing the following four objectives and their associated tasks:

A. Assembling experimental databases

Several databases were assembled for conducting this study, including the following:

- Adsorption data for several adsorbates over wide temperatures on activated carbons
- Adsorption data and its corresponding swelling and permeability data on several coals
- Adsorption data for methane, nitrogen and CO_2 on several shales

All the data acquired in the laboratory or compiled from literature sources were used for model development.

B. Modifying the SLD model to account for the temperature dependence of gas adsorption

Temperature variations as a function of reservoir depth can impact the adsorbed amounts of gas and should be taken into account for proper in-situ gas estimates. This requires an adsorption model capable of describing the temperature dependence of adsorption over significant temperature ranges. To accomplish this, the SLD model was modified by introducing a new temperature-dependence expression in the model. Specifically, temperature dependence was introduced for the adsorbed phase volume. The selected expression was tested using adsorption data on several activated carbons. Activated carbons were chosen in this study primarily because the adsorption data covering several temperatures are extremely limited for both coals and shales. Since activated carbons are simpler structural analogs of other carbon-based adsorbents such as coals and shales, a

model developed on the basis of activated carbons can be expected to perform satisfactorily for coals and shales.

C. Measuring adsorption capacities on New Albany shale, Woodford shale and Caney shale and extending the SLD model to describe adsorption behavior on shales

Production of natural gas from shale reservoirs has increased significantly in recent years. Gas-in-place estimates in shale reservoirs are useful for reservoir engineers to conduct economic feasibility studies. Thus, one of the focuses of this research was investigation of the SLD model efficacy in representing adsorption capacity on various shale samples from both newly acquired shale data and data from the literature.

Adsorption data on shale samples are extremely limited, especially at higher pressures. Therefore, in this study, new adsorption data were acquired on diverse shale samples to supplement the existing literature database. The New Albany shale, Woodford shale and Caney shale sample were selected in this project due to their high adsorption capacities. Further, the New Albany shale and Woodford shales are currently producing natural gas commercially [8]. These data, as well as literature data for adsorption of pure gases on shales, were utilized to extend the SLD model to shale gas adsorption.

D. Integrating the SLD adsorption and PC swelling models

The PC swelling model has been used earlier utilizing simpler adsorption models [6, 12, 13]. The present research utilizes the theoretically rigorous SLD adsorption model for integrating the PC swelling model. The SLD model contains several distinct advantages when compared to earlier approaches. Specifically:

1. The SLD adsorption model accounts explicitly for coal swelling during the modeling of gas adsorption on coals.

2. The generalized SLD model can provide *a priori* predictions of adsorption isotherms where experimental data are lacking. The generalized SLD model can predict adsorption isotherms solely on the basis of adsorbent characterization information such as proximate and ultimate analyses of coal.
3. The SLD model utilizes slit-shaped pore geometry that facilitates estimating the adsorbed-phase volume. The adsorbed-phase volume is required to calculate surface potential. However, it has been neglected in previous works with the Pan and Connell model. This term can be significant at higher pressures and the present study fully accounts for it.

To accomplish this objective, swelling data and their corresponding adsorption isotherms have been compiled from the literature for coals; no similar data are available for shales. Ultimately, in testing the combined SLD-PC model, the adsorbent swelling predictions were used as input for modeling permeability changes using the Shi and Durucan model [14]. The predicted permeability changes are compared with the available experimental data.

1.3 Thesis Organization

This dissertation is written in "manuscript style", and it is divided into four stand-alone chapters. Chapter 1 provides the rationale and the objectives of this work. Chapter 2 presents the development of the new temperature dependence expression for the SLD model. Chapter 3 deals with experimental procedures for measuring high-pressure adsorption of gases on the New Albany shale. Chapter 4 focuses on experimental procedures for measuring high-pressure adsorption of gases on shales from Oklahoma including the Woodford shale and the Caney shale. Chapter 5 presents the development of an integrated SLD and PC model for describing coal swelling phenomenon. The final chapter contains conclusions and recommendations from this study.

REFERENCES

1. Pini, R., et al., Role of adsorption and swelling on the dynamics of gas injection in coal. Journal of Geophysical Research: Solid Earth, 2009. 114(B4): p. B04203.
2. Robertson, E.P., Measurement and Modeling of Sorption Induced Strain and Permeability Changes in Coal. Idaho National Laboratory, 2005.
3. Pashin, J.C. and M.R. McIntyre, Temperature–pressure conditions in coalbed methane reservoirs of the Black Warrior basin: implications for carbon sequestration and enhanced coalbed methane recovery. International Journal of Coal Geology, 2003. 54(3–4): p. 167-183.
4. Weniger, P., et al., High-pressure methane and carbon dioxide sorption on coal and shale samples from the Paraná Basin, Brazil. International Journal of Coal Geology, 2010. 84(3–4): p. 190-205.
5. Rangarajan, B., C.T. Lira, and R. Subramanian, Simplified local-density model for adsorption over large pressure ranges. AIChE Journal, 1995. 41(4): p. 838-845.
6. Pan, Z. and L.D. Connell, A theoretical model for gas adsorption-induced coal swelling. International Journal of Coal Geology, 2007. 69(4): p. 243-252.
7. Mohammad, S.A., et al., Generalized Simplified Local-Density/Peng−Robinson Model for Adsorption of Pure and Mixed Gases on Coals. Energy & Fuels, 2009. 23(12): p. 6259-6271.

8. Cluff, R.M., Illinois State Geological Survey; Dickerson, Donald R, Natural Gas Potential of the New Albany Shale Group (Devonian-Mississippian) in Southeastern Illinois. Society of Petroleum Engineers 22, 1982.

9. Do, D.D., Adsorption analysis: Equilibria and kinetics. Imperial College Press, London. 1998.

10. Pan, Z., Modeling of Gas Adsorption Using Two Dimensional Equations of State. Ph.D. Dissertation. Oklahoma State University, 2004.

11. Sudribandriyo, M., A Generalized Ono-Kondo Lattice Model for High Pressure Adsorption of Gases on Carbon Adsorbents. Ph.D. Dissertation. Oklahoma State University, 2003.

12. Pan, Z. and L.D. Connell, Modelling of anisotropic coal swelling and its impact on permeability behaviour for primary and enhanced coalbed methane recovery. International Journal of Coal Geology, 2011. 85(3–4): p. 257-267.

13. Clarkson, C.R., Pan, Z., Palmer, I., and Harpalani, S, Predicting Sorption-Induced Strain and Permeability Increase With Depletion for Coalbed-Methane Reservoirs. Society of Petroleum Engineering 15, 2010: p. 152-159.

14. Shi, J.Q. and S. Durucan, Drawdown Induced Changes in Permeability of Coalbeds: A New Interpretation of the Reservoir Response to Primary Recovery. Transport in Porous Media, 2004. 56(1): p. 1-16.

CHAPTER II

MODELING THE TEMPERATURE DEPENDENCE OF SUPERCRITICAL GAS ADSORPTION ON ACTIVATED CARBONS, COALS AND SHALES

The content in this chapter has been published in the International Journal of Coal Geology*.

2.1 Introduction

Shale and coalbed methane reservoirs have become an important source of natural gas, and a significant portion of the gas in these reservoirs exists in an adsorbed state. Thus, knowledge of gas adsorption behavior over a range of pressures and temperatures is required to estimate the gas-in-place for these reservoirs. Further, some of these reservoirs can offer potential sites for CO_2 sequestration. Gases commonly encountered in these reservoirs are the natural gas components including carbon dioxide and nitrogen with the latter two being especially important in enhanced gas recovery and carbon dioxide sequestration. Since gas adsorption is temperature dependent, the presence of geothermal gradients in a reservoir affects the adsorption capacity of these gases. For example, in the Black Warrior basin the coal bed reservoir temperature varies from about 300 K to 325 K within the 0.3-1.8 km depth-range [1]. Thus, an accurate accounting for temperature dependence of gas adsorption is important for reliable gas-in-place estimates as well as CO_2 sequestration capacity of such reservoirs.

To date, few studies in the literature have focused on modeling the temperature dependence of supercritical gas adsorption. Among previous studies, the Dubinin micropore filling theory [2] was used by Clarkson and Bustin [3] and Ruppel et al. [4]. The theory offered a convenient method for

*Charoensuppanimit, P., et al., Modeling the temperature dependence of supercritical gas adsorption on activated carbons, coals and shales. International Journal of Coal Geology, 2015. 138(0): p. 113-126.

predicting adsorption capacities over a range of temperatures based on the linear and temperature-independent characteristic curves. Clarkson and Bustin and Ruppel et al. [3, 4] tested the validity of such characteristic curves. In their work, the characteristic curves appeared to be non-linear, especially at large temperature and pressure ranges, indicating that the temperature invariance of the characteristic curve may not be valid over a wide temperature range. Czerny et al. [5] observed that the temperature-independent characteristic energy of adsorption, ε in Dubinin's theory, varies linearly with temperature. Richard et al. [6] modified the Dubinin-Ashtakov (D-A) model by expressing ε as a linear function of temperature. They concluded that better model representations for adsorption were obtained after the modification of ε was introduced. Dundar et al. [7] utilized the multicomponent potential theory of adsorption (MPTA) model, which can be extended to describe adsorption of gas mixtures. Similar to the modification in Richard et al. [6], Dundar and co-workers replaced the constant adsorbed-phase volume, Z_0 in the Dubinin-Radushkevish-Astakov (DRA) potential, with the variable Z_0 expressed as a linear function of temperature. The modified DRA potential (MDP) was then used to account for the solid-gas interaction in MPTA model. The results obtained in Dundar's work indicated that the MPTA-MDP model improved the representations of adsorption on several activated carbons when compared to the results obtained from the MPTA-DRA model.

Although some success has been attained in modeling of supercritical gas adsorption, the adsorption models listed above have not been generalized to provide a priori predictions for a wide range of adsorbent/adsorbate pairs. In this work, we present a generalized model that is found capable of predicting temperature dependence of near-critical and supercritical gas adsorption for diverse adsorbate/adsorbent pairs over larger temperature ranges.

The simplified local-density (SLD) model has been used successfully in our previous studies. In a recent work, the SLD model was extended to represent adsorption behavior on shales [8]. Further, the SLD model was integrated with the Pan and Connell [9] (PC) swelling model to account for

adsorption-induced swelling of coals [10]. The swelling results obtained from the integrated SLD-PC model provided useful predictions of linear strain and gas permeability changes in coals due to gas adsorption. Details about the extension of the SLD model for representing shale data are provided in Chapter III and IV and details about the integrated SLD-PC model for coal swelling are provided in Chapter V. Thus, the SLD model offers distinct advantages in providing predictions for a spectrum of adsorption-related phenomena from adsorption to permeability on coals and shales, which are crucial for more realistic reservoir simulations.

Notwithstanding the progress in modeling these systems, our analysis indicated that the inherent temperature dependence in the original SLD model was inadequate over wider temperature ranges. To remedy this problem, a new temperature-dependence expression is incorporated in the SLD model in this work based on the volume-expansivity approach proposed by Do [11].

In this work, the SLD model was modified by introducing a new temperature dependence for the adsorbed-phase volume. The modified SLD model was tested initially using adsorption data on several activated carbons. Results indicate that inclusion of this new temperature dependence in the SLD model provided marked improvements for representations over larger temperature ranges compared to representations from the original SLD model. These initial evaluations utilized activated carbons since the adsorption data covering wide temperature ranges are extremely limited for both coals and shales. Further, since activated carbons are simpler structural analogs of other carbon-based adsorbents such as coals and shales, a model should be applicable to activated carbons as a precursor to extending it to coals and shales.

Some of the noteworthy aspects of this work include: (1) A large database for adsorption on activated carbons was compiled that contains adsorption data for 11 adsorbates on 18 adsorbents with a total of about 2600 data points (2) A generalized adsorption model was developed to predict the supercritical gas adsorption over significant temperature ranges (3) The generalized model was

validated with an external dataset, and (4) the modified model was tested to describe adsorption on coals and shales (additional 670 data points) at multiple temperatures.

The remainder of this Chapter is organized as follows: Section 2.2 describes the SLD model and the modifications undertaken to account for the temperature dependence of gas adsorption, Section 2.3 presents the literature database employed and Section 2.4 presents the results obtained in this work.

2.2 Adsorption Model

2.2.1 Original SLD Model

The SLD model envisions the adsorbent to be composed of rectangular-shaped slits and the adsorbate molecules reside within these two-surface slits. A molecule within a slit has interactions with both walls of the adsorbent slit. The SLD model accounts for both fluid-fluid and fluid-solid interactions in the slit-shaped pore. The model was first developed by Rangarajan et al. [12], who used the van der Waals equation of state (EOS) to account for the fluid-fluid interactions. Following our earlier work [13, 14] the Peng-Robinson EOS is used in this work. The following paragraphs provide the essential details of the SLD model as used in this work.

At equilibrium, the chemical potential of the fluid, μ, is expressed as the sum of the fluid-fluid and fluid-solid potentials at a position, "z", between the slit surfaces, as follows:

$$\mu(z) = \mu_{ff}(z) + \mu_{fs}(z) = \mu_{bulk} \tag{2.1}$$

where subscript "bulk" refers to the bulk fluid and "ff" and "fs" refer to the fluid-fluid and fluid-solid interactions, respectively. The equation shows how the chemical potential of the adsorbed fluid reflects the proximity of the fluid to the molecular wall of the adsorbent. Thus, the SLD model considers the inhomogeneity of the adsorbed phase in describing the molecular interactions of the adsorbed fluid with the adsorbent. The chemical potential of the bulk fluid can be expressed in terms of fugacity as

$$\mu_{bulk} = \mu_0(T) + RT \ln \frac{f_{bulk}}{f_0} \tag{2.2}$$

where subscript "0" designates an arbitrary reference state and "f" refers to fugacity. Similarly, the chemical potential from fluid-fluid interactions is given as

$$\mu_{ff}(z) = \mu_0(T) + RT \ln \frac{f_{ff}(z)}{f_0} \tag{2.3}$$

where "$f_{ff}(z)$" is fluid fugacity at position z and "f_0" refers to the same arbitrary reference state as in Equation (2.2).

The fluid-solid interactions in the model are accounted for through a potential energy function. In particular, the fluid-solid potential is given as

$$\mu_{fs}(z) = N_A\left[\Psi^{fs}(z) + \Psi^{fs}(L - z)\right] \tag{2.4}$$

where "N_A" is Avogadro's number, "$\Psi(z)$" and "$\Psi(L-z)$" are the fluid-solid interactions for the two surfaces of a slit of length L.

Substituting Equations (2.2), (2.3) and (2.4) into Equation (2.1) provides the equilibrium relationship for adsorption within the slit:

$$f_{ff}(z) = f_{bulk} \exp\left(-\frac{\Psi^{fs}(z) + \Psi^{fs}(L - z)}{kT}\right) \tag{2.5}$$

where k is the Boltzmann's constant.

Applying the SLD model, the excess adsorption (n^{Ex}) is given as

$$n^{Ex} = \frac{SA}{2} \int_{\text{Left Side of Slit}}^{\text{Right Side of Slit}} \left(\rho(z) - \rho_{bulk}\right) dz \tag{2.6}$$

where n^{Ex} is the excess adsorption of adsorbate in number of moles per unit mass of adsorbent, and "SA" is the surface area of the adsorbate on a particular solid. The lower limit in Equation (2.6) is 3/8 σ_{ff}, which is 3/8 of the diameter of an adsorbed molecule touching the left plane surface.

The upper limit is L-3/8σ_{ff}, the location of an adsorbed molecule touching the right plane surface. The local density is assumed to be zero for the distances less than 3/8σ_{ff} away from the wall. The left and right sides of the slit each comprise half of the total surface area. The selection of the lower and upper integration limits has been discussed in one of our previous works [14].

The fluid-solid interaction, $\Psi^{fs}(z)$, was represented by Lee's partially-integrated 10-4 potential [15], which is a truncated form of Steele's 10-4-3 potential [16].

$$\Psi^{fs}(z) = 4\pi\rho_{atoms}\varepsilon_{fs}\sigma_{fs}^{2}\left(\frac{\sigma_{fs}^{10}}{5(z')^{10}} - \frac{1}{2}\sum_{i=1}^{4}\frac{\sigma_{fs}^{4}}{(z'+(i-1)-\sigma_{ss})^{4}}\right) \tag{2.7}$$

$$\varepsilon_{fs} = \sqrt{\varepsilon_{ff} \times \varepsilon_{ss}} \tag{2.8}$$

where ε_{fs} and ε_{ss} are the fluid-solid and solid-solid interaction energy parameters, respectively, and ρ_{atoms} = 0.382 atoms/Å^2. The parameters σ_{ff} and σ_{ss} signify, respectively, the molecular diameter of the adsorbate and the carbon interplanar distances. The carbon interplanar distance was taken to be the value for graphite, 0.335 nm [17] and values of σ_{ff} and ε_{ff} were taken from [18]. The fluid-solid molecular diameter, σ_{fs} and dummy coordinate z' used in numerical integration of Equation (2.6) are defined as:

$$\sigma_{fs} = \frac{\sigma_{ff} + \sigma_{ss}}{2} \tag{2.9}$$

$$z' = z + \frac{\sigma_{ss}}{2} \tag{2.10}$$

Absolute adsorption (n_{ads}^{Abs}) can also be determined readily from the adsorbent geometry envisioned in the SLD slit-pore model [19]. Specifically, the absolute adsorption calculated in the SLD model is given as

$$n_{ads}^{Abs} = V_{ads}\rho_{ads} \tag{2.11}$$

where V_{ads} is adsorbed-phase volume per gram of adsorbent, ρ_{ads} is the adsorbed-phase density estimated by averaging the local adsorbed density across the slit. The adsorbed-phase volume appearing in Equation (2.11) is given as

$$V_{ads} = \frac{SA}{2}\left[L - \frac{3}{4}\sigma_{ff} \right] \tag{2.12}$$

In this manner, the original SLD model contains three regressed parameters: surface area, SA, slit length, L and solid-solid interaction energy, ε_{ss}/k. As explained below, the modification of the SLD model includes an initial regression of one more parameter, δ, the thermal expansion coefficient for the adsorbate.

2.2.2 Modifying the SLD Model for Improved Temperature Dependence of Adsorption

In this work, an additional modification was implemented in the SLD model to improve the modeling of gas adsorption over larger temperature ranges. The increase in temperature can lead to the expansion of the adsorbed phase. This gives rise to less dense packing of the adsorbed molecules within the adsorbent pore volume, thus decreasing the amount of gas adsorbed. Do [11] presented an approach for estimating the changes in adsorbed-phase volume as a function of temperature. In this work, we have implemented a similar approach within the SLD model and incorporated a temperature-dependent adsorbed-phase volume in the SLD model. Specifically, the changes in the adsorbed-phase volume can be related to temperature with the following expression:

$$\int_{V_{ads,0}}^{V_{ads}} \frac{dV}{V} = -\int_{T_0}^{T} \delta dT \tag{2.13}$$

Integrating Equation (2.13) yields

$$V_{ads} = V_{ads,0} \exp\left(-\delta\left(T - T_0\right)\right) \tag{2.14}$$

where V_{ads} is adsorbed-phase volume, $V_{ads,0}$ is adsorbed-phase volume at a reference temperature T_0 and is the thermal expansion coefficient. In this manner, Equation (2.14) was used to account for the changes in adsorbed-phase volume in the SLD model.

2.3 Database Employed and Modeling Methodology

2.3.1 Database Employed for Adsorption Modeling over Larger Temperature Ranges

To extend the temperature-dependence in SLD model, pure-gas adsorption data on activated carbons were used initially for several reasons, including:

A. Adsorption data on coals and shales over wide temperature ranges are extremely limited.
B. Adsorption data at multiple temperatures on several activated carbons are readily available in literature.
C. Activated carbons possess simpler chemical composition and structure relative to coals and shales while exhibiting similar qualitative adsorption behavior.

A large database was compiled for pure-gas adsorption of 11 adsorbates on 18 activated carbons over significant temperature ranges. Several of the systems were obtained from a database compiled recently by Talu [20], and additional systems were added to enlarge the database for adsorption of natural gas components on several activated carbons. An important criteria used in the database was the presence of adsorbates in the near-critical and supercritical region as well as availability of data for at least three temperatures. Table 2.1 provides details of the database on activated carbons used in this work. Overall, a total of 2650 adsorption data points were included in the database. About 2100 data points were used for model development and the remaining 500 data points were used as an external set for validation of the generalized model. Further, the available data in the literature on coals and shales at multiple temperatures was also included in the expanded database. These data included seven coals and six shale samples. The details of these

data are listed in Table 2.1. Thus, the complete database included adsorption measurements on activated carbons, coals and shales.

2.3.2 Modeling Methodology

The following methodology was used to develop the generalized model presented in this work:

1. The modified SLD model parameters (namely, surface area, SA, slit length (L), solid-solid interaction energy, ε_{ss}/k and thermal expansion coefficient, and δ) were first regressed to obtain precise representations of the adsorption data. For a given adsorbate/adsorbent pair, data at all temperatures were regressed simultaneously to obtain the parameters.
2. The regressed values of δ were then used to develop a generalized model in terms of available adsorbent and adsorbate molecular properties.
3. The generalized values of δ from the above step were then used in the modified SLD model to obtain *predictions* for the systems in the database as well as systems not used in the model development.

Since the experimental uncertainties in gas adsorption data were generally not provided with the original data in the literature, the objective function (OF) used in the model regressions was the average absolute percentage deviation (%AAD). The regressions were performed by minimizing %AAD in excess adsorption as given below.

$$OF = \frac{1}{N}\sum_{i=1}^{N}\left(\frac{n_{Cal}^{Ex} - n_{Exp}^{Ex}}{n_{Exp}^{Ex}}\right)_i \times 100 \qquad (2.15)$$

where N is the number of data points, n_{Cal}^{Ex} and n_{Exp}^{Ex} are the calculated and experimental excess adsorption, respectively.

2.3.3 Generalized Model Development

The regressed values for the thermal expansion coefficient, δ, were used to develop a generalized model in terms of adsorbate and adsorbent properties. The generalized expression for δ was developed by using techniques outlined in some of our earlier work [21]. Specifically, a sequential regression algorithm was used to identify properties that best correlate with δ. To prevent over-fitting and retain the predictive capability of the generalized model, the number of properties used in the model was restricted to five.

2.4 Results and Discussion

2.4.1 Modified SLD Model Representations for Gas Adsorption on Activated Carbons

The modified SLD model was used to represent gas adsorption data on several activated carbons from the literature. (In the following discussion, "representations" refer to results obtained with model parameter regressions and "predictions" refers to the results obtained with the generalized model.) Table 2.2 presents the model parameters for each of the datasets used in this work. The regression results yielded parameters that characterize adsorbent surface properties such as the surface area (in the range of 600-1200 m^2/g), effective pore width (in the range of 0.7-1.3 nm) and solid-solid interaction energy (in the range of 20-30 K). These regressed parameters were within the range expected for activated carbons. The thermal expansion coefficient, δ, had an average value of 1.8E-03 [1/R], which was comparable to the average value of 1.7E-03 [1/R] reported by [11]. Further, the values of δ were similar for closely-related adsorbates such as ethane-ethylene and propane-propylene. However, the values of δ were different for a specific gas adsorbed on different adsorbents. Thus, the thermal expansion coefficient varies as a function of *both* adsorbent and adsorbate properties.

Table 2.3 presents the overall percentage average absolute deviation (%AAD) obtained in representing gas adsorption on these activated carbons. Three distinct cases were considered in these model regressions. Case 1 utilized a constant adsorbed-phase volume (original SLD model),

Case 2 included a temperature-dependent adsorbed-phase volume (modified SLD model) and model regressions were undertaken, whereas Case 3 was based on the generalized model. As evident from Table 2.3, the overall %AADs for Cases 2 and 3 were about one-half those for Case 1, indicating significant improvement of model representations obtained with the modified SLD model.

Figures 2.1(a)-(c) depict deviations in excess adsorption from Cases 1 and 2 for selected datasets and clearly show improvement in model representations. As evident in Figure 1, the improved representations were attributed to the datasets that have wider temperature range. Thus, the major advantage of the modification in the work would be the improved descriptions of the temperature dependence of adsorption over larger temperature ranges. Figures 2.2(a)-(e) illustrate typical examples of model representations obtained from the modified SLD model. These figures also provide comparisons between the original and the modified SLD models and show significantly better fits obtained from the modified SLD model (Case 2). Thus, the adsorbed-phase volume expression utilized in the modified SLD model appears to be effective in improving the temperature-dependence in the model.

The adsorbed-phase volumes from Equation 2.14 were compared with the volumes obtained from the original SLD model. This was performed on datasets that have adsorption data over wider temperature ranges. In Figure 2.3, the straight line represents adsorbed-phase volumes determined from Equation 2.14, whereas each data point represents the adsorbed phase volume obtained from the original SLD model through regressions at each temperature conducted separately. As evident from Figure 2.3, the new expression for temperature-dependence of adsorbed-phase volume allows us to predict the variation of adsorbed-phase volume with reasonable accuracy.

2.4.2 Generalized Model for Predicting Temperature-Dependence of Adsorption

The regressed values for thermal expansion coefficient, δ in Table 2.2 were used to develop a generalized model in terms of adsorbate and adsorbent properties. A sequential search algorithm outlined elsewhere [15] was used to identify the most significant properties and correlate these properties to describe thermal expansion coefficient, δ. Table 2.4 lists the properties of adsorbates and adsorbents that were found to be significant in predicting the thermal expansion coefficient. Thus, the thermal expansion coefficient, δ, was generalized with the following expression determined from the approach discussed above.

$$\delta = 6.03\text{E-}08\,M_1^2 - \frac{6.37\text{E-}03}{M_2} + 4.62\text{E-}02\,M_3^2 - \frac{5.85\text{E-}01}{M_4} - 3.73\text{E}-01\log(M_5) + 8.95\text{E-}03 \quad (2.15)$$

where the M_1 to M_5 denote the properties of adsorbates and adsorbents listed in Table 2.4.

In this manner, Equation (2.15) was used to obtain generalized values of δ for the systems considered. These values were used in the modified SLD model to obtain the generalized predictions. The statistics for the modified SLD model predictions are listed in Table 2.3. The overall %AAD for predictions was about 4.9%, which is close to the overall %AAD of 4.3% from direct regressions. Thus, using the generalized expression for δ was useful in obtaining improved accuracy in predictions on these activated carbons, as illustrated in Figures 2.4(a)-(c).

2.4.3 Validation of the Generalized Model

The generalized model was validated by testing the model on four additional datasets that were not included in the model development. Thus, these systems were ideally suited to test the model for more realistic predictive capability. Table 2.5 presents the predictions obtained for each of these datasets. As shown in the table, the overall %AAD for the generalized predictions on these systems was about 6.4%. This compares with %AAD of 5.1% when direct parameter regressions were performed. Note that the generalized predictions on these systems were obtained by using the δ values from Equation (2.15). Thus, the comparable level of errors observed for the systems in Table 2.5 illustrates the promise of the generalized model. An example of this generalized prediction is

shown in Figures 2.5(a)-(b) for adsorbents used for validation. Other systems produced similar predictions, but are not shown here for brevity.

2.4.4 Comparisons between the Modified SLD Model and Adsorption Models in the Literature

The representations from the modified SLD model were also compared with two adsorption models from the literature, the MPTA-MDP and the modified D-A models [6, 7]. Note that for each adsorbent/adsorbate pair, the MPTA-MDP model contains four parameters of which three are specific to the adsorbate and one is specific for the adsorbent, whereas the modified D-A model has five parameters and all five are specific to the adsorbate. The modified SLD model contains four parameters and two of them are specific to particular gas adsorbed. Thus, for an example of one adsorbent with three adsorbates, the MPTA-MDP, the modified DA and the modified SLD models will require 10, 15 and 8 parameters, respectively.

Adsorption data for methane and nitrogen on activated carbons [6, 7] were represented by the SLD model for comparative purposes. The statistics for the SLD, modified D-A, and MPTA-MDP models are provided in Table 2.6. The RMSEs for the SLD model representation are comparable for nitrogen, but slightly higher for methane compared the modified D-A and MPTA-MDP models. Note that the number of regressed parameters used in the modified SLD model is lowest among these adsorption models. Further, the SLD model has been generalized in terms of molecular properties, which has not been performed with the literature models. Figures 2.6(a) and (b) present a comparison of deviations obtained from these models for the above systems. As evident from these figures, the modified SLD model provides a uniform distribution of deviations throughout the pressure and temperature range of measurements for these systems.

Each of the models can provide estimates of the adsorbed-phase density; results are compared in Table 2.6. The adsorbed phase density is generally needed for estimating absolute adsorption

values, which are required for reservoir simulation. Since gas in the adsorbed state is liquid-like, commonly used estimates for the adsorbed-phase densities of methane and nitrogen are the liquid densities at their normal boiling points [23]. As evident from Table 2.6, among these adsorption models the adsorbed-phase densities predicted by the modified SLD model are closest to the densities of methane and nitrogen at normal boiling points, which are reported to be 0.42 g/cc [24] and 0.8 g/cc [25], respectively. Thus, the modified SLD model provides consistent predictions of the adsorbed-phase density based on the experimentally measured excess adsorption.

2.4.5 Modified SLD Model Predictions at Multiple Temperatures based on Data at a Single Temperature

As part of this work, we tested the efficacy of the modified SLD model to predict adsorption data at multiple temperatures based on adsorption data available at a single temperature. The activated carbon data were obtained from Berlier and Frère [26], Frère and De Weireld [27], Payne et al. [28] and [29]. The values of δ were predicted from the generalized correlation developed in this work (Equation 2.15). The steps contained in this prediction case include: (1) the parameters in the original SLD model, i.e. SA, $\varepsilon_{ss/k}$ and L were regressed based on a single adsorption isotherm and (2) the modified SLD model with the generalized δ values obtained from Equation (2.15) was then used to predict the adsorption at other temperatures.

The overall %AAD for these datasets was about 3.7%, as shown in Table 2.7. Figures 2.7(a)-(c) illustrate modified SLD model predictions for adsorption obtained with this approach. The modified SLD model appears capable of providing reliable predictions at several temperatures based on available measurements at only a single temperature.

2.4.6 Modified SLD Model Results for Gas Adsorption at Multiple temperatures on Coals

Based on the promising results of our study of adsorption on activated carbons, we investigated the capability of the modified SLD model to describe gas adsorption at multiple temperatures on coals.

The adsorption data on coals were obtained from Sakurovs et al. [30] and Li et al. [31]. Two specific case studies were conducted depending on the type of available adsorption data. If the adsorption measurements were available at only two temperatures for a gas, the modified SLD model parameters were regressed to obtain model representations. If the adsorption measurements were available at more than two temperatures, then the model parameters were obtained based on two temperature levels and the remaining isotherms were then predicted.

The adsorption data from [30] were available at 308 and 328 K and therefore, the modified SLD model parameters were regressed from these data. Table 2.8 lists the regressed SLD model parameters on these coals. The regressed parameters SA, $\varepsilon_{ss/k}$ and L were within the range observed in our previous study on coals [13]. Further, the regressed values of δ were comparable to those obtained for activated carbons in this study.

Table 2.9 presents the statistics for model regressions on these coals. The %AADs for adsorption of CO_2 at temperatures of 308 and 328 K were relatively higher than those of other gases, which can be attributed to errors in gas density predictions from the equation of state at conditions very close to critical state of CO_2. Overall, the modified SLD model appeared capable of providing precise representations of gas adsorption on coals at different temperatures, as evident from the overall %AAD of about 3%. For illustration purposes, Figure 2.8 depicts the SLD model representations on Pocahontas coal. Other systems listed in Table 2.9 produced similar representations, but are not shown here for brevity.

The adsorption data from [31] were available at 308, 318 and 328 K and therefore, the SLD parameters were obtained by using the data at 308 and 318 K. Then, using these parameters, the adsorption isotherms for 328 K were predicted. Table 2.10 presents the SLD model parameters obtained from the isotherms at 308 and 318 K. Using the parameters listed in Table 2.10, the adsorption at 328 K was predicted. The model statistics for these predictions are listed in Table

2.11, along with results for 308 and 318 K. For illustration purposes, Figure 2.9 presents the model predictions obtained at 328 K. Overall, the %AAD for adsorption of methane and CO_2 at 328 K was about 2%, based on the model parameters obtained from other temperatures. Thus, the modified SLD model appears capable of useful predictions of adsorption on these coals. Notwithstanding this result, the approach presented in this study requires additional testing with adsorption data on more coals at wider ranges of temperature.

2.4.7 Modified SLD Model Representations of Gas Adsorption at Multiple Temperatures on Shales

The modified SLD model was also used to describe adsorption data on shales. The adsorption data on shales were obtained from [32]. Table 2.12 presents the SLD model parameters for representations on shale samples. The regressed SLD model parameters such as SA, $\varepsilon_{ss/k}$ and L were within ranges observed in our previous work on shale gas adsorption [8] and the regressed thermal expansion coefficients were also comparable to the values obtained for activated carbons and coals.

Table 2.13 presents the statistics for model representations on shale samples. The %AAD for each sample varied from about 3 to 6% and the overall %AAD was about 4%. Figures 2.10(a)-(c) illustrate typical model representations obtained, which indicate useful representations provided by the modified SLD model. Thus, the modified SLD model appears capable of describing the supercritical gas adsorption at multiple temperatures on these shale samples.

2.5 Conclusion

A modeling study was conducted to extend the SLD model's predictive capability for the temperature dependence of supercritical gas adsorption. The SLD model was modified by including a temperature-dependent expression for the adsorbed-phase volume. The expression accounts for the changes in adsorbed-phase volume with temperature. The thermal expansion coefficient, δ, used to extend the temperature dependence was developed based on data for

activated carbons. The modified SLD model thus obtained provided improved representations of gas adsorption on activated carbons over wider ranges of temperature.

The model for thermal expansion coefficient was generalized in terms of molecular properties of adsorbates and adsorbents. Results obtained from the generalized model were comparable to the results obtained from direct regressions. A validation of the generalized model was performed by testing with data on systems that were not utilized in the model development. The generalized model was also used to obtain predictions at multiple temperatures based on available adsorption isotherm at only a single temperature. The modified model was utilized to describe supercritical gas adsorption on coals and shales at multiple temperatures. The model was found capable of providing accurate description of adsorption at multiple temperatures on these adsorbents. The modeling results on coals and shales indicated that the model is capable of describing gas adsorption at several temperatures. The generalized model presented in this work can be further tested once additional data on coals and shales at wider ranges of temperatures becomes available.

Table 2.1. Database for Pure-Gas Adsorption on Activated Carbons, Coals and Shales

Adsorbent	Adsorbate	Pressure Range (MPa)	Temperature Range (K)	BET Surface Area (m^2/g)	NDP*	Reference
Data Set for Activated Carbons						
PCB	CH_4	0.1-3.7	296-480	1150	65	[33]
	CO_2	0.2-5.8				
	CO	0.1-1.3				
	H_2S	0.3-6.7				
Norit-RB1	CH_4	0.1-0.8	294-350	1100	128	[34]
	CO_2					
Nuxit-Al	CH_4	0.01-0.6	293-363	1200	447	[35]
	C_2H_2	0.001-0.1				
	C_2H_6	0.01-0.7				
	C_2H_4	0.01-0.6				
	C_3H_8	0.01-0.7				
	C_3H_6	0.01-0.8				
	nC_4H_{10}	0.001-0.1				
Columbia Grade L	CH_4	0.02-1.5	311-478	1152	272	[36]
	N_2	0.03-1.5				
	C_2H_2	0.01-0.1				
	C_2H_6	0.01-1.5				
	C_2H_4	0.01-1.5				
	C_3H_8	0.01-0.7				
	C_3H_6	0.01-0.1				
BPL	CH_4	0.01-3.8	213-301	988	233	[37]
	CO_2	0.003-3.84				
	C_2H_6	0.001-1.71				
	C_2H_4	0.001-1.70				
F30/470	CH_4	0.44-6.0	303-383	993	154	[26]
	N_2	0.39-6.0				
F30/470	CO_2	0.05-2.5	288-328	993	113	[27]

Table 2.1. Database for Pure-Gas Adsorption on Activated Carbons, Coals and Shales – Cont'd

Adsorbent	Adsorbate	Pressure Range (MPa)	Temperature Range (K)	BET Surface Area (m2/g)	NDP*	Reference
LAC	C_3H_8	0.001-0.1	273-343	1011	102	[38]
	C_3H_6					
Carbotech	CH_4	0.006-3.4	300-318	885	32	[39]
KT	CH_4	0.6-3.4	300-318	668	31	
Maxsorb II	CH_4	0.1-1.2	281-343	2768	126	[40]
Templated Carbon	CH_4	0.05-4.6	263-303	1500	71	[41]
	C_2H_6	0.02-2.0				
Maxsorb III	CH_4	0.06-2.4	263-303	3140	128	[42]
Columbia Grade G	CH_4	0.1-13.8	283-343	1157	141	[28]
	nC_4H_{10}	0.003-0.8				
	C_3H_8	0.001-1.4				
JX101	CH_4	0.01-1.0	283-313	1500	107	[43]
External Data Set For Activated Carbons Used for Validation						
Coconut shell-derived carbon	CH_4	0.1-9.3	235-333	3106	122	[29]
	N_2	0.5-9.0	198-298		61	
F-400	CO_2	0.14-9.4	303-318	850	116	[44]
CNS-201	CH_4	0.01-6.8	243-333	2000	62	[7]
CO-64	N_2	0.01-6.6	153-298	1150	135	
Data Set for Coals						
Pocahontas	CH_4	1.4-13.8	308-328	N/A*	20	[30]
	N_2		298-328		20	
	CO_2		308-328		20	
Illinois-6	CH_4	14-13.8	308-328	N/A	20	
	N_2		298-328		20	
	CO_2		308-328		20	

Table 2.1. Database for Pure-Gas Adsorption on Activated Carbons, Coals and Shales – Cont'd

Adsorbent	Adsorbate	Pressure Range (MPa)	Temperature Range (K)	BET Surface Area (m2/g)	NDP*	Reference
Data Set for Coals (Cont'd)						
Beulah Zap	CH_4	14-13.8	308-328	N/A	20	[30]
	N_2		298-328		20	
	CO_2		308-328		20	
Hulun Buir	CH_4	2.5-19.1	308-328	N/A	41	[31]
	CO_2	3.8-24.2			80	
Pingdingshan	CH_4	3.0-19.7	308-328	N/A	43	
	CO_2	5.2-24.6			71	
Jingcheng	CH_4	1.2-19.0	308-328	N/A	48	
	CO_2	3.6-24.6			67	
Data Set for Shales						
WIC7145	CH_4	0.07-12.5	318-358	6.7	26	[32]
WIC7155		0.05-13.0		4.3	28	
HAR7038		0.02-12.0		N/A	25	
HAR7060		0.06-13.5		N/A	14	
HAD7090		0.05-12.8		25.1	23	
HAD7119		0.07-13.8		21.0	29	
Total					**3321**	

*****NDP is number of data points and N/A denotes not available.

Table 2.2 Modified SLD Model Parameters for Gas Adsorption on Activated Carbons

Adsorbent	Adsorbate	Model Parameters			
		SA (m^2/g)	δ (1/R)	L (nm)	$\varepsilon_{ss/k}$ (K)
PCB	CH_4	708.1	1.42E-03	0.94	29.0
	CO_2	849.3	1.82E-03		
	CO	755.8	6.66E-04		
	H_2S	971.5	9.23E-04		
Norit-RB1	CH_4	639.2	1.26E-03	1.04	35.3
	CO2	647.0	3.16E-03		
Nuxit-Al	CH_4	512.7	2.40E-03	1.09	34.2
	C_2H_2	664.2	2.56E-03		
	C_2H_6	685.5	2.39E-03		
	C_2H_4	699.9	2.42E-03		
	C_3H_8	827.1	1.74E-03		
	C_3H_6	798.4	1.80E-03		
	nC_4H_{10}	825.3	1.11E-03		
Columbia Grade L	CH_4	694.6	1.59E-03	1.16	36.6
	N_2	636.7	9.39E-04		
	C_2H_2	709.7	3.98E-03		
	C_2H_6	826.9	1.41E-03		
	C_2H_4	795.6	1.05E-03		
	C_3H_8	844.4	1.10E-03		
	C_3H_6	956.1	1.93E-03		
BPL	CH_4	524.4	1.89E-03	1.00	30.5
	CO_2	627.9	2.71E-03		
	C_2H_6	710.9	1.90E-03		
	C_2H_4	686.8	1.97E-03		
F30/470	CH_4	580.2	1.76E-03	1.07	36.2
	N_2	477.4	1.63E-03		
F30/470	CO_2	667.4	2.49E-03	1.07	36.2
LAC	C_3H_8	924.8	2.61E-03	1.00	33.9
	C_3H_6	1006.9	1.80E-03		
Carbotech	CH_4	449.5	1.38E-03	1.27	37.2
KT	CH_4	407.3	5.36E-04	0.86	41.2
Maxsorb II	CH4	1813.8	1.76E-03	0.71	14.7

Table 2.2 Modified SLD Model Parameters for Gas Adsorption on Activated Carbons - Cont'd

Adsorbent	Adsorbate	Parameters			
		SA (m^2/g)	δ (1/R)	L (nm)	$\varepsilon_{ss/k}$ (K)
Templated Carbon	CH_4	973.6	4.71E-04	1.39	21.7
	C_2H_6	1076.6	2.16E-03		
Maxsorb III	CH_4	1088.6	1.64E-03	1.85	23.7
Columbia Grade G	CH_4	770.2	1.68E-03	1.11	29.6
	nC_4H_{10}	984.6	6.95E-04		
	C_3H_8	1127.6	1.10E-03		
JX101	CH_4	665.3	2.57E-03	0.76	26.7
	N_2	634.3	2.13E-03		

Table 2.3. SLD Results for Modeling Temperature Dependence of Adsorption on Activated Carbons

Adsorbent	Adsorbate	NDP	%AAD in Excess Adsorption		
			Original SLD Model (Case 1)	Modified SLD Model	
				Regressed δ (Case 2)	Generalized δ (Case 3)
PCB	CH_4	22	14.9	3.3	3.9
	CO_2	12	19.0	5.2	11.5
	CO	15	10.3	5.7	5.8
	H_2S	16	9.9	4.3	5.8
Norit RB-1	CH_4	64	7.3	4.5	4.3
	CO_2	64	9.5	5.1	5.4
Nuxit Al	CH_4	29	6.3	3.4	3.5
	C_2H_2	99	10.7	5.5	5.6
	C_2H_6	92	10.7	4.1	4.5
	C_2H_4	72	3.2	3.2	3.2
	C_3H_8	67	4.8	4.8	4.8
	C_3H_6	54	5.1	2.8	2.9
	nC_4H_{10}	34	10.9	4.4	5.0
Columbia Grade L	CH_4	43	11.4	5.2	5.1
	N_2	32	9.5	4.7	4.6
	C_2H_2	11	12.7	6.1	8.4
	C_2H_6	57	10.9	4.9	12.4
	C_2H_4	62	9.9	6.3	9.7
	C_3H_8	46	15.8	6.2	6.4
	C_3H_6	21	7.2	5.7	9.0
BPL	CH_4	60	16.2	6.2	6.9
	CO_2	49	11.6	4.9	4.9
	C_2H_6	52	11.4	3.9	3.7
	C_2H_4	72	10.5	2.7	4.7
F30/470	CH_4	82	9.0	4.5	4.2
	N_2	72	7.1	1.9	1.7
F30/470	CO_2	113	5.0	2.6	2.6
LAC	C_3H_8	51	12.2	7.9	7.9
	C_3H_6	51	12.6	6.9	9.2
Carbotech	CH_4	32	3.0	2.5	2.5
KT	CH_4	31	1.1	1.0	1.3
Maxsorb II	CH_4	126	5.9	2.3	2.3
Templated Carbon	CH_4	41	7.7	6.3	8.1
	C_2H_6	30	7.6	4.3	4.4
Maxsorb III	CH_4	128	6.2	3.3	3.5

Table 2.3. SLD Results for Modeling Temperature Dependence of Adsorption on Activated Carbons – Cont'd

Adsorbent	Adsorbate	NDP	%AAD in Excess Adsorption		
			Original SLD Model (Case 1)	Modified SLD Model	
				Regressed δ (Case 2)	Generalized δ (Case 3)
Columbia Grade G	CH_4	39	4.8	4.8	4.8
	nC_4H_{10}	55	4.8	3.5	3.5
	C_3H_8	47	4.7	3.8	3.9
JX101	CH_4	52	5.8	4.9	4.7
	N_2	55	5.5	3.5	3.8
Overall		**2150**	**8.2**	**4.3**	**4.9**

Table 2.4. Molecular Properties of Adsorbates and Adsorbents Used in Generalized Expression for Thermal Expansion Coefficient, δ

Notation from Equation (2.15)	Molecular Property	Description	Type of Molecular Property
M_1	%C	% of carbon atoms	constitutional index
M_2	Mor13m	signal 13 weighted by mass	3-D geometrical index
M_3	Mor06v	signal 06 weighted by van der Waals volume	3-D geometrical index
M_4	BET	BET surface area of adsorbent	adsorbent surface property
M_5	Di	D total accessibility index / weighted by ionization potential	whim descriptor

Table 2.5. Validation Results for the Modified SLD Model on Datasets Not Used in the Model Development

Adsorbent	Adsorbate	NDP	%AAD in Excess Adsorption		Reference
			Regressed δ	Generalized δ	
Coconut shell-derived carbon	CH_4, N_2	183	2.7	4.0	[29]
F-400	CO_2	116	9.1	9.3	[44]
CNS-201	CH_4	62	3.9	5.4	[7]
CO-64	N_2	135	4.6	7.0	
Overall		**496**	**5.1**	**6.4**	

Table 2.6. Pure-Gas Adsorption on CNS-201 and CO-64 Activated Carbons: Comparison with Literature Models

Model	Number of Regressed Parameters	Overall RMSE* (mmol/g)		Adsorbed Phase Density Prediction (g/cc)		Liquid Density at Normal Boiling Point (g/cc)		Reference
		CH_4 on CNS-201	N_2 on CO-64	CH_4 on CNS-201	N_2 on CO-64	CH_4	N_2	
MPTA-MDP	10	0.10	0.35	0.49	0.96	0.42	0.81	**[7]**
Modified DA	15	0.11	0.58	0.58	1.01			**[7]**
Modified SLD	8	0.19	0.35	0.36	0.73			This work

*RMSE is the root-mean-squared error in excess adsorption.

Table 2.7. Modified SLD Model Results for Predicting Adsorption Based on Data at a Single Temperature

Adsorbent	Adsorbate	Temperature (K)	NDP	%AAD in Excess Adsorption*
F30/470	CH_4	303	16	1.6
		323	16	2.0
		343	17	2.0
	N_2	303	16	3.4
		323	12	2.4
		343	15	3.3
	CO_2	303	16	3.1
		308	32	3.1
		318	16	4.1
		328	17	4.0
Columbia Grade G	C_3H_8	303	10	3.4
		313	11	6.1
		323	10	7.5
		333	10	5.7
	CH_4	303	12	1.6
		313	10	2.1
		323	13	2.7
Coconut shell-derived carbon	CH_4	313	20	1.2
		333	19	2.9
Overall				**3.7**

*%AADs in the highlighted rows are percentage average absolute deviation for SLD model representations with respect to experimental data at 303 or 313 K. Overall %AAD does not include the highlighted isotherms for which parameters were regressed.

Table 2.8. Modified SLD Model Parameters for Gas Adsorption on Coals (Data from [30])

Adsorbent	Adsorbate	Model Parameters			
		SA (m^2/g)	L (nm)	$\varepsilon_{ss/k}$ (K)	δ (1/R)
Pocahontas	CH_4	71.6	1.02	33.7	1.91E-03
	N_2	53.2			2.74E-03
	CO_2	79.3			2.02E-03
Illinois-6	CH_4	61.5	1.21	26.1	1.81E-03
	N_2	50.2			2.24E-03
	CO_2	93.3			1.02E-03
Beulah Zap	CH_4	51.5	1.31	39.5	4.10E-03
	N_2	38.2			3.51E-03
	CO_2	85.3			1.96E-03

Table 2.9. Modified SLD Model Representations on Coals

Adsorbent	Adsorbate	Temperature (K)	NDP	Modified SLD Model		Reference
				%AAD	Overall	
Pocahontas	CH_4	308	10	1.9	1.4	[30]
		328	10	1.0		
	N_2	298	10	1.1	1.1	
		328	10	1.0		
	CO_2	308	10	6.7	6.7	
		328	10	6.6		
Illinois-6	CH_4	308	10	1.9	2.5	
		328	10	3.1		
	N_2	298	10	2.3	2.2	
		328	10	2.1		
	CO_2	308	10	5.7	4.6	
		328	10	3.6		
Beulah Zap	CH_4	308	10	2.4	1.6	
		328	10	0.7		
	N_2	298	10	1.2	1.3	
		328	10	1.5		
	CO_2	308	10	5.8	5.4	
		328	10	4.9		
Overall			**180**		**3.0**	

Table 2.10. Modified SLD Model Parameters for Gas Adsorption on Coals (Data from [31])

Adsorbent	Adsorbate	Model Parameters*			
		SA (m^2/g)	L (nm)	$\varepsilon_{ss/k}$ (K)	δ (1/R)
Hulun Buir	CH_4	69.6	1.24	31.3	7.45E-03
	CO_2	98.9			1.94E-03
Pingdingshan	CH_4	58.2	1.27	30.5	2.22E-03
	CO_2	62.4			1.37E-03
Jingcheng	CH_4	105.3	0.93	34.5	1.77E-03
	CO_2	115.2			2.86E-03

*Model parameters were obtained from SLD model regression using adsorption data of methane and CO_2 at 308 and 318 K from [31]. These sets of parameters were used for predicting adsorption at 328 K.

Table 2.11. Modified SLD Model Representations and Predictions for Gas Adsorption on Coals

Adsorbent	Adsorbate	NDP	Temperature (K)	%AAD* in Excess Adsorption	Reference
Hulun Buir	CH_4	12	308	1.0	[31]
		15	318	0.6	
		14	328	2.2	
	CO_2	27	308	4.2	
		26	318	2.6	
		27	328	2.5	
Pingdingshan	CH_4	12	308	2.3	
		15	318	1.8	
		16	328	2.3	
	CO_2	24	308	4.9	
		25	318	3.9	
		22	328	2.3	
Jingcheng	CH_4	16	308	0.6	
		15	318	0.6	
		17	328	0.8	
	CO_2	24	308	4.3	
		22	318	2.9	
		21	328	2.7	
Overall		**117**		**2.2**	

*%AADs in the highlighted rows are percentage average absolute deviation for SLD model representations with respect to experimental data at 308 and 318 K. Overall %AAD does not include the highlighted isotherms for which parameters were regressed.

Table 2.12. Modified SLD Model Parameters for Gas Adsorption on Shales

Adsorbent	Adsorbate	Sample#	Model Parameters			
			SA (m^2/g)	L (nm)	$\varepsilon_{ss/k}$ (K)	δ (1/R)
Posidonia Shales	CH_4	WIC7145	8.7	1.85	26.4	1.93E-03
		WIC7155	8.9	1.79	21.6	2.31E-03
		HAR7038	11.81	0.71	8.45	2.08E-03
		HAR7060	9.3	0.70	8.6	1.40E-03
		HAD7090	10.0	1.14	29.3	1.75E-03
		HAD7119	9.6	1.04	20.5	1.43E-03

Table 2.13. Modified SLD Model Representations on Shales

Adsorbent	Adsorbate	Sample#	NDP	Temperature (K)	Modified SLD Model		Reference
					%AAD	Overall	
Posidonia Shales	CH_4	WIC7145	26	318	5.3	5.3	[32]
				338	5.6		
				358	5.2		
		WIC7155	28	318	3.2	3.6	
				338	4.0		
				358	3.8		
		HAR7038	25	318	6.6	5.7	
				338	5.2		
				358	5.5		
		HAR7060	14	318	3.9	5.0	
				338	6.2		
				358	4.6		
		HAD7090	23	318	4.1	3.7	
				338	2.9		
				358	4.0		
		HAD7119	29	318	3.7	2.7	
				338	2.8		
				358	1.7		
Overall			**145**			**4.2**	

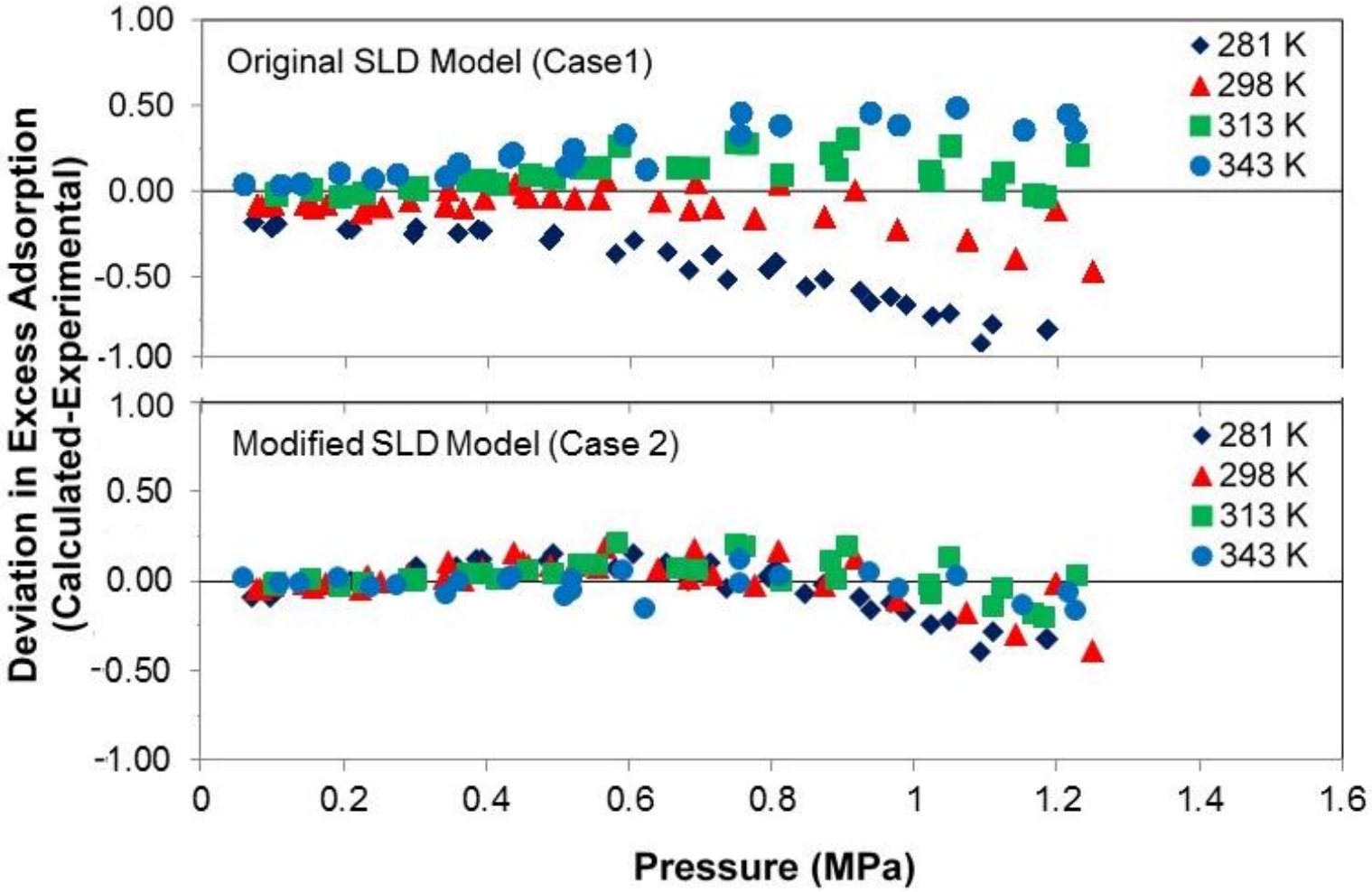

Figure 2.1(a). Deviations of SLD Model Representations for Methane Adsorption in mmol/g on Maxsorb II (Points are Data from [40])

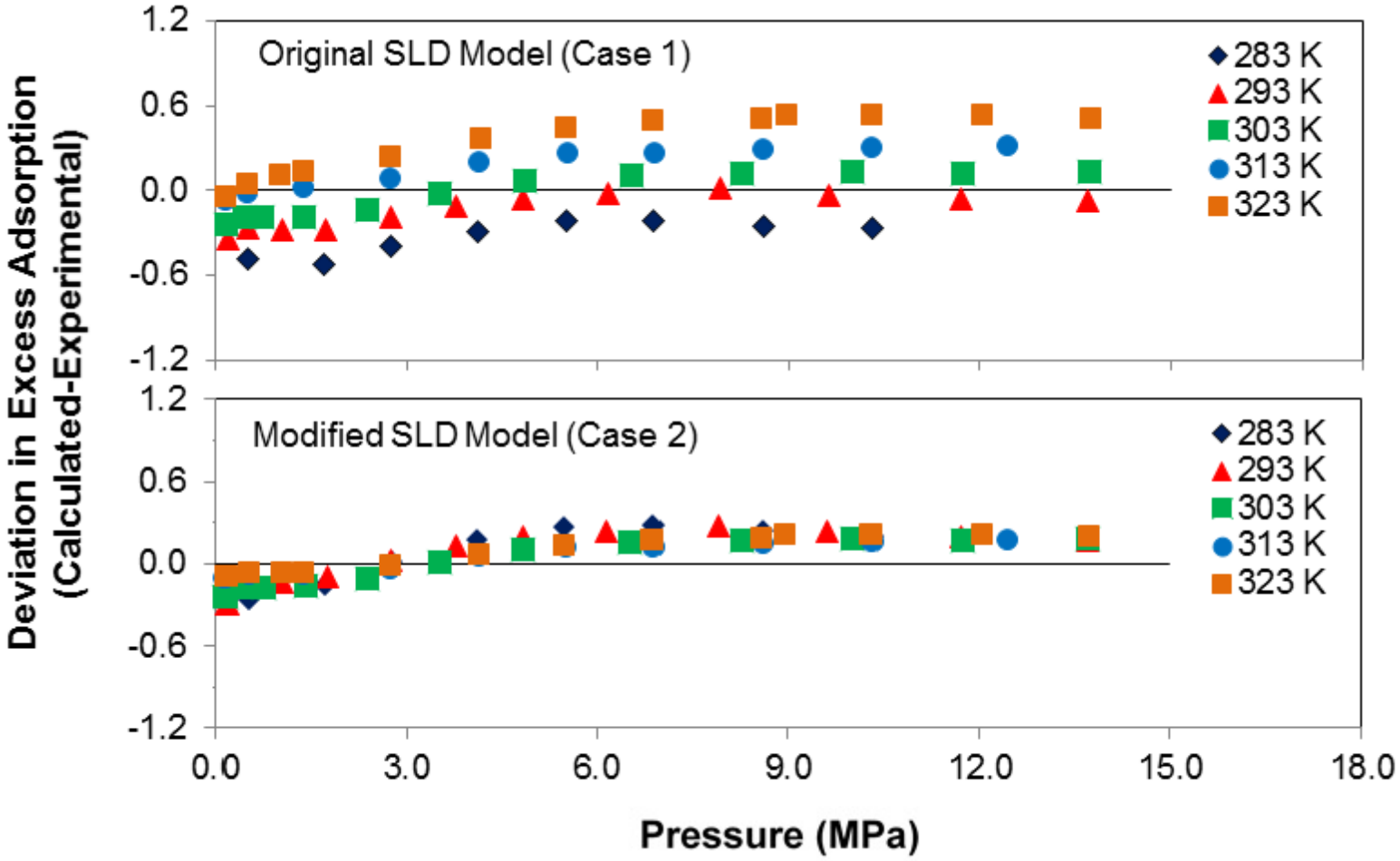

Figure 2.1(b). Deviations of SLD Model Representations for Methane Adsorption in mmol/g on Columbia Grade G (Points are Data from [28])

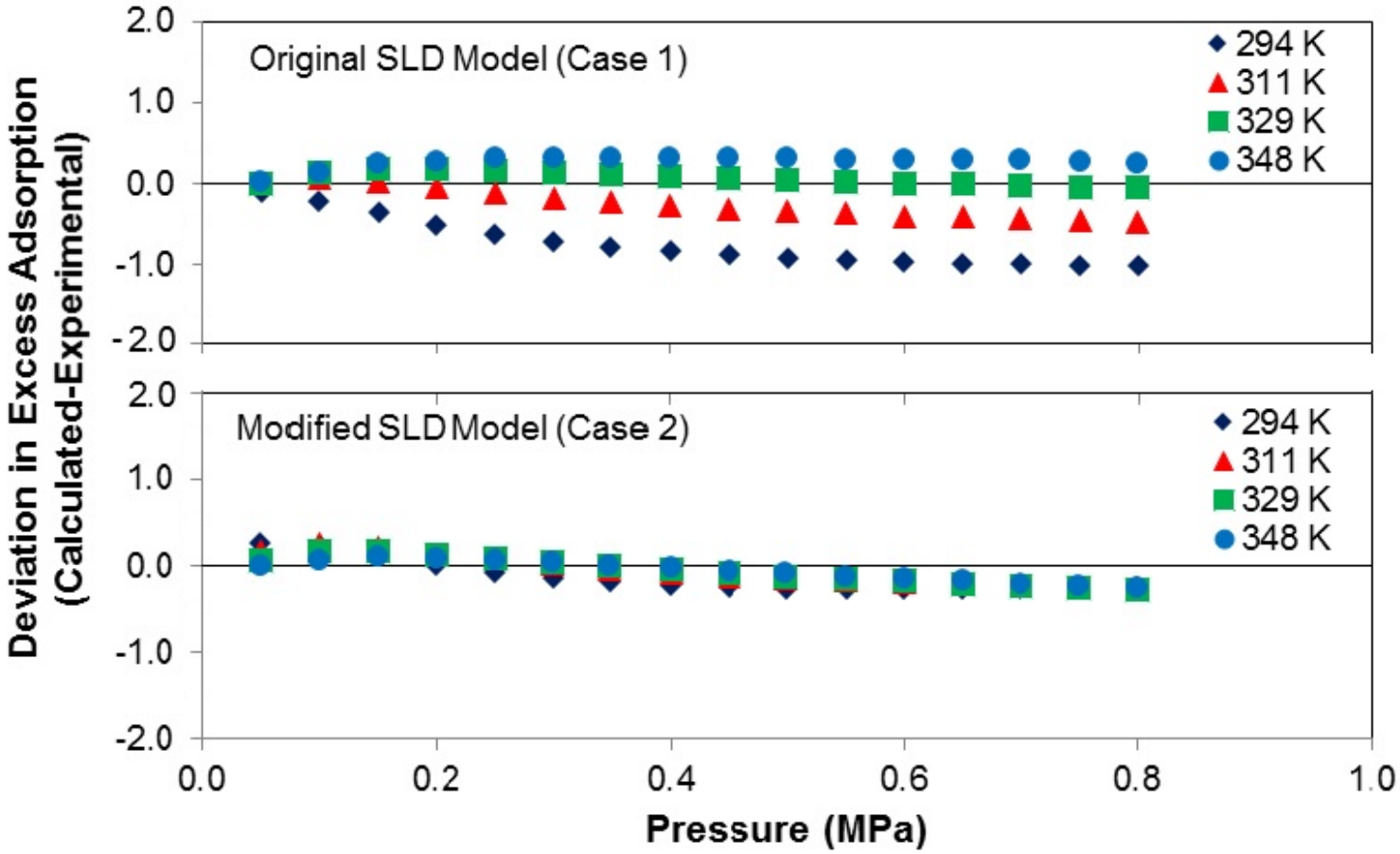

Figure 2.1(c). Deviations of SLD Model Representations for CO_2 Adsorption in mmol/g on Norit-RB1 (Points are Data from [34])

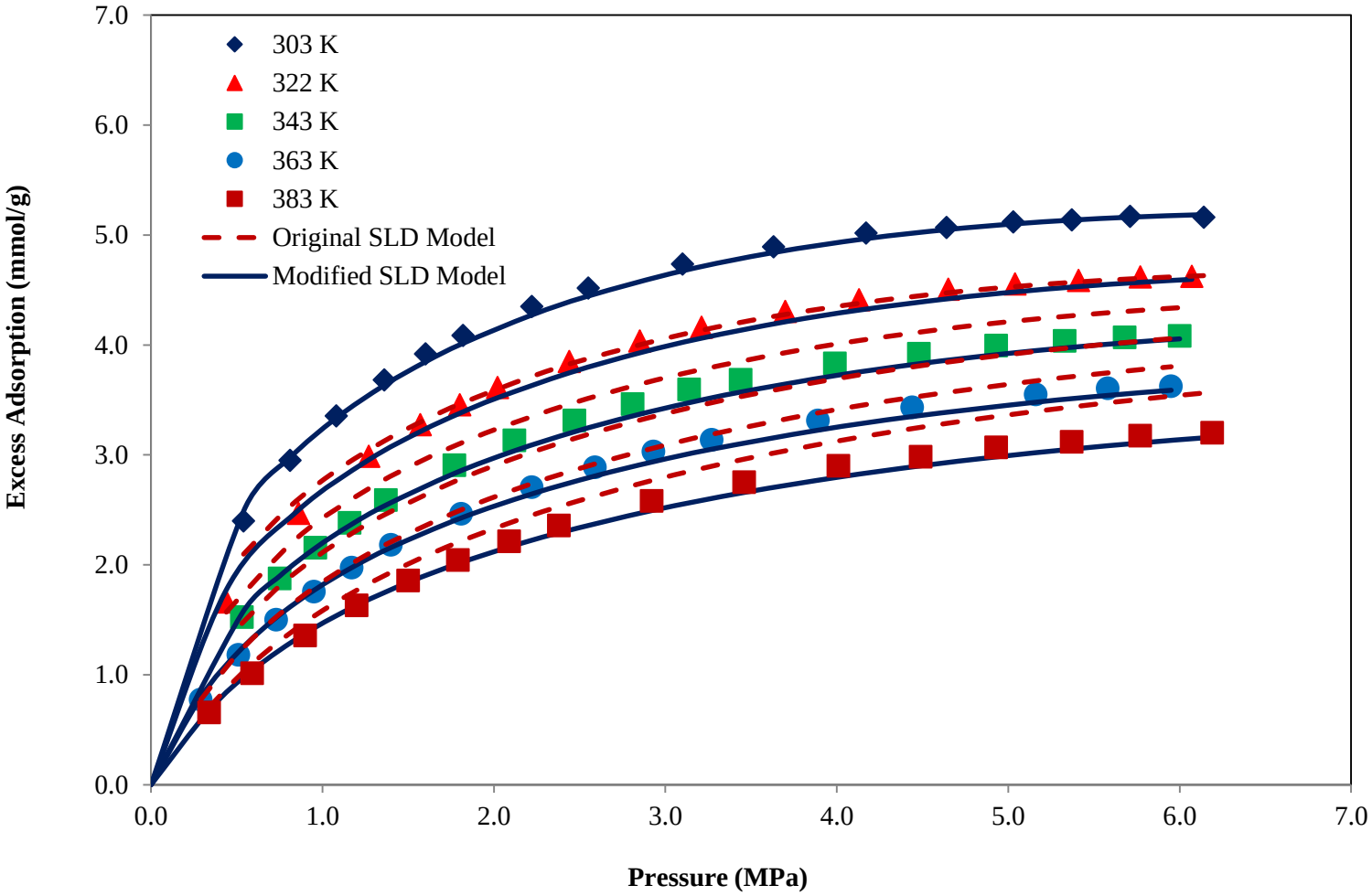

Figure 2.2(a). Modified SLD Model Representations for Methane Adsorption on F30/470 (Points are Data from [26])

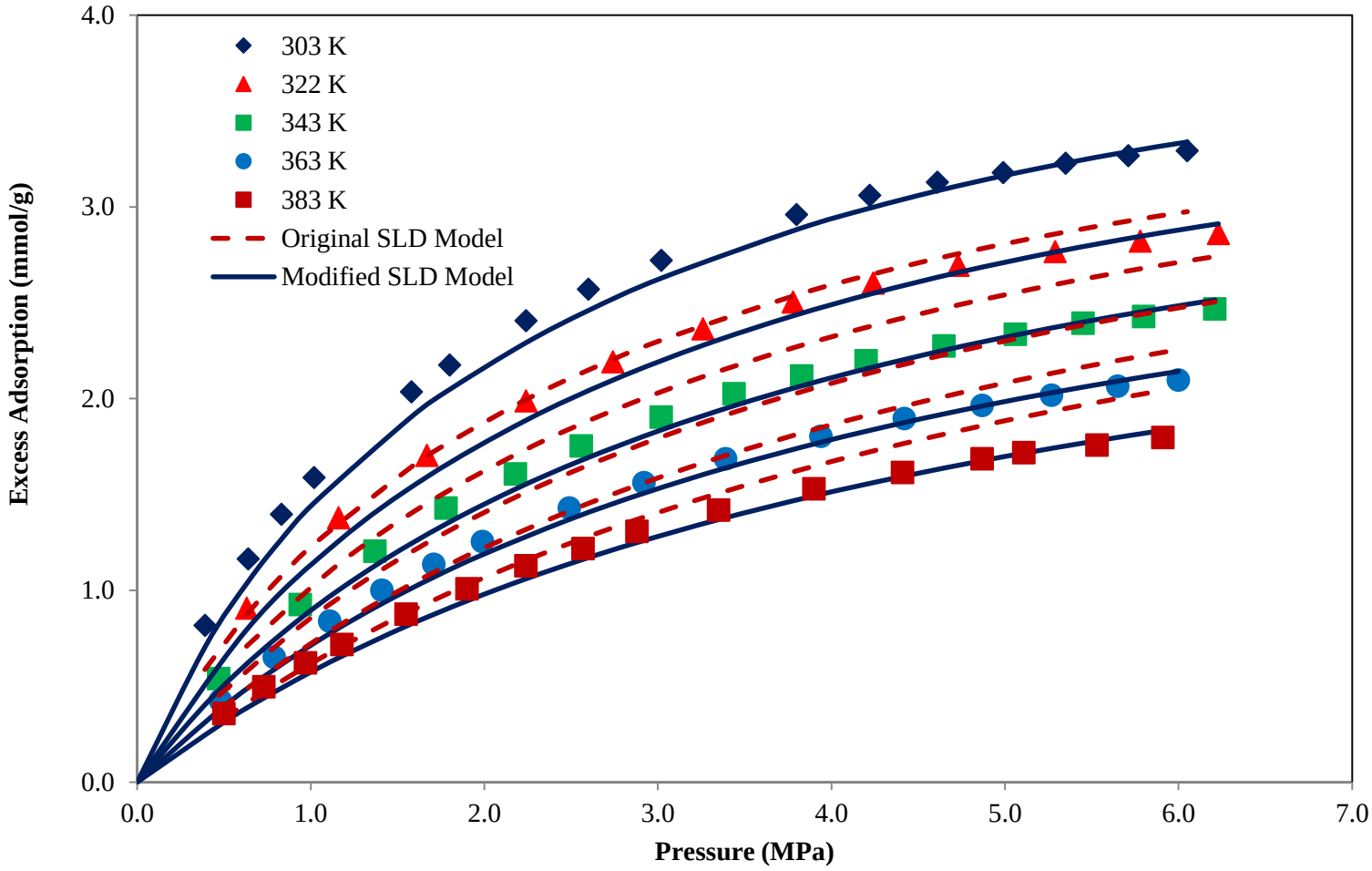

Figure 2.2(b). Modified SLD Model Representations for Nitrogen Adsorption on F30/470 (Points are Data from [26])

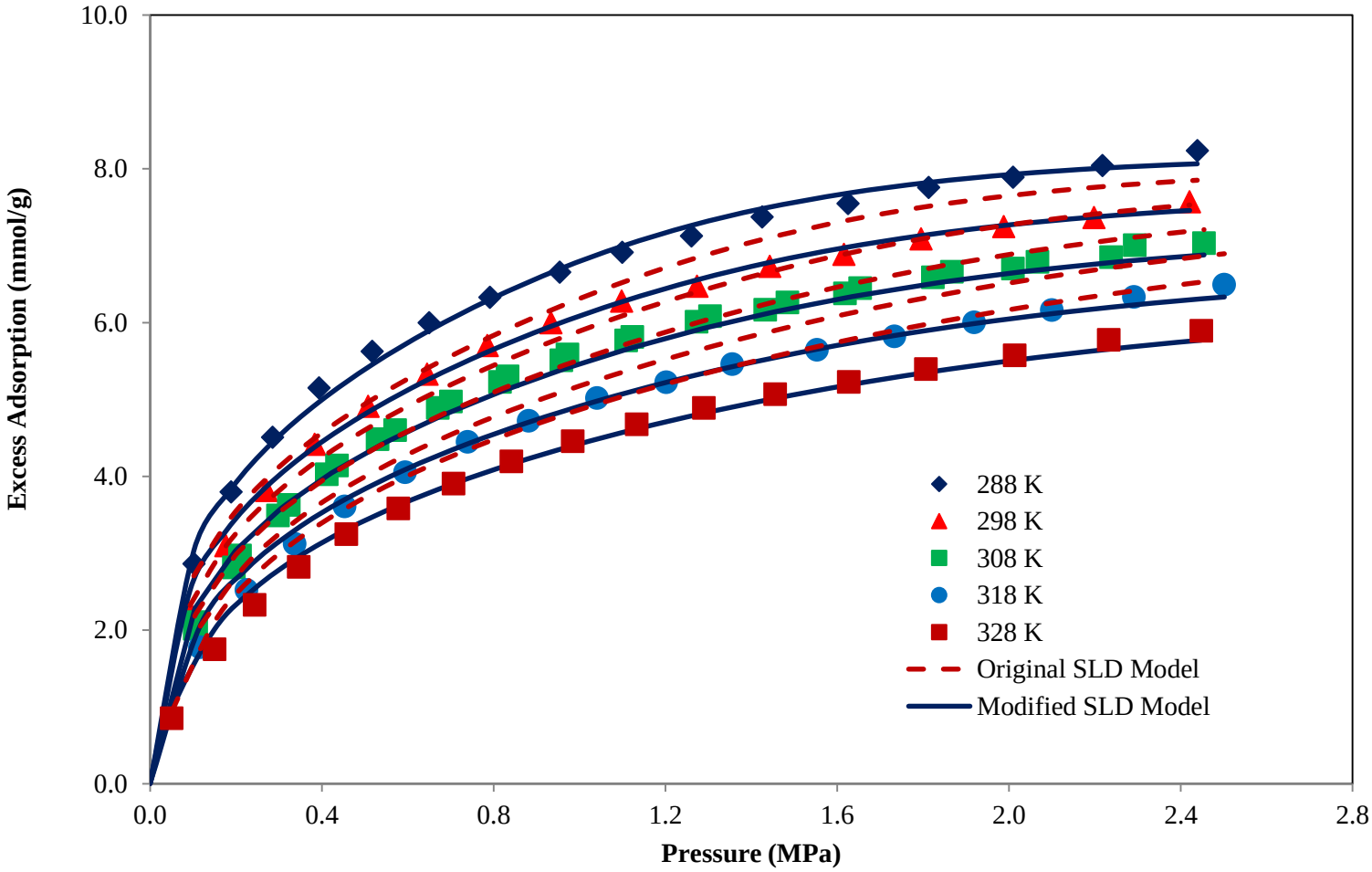

Figure 2.2(c). Modified SLD Model Representations for CO_2 Adsorption on F30/470 (Points are Data from [27])

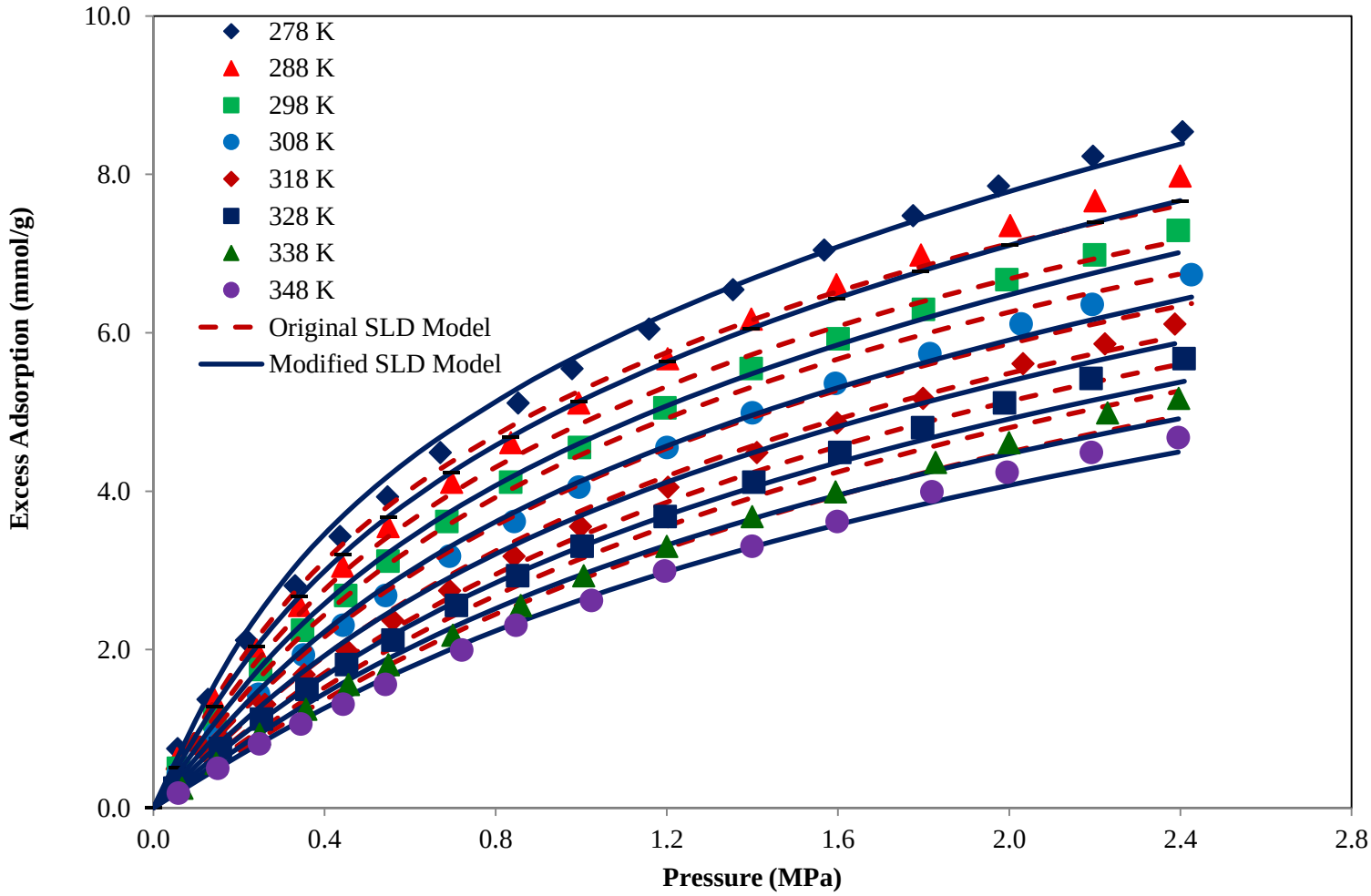

Figure 2.2(d). Modified SLD Model Representations for Methane Adsorption on Maxsorb III (Points are Data from [42])

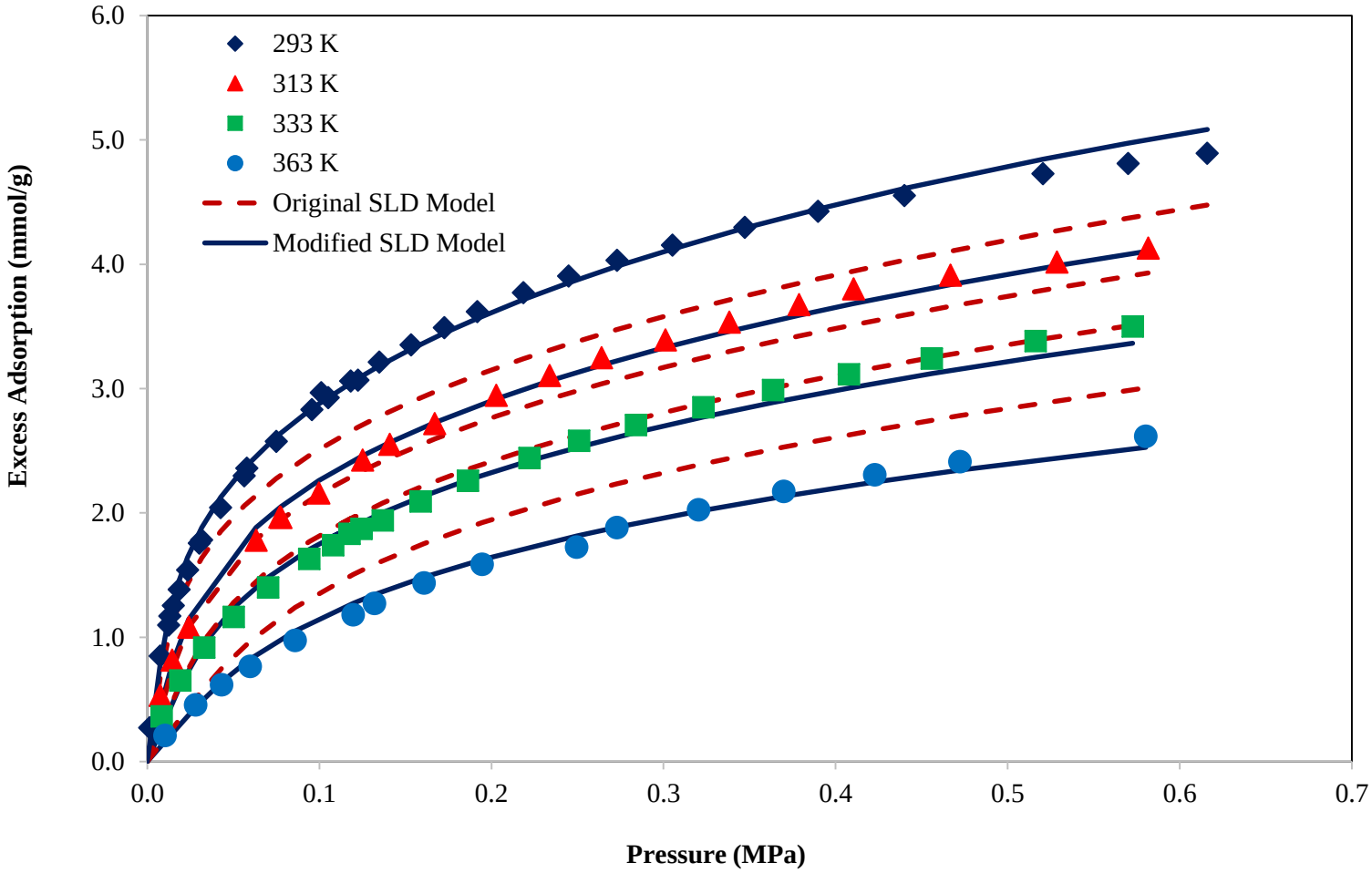

Figure 2.2(e). Modified SLD Model Representations for Ethylene Adsorption on Nuxit-Al (Points are Data from [35])

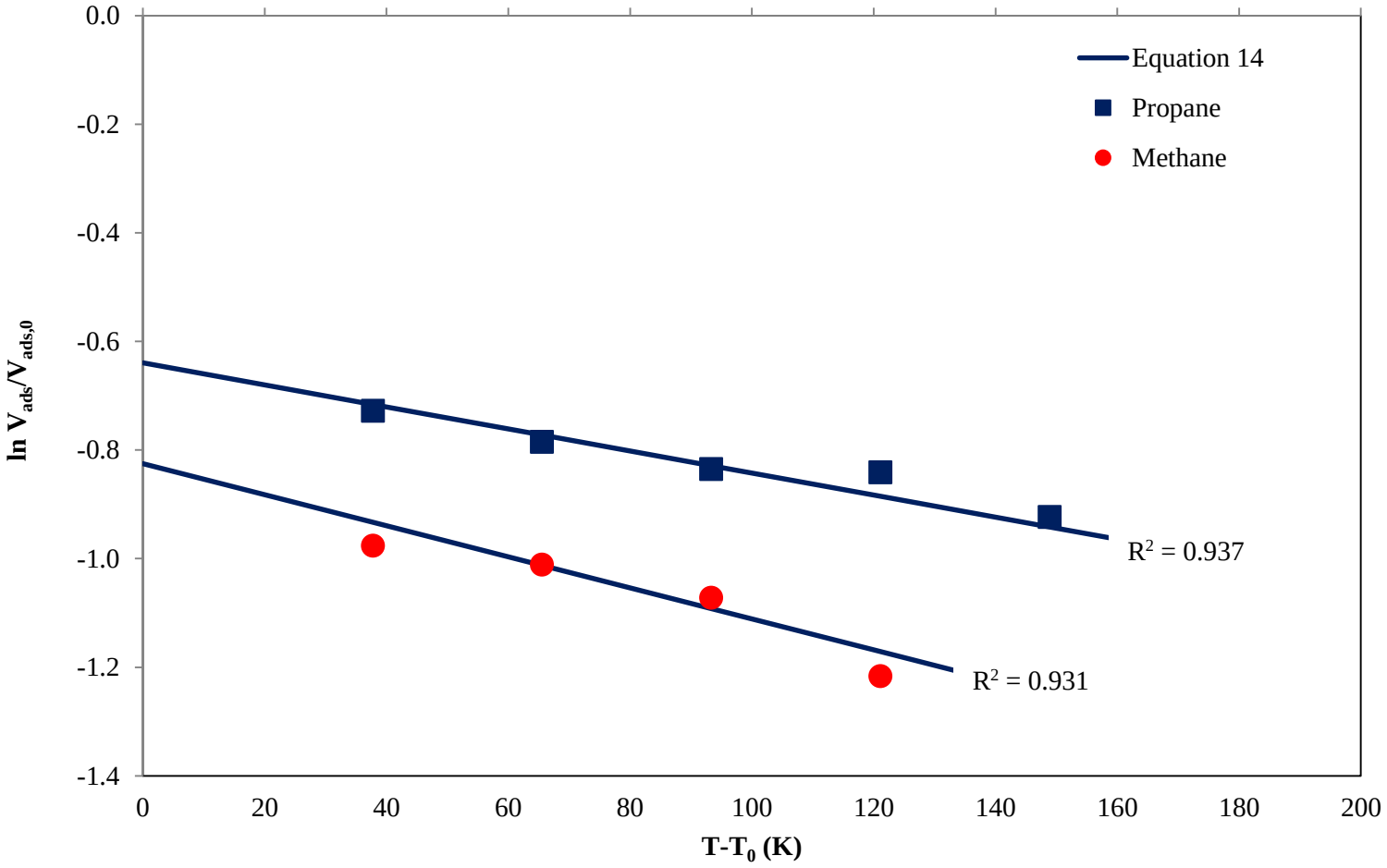

Figure 2.3. Temperature Effect on Adsorbed-Phase Volume
(Points are based on Data from [36])

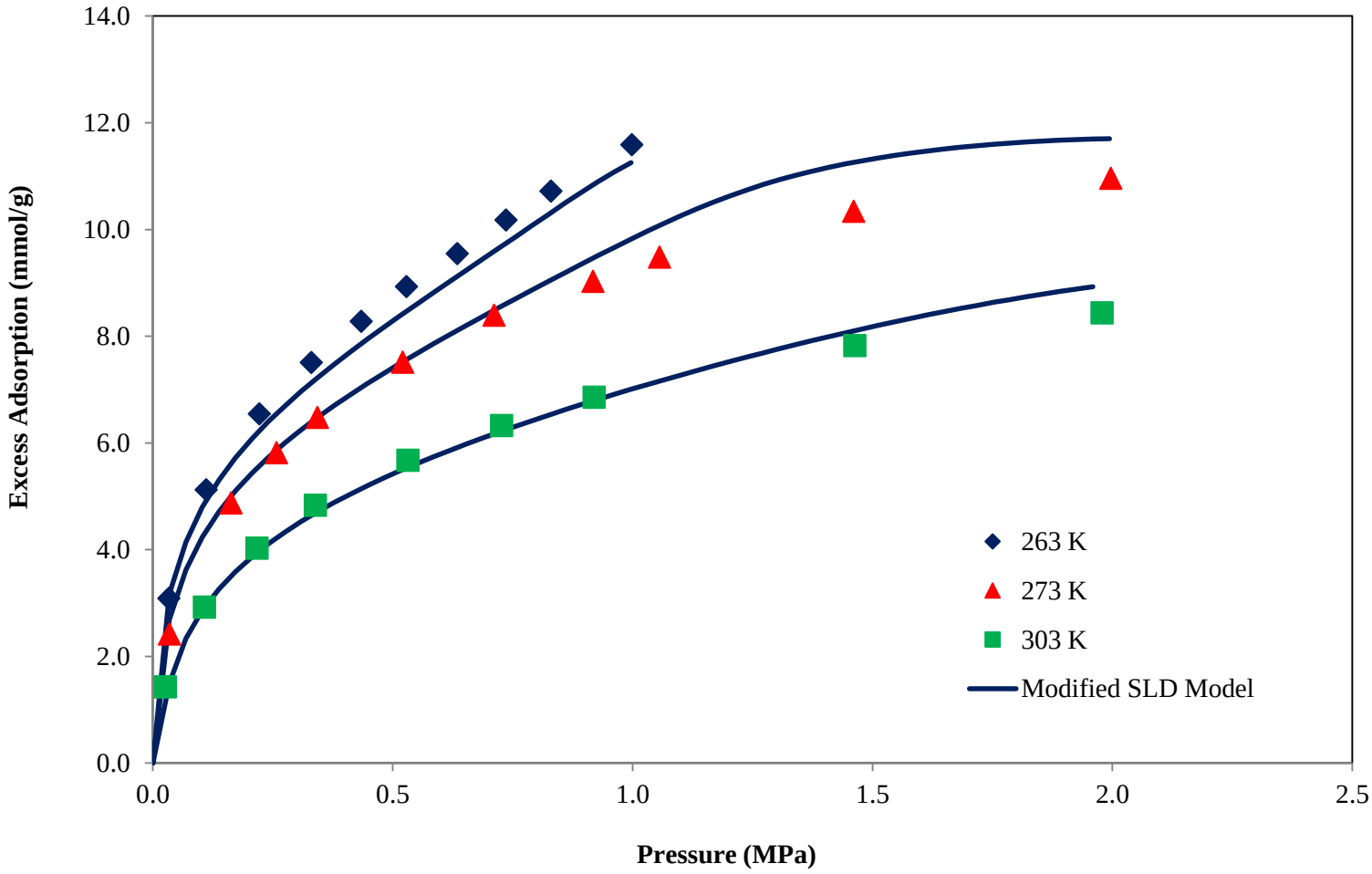

Figure 2.4(a). Generalized Predictions of the Modified SLD Model for Ethane Adsorption on Templated Carbon (Points are Data from [41])

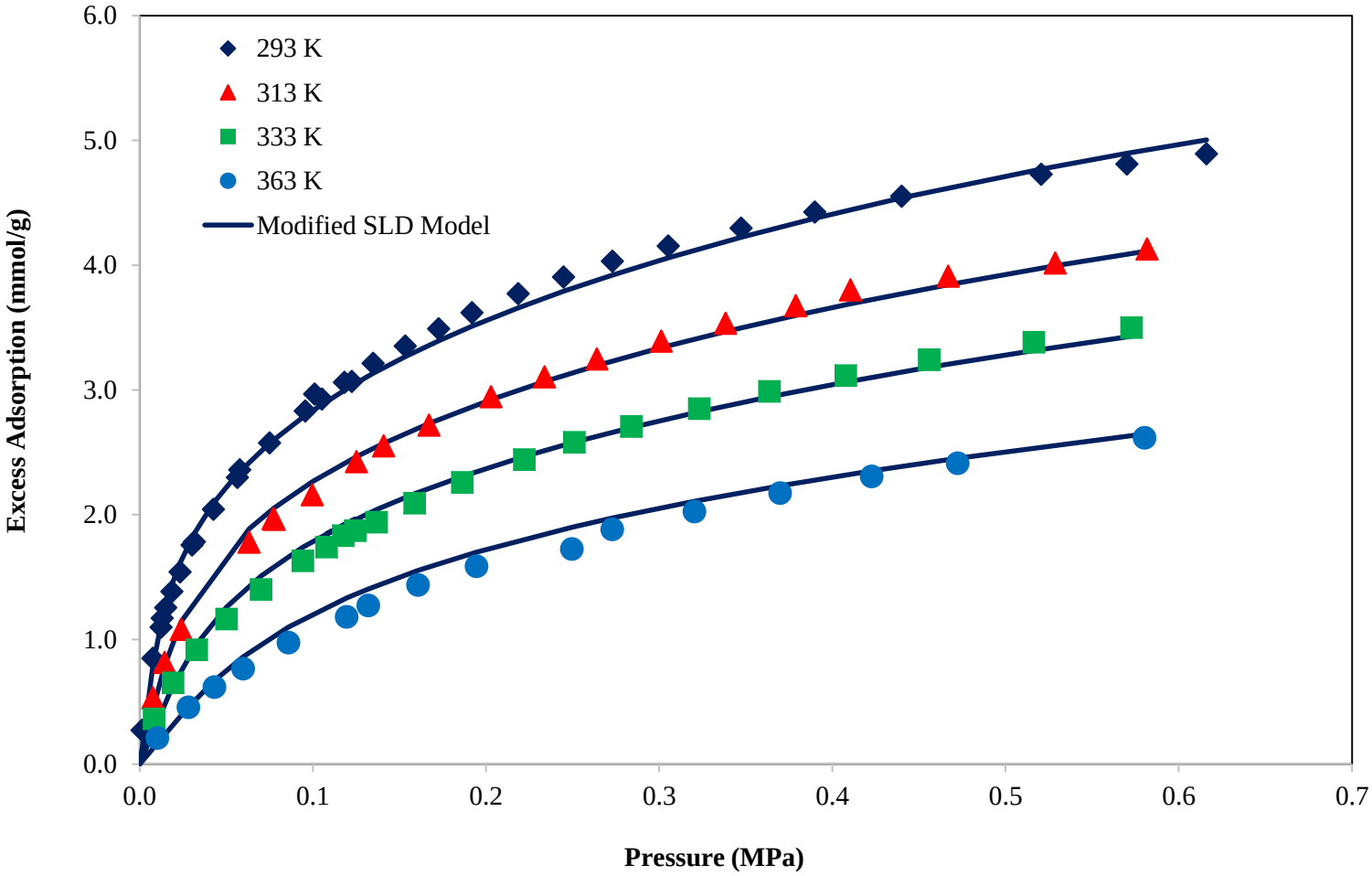

Figure 2.4(b). Generalized Predictions of the Modified SLD Model for Ethylene Adsorption on Nuxit-Al (Points are Data from [35])

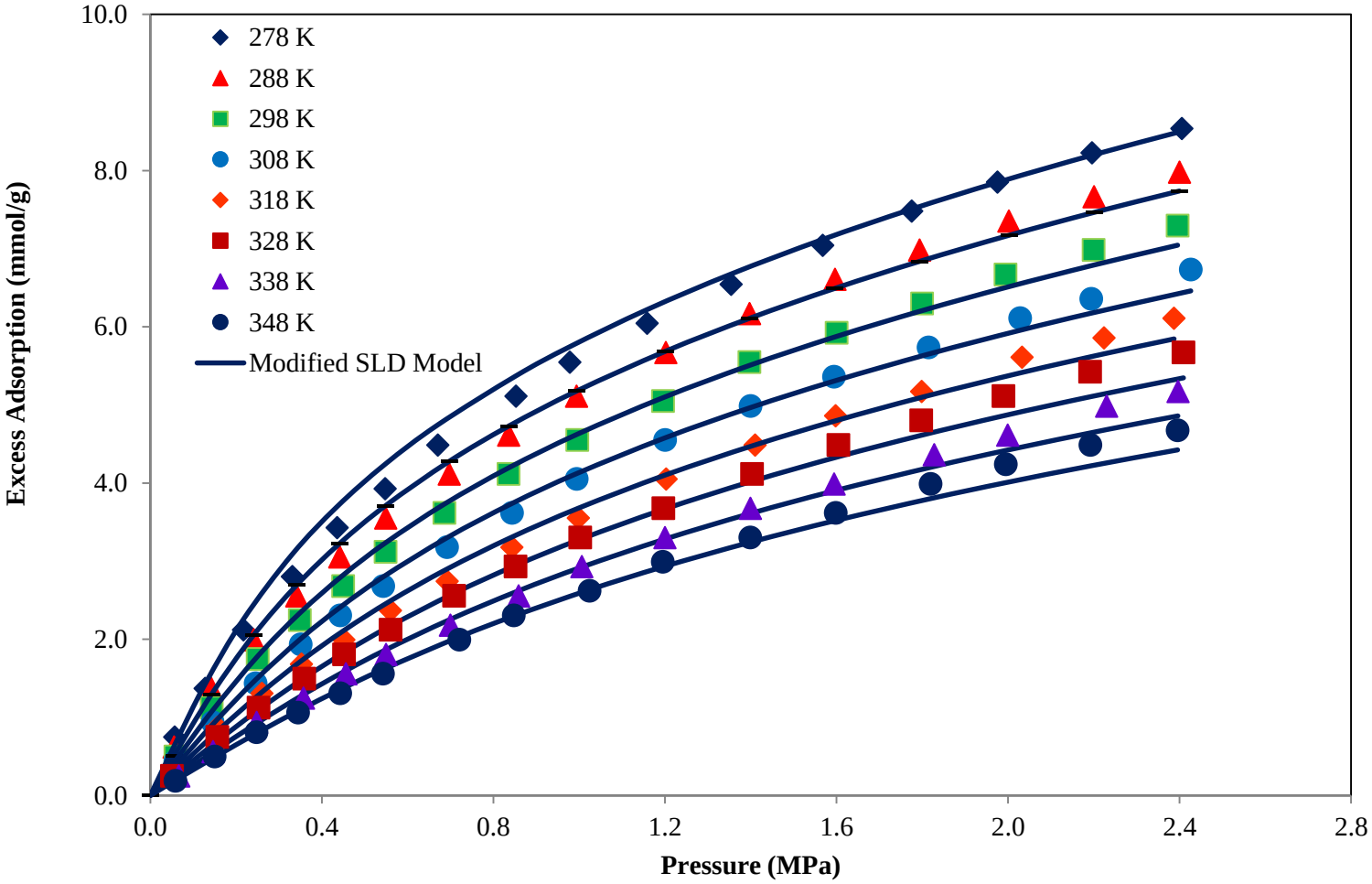

Figure 2.4(c). Generalized Predictions of the Modified SLD Model for Ethylene Adsorption on Maxsorb III (Points are Data from [42])

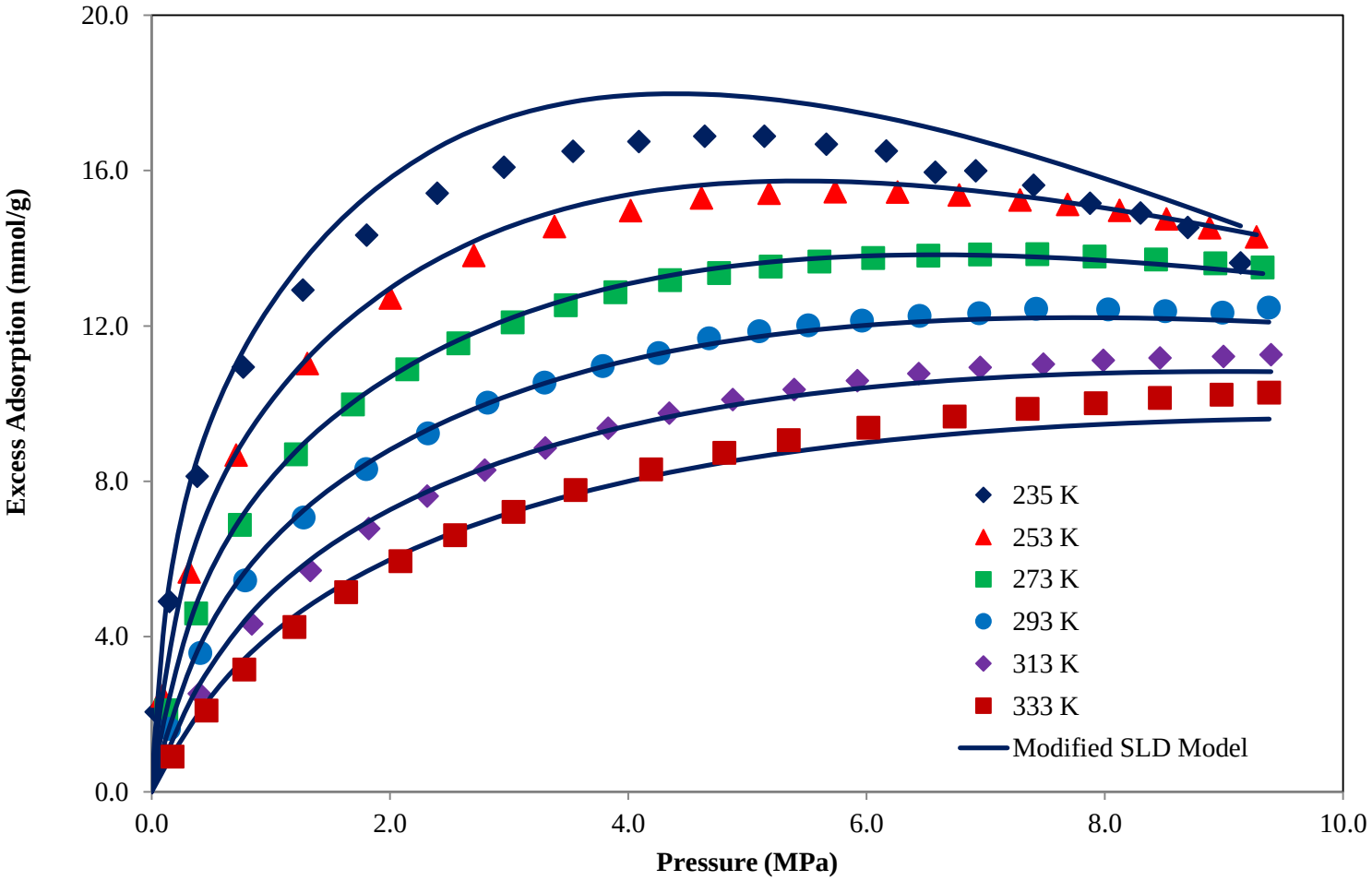

Figure 2.5(a). Generalized Predictions of the Modified SLD Model for Methane Adsorption on Coconut shell-derived carbon (Points are Data from [29])

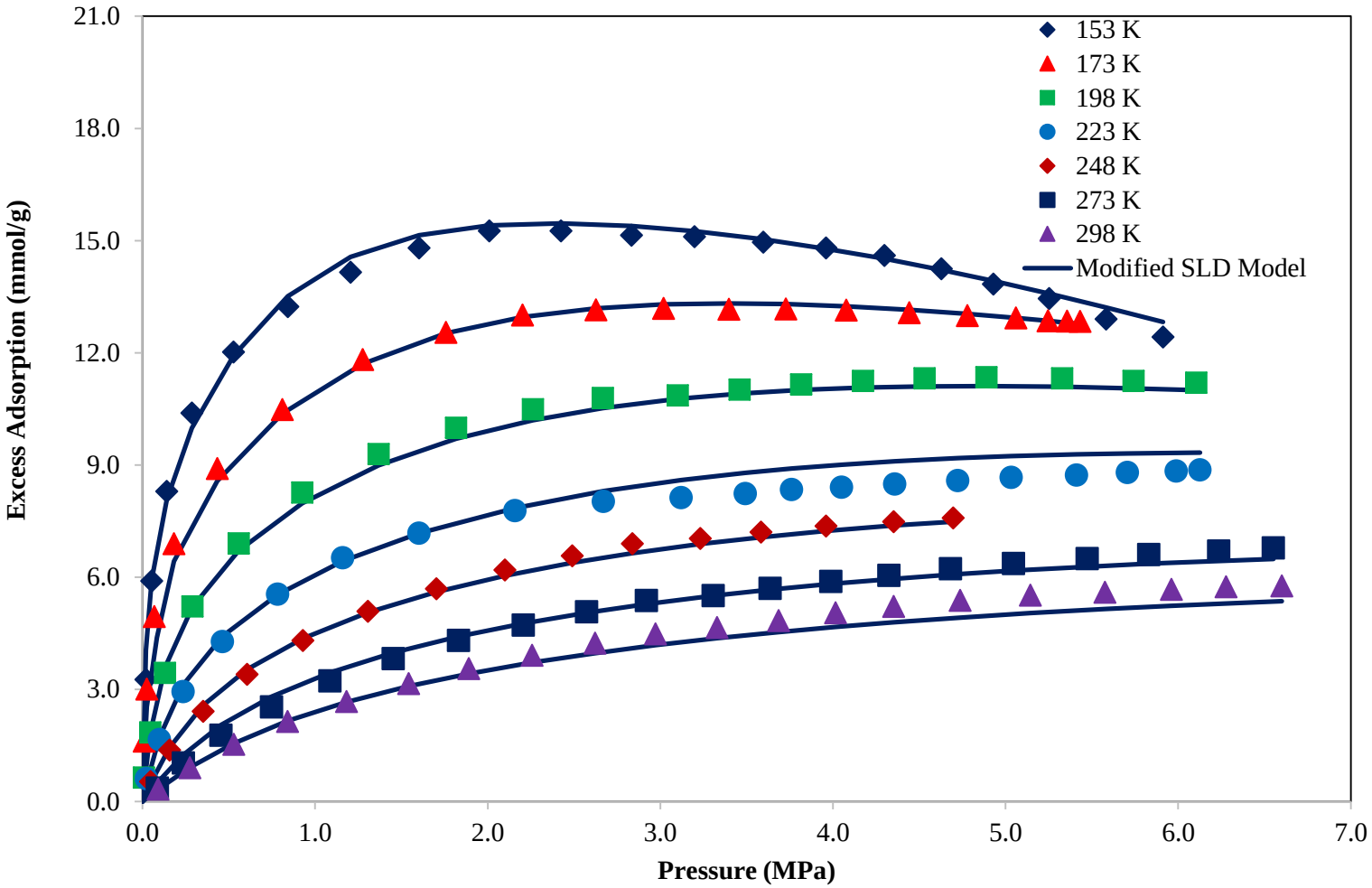

Figure 2.5(b). Generalized Predictions of the Modified SLD Model for Nitrogen Adsorption on CO-64 (Points are Data from [7])

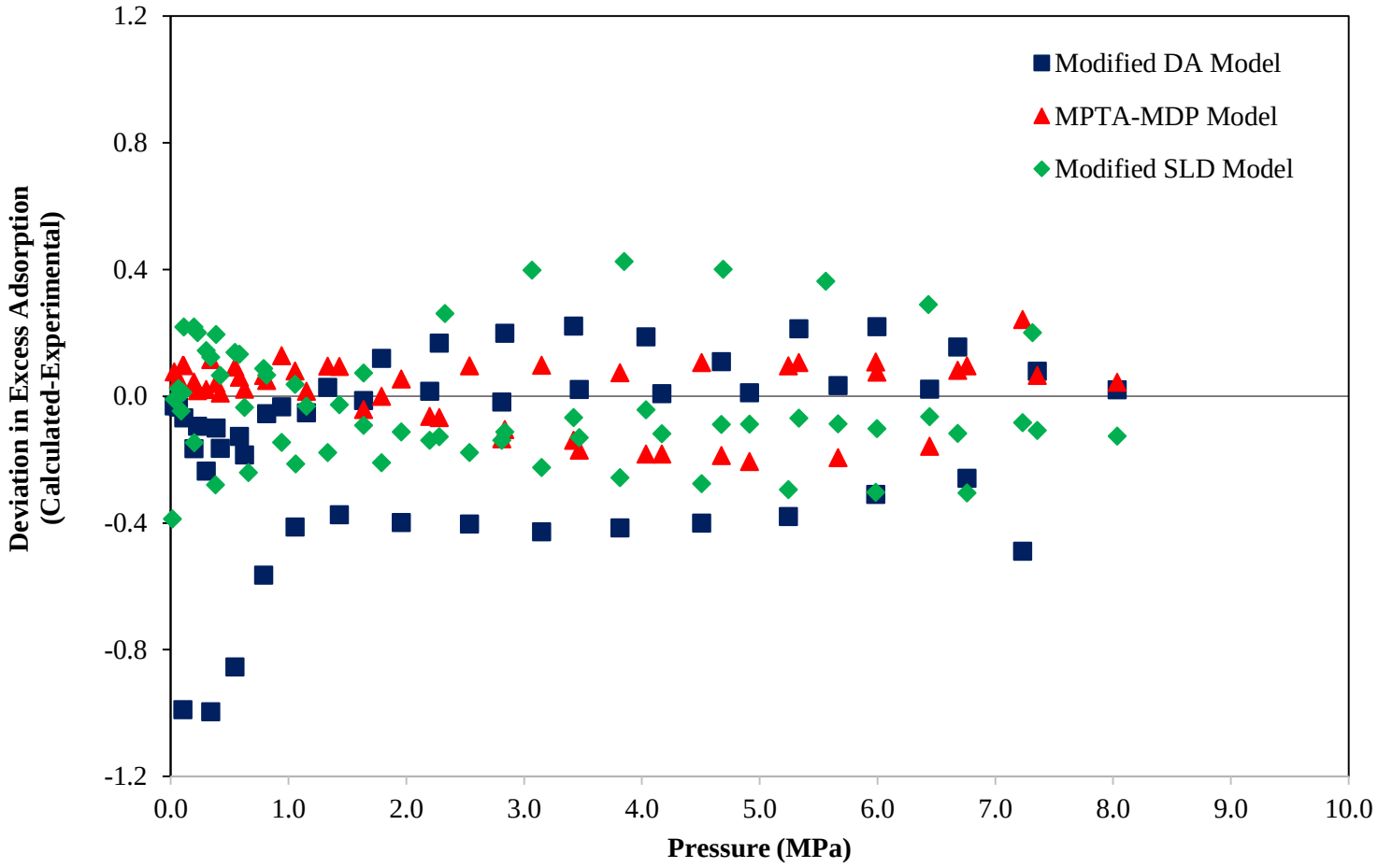

Figure 2.6(a). Deviations of Modified DA, MPTA-MDP and SLD Model Representations for Methane Adsorption on CNS-201 (Points are Data from [7])

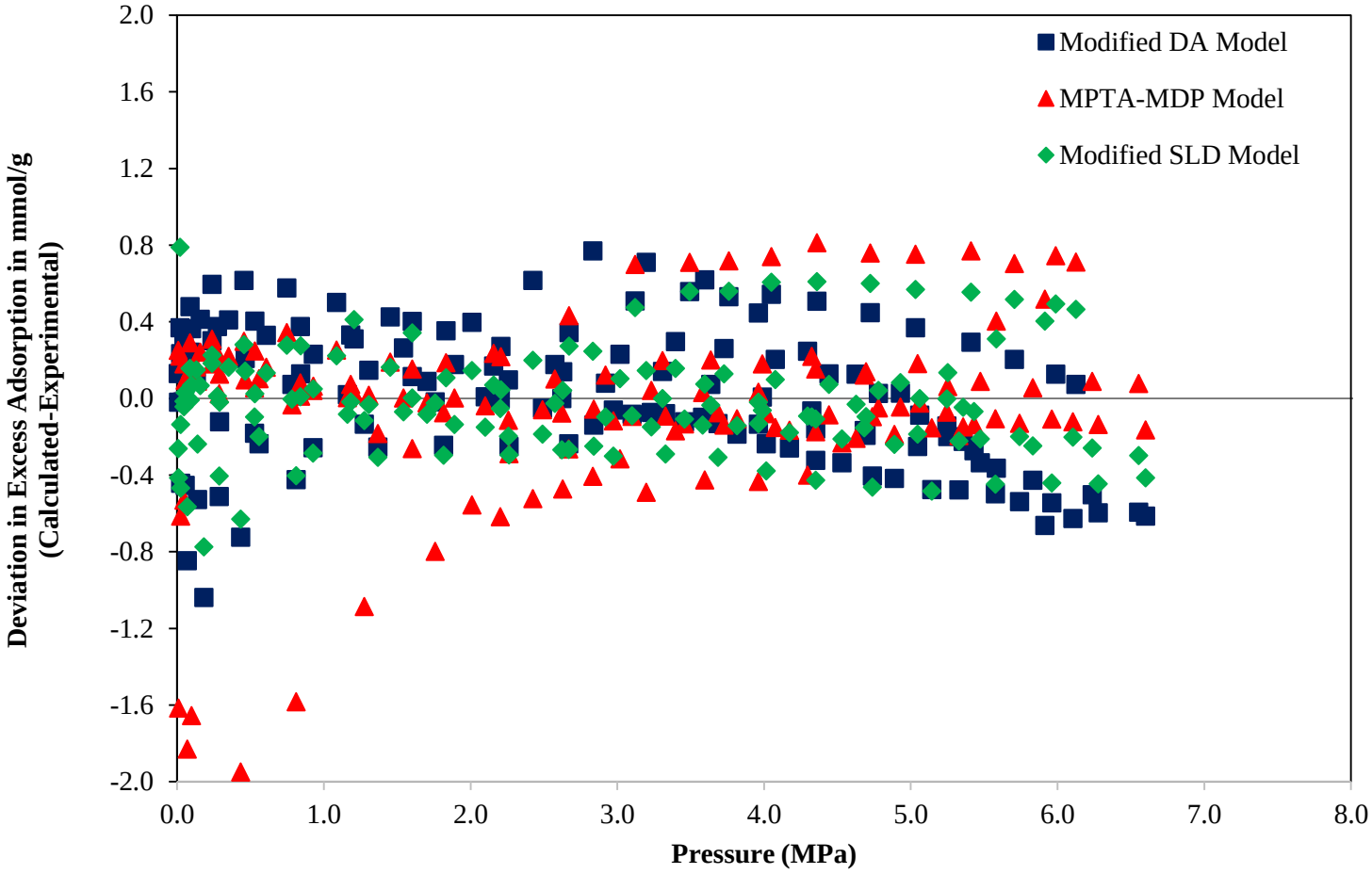

Figure 2.6(b). Deviations of Modified DA, MPTA-MDP and SLD Model Representations for Nitrogen Adsorption on CO-64 (Points are Data from [7])

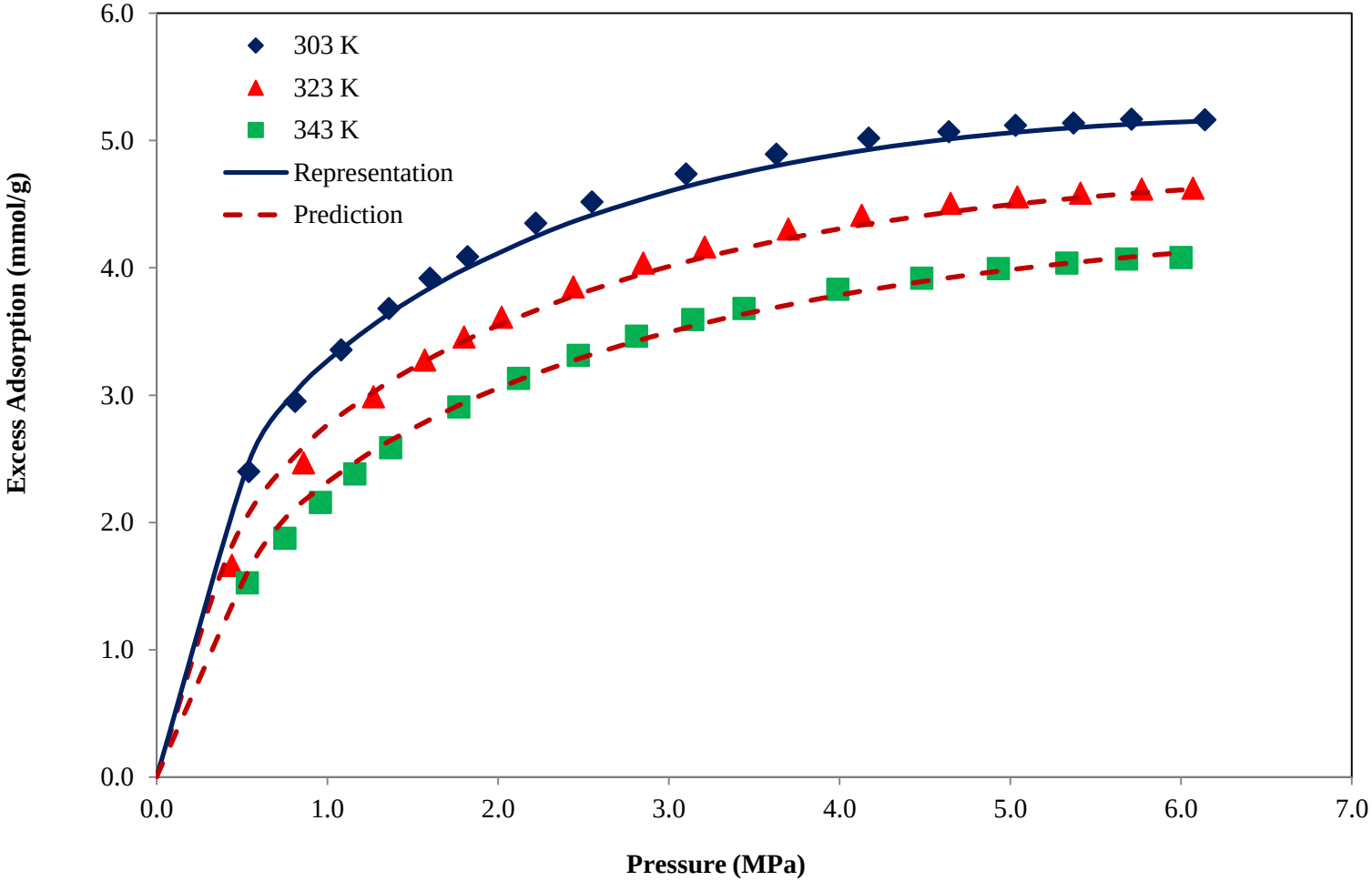

Figure 2.7(a). Modified SLD Model Predictions for Methane Adsorption on F30/470 Based on a Single Adsorption Isotherm (Points are Data from [26])

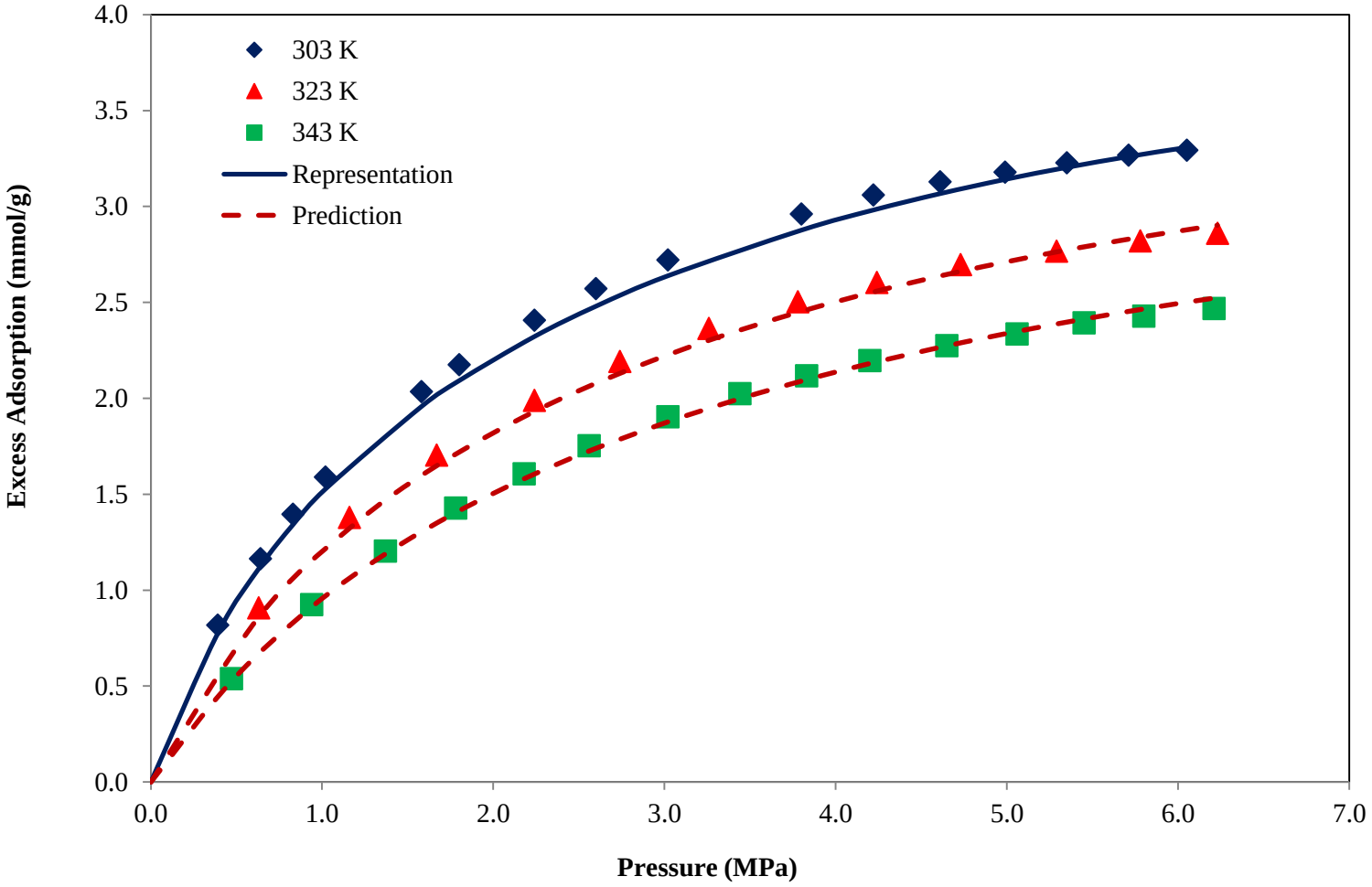

Figure 2.7(b). Modified SLD Model Predictions for Nitrogen Adsorption on F30/470 Based on a Single Adsorption Isotherm (Points are Data from [26])

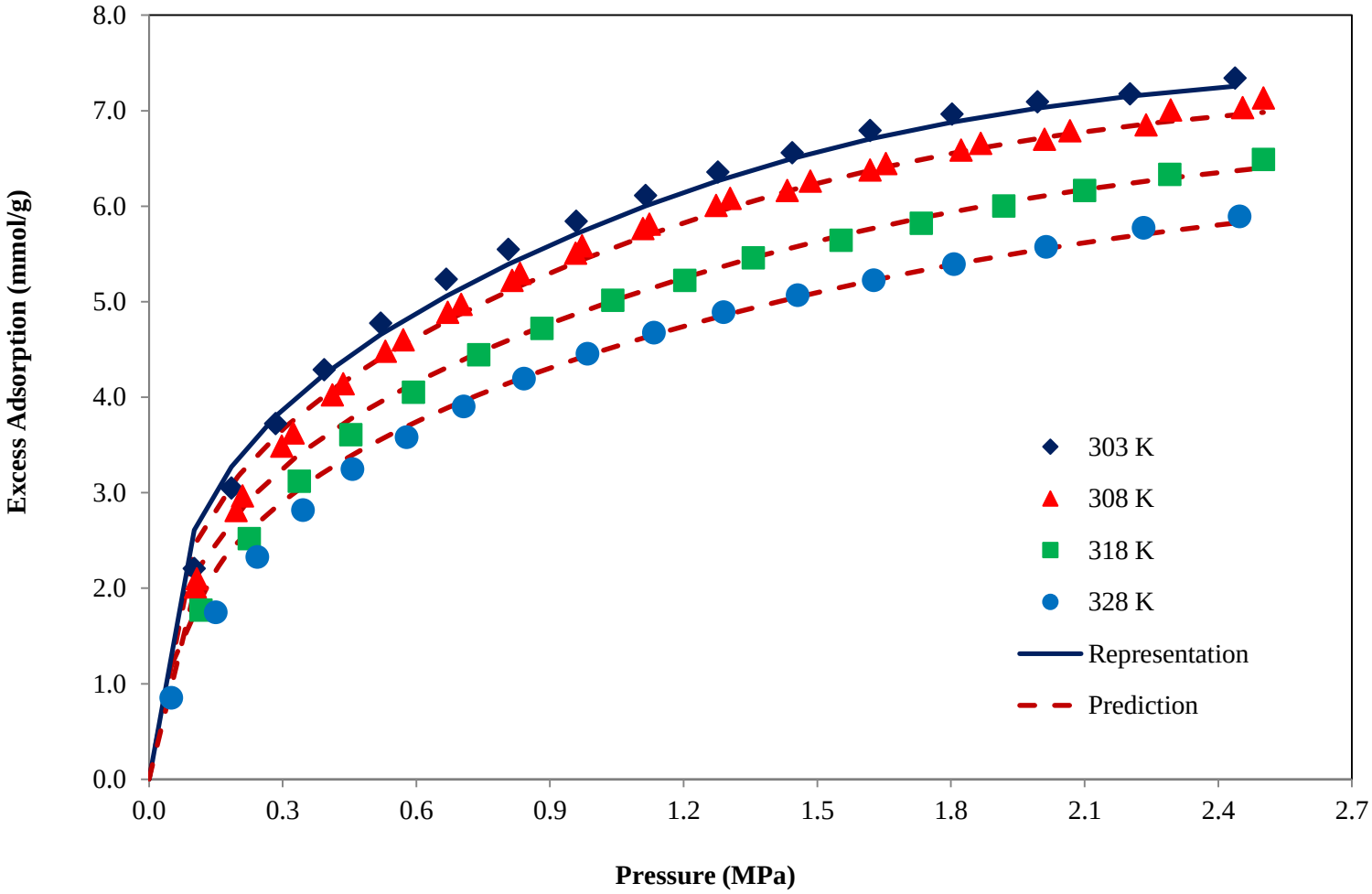

Figure 2.7(c). Modified SLD Model Predictions for CO_2 Adsorption on F30/470 Based on a Single Adsorption Isotherm (Points are Data from [27])

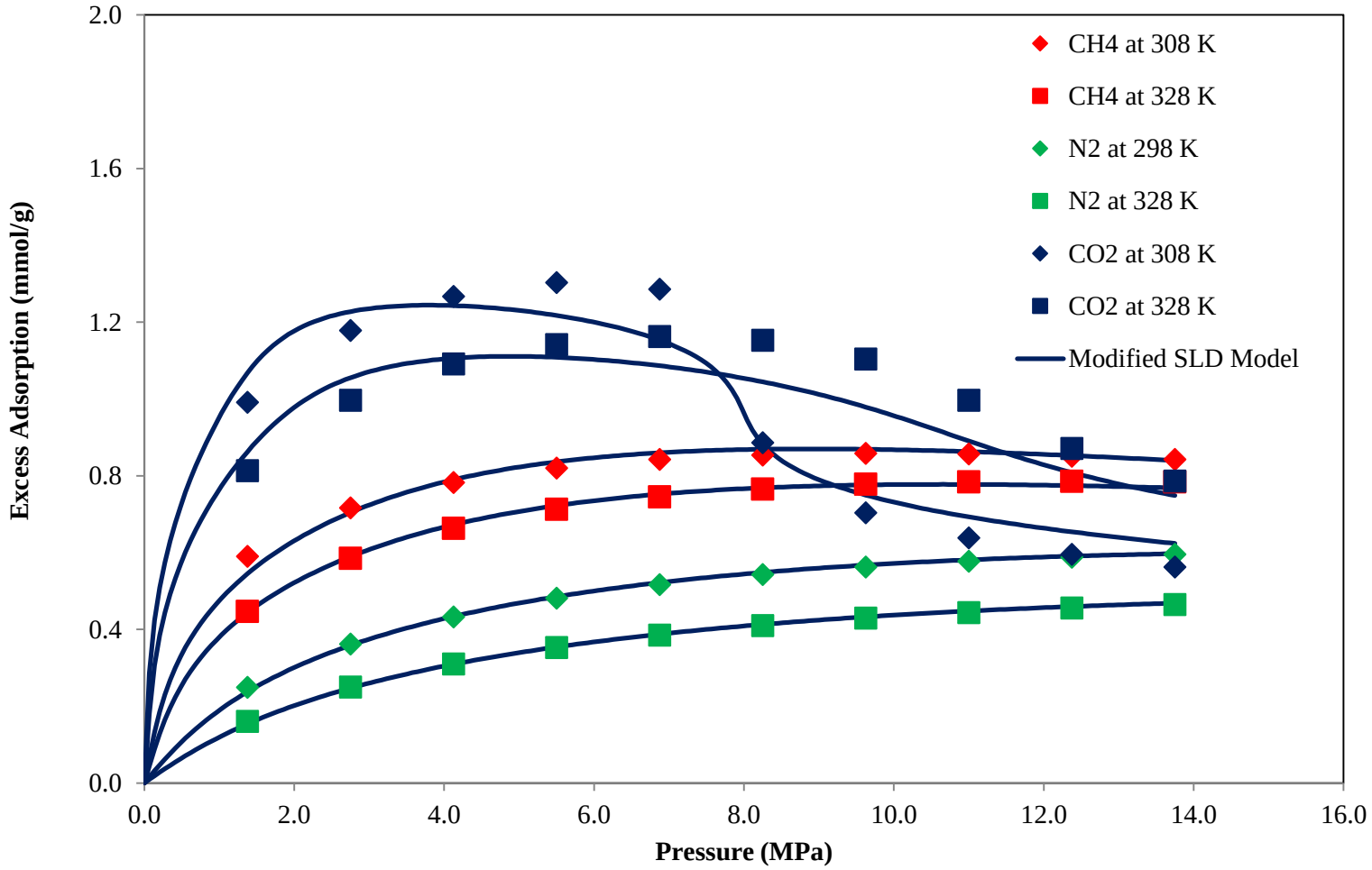

Figure 2.8. Modified SLD Model Representations for Methane, Nitrogen and CO_2 Adsorption on Pocahontas Coal (Points are Data from [30])

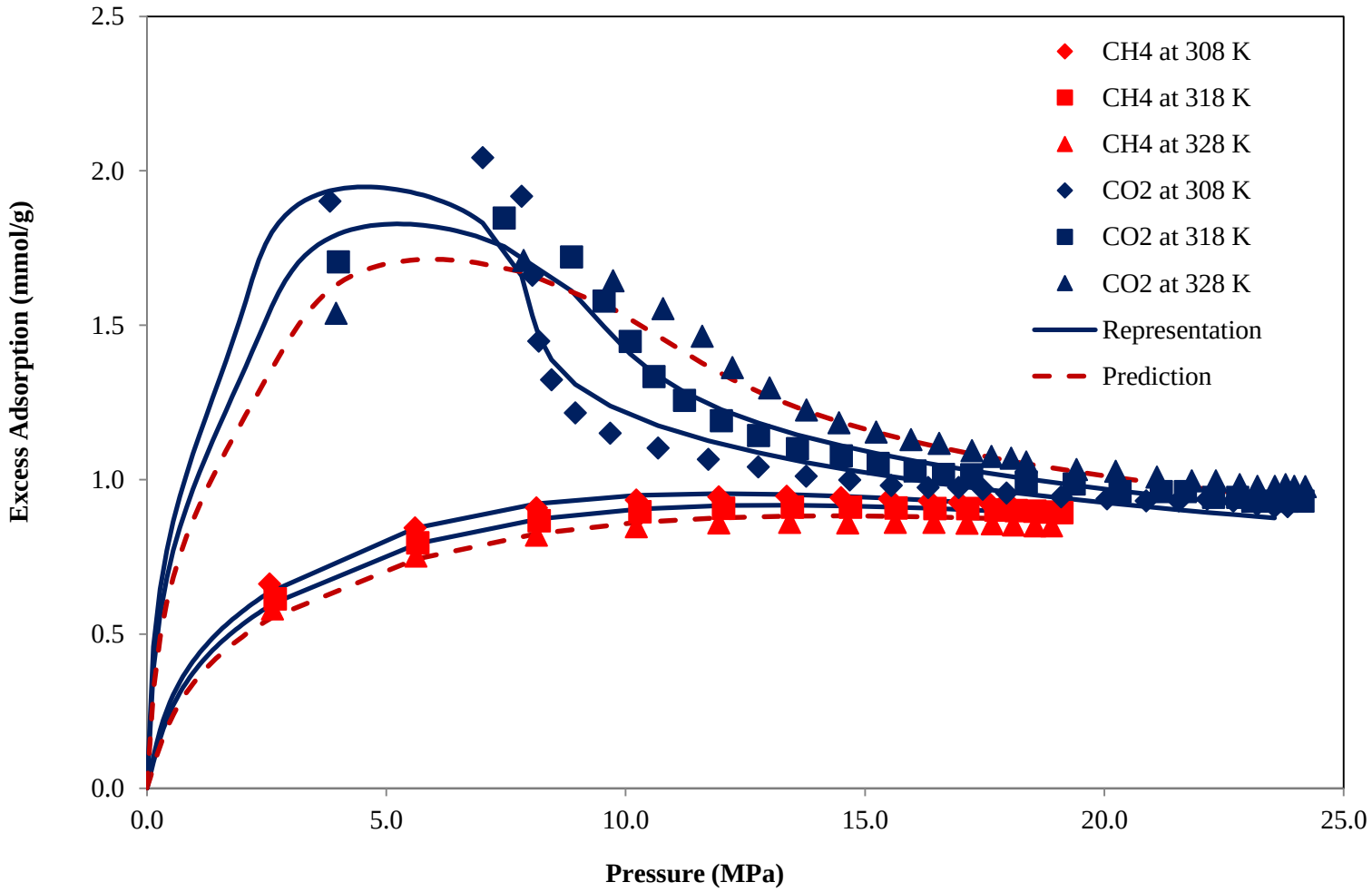

Figure 2.9. Modified SLD Model Predictions for Methane and CO_2 Adsorption at 328 K on Hulun Buir Coal (Points are Data from [31])

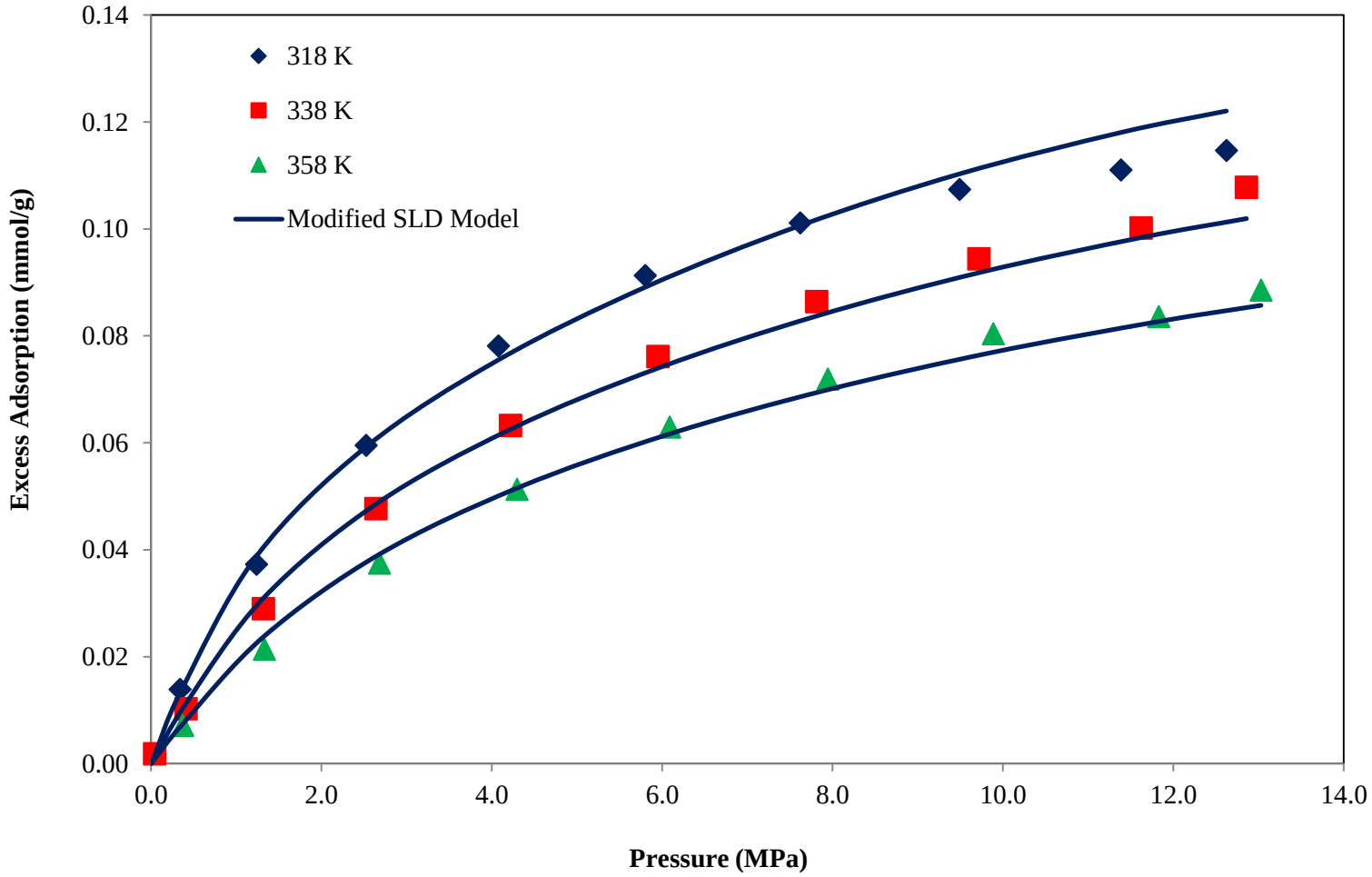

Figure 2.10(a). Modified SLD Model Representations for Methane Adsorption on Posidonia Shale (WIC7115) (Points are Data from [32])

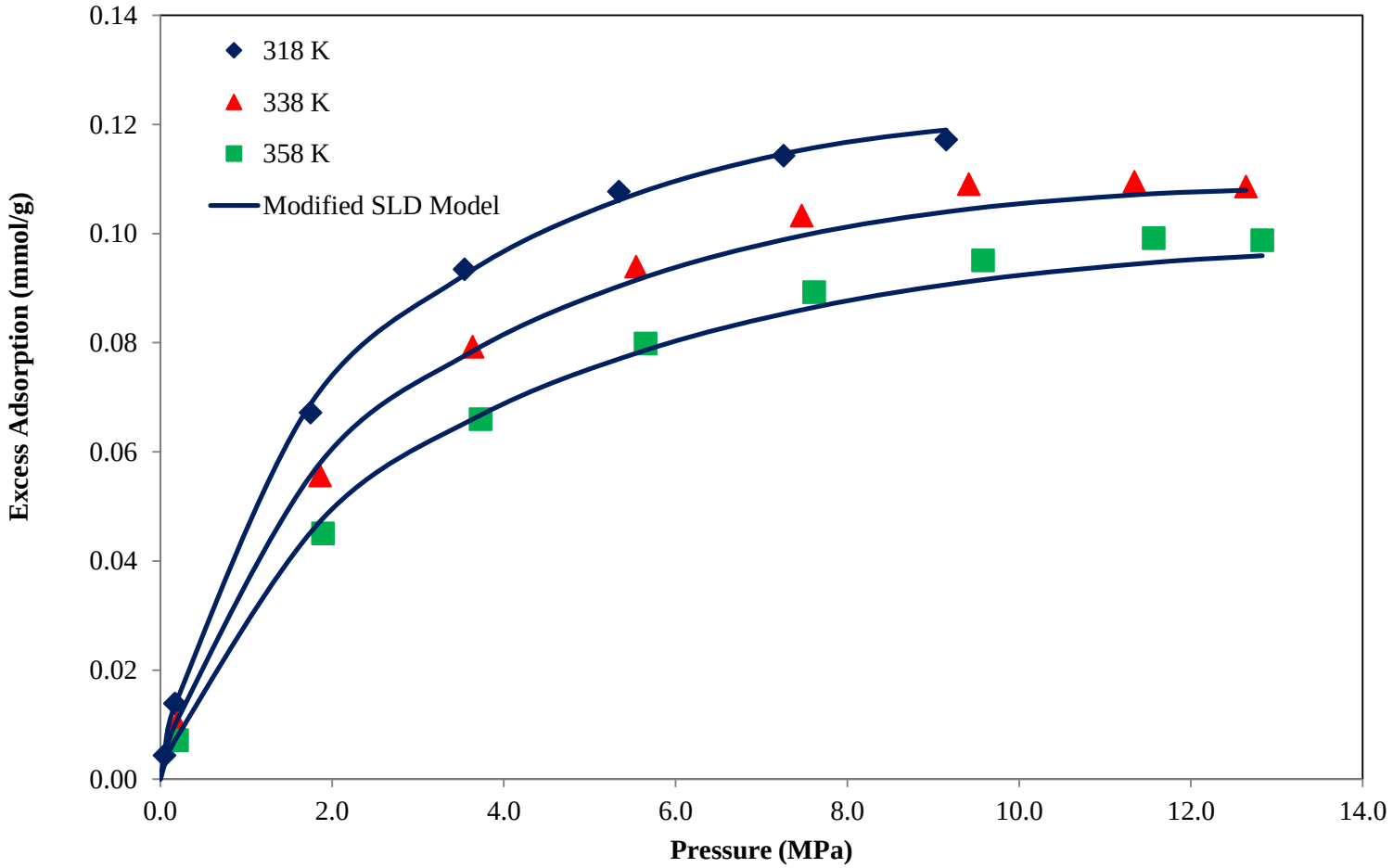

Figure 2.10(b). Modified SLD Model Representations for Methane Adsorption on Posidonia Shale (HAD7090) (Points are Data from [32])

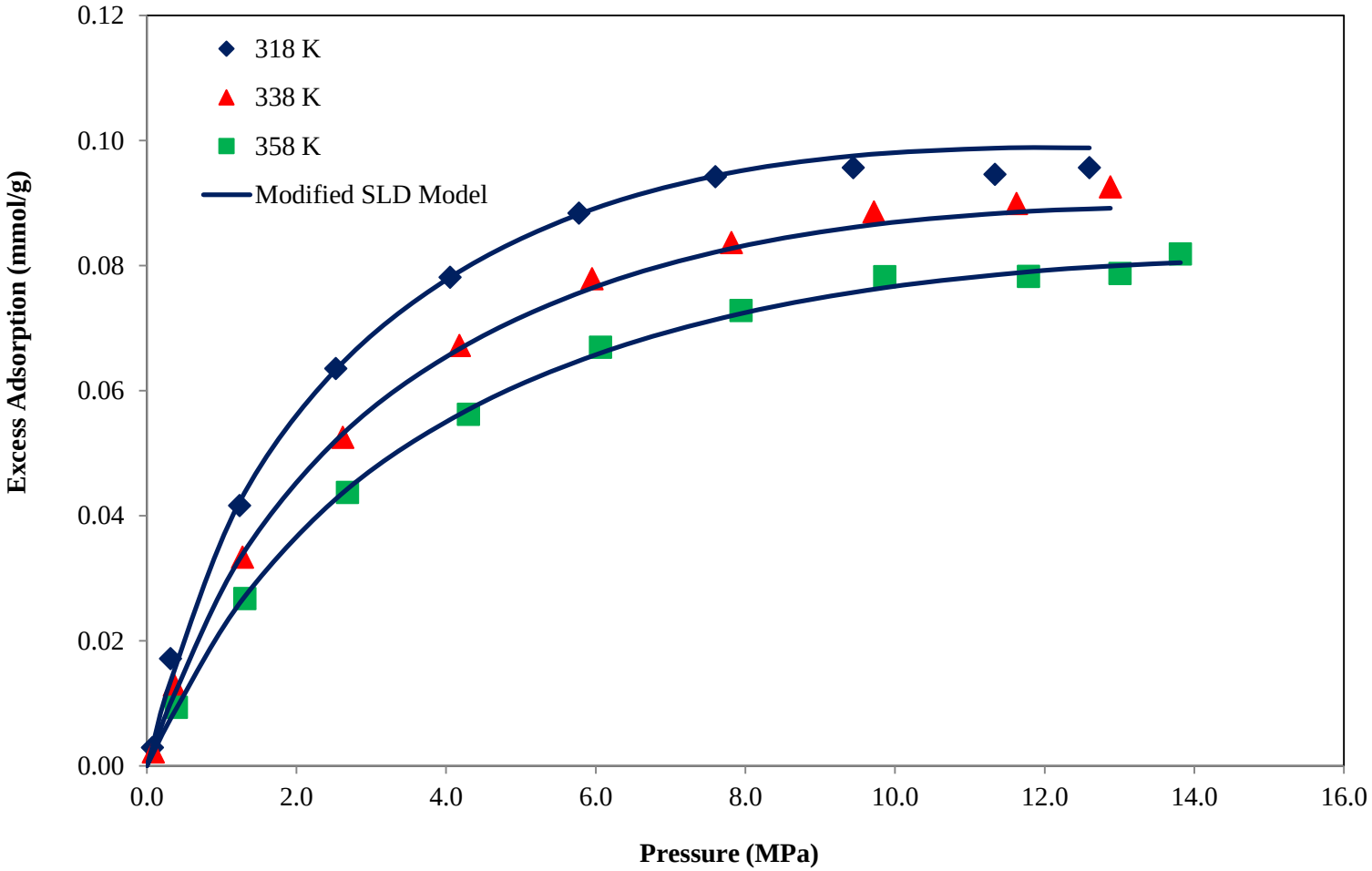

Figure 2.10(c). Modified SLD Model Representations for Methane Adsorption on Posidonia Shale (HAD7119) (Points are Data from [32])

REFERENCES

1. Pashin, J.C. and M.R. McIntyre, Temperature–pressure conditions in coalbed methane reservoirs of the Black Warrior basin: implications for carbon sequestration and enhanced coalbed methane recovery. International Journal of Coal Geology, 2003. 54(3–4): p. 167-183.
2. Dubinin, M.M., The Potential Theory of Adsorption of Gases and Vapors for Adsorbents with Energetically Nonuniform Surfaces. Chemical Reviews, 1960. 60(2): p. 235-241.
3. Clarkson, C.R., R.M. Bustin, and J.H. Levy, Application of the mono/multilayer and adsorption potential theories to coal methane adsorption isotherms at elevated temperature and pressure. Carbon, 1997. 35(12): p. 1689-1705.
4. Ruppel, T.C., C.T. Grein, and D. Bienstock, Adsorption of methane on dry coal at elevated pressure. Fuel, 1974. 53(3): p. 152-162.
5. Czerny, A.M., P. Bénard, and R. Chahine, Adsorption of Nitrogen on Granular Activated Carbon: Experiment and Modeling. Langmuir, 2005. 21(7): p. 2871-2875.
6. Richard, M.A., P. Bénard, and R. Chahine, Gas adsorption process in activated carbon over a wide temperature range above the critical point. Part 1: modified Dubinin-Astakhov model. Adsorption, 2009. 15(1): p. 43-51.
7. Dundar, E., et al., Modified potential theory for modeling supercritical gas adsorption. International Journal of Hydrogen Energy, 2012. 37(11): p. 9137-9147.
8. Chareonsuppanimit, P., et al., High-pressure adsorption of gases on shales: Measurements and modeling. International Journal of Coal Geology, 2012. 95(0): p. 34-46.

9. Pan, Z. and L.D. Connell, A theoretical model for gas adsorption-induced coal swelling. International Journal of Coal Geology, 2007. 69(4): p. 243-252.

10. Chareonsuppanimit, P., et al., Modeling gas-adsorption-induced swelling and permeability changes in coals. International Journal of Coal Geology, 2014. 121(0): p. 98-109.

11. Do, D.D., Adsorption analysis: Equilibria and kinetics. 1998, London: Imperial College Press.

12. Rangarajan, B., C.T. Lira, and R. Subramanian, Simplified local-density model for adsorption over large pressure ranges. AIChE Journal, 1995. 41(4): p. 838-845.

13. Mohammad, S.A., et al., Generalized Simplified Local-Density/Peng−Robinson Model for Adsorption of Pure and Mixed Gases on Coals. Energy & Fuels, 2009. 23(12): p. 6259-6271.

14. Fitzgerald, J.E., R.L. Robinson, and K.A.M. Gasem, Modeling High-Pressure Adsorption of Gas Mixtures on Activated Carbon and Coal Using a Simplified Local-Density Model. Langmuir, 2006. 22(23): p. 9610-9618.

15. Lee, L.L., Molecular Thermodynamics of Non-ideal Fluids. 1988, Stoneham, MA Butterworth.

16. Steele, W.A., The Interaction of Gases with Solid Surfaces. 1974, Oxford: Pergamon Press.

17. Subramanian, R., H. Pyada, and C.T. Lira, Engineering model for adsorption of gases onto flat surfaces and clustering in supercritical fluids. Industrial & Engineering Chemistry Research, 1995. 34(11): p. 3830.

18. Reid, R.C., J.M. Prausnitz, and B.E. Poling, The Properties of Gases and Liquids. 1987, New York: McGraw-Hill

19. Fitzgerald, J.E., et al., Modeling the adsorption of pure gases on coals with the SLD model. Carbon, 2003. 41(12): p. 2203-2216.

20. Talu, O., The Landolt-Börnstein Adsorption Database. Springer, 2013.

21. Golla, S., et al., Quantitative structure–property relationship modeling of skin sensitization: A quantitative prediction. Toxicology in Vitro, 2009. 23(3): p. 454-465.

22. Golla, S., et al., Quantitative structure–property relationships modeling of skin irritation. Toxicology in Vitro, 2009. 23(1): p. 176-184.

23. Arri, L.E. and D. Yee. Modeling Coalbed Methane production with binary gas sorption, SPE paper 24363. in SPE Rocky Mountain regional meeting. 1992. Casper, WY.

24. Daniel G. Friend, J.F.E., Hepburn Ingham, Thermophysical Properties of Methane. Thermophysics Division, National Institute of Standard and Technology, 1988.

25. Jacobsen, R.T. and R.B. Stewart, Thermodynamic Properties of Nitrogen Including Liquid and Vapor Phases from 63K to 2000K with Pressures to 10,000 Bar. Journal of Physical and Chemical Reference Data, 1973. 2(4): p. 757-922.

26. Berlier, K. and M. Frère, Adsorption of CO2 on Microporous Materials. 1. On Activated Carbon and Silica Gel. Journal of Chemical & Engineering Data, 1997. 42(3): p. 533-537.

27. Frère, M.G. and G.F. De Weireld, High-Pressure and High-Temperature Excess Adsorption Isotherms of N2, CH4, and C3H8 on Activated Carbon. Journal of Chemical & Engineering Data, 2002. 47(4): p. 823-829.

28. Payne, H.K., G.A. Sturdevant, and T.W. Leland, Improved Two-Dimensional Equation of State to Predict Adsorption of Pure and Mixed Hydrocarbons. Industrial & Engineering Chemistry Fundamentals, 1968. 7(3): p. 363-374.

29. Zhou, L., et al., Experimental and Modeling Study of the Adsorption of Supercritical Methane on a High Surface Activated Carbon†. Langmuir, 2000. 16(14): p. 5955-5959.

30. Sakurovs, R., et al., Temperature dependence of sorption of gases by coals and charcoals. International Journal of Coal Geology, 2008. 73(3–4): p. 250-258.

31. Li, D., et al., High-pressure sorption isotherms and sorption kinetics of CH4 and CO2 on coals. Fuel, 2010. 89(3): p. 569-580.

32. Rexer, T.F., et al., High-Pressure Methane Adsorption and Characterization of Pores in Posidonia Shales and Isolated Kerogens. Energy & Fuels, 2014. 28(5): p. 2886-2901.

33. Ritter, J.A. and R.T. Yang, Equilibrium adsorption of multicomponent gas mixtures at elevated pressures. Industrial & Engineering Chemistry Research, 1987. 26(8): p. 1679-1686.

34. Van Der Vaart, R., et al., Single and Mixed Gas Adsorption Equilibria of Carbon Dioxide/Methane on Activated Carbon. Adsorption, 2000. 6(4): p. 311-323.

35. Szepesy, L., and 1lles, V., Adsorption of gases and gas mixtures. II. Measurement of the adsorption isotherms of gases on active carbon under pressures of 1 to 7 atm. Acad. Sci. Hung. Acta Chim., 1963: p. 53-60.

36. Ray, G.C. and E.O. Box, Adsorption of Gases on Activated Charcoal. Industrial & Engineering Chemistry, 1950. 42(7): p. 1315-1318.

37. Reich, R., W. T. Ziegler, and K. A. Rogers, Adsorption of methane, ethane, and ethylene gases and their binary and ternary mixtures and carbon dioxide on activated carbon at 212-301 K and pressures to 35 atmospheres. Industrial and Engineering Chemistry Process Design and Development, 1980. 19: p. 336-344.

38. Mofarahi, M., M. Sadrameli, and J. Towfighi, Characterization of Activated Carbon by Propane and Propylene Adsorption. Journal of Chemical & Engineering Data, 2003. 48(5): p. 1256-1261.

39. Martin, A., et al., Adsorption Isotherms of CH4 on Activated Carbon from Indonesian Low Grade Coal. Journal of Chemical & Engineering Data, 2011. 56(3): p. 361-367.

40. Wang, X., et al., Adsorption Measurements of Methane on Activated Carbon in the Temperature Range (281 to 343) K and Pressures to 1.2 MPa. Journal of Chemical & Engineering Data, 2010. 55(8): p. 2700-2706.

41. Chen, J., L.S. Loo, and K. Wang, An Ideal Absorbed Solution Theory (IAST) Study of Adsorption Equilibria of Binary Mixtures of Methane and Ethane on a Templated Carbon. Journal of Chemical & Engineering Data, 2011. 56(4): p. 1209-1212.

42. Loh, W.S., et al., Improved Isotherm Data for Adsorption of Methane on Activated Carbons. Journal of Chemical & Engineering Data, 2010. 55(8): p. 2840-2847.

43. Qin Wu, L.Z., Jiaquan Wu, and Yaping Zhou, Adsorption Equilibrium of the Mixture CH4+ N2+ H2on Activated Carbon. J. Chem. Eng. Data, 2005. 50: p. 635-642.

44. Humayun, R. and D.L. Tomasko, High-resolution adsorption isotherms of supercritical carbon dioxide on activated carbon. AIChE Journal, 2000. 46(10): p. 2065-2075.

CHAPTER III

HIGH-PRESSURE ADSORPTION OF GASES ON THE NEW ALBANY SHALE

The content in this chapter has been published in the International Journal of Coal Geology*.

3.1 Introduction

The significant increase in natural gas usage has stimulated the recovery of natural gas from unconventional gas reservoirs such as coal beds and shales. Due to recent advances in drilling and recovery techniques, natural gas production from shales has increased steadily in the U.S. over the past five years [1]. Among the shale plays in the U.S., the New Albany shales in the Illinois basin are regarded as one of the "current" shale plays with substantial reserves of natural gas. A recent study commissioned by the Energy Information Administration (EIA) estimated that the technically recoverable reserves from the New Albany shales in Illinois basin are about 11 tcf [1].

The need to mitigate CO_2 concentrations in the atmosphere has also led to studies of the potential for sequestration of CO_2 in geologic formations such as deep, unmineable coal beds, saline aquifers and shales [2-6]. A road-map and criteria for the site selection for CO_2 sequestration in geological media has been presented [7]. Nuttall et al. [8] investigated the CO_2 sequestration potential in the organic-rich Devonian black shales and estimated the sequestration capacity to be about 6.8 billion tons over the Big Sandy gas field of Eastern Kentucky. In another study, Busch et al. [4] investigated the diffusion transport and gas sorption behavior of Muderong shales, Australia.

* Chareonsuppanimit, P., et al., High-pressure adsorption of gases on shales: Measurements and modeling. International Journal of Coal Geology, 2012. 95(0): p. 34-46.

Their experiments indicated a significant CO_2 storage capacity in the shale formations, which was attributed to CO_2 dissolution in water, physical sorption on clay minerals of the shale samples and geochemical reactions. Since a significant fraction of the gas in shale reservoirs is in the adsorbed state, knowledge of adsorption behavior of natural gas components is important in developing gas-in-place estimates and conducting feasibility studies for CO_2 sequestration in shale-gas reservoirs. Strąpoć et al. [9] studied the gas content of New Albany shale in the eastern Illinois basin through gas desorption tests. They observed that the gas content was dependent on the total organic carbon content and the micropore volume of the shales. Beaton et al. [10] measured methane adsorption isotherms on several shale samples from the Duvernay, Muskwa, Banff and Exshaw formations. Nuttall et al. [8] reported methane and carbon dioxide adsorption isotherms on New Albany shales and Ohio shales extracted from various depths below the surface. They observed a correlation between percent total organic carbon (% TOC) and depth. In a recent study, Weniger et al. [11] investigated the high-pressure adsorption behavior of methane and carbon dioxide on several coal and shale samples from the Paraná Basin, Brazil. They observed that the sorption capacities of methane and carbon dioxide were correlated with % TOC. They reported CO_2:CH_4 sorption capacity ratios that varied between 1.9 to 6.9 for several coals and carbonaceous shale samples.

In this work, the high-pressure adsorption behavior of methane, nitrogen and CO_2 on New Albany shale at 328.2 K and pressures up to 12.4 MPa were investigated. Data were obtained using the existing apparatus [12], which utilizes a volumetric method of measuring adsorption. Prior to beginning the shale isotherm measurements, a sensitivity analysis was conducted on the experimental technique. This led to modifications in the apparatus, resulting in a reduction in the expected experimental uncertainties for the new measurements. The simplified local-density (SLD) model was used to represent the newly-acquired data. Further, adsorption data on shales in the literature were also used to test the viability of the SLD model to describe adsorption on several shale samples.

Details of this chapter are presented as follows: Section 3.2 - the experimental procedures used in this study; Section 3.3 - the SLD model; and Section 3.4 - the steps undertaken to reduce expected uncertainties for gas adsorption isotherms on shales and presentation of the experimental and modeling results.

3.2 Experimental Methods and Procedures

3.2.1 Adsorption Measurements

The experimental method used in this study is based on the volumetric method of measuring adsorption isotherms. The volumetric method is based on the mass balance principle and requires precise measurements of pressure, volume and temperature. The experimental apparatus, shown schematically in Figure 3.1, has been used successfully in previous measurements [12-14].

Briefly, the entire apparatus is maintained in a constant temperature air bath. The equilibrium cell (Figure 3.1) is filled with the adsorbent to be studied, and the cell is placed under vacuum prior to gas injection. The void volume, V_{void}, in the equilibrium cell is then determined by injecting a known quantity of helium from a calibrated injection pump (Ruska). Since helium adsorption is considered negligible at these conditions, the void volume can be determined from measured values of the temperature, pressure and amount of helium injected into the cell.

The mass balance equation is:

$$V_{void} = \frac{\left(\frac{P\Delta V}{ZT}\right)_{pump}}{\left(\frac{P_2}{Z_2T} - \frac{P_1}{Z_1T}\right)_{cell}} \tag{3.1}$$

where ΔV is the volume of the gas injected from the pump, Z is the compressibility factor of helium, T is the temperature, P is the pressure, subscripts “cell” and “pump” refer to conditions in the cell and pump sections of the apparatus, respectively, and “1” and “2” refer to conditions in the cell

before and after injection of gas from the pump, respectively. The helium void volume measurements were performed at the same temperature as the gas adsorption isotherms (328.2 K) and over a range of pressures from atmospheric to about 12.4 MPa (1800 psia) in intervals of 1.4 MPa (200 psia).

Generally, the void volume calculated from sequential injections varied less than 0.3 cm^3 from the average value of approximately 60 cm^3 for the measurements in this study. The helium void volume includes all the volume of the cell section exclusive of the adsorbent volume that is impenetrable to helium gas. The constancy of the calculated void volume from the incremental injections over a range of pressures confirmed our assumption that adsorption of helium is negligible at the conditions of the measurements.

The Gibbs or excess adsorption can be calculated directly from experimentally measured quantities. For pure-gas adsorption measurements, a known quantity, n_{inj}, of gas (e.g., methane) is injected from the pump section into the cell section. Some of the injected gas will be adsorbed, and the remainder, n_{unads}^{Gibbs}, will exist in the equilibrium bulk gas phase in the cell. A material balance is used to calculate the amount adsorbed, n_{ads}^{Gibbs}, as

$$n_{ads}^{Gibbs} = n_{inj} - n_{unads}^{Gibbs} \tag{3.2}$$

The amount injected can be determined from pressure, temperature and volume measurements of the pump section

$$n_{inj} = \left(\frac{P\Delta V}{ZRT} \right)_{pump} \tag{3.3}$$

The amount of unadsorbed gas is calculated from conditions at equilibrium in the cell

$$n_{unads}^{Gibbs} = \left(\frac{PV_{Void}}{ZRT} \right)_{cell} \tag{3.4}$$

where the pressure P is the equilibrium pressure, and Z is the compressibility factor of the gas. The cell pressure was recorded periodically and equilibrium was indicated by the constancy of the recorded pressure (usually within 6 to 12 hours). Further, prior to measuring adsorption isotherms, the apparatus was checked for pressure leaks. The adsorption isotherms were measured only when no leaks were observed in the system over a period of 24 hours.

The above steps are repeated at sequentially higher pressures to measure a complete adsorption isotherm. The amount adsorbed is presented as mmol/g of shale on a dry mass basis (1 mmol/g = 759 SCF/ton). Equations 3.2-3.4 show that the amount adsorbed may be calculated in a straightforward manner from the experimental measurements of pressures, temperatures and volumes, coupled with independent knowledge of the gas compressibility factors, Z, from an accurate equation of state.

Frequent instrument calibrations were conducted during the course of the experiments. The thermocouples and RTDs were calibrated against a Minco platinum reference RTD. Super TJE pressure transducers (range: 0 – 13.8 MPa) were calibrated using helium as the working fluid against a Ruska deadweight tester with a calibration traceable to the National Institute of Standards and Technology. Detailed information on calibration is available elsewhere [15]. The uncertainties in the experimentally measured quantities after calibrations were estimated as follows: temperature, 0.1 K; pressure, 6.9 kPa; and injected gas volume, 0.02 cm^3.

3.2.2 Gas Compressibility Factors

As evident from the above equations, compressibility factors are required for the pure gases for proper data analysis. The compressibility factors for the pure gases were calculated from highly accurate equations of state [16-18]. For void volume determination, the helium compressibility factor was calculated with an expression based on experimental data from the National Bureau of Standards Technical Note 631 for helium [19].

3.2.3 Materials

The pure gases used in this study were obtained from Airgas with reported purities of 99.99% and were used as-received. The shale samples were provided by the Illinois State Geological Survey (ISGS). The samples were retrieved at 4,541-4,544 feet below the surface in the Illinois basin. The sample was pulverized to 250 μm size in a helium environment to avoid possible oxidation of the sample. The pulverized samples were stored in an inert environment until their use for measuring the adsorption isotherms. The gas adsorption isotherms were measured on the "as-received" sample without any drying of the sample. Table 3.1 presents the compositional analysis of the New Albany shale sample. The shale sample contained about 5.5% total organic carbon, 0.4% moisture and 90% ash content. For comparison, Table 3.1 also lists the compositional analyses for five coals from the Argonne coal sample program [20]. The newly acquired adsorption data on shale is compared with the adsorption on these coal samples in a later section.

Table 3.2 lists the details provided by the ISGS [21] regarding the New Albany shale samples utilized in this work. The New Albany shale was cored in 1997 and the core sample was transferred to the ISGS, where it was stored in a temperature-controlled environment at 65°F until they were supplied to our adsorption laboratory for isotherm measurements in 2011. Once the shale samples were received from ISGS, the samples were stored in inert nitrogen atmosphere until isotherm measurements. Table 3.2 also lists the stratigraphy of the shale sample, which shows that the samples used in this work belonged to the Grassy Creek member of the New Albany group. This member is the thickest of the organic-rich units in the New Albany shale.

3.2.4 Gas Solubility in Water

In previous studies at Oklahoma State University (OSU) on wet/moist adsorbents [12, 13], we included a term in Equation (3.2) to account for the amount of gas, n_{sol}, dissolved in the water (rather than adsorbed on the coal surface).

$$n_{ads}^{Gibbs} = n_{inj} - n_{unads}^{Gibbs} - n_{sol} \tag{3.5}$$

To calculate the gas solubility in water as a function of pressure, an empirical equation was used for temperatures around 318 K.

$$x_{gas} = \frac{P}{a + bP + cP^2} \tag{3.6}$$

Since the solubilities of methane and nitrogen in water are small; the same equation and parameter values were used at other temperatures (e.g., 328.2 K in this study). Table 3.3 lists the values of parameters in Equation (3.6). In comparison to nitrogen and methane, the solubility of CO_2 is significant at temperatures near 318 K. To calculate the gas dissolved in water for use in Equation (3.5), literature data [22-24] were used to construct an empirical relationship for CO_2/water solubility at temperatures from 313.2 K to 348.2 K. In the 0-15 MPa range, the empirical function represents their data with an average absolute deviation of 1.5%. Thus, the mole fraction of CO_2 present in water at temperature T (in K) and pressure P (in MPa) is given as:

$$x_{CO2} = \frac{P}{a + (b_1 + b_0 T)P + (c_1 + c_0 T)P^2} \tag{3.7}$$

The amount of CO_2 dissolved in water can be given as

$$n_{sol} = \frac{x_{co_2} n_{water}}{(1 - x_{co_2})} \tag{3.8}$$

The denominator in Equation (3.8) is close to unity and therefore, the amount of gas dissolved in water was taken (approximately) as the product of mole fraction of CO_2 and the amount of water in moles in the system. Thus, the amount of CO_2 dissolved in water per unit mass of coal is expressed as

$$n_{sol} \approx \frac{x_{co_2} n_{water}}{m_{coal}} \tag{3.9}$$

where n_{water} is the amount of water in moles and m_{coal} is the mass of coal in the system.

The solubility of CO_2 in water calculated with Equation (3.7) is a monotonic increasing function of pressure at a given temperature. Thus, the maximum solubility of CO_2 in water was observed at 12.4 MPa and was about 2 mole percent. Table 3.4 lists the values of parameters in Equation (3.7).

As evident from the above discussion (Equation 3.5), accounting for the solubility of gas in water-rich adsorbed phase lowers the calculated Gibbs adsorption values. In the above discussion, it is assumed that all the water present in the system is adsorbed and, therefore, the amount of gas dissolved in water was estimated based on all the water present in the system. In other words, all the water present in the adsorbent was considered to be accessible to the gas. Further, we assumed that the bulk gas-phase was water-free.

Due to the low levels of moisture present in the shale sample, the correction for gas solubility in water was quite small. The difference in amounts of gas adsorbed (with and without solubility) correction ranged from 2-5% of the gas adsorbed. Thus, the correction was not significant when compared with the experimental uncertainties of the isotherms. Nonetheless, the method is highlighted here since the data reduction method typically *includes* these corrections to gas adsorption isotherms.

3.2.5 Swelling of Shale

Some authors have investigated the effect of gas adsorption and treatment on the potential swelling and/or structural changes of shales. Recently, Lahann et al. [25] investigated the effect of CO_2 on pore structure and mineralogy of New Albany shale. They observed no distinct changes to the pore structure of shales for samples saturated with CO_2 when compared with samples that had no exposure to CO_2. However, their experiments were conducted at low-pressures of CO_2 and thus, the concentration of CO_2 was small in the experiments. Kumar et al. [26] studied the evolution of

permeability in Marcellus shale that can be caused by swelling when exposed to helium, CH_4 and CO_2. They found that adsorption of CO_2 on Marcellus shale reduced the permeability to half the original value; however, they observed that this change was temporary and the permeability of the sample returned to its original value after sufficient interaction with the sample. The return of permeability to its original value does not necessarily imply that there was no swelling, but only that it was *reversible*. Similar studies have also been conducted on coals. For example, Mitra and Harpalani [27] reported recently a measurement and modeling study of permeability variation on coal-gas reservoirs that showed that the permeability of coal increases continuously with gas production. The increase in coal permeability was attributed primarily to the sorption-induced volumetric strain.

As part of the present adsorption study, we measured the helium void volume before and after the adsorption isotherm measurements. The void volume remained constant within its experimental uncertainty of 0.3 cm^3 (or 0.5% of the void volume), indicating that if there was any swelling *during* the isotherm measurement, it was reversible. Further, our previous work with the SLD model has shown that the model is capable of accurate predictions of high-pressure adsorption data on a variety of coals *without* the inclusion of a swelling term or correction [28, 29]. Thus, the inclusion of a separate swelling term in the model could not be justified on the basis of adsorption measurements alone. Measurements beyond adsorption will be required to establish the effects of any potential swelling. In fact, the detailed investigation of swelling on shales falls under the purview of rock-mechanics and is beyond the scope of this paper. Thus, no swelling corrections were made in the data reduction of this study, and this is the case for essentially all similar studies in the literature.

3.3 Simplified Local-Density Adsorption Model

The simplified local-density (SLD) model was used to describe the adsorption behavior of pure gases on several shale samples. The SLD model has been used in our previous studies on gas adsorption [29, 30]. The SLD model envisions the adsorbent to be composed of a rectangular-shaped slit and the adsorbate molecules reside within this two-surface slit, as illustrated in Figure 3.2. The distance between the slit surfaces is L, and the position of a molecule within the slit, z, is orthogonal to the one of the solid surfaces formed by carbon atoms. A molecule within the slit has interactions with both walls of the adsorbent slit (at distances z and L-z).

The SLD model accounts for both fluid-fluid and fluid-solid interactions in the slit-shaped pore. The model was first developed by Rangarajan et al. [31], who used the van der Waals equation of state (EOS) to account for the fluid-fluid interactions. Several researchers have used different equations of state within the SLD framework [32-35]. Following our earlier work [29, 30], the Peng-Robinson EOS is used in this study.

At equilibrium, the chemical potential of the fluid, μ, is expressed as the sum of the fluid-fluid and fluid-solid potentials at a position, "z", as follows:

$$\mu(z) = \mu_{ff}(z) + \mu_{fs}(z) = \mu_{bulk} \tag{3.10}$$

where subscript "bulk" refers to the bulk fluid and "ff" and "fs" refer to the fluid-fluid and fluid-solid interactions, respectively. The equation denotes that the chemical potential of the adsorbed fluid reflects the proximity of the fluid to the molecular wall of the adsorbent. Thus, the SLD model considers the inhomogeneity of the adsorbed phase in describing the molecular interactions of the adsorbed fluid with the adsorbent.

The chemical potential of the bulk fluid can be expressed in terms of fugacity as

$$\mu_{bulk} = \mu_0(T) + RT\ln\left(\frac{f_{bulk}}{f_0}\right) \tag{3.11}$$

where subscript "0" designates an arbitrary reference state and "f" refers to fugacity. Similarly, the chemical potential from fluid-fluid interactions is given as

$$\mu_{ff}(z) = \mu_0(T) + RT\ln\left(\frac{f_{ff}(z)}{f_0}\right) \tag{3.12}$$

where "$f_{ff}(z)$" is fluid fugacity at position z and "f_0" refers to the same arbitrary reference state as in Equation (3.11).

The fluid-solid interactions in the model are accounted for through a potential energy function. In particular, the fluid-solid potential is given as

$$\mu_{fs}(z) = N_A\left[\Psi^{fs}(z) + \Psi^{fs}(L - z)\right] \tag{3.13}$$

where "N_A" is Avogadro's number, "$\Psi(z)$" and "$\Psi(L-z)$" are the fluid-solid interactions for the two surfaces of a slit of length L.

Substituting Equations (3.11), (3.12) and (3.13) into Equation (3.10) provides the equilibrium relationship for adsorption within the slit:

$$f_{ff}(z) = f_{bulk}\exp\left(-\frac{\Psi^{fs}(z) + \Psi^{fs}(L-z)}{kT}\right) \tag{3.14}$$

where k is the Boltzmann's constant.

Applying the SLD model, the excess adsorption (n^{Ex}) is given as

$$n^{Ex} = \frac{A}{2}\int_{\text{Left Side of Slit}}^{\text{Right Side of Slit}}\left(\rho(z) - \rho_{bulk}\right)dz \tag{3.15}$$

where n^{Ex} is the excess adsorption of adsorbate in number of moles per unit mass of adsorbent, and "A" is the surface area of the adsorbate on a particular solid. The lower limit in Equation (3.15) is 3/8 σ_{ff}, which is 3/8 of the diameter of an adsorbed molecule touching the left plane surface. The upper limit is L-3/8σ_{ff}, the location of an adsorbed molecule touching the right plane surface. The local density is assumed to be zero for the distances less than 3/8σ_{ff} away from the wall. The value

3/8 σ_{ff} is chosen to account for most of the adsorbed gas; details are given elsewhere [36]. The left and right sides of the slit each comprise half of the total surface area, A/2.

The Peng-Robinson equation of state [37] was used to provide the bulk fluid density and fugacity. The EOS, expressed in terms of density, is given as:

$$\frac{P}{\rho RT} = \frac{1}{(1-\rho b)} - \frac{a(T)\rho}{RT\left[1+\left(1-\sqrt{2}\right)\rho b\right]\left[1+\left(1+\sqrt{2}\right)\rho b\right]} \tag{3.16}$$

where

$$a(T) = \frac{0.457535\,\alpha(T)R^2T_C^2}{P_C} \tag{3.17}$$

$$b = \frac{0.077796\,RT_C}{P_C} \tag{3.18}$$

The term, α(T), in Equation (3.17) was calculated using the following expression developed at Oklahoma State University in an earlier work [38]

$$\alpha(T) = \exp\left(\left(A + BT_r\right)\left(1 - T_r^{C+D\omega+E\omega^2}\right)\right) \tag{3.19}$$

where A, B, C, D and E are correlation parameters and their values, respectively, are 2.0, 0.8145, 0.134, 0.508 and -0.0467. The values used were based on accurate description of saturation pressures for the pure gases under conditions encountered in coal bed operations. Other fluid properties used in this study are listed in Table 3.5.

The fugacity of the bulk fluid using PR EOS is

$$\ln\frac{f_{bulk}}{P} = \frac{b\rho}{1-b\rho} - \frac{a(T)\rho}{RT\left(1+2b\rho - b^2\rho^2\right)} - \ln\left[\frac{P}{RT\rho} - \frac{Pb}{RT}\right] - \frac{a(T)}{2\sqrt{2}bRT}\ln\left[\frac{1+(1+\sqrt{2})\rho b}{1+(1-\sqrt{2})\rho b}\right] \tag{3.20}$$

For the adsorbing fluid, the fugacity for fluid-fluid interactions is

$$\ln\frac{f_{ff}(z)}{P}=\frac{b\rho(z)}{1-b\rho(z)}-\frac{a_{ads}(z)\rho(z)}{RT\left(1+2b\rho(z)-b^2\rho^2(z)\right)}$$

$$-\ln\left[\frac{P}{RT\rho(z)}-\frac{Pb}{RT}\right]-\frac{a_{ads}(z)}{2\sqrt{2}bRT}\ln\left[\frac{1+(1+\sqrt{2})\rho(z)b}{1+(1-\sqrt{2})\rho(z)b}\right] \quad (3.21)$$

The parameter "$a_{ads}(z)$" in Equation (3.21) varies with the position within the slit. Chen et al. [32] provided equations for "$a_{ads}(z)$," which depends on the ratio of slit length L to the molecular diameter σ_{ff}.

In one of the earlier works with the SLD model [28], the covolume "b" in the PR EOS was adjusted, using a simple empirical correction, to describe more accurately the repulsive interactions of adsorbed fluid at high pressures. The covolume is corrected by an adjustable parameter, Λ_b, as

$$b_{ads}=b\left(1+\Lambda_b\right) \quad (3.22)$$

Equation (3.21) then becomes

$$\ln\frac{f_{ff}(z)}{P}=\frac{b_{ads}\rho(z)}{1-b_{ads}\rho(z)}-\frac{a_{ads}(z)\,\rho(z)}{RT\left[1+2b_{ads}\rho(z)-b_{ads}^2\rho(z)^2\right]}$$

$$-\ln\left[\frac{1-b_{ads}\rho(z)}{RT\rho(z)}\right]-\frac{a_{ads}(z)}{2\sqrt{2}b_{ads}RT}\ln\left[\frac{1+(1+\sqrt{2})\rho(z)b_{ads}}{1+(1-\sqrt{2})\rho(z)b_{ads}}\right] \quad (3.23)$$

In this work, we used a fixed value of Λ_b = -0.2 for all three gases (methane, nitrogen and CO_2) following an earlier work [29].

The fluid-solid interaction, $\Psi^{fs}(z)$, was represented by Lee's partially-integrated 10-4 potential [39], which is a truncated form of Steele's 10-4-3 potential [40]

$$\Psi^{fs}(z)=4\pi\rho_{atoms}\varepsilon_{fs}\sigma_{fs}^2\left(\frac{\sigma_{fs}^{10}}{5(z')^{10}}-\frac{1}{2}\sum_{i=1}^{4}\frac{\sigma_{fs}^4}{\left(z'+(i-1)\cdot\sigma_{ss}\right)^4}\right) \quad (3.24)$$

$$\varepsilon_{fs}=\sqrt{\varepsilon_{ff}\times\varepsilon_{ss}} \quad (3.25)$$

Where ε_{fs} and ε_{ss} are the fluid-solid and solid-solid interaction energy parameters, respectively, and ρ_{atoms} = 0.382 atoms/Å^2. The parameters σ_{ff} and σ_{ss} signify, respectively, the molecular diameter of the adsorbate and the carbon interplanar distances. The carbon interplanar distance was taken to be the value for graphite, 0.335 nm [41] and values of σ_{ff} and ε_{ff} were taken from Reid et al. [42]. The fluid-solid molecular diameter, σ_{fs} and dummy coordinate z' used in numerical integration of Equation (3.15) are defined as:

$$\sigma_{fs} = \frac{\sigma_{ff} + \sigma_{ss}}{2} \tag{3.26}$$

$$z' = z + \frac{\sigma_{ss}}{2} \tag{3.27}$$

For the adsorbed phase, the slit is divided into two halves and each half is subdivided into 50 intervals. The local density is then calculated by solving Equations (3.20) and (3.23) simultaneously for each interval. Once the local density is determined across the slit, the excess adsorption is calculated by integrating Equation (3.15) numerically using Simpson's rule. Thus, the SLD model contains the following three regressible parameters: surface area, A; solid-solid interaction energy, ε_{ss}/k; and the slit length, L. These model parameters are helpful in characterizing the adsorbent surface and in estimating the accessibility of each gas. Specifically, the surface areas denote the accessible areas for each gas on the adsorbent, the solid-solid interaction energy characterizes the molecular interactions between the solid adsorbent atoms and the slit length characterizes the pores of the adsorbent and represents the *effective* pore-width of the adsorbent.

For describing the pure-gas adsorption of three gases, the SLD model thus requires five parameters. They are the three surface areas A_i, (one for each gas), solid-solid interaction energy, ε_{ss}/k and the slit length, L. Thus, there is only one *gas-specific* parameter (A_i) for each gas. In particular, this accessible surface area, A_i, is specific to the adsorbing gas species whereas the other two parameters (solid-solid interaction energy and slit length) are the same for all gases on a specific adsorbent.

Thus, only five parameters are required for simultaneous representation of pure-gas adsorption of *three* gases. In previous studies, we have shown that with these five pure-component parameters, different predictive scenarios/cases can be constructed with the SLD model. For example, in a recent work [43], the model has been shown capable of predicting adsorption of other gases based on a single gas isotherm (e.g., predicting nitrogen and CO_2 adsorption based solely on methane adsorption isotherms and adsorbent surface characterization). The SLD model has also been shown to yield useful predictions of mixture adsorption based solely on pure-component isotherm data [29, 30].

3.4 Results and Discussion

3.4.1 Analysis of Experimental Uncertainties for Gas Adsorption on Shales

Shales typically adsorb considerably less gas than other carbonaceous adsorbents such as activated carbons and coals. This is especially true for shale samples that contain very low levels of organic carbon [44]. As a result, an experimental design that is adequate for gas adsorption measurements on coals may not be suitable for adsorption measurements on shales. A similar conclusion was reached by Lu et al. [45], who measured gas adsorption on shales after undertaking appropriate modifications to their experimental design.

Prior to measuring the isotherms in this study, the experimental set-up and design of our apparatus were re-optimized to reduce the expected experimental uncertainties from the measurements. A detailed analysis of factors (random errors) affecting the experimental uncertainties in the amounts of gas adsorbed for measurements based on the volumetric method was presented in an earlier study [46]. The study identified the major contributors to the experimental uncertainty to be the void volume of the equilibrium cell and the pressure in the injection pump. Therefore, in this study, we modified our apparatus to reduce, as much as possible, the void volume in the equilibrium cell. An injection pressure of 7 MPa (about 1000 psia) was used since this gives the optimal overall

performance for a fixed-pressure, experimental apparatus. Our apparatus modifications resulted in a 34% reduction in void volume, and this lowered the expected uncertainties in adsorption by more than two-fold relative to the previous configuration of the apparatus used in our adsorption work on coals [43]. In particular, the void volume was minimized by (1) filling the equilibrium cell with as much of the shale sample as possible and (2) minimizing the remaining dead space within the apparatus (in lines, fittings, etc.). Detailed error propagation calculations from the newly acquired adsorption data showed that the modifications in the apparatus led to an overall reduction of about 78%, 68% and 51% in the experimental uncertainties for the adsorption of CO_2, methane and nitrogen, respectively, over the previous case. This experimental observation confirmed the predictions obtained in the analysis of expected uncertainties discussed above. For brevity, the detailed analysis is not reproduced here, and the reader is referred to our earlier study on adsorption error analysis [46] for the methodology utilized in this work.

3.4.2 Experimental Results

Table 3.6 presents the newly acquired experimental data for the adsorption of methane, nitrogen and CO_2 on the New Albany shale. The table lists the pressure, excess adsorption and the expected experimental uncertainty for each datum. Two replicate runs were conducted to investigate the reproducibility of the isotherm measurements. The data from the two runs agreed within 9%, 32% and 7% for adsorption of methane, nitrogen and CO_2, respectively. This compares with expected experimental uncertainties of 31%, 136% and 26% for methane, nitrogen and CO_2 adsorptions, respectively. When compared to the reproducibility of the data, the expected uncertainties appear relatively large; this is because the reported uncertainties account for both the precision *and* accuracy of the measurements. In other words, the precision of the measurements was higher than the accuracies, which were included in the uncertainty estimates listed in Table 3.6. Further, the large expected percentage uncertainties (especially for N_2) are an artifact of low levels of gas adsorption on the shale sample. That is, the large *percentage* uncertainties correspond to small

errors in the *amounts* of gas adsorbed. This experimental artifact can also be inferred from a comparison of gas adsorption amounts (and their expected errors) on the shale and coals. Specifically, the adsorption on New Albany shale is an order of magnitude lower than on several coals studied previously using the same apparatus [43]. In fact, we observed that the expected errors for the amounts adsorbed on shale were quite comparable to those obtained for the adsorption on coals. However, the low levels of adsorption on the New Albany shale *inflate* the percentage errors; thus, the absolute errors are probably more meaningful for interpretation of gas adsorption data on shales with low adsorbing nature.

For nitrogen adsorption on New Albany shale, the datum at 1.5 MPa contributed significantly to the overall percentage experimental uncertainty. Specifically, the average percentage uncertainty for nitrogen adsorption isotherm without the first datum (which has near-zero adsorption) was about 77%, instead of the 136% when the first datum is included in the estimates. Overall, the average experimental uncertainties corresponded to about 0.0095, 0.0081 and 0.024 mmol/g shale for the adsorption of methane, nitrogen and CO_2, respectively.

Figure 3.3 presents the adsorption isotherms for methane, nitrogen and CO_2 on New Albany shale. The solid lines in these figures are SLD model representations (described in Section 3.4.3). At 7 MPa, the ratio of excess adsorption for methane, nitrogen and CO_2 were 1:3.2: 9.3. This N_2:CH_4 ratio is similar to that obtained earlier for gas adsorption on coals and activated carbons [12, 14]. However, CO_2 adsorption ratios (CO_2:CH_4 and CO_2:N_2) on New Albany shale was much higher than seen in coals, where a typical CO_2:CH_4) ratio might be on the order of 2.5:1 [43]. This indicates a strong preference of these shale samples for adsorbing CO_2 compared to other gases and, thus, points to the possible CO_2 storage potential in these shales.

The adsorption on shales was much lower than the coals that we studied previously [12, 13]. Specifically, the adsorption of the three gases on shales was about 10 to 30 times lower than the

adsorption on coals. Figures 3.4-3.6 compare the adsorption isotherms for methane, nitrogen and CO_2, respectively, on New Albany shale and five coals that we measured in an earlier study [43]. The figures illustrate the difference in adsorption levels observed between coals and shales. The lower levels of adsorption on shales reflects the low levels of total organic carbon on shales, since the adsorption is related significantly to the carbon content of the samples. The higher levels of ash in the shale sample also decrease adsorption, since ash is largely inert to gas adsorption. In a recent study, Weniger et al. [11] observed that the %TOC was correlated positively with the maximum excess adsorption, while the ash content exhibited the reverse behavior. As evident from Table 3.1, the shale has a carbon content of about 34%. In comparison, the percent carbon of coals ranges from about 73-91%. Further, the total organic carbon content of shale sample used in this study was only 5.5%. In addition, the shale sample contained about 90% ash on an as-received basis. The lower organic carbon content and higher ash content of the New Albany sample led to very low levels of gas adsorption.

3.4.3 SLD Model Representations of Gas Adsorption on Shales

3.4.3.1 Data from Oklahoma State University (OSU)

The SLD model was used to represent the adsorption data on the shale in this study. Five parameters in the SLD model were regressed to fit the data, namely: surface area, A_i (one for each gas), solid-solid interaction energy, ε_{ss}/k, and slit length, L. The objective function used in the model regressions was the weighted root-mean-squared (WRMS), where the assigned weights were the estimated experimental uncertainties in the adsorption data. Note that in the representations of the data, the datum for N_2 at 1.5 MPa yields an anomalously high error; as a result, this suspect datum was removed from the modeling analysis and is not included in the statistics reported in Table 3.7.

Table 3.7 presents the regressed model parameters and statistics for this system, including the weighted average absolute deviation (WAAD), the root-mean-squared error (RMSE) and the

average absolute percentage deviation (%AAD). The surface area of each gas was allowed to vary to account for different accessibilities of the coal surface for the three gases. The accessible surface area for CO_2 was the largest among the three gases and nitrogen had the smallest surface area in the SLD regressions. As evident from the table, the SLD model is capable of describing the adsorption data of the three gases within the experimental uncertainties. In particular, the %AADs for methane, nitrogen and CO_2 were 10%, 6% and 5%, respectively. Figure 3.3 presents the SLD model representations for methane, nitrogen and CO_2 adsorption on the New Albany shale sample.

A comparison of the SLD model parameters for shale and coals is provided in Table 3.8. The model parameters for coals were obtained in an earlier study [47]. The low surface areas obtained for shales reflect the lower adsorption capacity of shale samples compared to coals. The ε_{ss}/K of the shale is about one-third of the value obtained for the coals. In the SLD model, the ε_{fs}/k (or the fluid-solid energy parameter) is a geometric mean of ε_{ss}/K and ε_{ff}/k, as given in Equation (3.25). Since the fluid-fluid energy parameter is fixed for each gas independent of the adsorbent, the lower values of ε_{ss}/k signify weaker *fluid-solid* interactions. Thus, the shale used in this study appear to have much smaller affinity for gas adsorption than most coals we have studied, and this fact is reflected in the model parameters obtained for these systems.

3.4.3.2 Literature Data

As part of this study, an adsorption database was compiled for gas adsorption measurements on shales from the literature. Table 3.9 presents the literature adsorption database compiled in this work. The table lists the sample number, ranges of pressure and temperature, adsorbates and characterization information available for each system. These data were available from the following three sources: [8, 10, 11]. Overall, the database contains 34 systems of methane and CO_2 adsorption isotherm measurements from the respective authors. Figure 3.7 presents maximum excess adsorption for both methane and CO_2 as a function of total organic content (%TOC). The

maximum excess adsorption increases with %TOC; however, there is considerable scatter from a linear trend, indicating that other factors also play a significant role in determining adsorption capacities of these shales.

The SLD model was used to represent the adsorption data for each of the systems listed in Table 3.9. In each case, the model parameters were regressed by minimizing the percentage average absolute deviation in excess adsorption, since detailed experimental uncertainties were not reported with these literature data. The model parameters and statistics for each system are listed in Table 3.10. As shown in the table, the SLD model provides satisfactory representations of adsorption data for these systems. The overall %AAD for methane and CO_2 adsorption were 4 and 9, respectively. Further, the largest percentage deviations were obtained on sample number 107928-1 for CH_4 adsorption (12%) and sample numbers 170 and 181 for CO_2 adsorption (14%), as shown in Table 3.10.

For illustrative purposes, Figures 3.8 and 3.9 present the SLD model representations for the adsorption of methane and CO_2 on several shale samples from the literature. The adsorption data on shales from literature sources were represented precisely, in general. However, the CO_2 adsorption data from Weniger et al. [11] contained a steep maxima between 8 to 11 MPa, which could not be represented adequately by the SLD model. Weniger et al. [11] also found similar problems in representing their data in this region with a modified Langmuir model.

Figures 3.10(a)-(f) present the percentage deviations for all the adsorption data considered in this study. These figures show the deviations obtained for adsorption data from the three literature sources (listed in Table 3.9 and 3.10) and also include deviations for adsorption data measured in this study. Figure 3.10(a) depicts the percentage deviations for adsorption of methane on 12 shale samples from Beaton et al. [10]. Figures 3.10(b) and (c) present the deviations for methane and CO_2 adsorption data, respectively, originating from Nuttall et al. [8]. Similarly, Figures 3.10(d) and

(e) present the deviations for methane and CO_2 adsorption data from Weniger et al. [11]. The legend entries in these figures list the shale sample number and the literature source of that data. The percentage deviations obtained for the adsorption of methane, nitrogen and CO_2 on New Albany shale measured in this study are presented in Figure 3.10(f). Overall, about 91% of all the methane adsorption data were predicted with deviations of less than 10% and about 65% the CO_2 adsorption data was predicted within 10% deviation. Further, the percentage deviations are higher at lower pressures due to the low values of excess adsorption at these pressures. Thus, the large *percentage* deviations at low pressures represent *small* errors in terms of amounts of gas adsorbed.

The adsorbed-phase density for supercritical adsorbates such as CO_2 can also be estimated graphically from high-pressure adsorption data that extends to the "linear region" of the isotherm. Specifically, when the absolute adsorption, $V_{ads}\rho_{ads}$, becomes constant at higher pressures, the excess adsorption isotherm becomes linear as a function of gas density, ρ_{gas}. The extrapolation of this linear relation to zero excess adsorption provides $\rho_{ads} = \rho_{gas}$ [48]. In this manner, the adsorbed-phase density can be estimated graphically from a plot of excess adsorption vs. gas density. Such a method was utilized by Sudibandriyo et al. [14], who estimated the adsorbed-phase density of CO_2 on activated carbon to be about 1.02 g/cm^3 or 22.5 mol/L. In this work, we utilized the adsorption data from Weniger et al. [11] to estimate the adsorbed-phase densities of CO_2 on several shale samples. For illustrative purposes, Figure 3.11 shows the method applied to CO_2 adsorption data on a shale sample reported by Weniger et al. [11]. Using this (somewhat subjective) graphical method, the CO_2 adsorbed-phase density for sample number 154 (Figure 3.11) was about 1.08 g/cm^3 or 24.6 mol/L, which is comparable to the adsorbed-phase density of CO_2 on activated carbon found earlier [14]. The density estimates obtained for other shale samples using the same technique are shown in Table 3.11, which shows that the adsorbed-phase densities for these samples vary between 0.8 to 1.1 g/cm^3.

We also considered the possibility of developing a shale structure-based generalized model for gas adsorption on shales, similar to our previous effort on coals [29]. However, this requires the availability of surface characterization information for the shales. Unfortunately, the information available from the original references in the literature for gas adsorption data on shales was insufficient to undertake this effort. Thus, a model generalization on shales could not be realized at the time of this writing.

3.5 Conclusion

High-pressure adsorption isotherms of methane, nitrogen and CO_2 were measured on a New Albany shale sample from the Illinois basin. The newly acquired data yielded expected uncertainties of about 0.0095, 0.0081 and 0.024 mmol/g for the methane, nitrogen and CO_2 adsorption isotherms, respectively.

The adsorption on shales is about an order of magnitude lower than the adsorption on coals. The lower organic carbon content and higher ash content of these shales resulted in reduced gas adsorption capacity of shales compared to coals. The N_2:CH_4 excess adsorption ratio on the shale sample was similar to gas adsorption on coals and activated carbons. The CO_2:N_2 and CO_2:CH_4 ratios on shale were much higher and reflect strong affinity of the New Albany shale sample to CO_2 adsorption.

The SLD model was used to correlate adsorption data on the shale from this work as well as data available in the literature for adsorption on 34 shale samples. The model was capable of describing the adsorption data from this work within the experimental uncertainties. Further, the model provided representations of literature data on several shale samples with an overall %AAD of 4 and 9 for the adsorption of methane and CO_2, respectively.

Table 3.1. Compositional Analyses of New Albany Shale[a] and Argonne Coals[b]

Analyses	New Albany Shale	Beulah Zap Coal	Wyodak Coal	Illinois-6 Coal	Upper Freeport Coal	Poca--hontas Coal
Ultimate	**(Dry-ash-free basis)**					
Carbon %	34.6	72.9	75.0	77.7	85.5	91.1
Hydrogen %	4.13	4.83	5.35	5.00	4.70	4.44
Oxygen %	46	20.3	18.0	13.5	7.5	2.5
Sulfur %	13	0.80	0.63	4.83	2.32	0.66
Proximate	**(As-received basis)**					
Moisture %	0.44	32.2	28.1	8.0	1.1	0.7
TOC%	5.54	-	-	-	-	-
Ash %	89.4	9.7	8.8	15.5	13.2	4.8

[a]Huffman Laboratories Inc., Colorado
[b]Argonne National Laboratory, Illinois

Table 3.2. Properties of the New Albany Shale Sample Used in this Study

Well Name	Mid-Continent Methane, Inc., Meadowlark #2
Location	Sec 10, T9S, R5E in Saline County, IL
API #	121652637600
Core ID#	C-14907
Well Completion Date	November 1997
New Albany Group (4460-4726)[a]	Hanibal-Saverton Member (4460-4485) Grassy Creek Member (4485-4577) Sweetland Creek Member (4577-4689) Blocher Member (4689-4726)

[a]Depth in Feet

Table 3.3. Parameters for CH_4 and N_2 Solubility in Water at Temperatures Around 318 K

Constant	Units of Constant	Methane	Nitrogen
a	MPa	5302.07	10204.24
b	-	150.4	127.3
c	1/MPa	-0.78	-0.09

Table 3.4. Parameters for CO_2 Solubility in Water at Multiple Temperatures

Constant	Value	Units of Constant
a	272.21	MPa
b_1	-332.637	-
b_0	1.06683	1/K
c_1	19.18	1/MPa
c_0	-0.05609	1/(MPa K)

Table 3.5. Physical Properties of Fluids Used in this Study [42, 49]

	CH_4	N_2	CO_2
T_C (K)	190.56	126.19	304.13
P_C (MPa)	4.60	3.40	7.38
σ_{ff} (nm)	0.3758	0.3798	0.3941
ε_{ff}/k (K)	148.6	71.4	195.2

Table 3.6. Excess Adsorption of CH_4, N_2 and CO_2 on New Albany Shale at 328.2 K

CH_4			N_2			CO_2		
Pressure (MPa)	**Excess Adsorption (mmol/g)**	**σ Excess Adsorption (mmol/g)**	**Pressure (MPa)**	**Excess Adsorption (mmol/g)**	**σ Excess Adsorption (mmol/g)**	**Pressure (MPa)**	**Excess Adsorption (mmol/g)**	**σ Excess Adsorption (mmol/g)**
1.45	0.0138	0.0091	1.47	0.0012	0.0076	1.70	0.0479	0.0200
2.85	0.0253	0.0090	2.86	0.0052	0.0076	3.06	0.0715	0.0197
4.23	0.0316	0.0090	4.23	0.0083	0.0076	4.76	0.0916	0.0194
5.63	0.0352	0.0091	5.62	0.0109	0.0077	5.66	0.0985	0.0192
6.99	0.0374	0.0093	6.99	0.0116	0.0079	6.96	0.1085	0.0194
8.36	0.0386	0.0095	8.37	0.0133	0.0081	8.26	0.1136	0.0225
9.76	0.0395	0.0099	9.77	0.0145	0.0084	9.75	0.1179	0.0259
11.12	0.0397	0.0103	11.14	0.0147	0.0088	11.14	0.1150	0.0309
12.52	0.0412	0.0107	12.56	0.0147	0.0091	12.60	0.0942	0.0389

Table 3.7. SLD Model Representations for CH_4, N_2 and CO_2 Excess Adsorption on New Albany Shale

Adsorbate	A (m^2/g)	Slit Length (nm)	ε_{ss}/k (K)	WAAD	%AAD	RMSE
CH_4	5.2	1.23	10.1	0.3	10	0.0033
N_2	2.8			0.1	6	0.0009
CO_2	8.6			0.2	5	0.0070
Overall				**0.2**	**12**	**0.005**

Table 3.8. Comparison of SLD Model Parameters for CH_4, N_2 and CO_2 Excess Adsorption on New Albany Shale and Argonne Coals[a]

Adsorbent	Surface area (m^2/g)			Slit length (nm)	ε_{ss}/k (K)
	CH_4	CO_2	N_2		
New Albany Shale	5.2	8.6	2.8	1.23	10.1
Dry Illinios-6	60.5	77.4	44.1	1.34	30.3
Dry Beulah Zap	49.8	93.0	34.8	1.30	37.4
Dry Wyodak	57.0	96.3	43.8	1.32	31.5
Dry Upper Freeport	47.1	54.1	35.1	1.18	37.2
Dry Pocahontas	63.1	69.5	46.8	1.15	36.8

[a]Model representations for the coals are from Mohammad et al. [47]

Table 3.9. Literature Sources for Gas Adsorption Data on Shales

Adsorbate	Sample Number	Temp. (K)	Pressure Range (MPa)	%TOC	% Moisture	NPTS	Source
CH_4	8995	343	0.4-20	1.11	1.24	9	[10]
CH_4	9373	340	0.4-15	2.34	1.72	9	[10]
CH_4	9261	358	0.8-27	4.03	0.26	9	[10]
CH_4	9264	355	0.8-27	1.32	0.2	9	[10]
CH_4	9265	345	0.8-26	2.84	0.92	9	[10]
CH_4	9364	345	0.8-26	1.29	0.26	9	[10]
CH_4	9262	340	0.9-28	1.73	0.55	9	[10]
CH_4	9263	353	0.8-27	0.45	0.61	9	[10]
CH_4	6517	311	0.4-15	4.48	0.77	12	[10]
CH_4	6534	311	0.3-16	3.25	1.47	13	[10]
CH_4	6543	311	0.4-16	0.75	0.59	13	[10]
CH_4	8046	323	0.4-20	1.66	1.42	9	[10]
CH_4 CO_2	107928-1	303	0.4-6 0.5-9	0.69	-	9 12	[8]
CH_4 CO_2	107928-2	303	0.3-6 0.3-9	2.95	-	9 12	[8]
CH_4 CO_2	107928-3	303	0.3-6 0.3-10	1.6	-	9 12	[8]
CO_2	124789-3	303	0.2-5	1.78	-	11	[8]
CO_2	123486-1	303	0.2-4	2.44	-	11	[8]
CO_2	121162-1	303	0.1-3	2.37	-	10	[8]
CO_2	121464-1	303	0.1-3	1.18	-	10	[8]
CO_2	121464-2	303	0.1-3	3.6	-	10	[8]
CO_2	121464-3	303	0.2-3	2.31	-	10	[8]
CH_4	119139-1	303	0.3-11	11.79	1.91	14	[8]
CH_4	119139-2	303	0.3-11	5.37	2.3	15	[8]
CH_4	123957-1	303	0.3-9	2.34	2.82	13	[8]
CH_4	123957-2	303	0.3-11	4.73	3.83	15	[8]
CH_4	125651-1	303	0.3-10	1.96	1.98	14	[8]
CH_4	125651-2	303	0.3-8	3.05	1.67	12	[8]
CH_4	125651-3	303	0.3-10	0.73	3.1	13	[8]
CH_4	AEP1-1	303	0.3-9	1.54	1.96	13	[8]
CH_4 CO_2	168	318	6-17 1-25	24.21	1.65	15 20	[11]
CH_4 CO_2	170	318	1-16 3-20	11.66	1.2	28 14	[11]
CH_4 CO_2	181	318	2-18 2-19	11.13	0.82	18 16	[11]
CH_4 CO_2	114	318	2-17 0.6-21	1.73	1.38	17 45	[11]
CH_4 CO_2	154	318	1-16 2-17	1.62	0.92	16 23	[11]

Table 3.10. SLD Model Representations for CH_4 and CO_2 Adsorption on Literature Data for Shales

Adsorbate	Sample Number	Area (m^2/g)		Slit length (nm)	ε_{ss}/k (K)	%AAD	
		CH_4	CO_2			CH_4	CO_2
CH_4	8995	1.9	-	1.28	11.6	7	-
CH_4	9373	1.9	-	1.90	15.1	3	-
CH_4	9261	1.3	-	1.85	14.9	2	-
CH_4	9264	0.5	-	1.64	14.7	6	-
CH_4	9265	1.2	-	2.04	16.5	3	-
CH_4	9364	2.2	-	1.44	10.3	2	-
CH_4	9262	1.1	-	1.85	16.8	3	-
CH_4	9263	1.9	-	1.13	16.4	3	-
CH_4	6517	1.8	-	2.20	18.9	3	-
CH_4	6534	2.1	-	1.78	7.1	3	-
CH_4	6543	1.1	-	2.78	7.6	8	-
CH_4	8046	2.3	-	2.25	14.5	5	-
CH_4,CO_2	107928-1	0.6	1.8	1.10	10.3	12	9
CH_4,CO_2	107928-2	5.8	8.4	0.74	8.3	3	4
CH_4,CO_2	107928-3	0.5	1.6	1.33	25.7	8	10
CO_2	124789-3	-	4.2	1.51	10.2	-	9
CO_2	123486-1	-	4.4	1.51	9.0	-	8
CO_2	121162-1	-	5.4	1.46	7.7	-	11
CO_2	121464-1	-	2.1	1.56	11.6	-	9
CO_2	121464-2	-	9.6	1.57	11.8	-	9
CO_2	121464-3	-	5.7	1.61	8.4	-	12
CH_4	119139-1	7.9	-	1.44	10.2	2	-
CH_4	119139-2	4.6	-	1.36	8.6	4	-
CH_4	123957-1	2.2	-	1.21	6.3	2	-
CH_4	123957-2	3.9	-	1.09	8.1	2	-
CH_4	125651-1	2.3	-	1.98	9.0	3	-
CH_4	125651-2	1.5	-	1.47	8.8	3	-
CH_4	125651-3	1.5	-	0.56	2.3	9	-
CH_4	AEP1-1	2.6	-	0.90	5.5	3	-
CH_4,CO_2	168	51.3	80.0	1.08	2.95	2	8
CH_4,CO_2	170	27.9	53.1	0.98	2.98	7	14
CH_4,CO_2	181	34.1	58.2	1.02	2.5	5	14
CH_4,CO_2	114	9.2	31.7	0.88	6.0	2	6
CH_4,CO_2	154	4.5	13.9	1.06	5.7	4	4

Table 3.11. CO_2 Adsorbed Phase Densities Based on Graphical Estimation Method (Adsorption Data from [11])

Sample number	CO_2 Adsorbed Phase Density	
	mole/L	g/cm^3
168	21.82	0.96
170	19.55	0.86
181	17.95	0.79
114	24.32	1.07
154	24.55	1.08

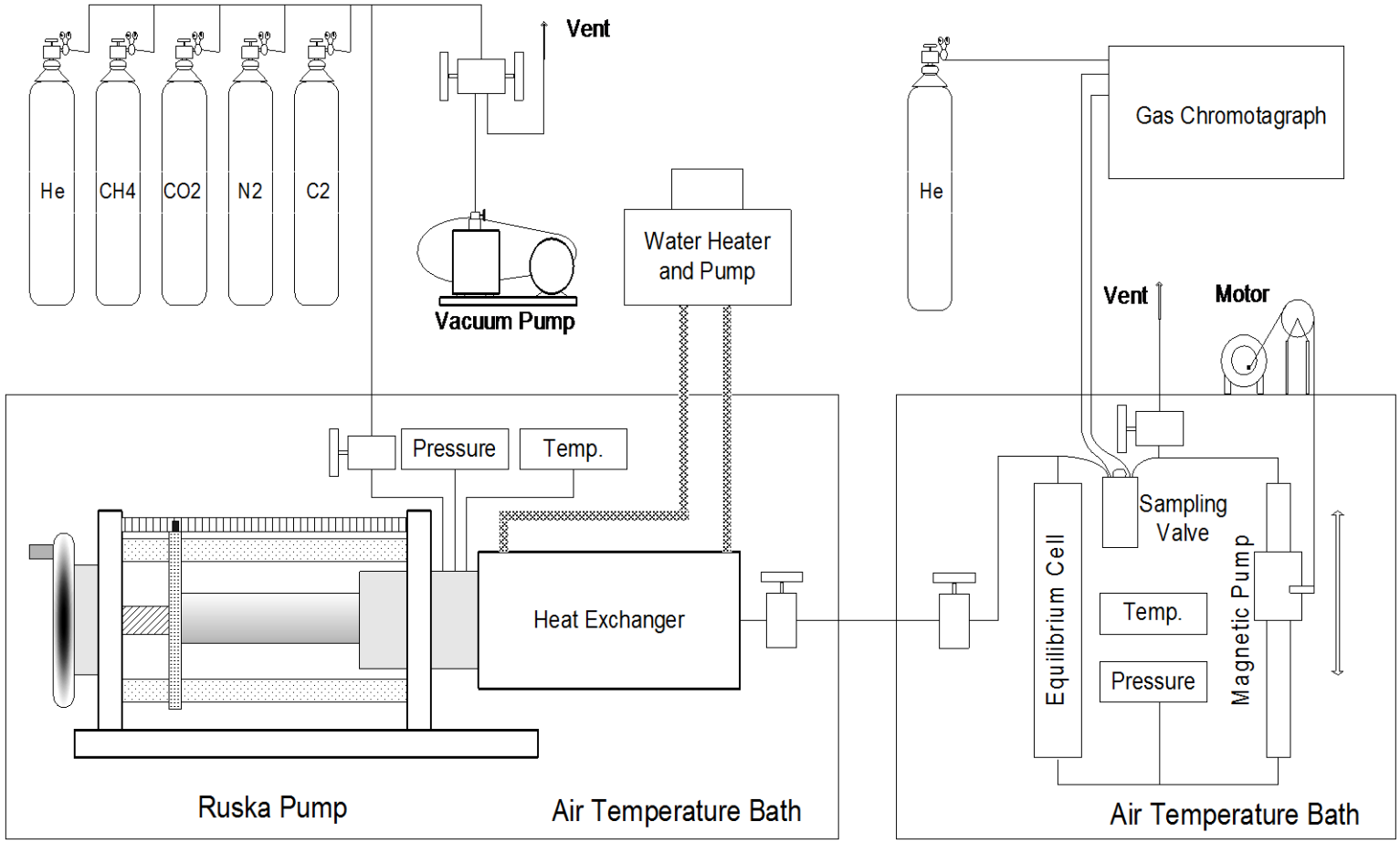

Figure 3.1. Schematic Diagram of the Experimental Apparatus

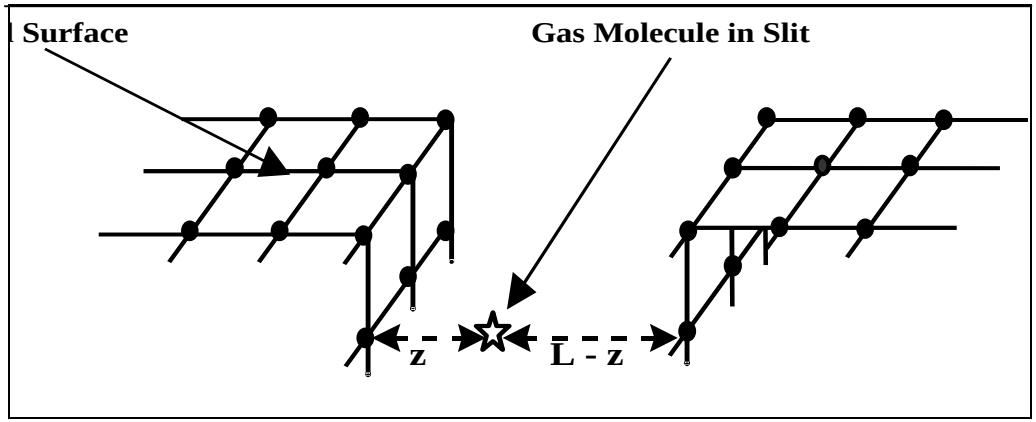

Figure 3.2. SLD Model Slit Geometry

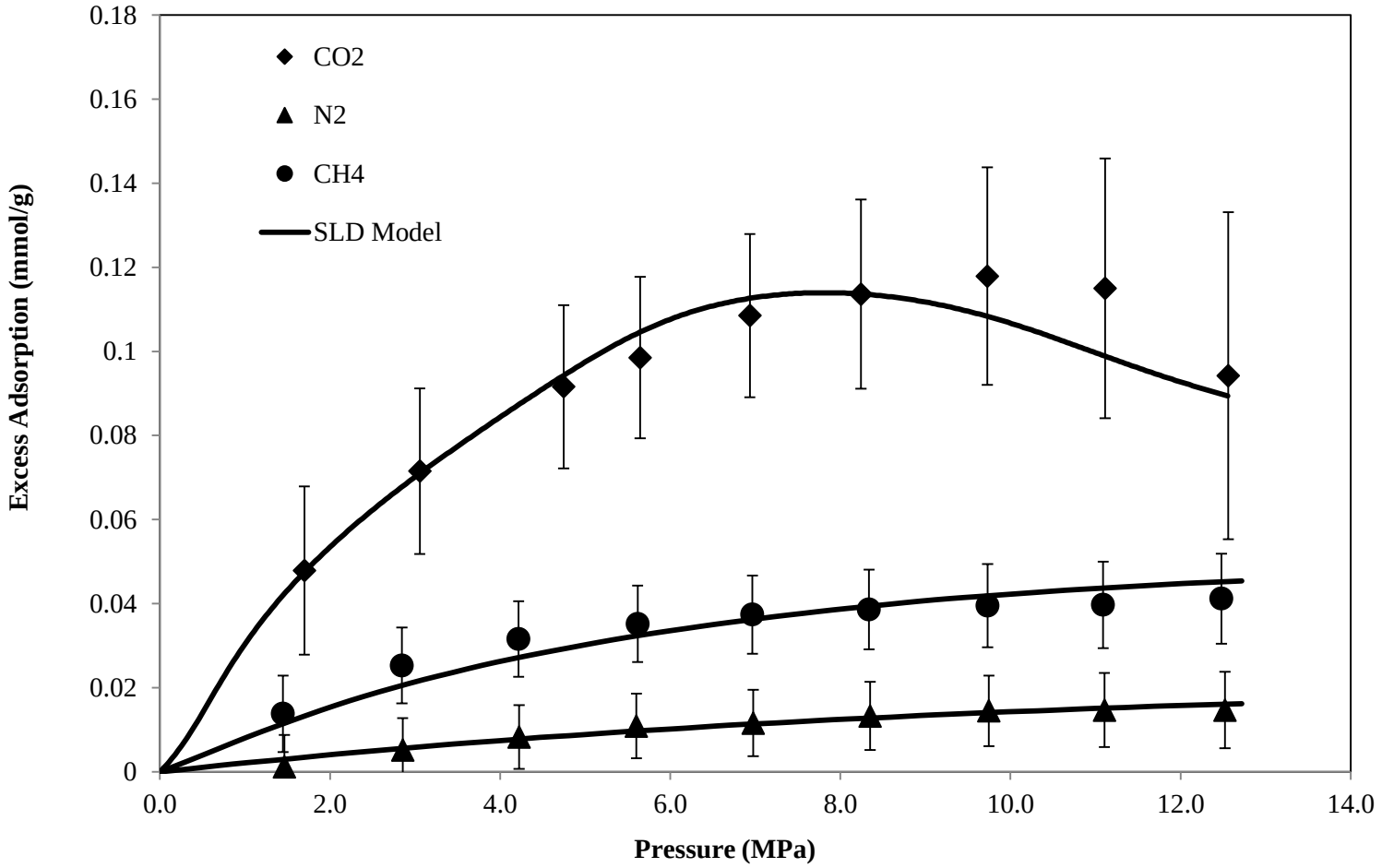

Figure 3.3. Excess Adsorption of CH_4, N_2 and CO_2 on New Albany Shale at 328.2 K

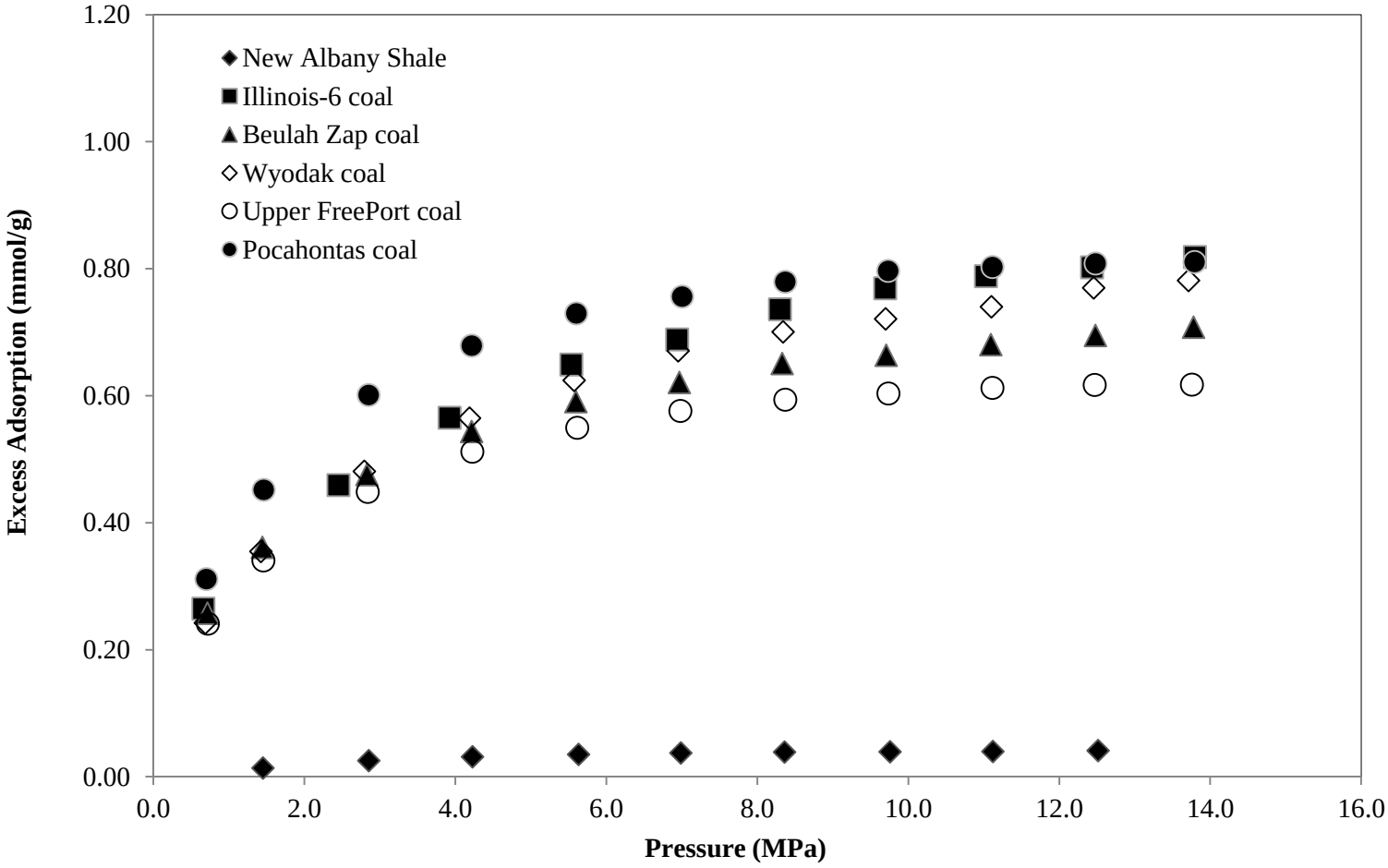

Figure 3.4. Comparison of CH_4 Adsorption on New Albany Shale and Argonne Coals at 328.2 K

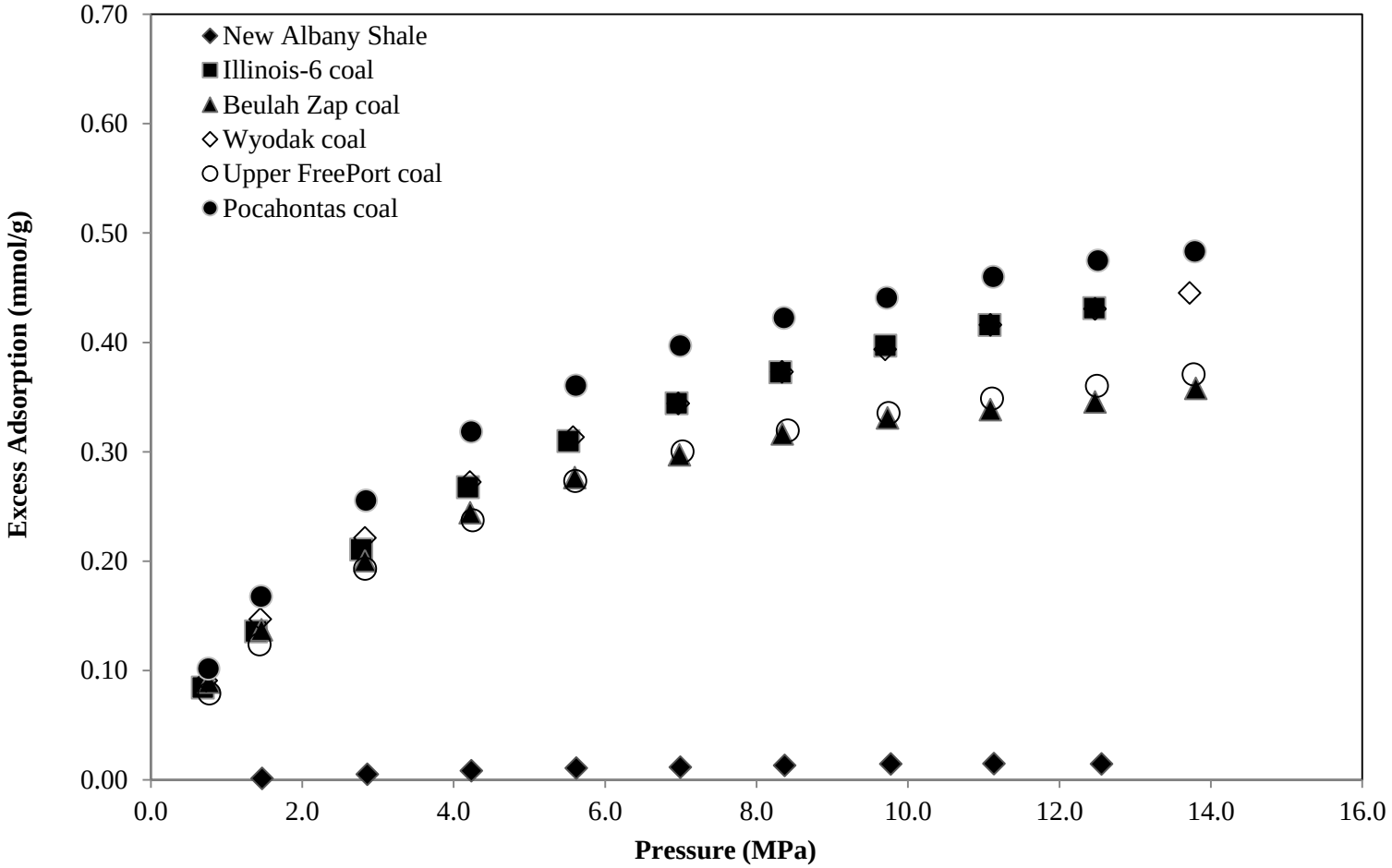

Figure 3.5. Comparison of N_2 Adsorption on New Albany Shale and Argonne Coals at 328.2 K

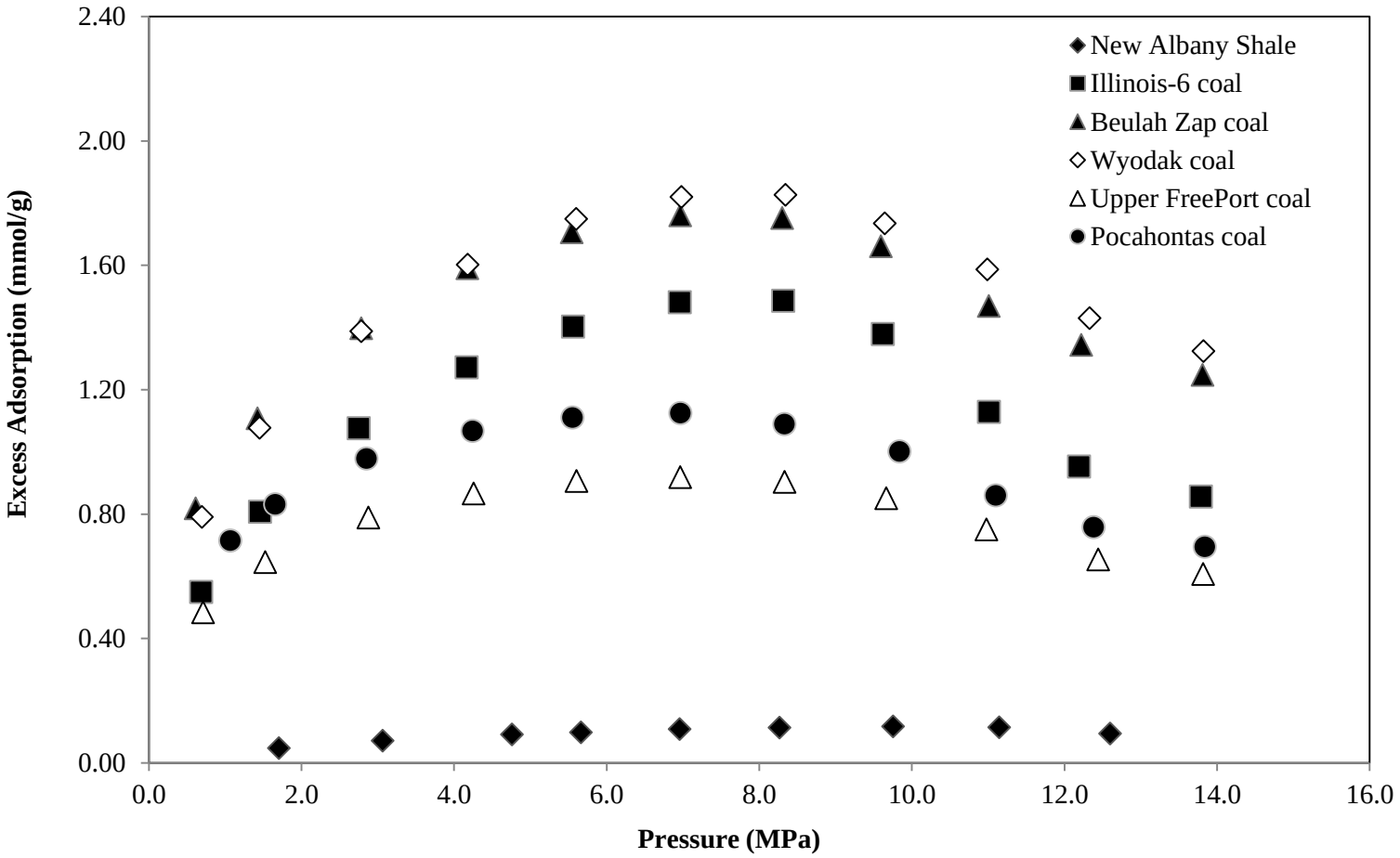

Figure 3.6. Comparison of CO_2 Adsorption on New Albany Shale and Argonne Coals at 328.2 K

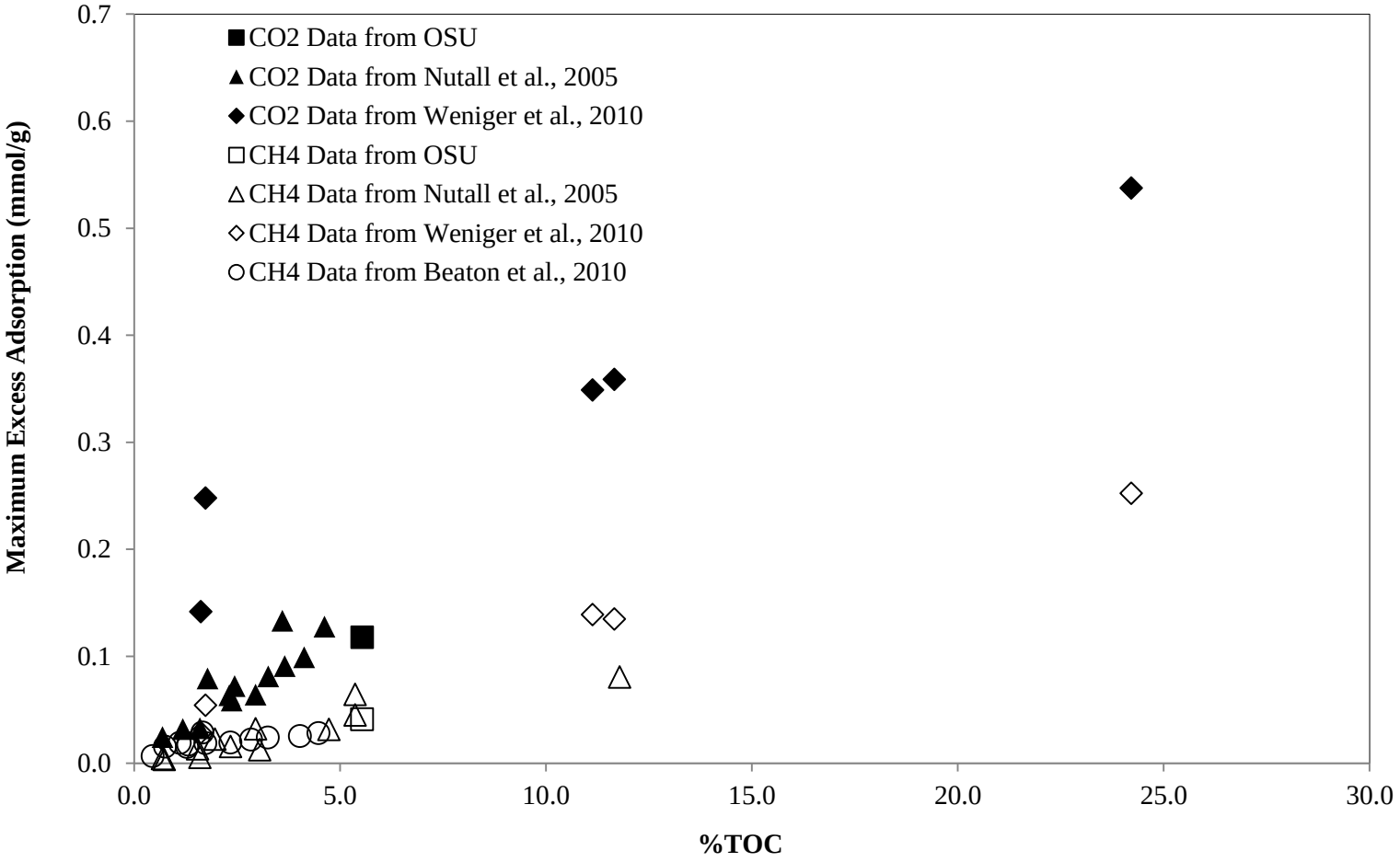

Figure 3.7. Maximum Excess Adsorption of CH_4 and CO_2 as a Function of Total Organic Carbon Content: Data from the Literature and Measured in this Study

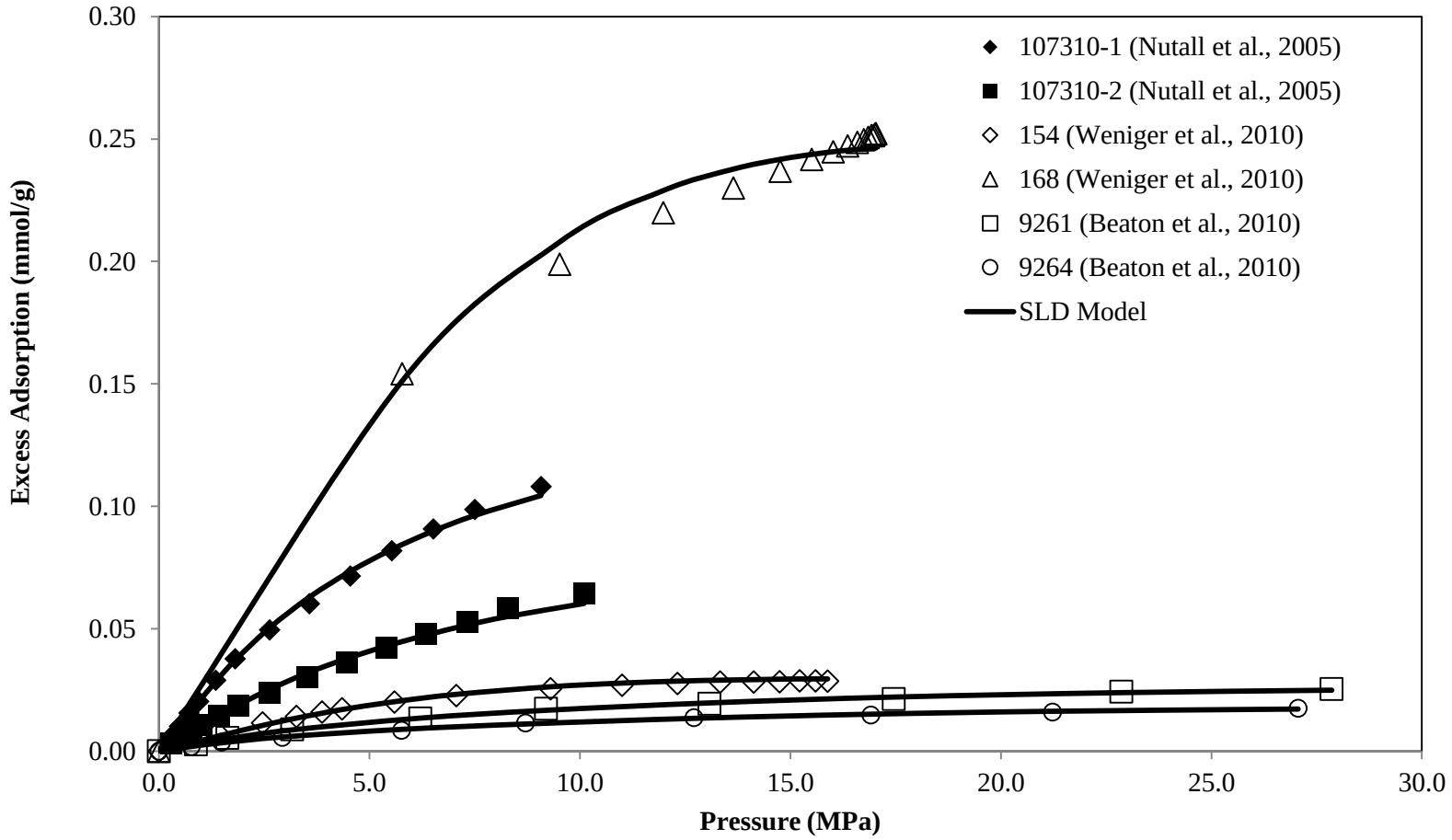

Figure 3.8. SLD Model Representations for CH_4 Adsorption on Shales: Data from the Literature

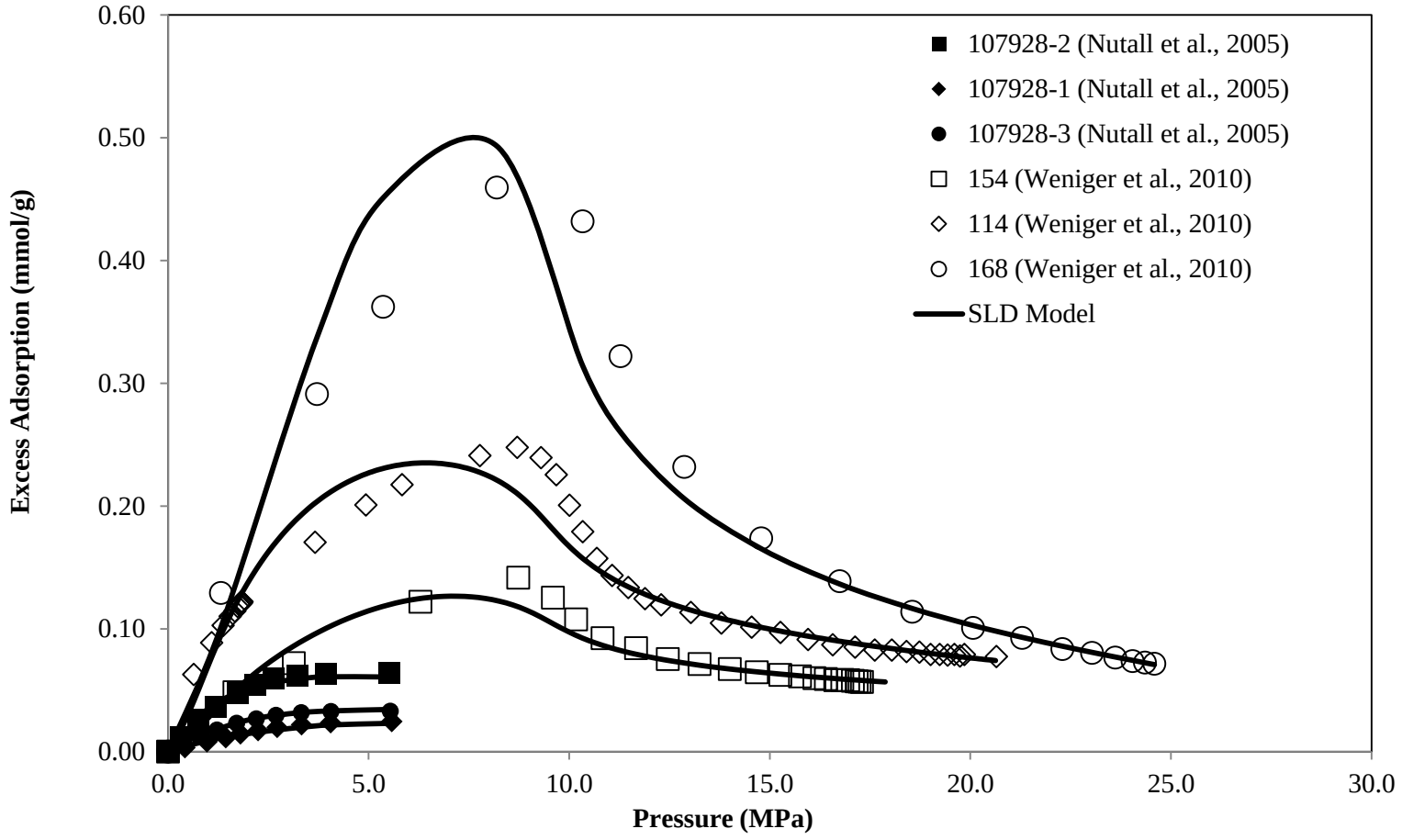

Figure 3.9. SLD Model Representations for CO_2 Adsorption on Shales: Data from the Literature

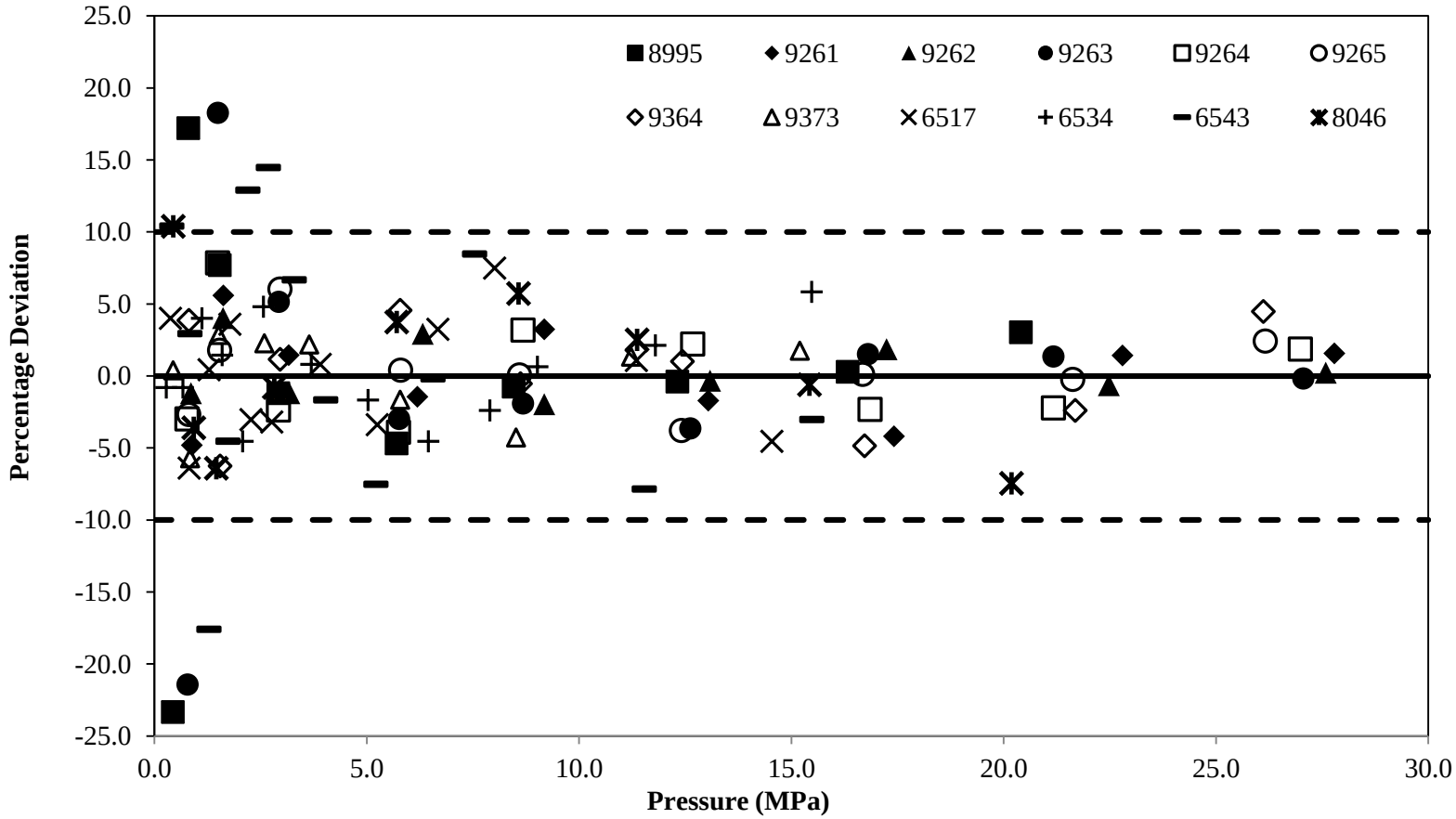

Figure 3.10(a). Percentage Deviation of SLD Model Representations for CH_4 Adsorption on Shales: Data from Beaton et al. [10]

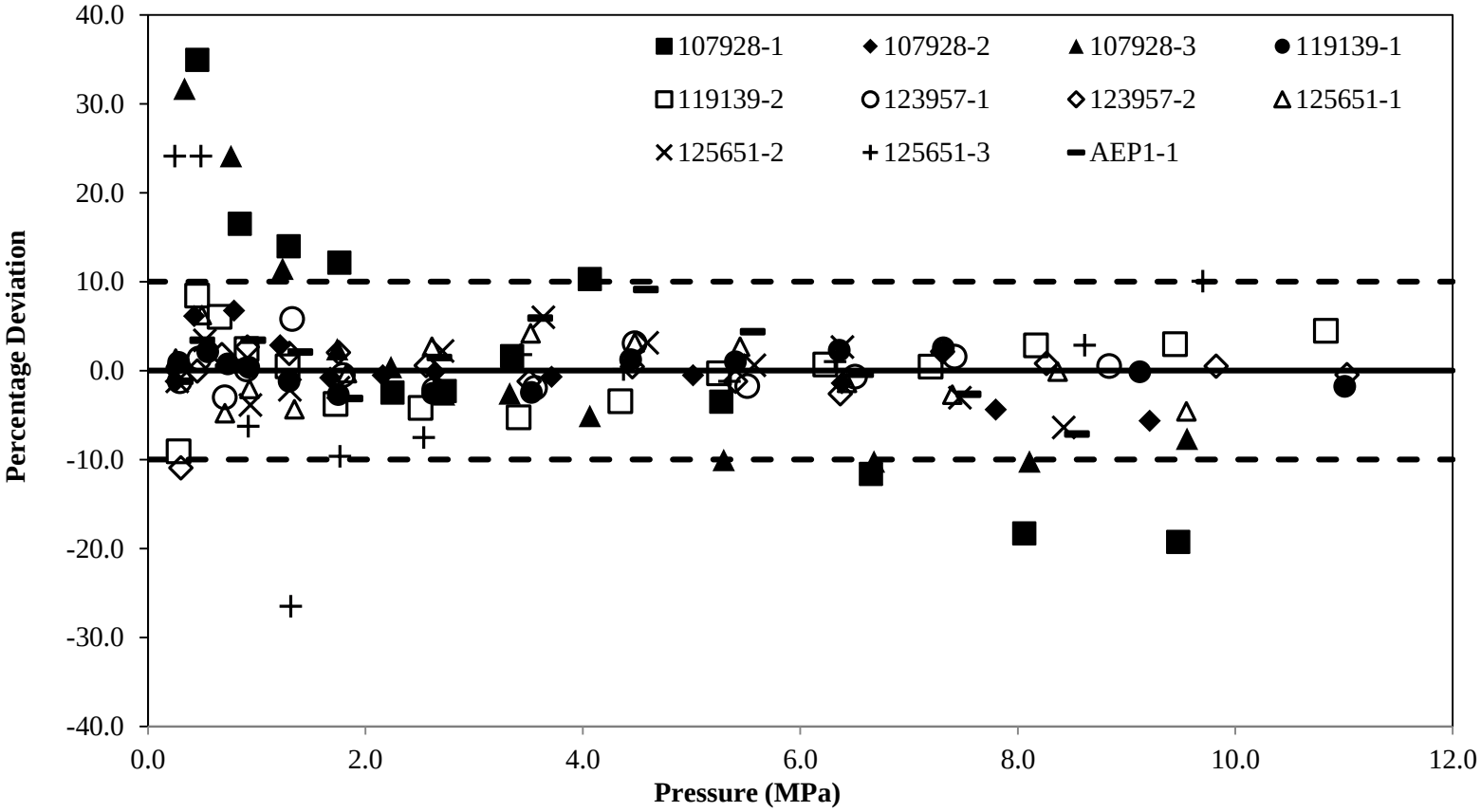

Figure 3.10(b). Percentage Deviation of SLD Model Representations for CH_4 Adsorption on Shales: Data from Nuttall et al. [8]

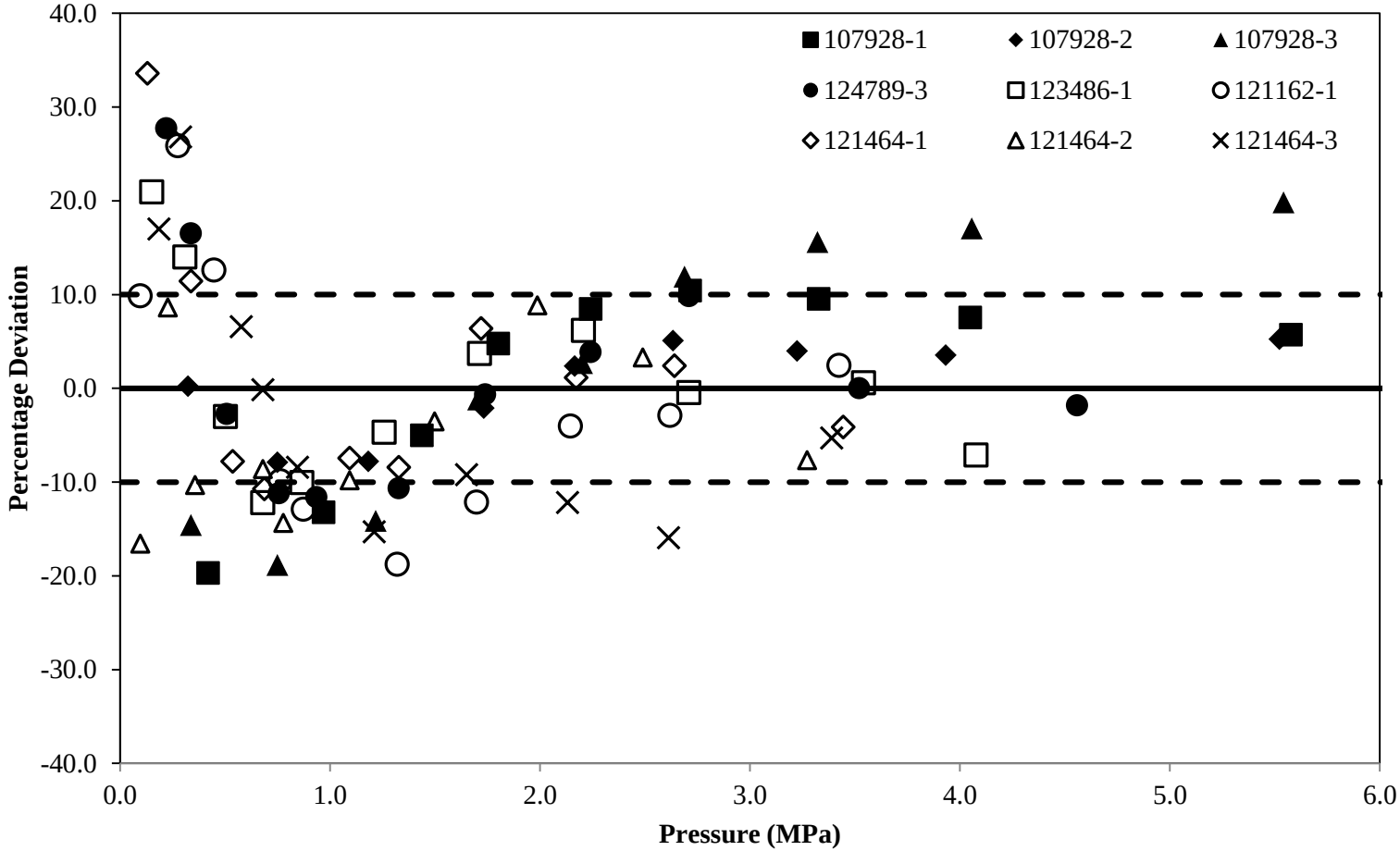

Figure 3.10(c). Percentage Deviation of SLD Model Representations for CO_2 Adsorption on Shales: Data from Nuttall et al. [8]

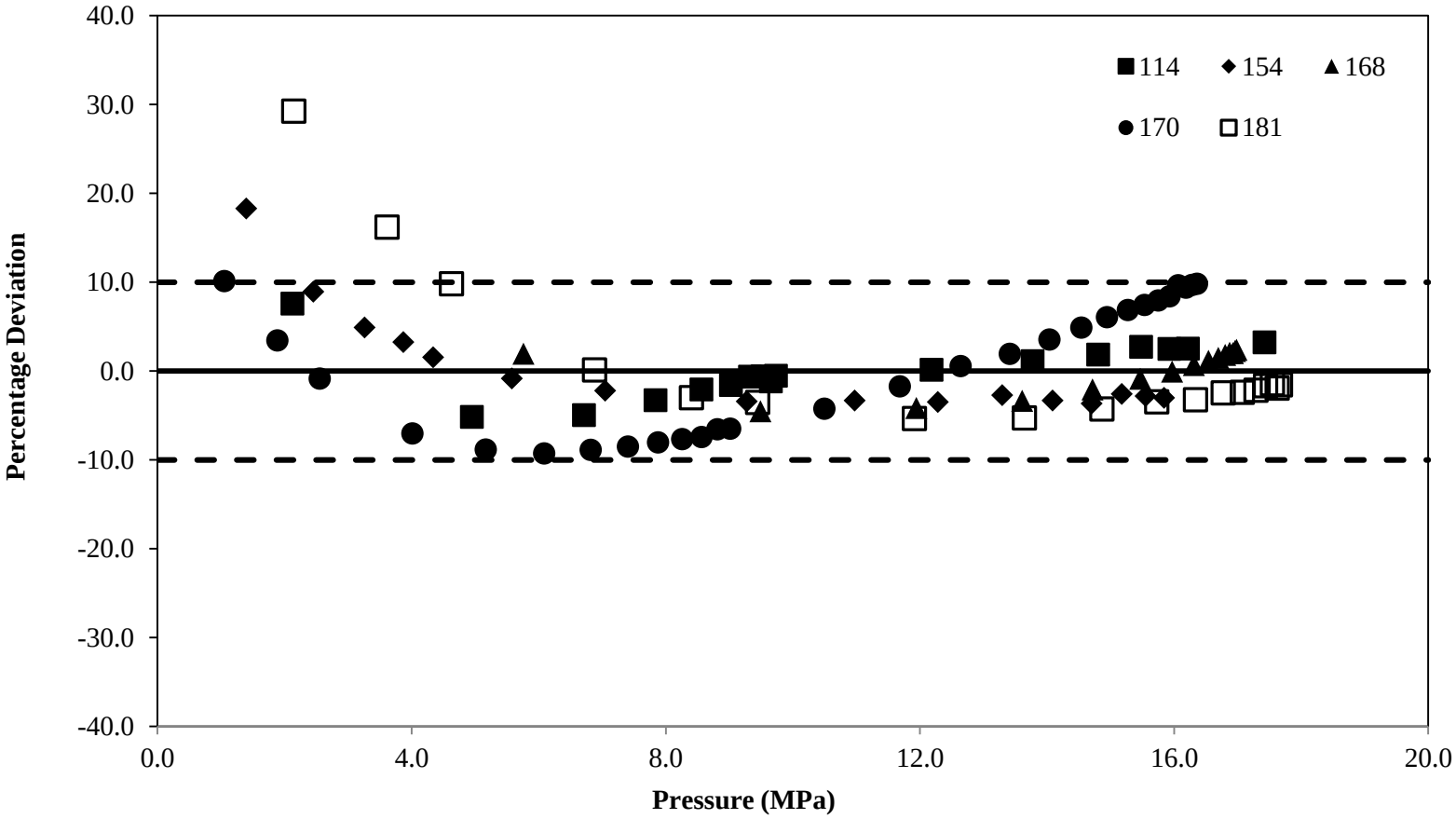

Figure 3.10(d). Percentage Deviation of SLD Model Representations for CH_4 Adsorption on Shales: Data from Weniger et al. [11]

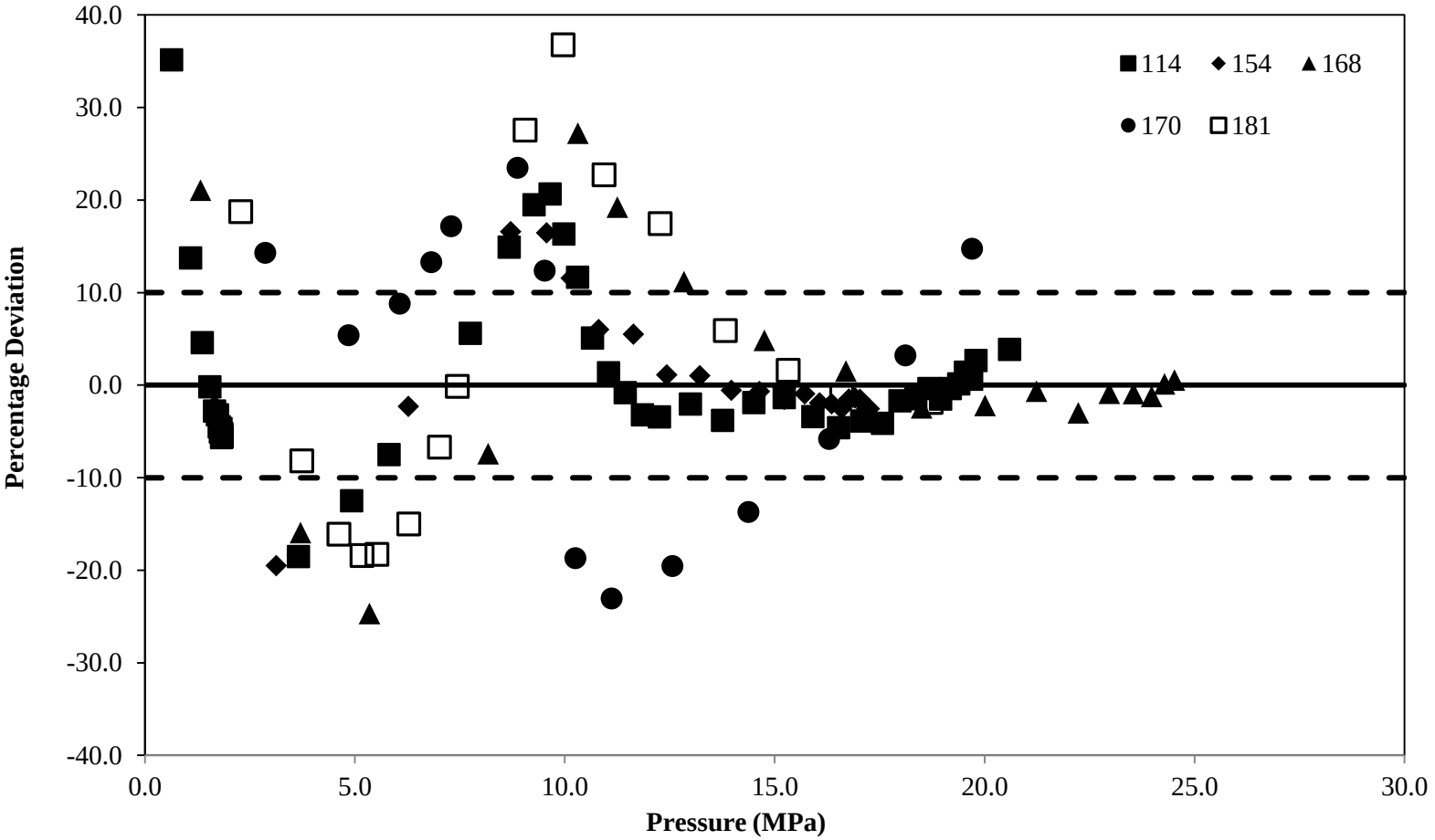

Figure 3.10(e). Percentage Deviation of SLD Model Representations for CO_2 Adsorption on Shales: Data from Weniger et al. [11]

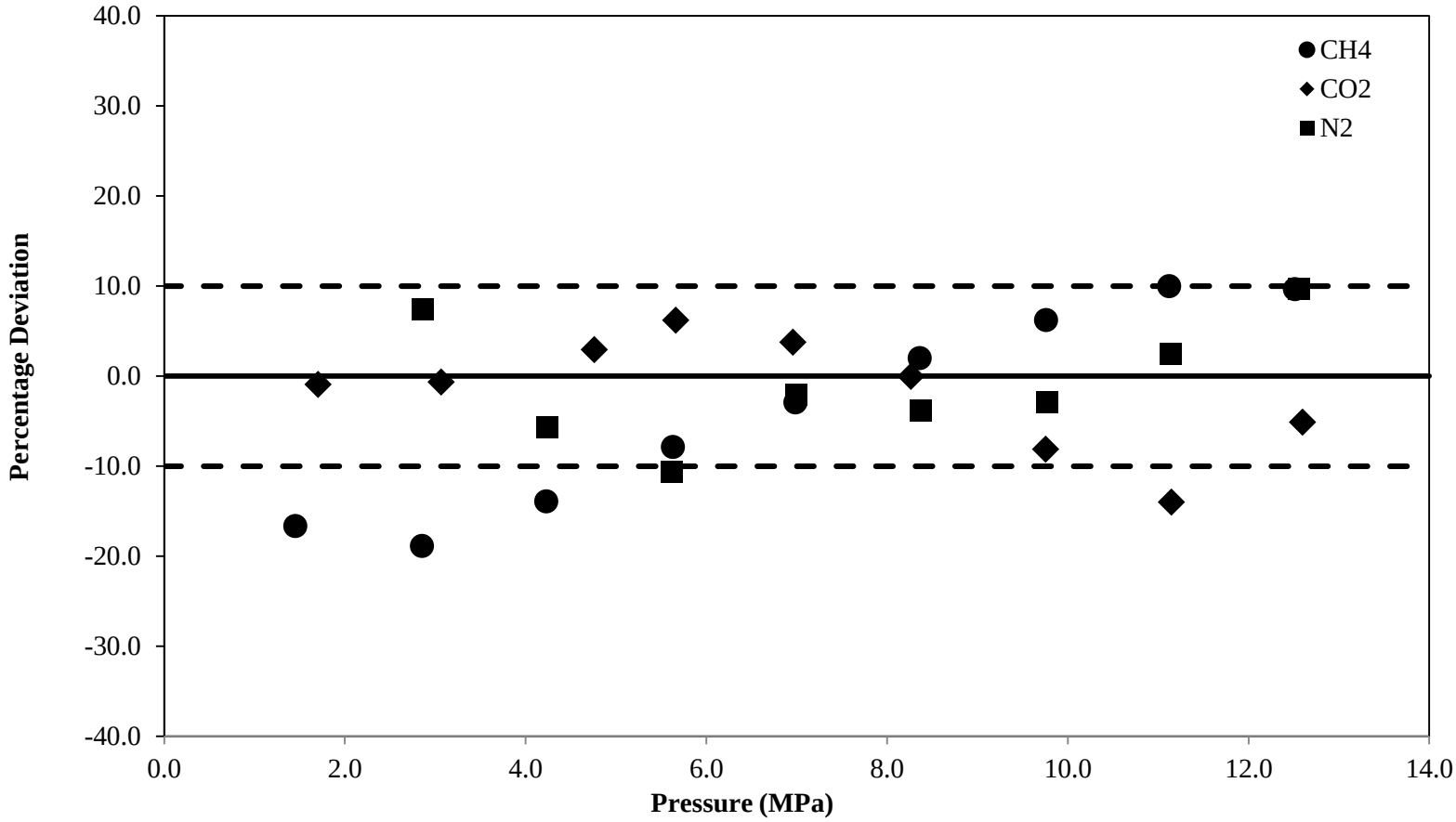

Figure 3.10(f). Percentage Deviation of SLD Model Representations for Pure-Gas Adsorption on New Albany Shale: Data Measured in this Study

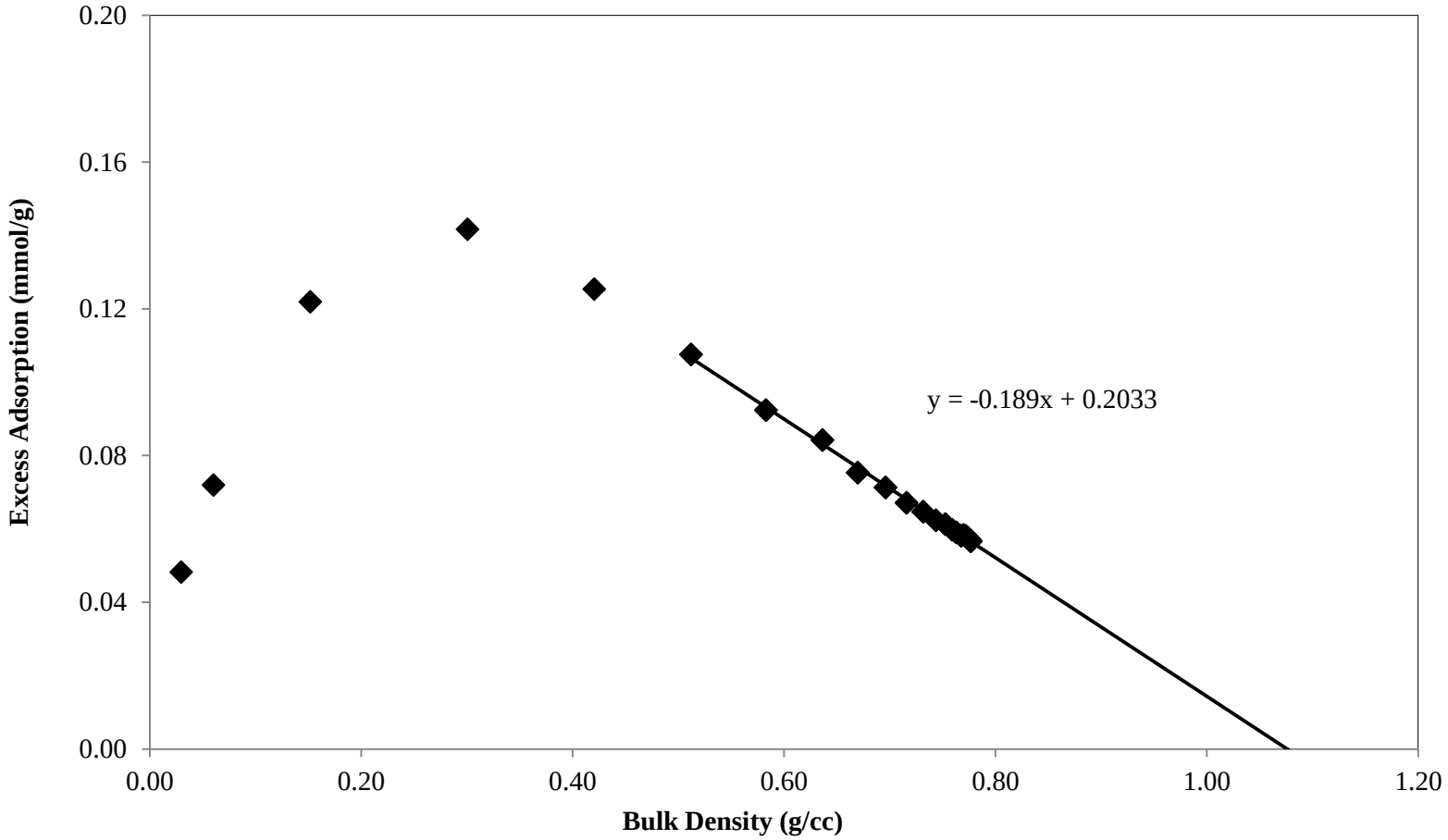

Figure 3.11. Graphical Estimation of CO_2 Adsorbed-Phase Density at 318 K: (Sample Number 154: Adsorption Data from Weniger et al. [11])

REFERENCES

1. EIA. Review of Emerging Resources: U.S. Shale Gas and Shale Oil Plays, U.S. Energy Information Administration. 2011 July 8, 2011 Accessed October 2011]; Available from: http://www.eia.gov/analysis/studies/usshalegas/.
2. White, C.M., et al., Sequestration of Carbon Dioxide in Coal with Enhanced Coalbed Methane Recovery-A Review. Energy Fuels, 2005. 19(3): p. 659-724.
3. Bachu, S., W.D. Gunter, and E.H. Perkins, Aquifer disposal of CO2: Hydrodynamic and mineral trapping. Energy Conversion and Management, 1994. 35(4): p. 269-279.
4. Busch, A., et al., Carbon dioxide storage potential of shales. International Journal of Greenhouse Gas Control, 2008. 2(3): p. 297-308.
5. Grimm, R.P., et al., Seal evaluation and confinement screening criteria for beneficial carbon dioxide storage with enhanced coal bed methane recovery in the Pocahontas Basin, Virginia. International Journal of Coal Geology, 2012. 90–91(0): p. 110-125.
6. Kalantari-Dahaghi, A. Numerical simulation and modeling of enhanced gas recovery and CO2 sequestration in shale gas reservoirs: A feasibility study. in SPE International Conference on CO2 Capture, Storage, and Utilization 2010. 2010. New Orleans, LA, U.S.A.: Society of Petroleum Engineers.
7. Bachu, S., Sequestration of CO2 in geological media in response to climate change: road map for site selection using the transform of the geological space into the CO2 phase space. Energy Conversion and Management, 2002. 43(1): p. 87-102.

8. Nuttall, B.C., et al., Analysis of Devonian Black shales in Kentucky for potential carbon dioxide sequestration and enhanced natural gas production, in Kentucky Geological Survey. 2005, University of Kentucky: Lexington, Kentucky.

9. Strąpoć, D., et al., Geochemical constraints on the origin and volume of gas in the New Albany Shale (Devonian–Mississippian), Eastern Illinois Basin AAPG Bulletin, 2010. 94: p. 1713-1740.

10. Beaton, A.P., et al., Total organic carbon and adsorption isotherms of the Duvernay and Muskwa formations in Alberta:shale gas data release. 2010, Energy Resources Conservation Board, ERCB/AGS: Edmonton, Alberta. p. 33.

11. Weniger, P., et al., High-pressure methane and carbon dioxide sorption on coal and shale samples from the Paraná Basin, Brazil. International Journal of Coal Geology, 2010. 84(3-4): p. 190-205.

12. Mohammad, S.A., et al., Adsorption of Pure Carbon Dioxide on Wet Argonne Coals at 328.2 K and Pressures up to 13.8 MPa. Energy & Fuels, 2009. 23(2): p. 1107-1117.

13. Hall, F., et al., Adsorption of Pure Methane, Nitrogen, and Carbon Dioxide and Their Binary Mixtures on Wet Fruitland Coal, in SPE Eastern Regional Conference & Exhibition, SPE Paper 29194. 1994: Charleston, S.C.

14. Sudibandriyo, M., et al., Adsorption of Methane, Nitrogen, Carbon Dioxide, and Their Binary Mixtures on Dry Activated Carbon at 318.2 K and Pressures up to 13.6 MPa. Langmuir, 2003. 19(13): p. 5323-5331.

15. Hall, F.E., Adsorption of Pure and Multicomponent Gases on Wet Fruitland Coal, in Chemical Engineering. 1993, Oklahoma State University: Stillwater.

16. Angus, S., B. Armstrong, and K.M. de Reuck, International Thermodynamic Tables of the Fluid State-5: Methane. IUPAC Chemical Data Series No.16. 1978, New York: Pergamon Press.

17. Angus, S., K.M. de Reuck, and B. Armstrong, International Thermodynamic Tables of the Fluid State-6: Nitrogen. IUPAC Chemical Data Series No.20. 1979, New York: Pergamon Press.

18. Span, R. and W. Wagner, A New Equation of State for Carbon Dioxide Covering the Fluid Region from the Triple Point Temperature to 1100 K at Pressures up to 800 MPa. J. Phys. Chem. Ref. Data, 1996. 25: p. 1509-1590.

19. McCarty, R.D., Thermophysical Properties of Helium-4 from 2 to 1500 K with Pressures to 1000 Atmospheres. 1972, U.S. Dept. of Commerce

20. Vorres, K.S., The Argonne Premium Coal Sample Program. Energy and Fuels, 1990. 4(5): p. 420-426.

21. Morse, D.G. 2012.

22. Dhima, A., J. de Hemptinne, and J. Jose, Solubility of Hydrocarbons and CO2 Mixtures in Water under High Pressure. Ind. & Eng. Chem. Res., 1999. 38(8): p. 3144-3161

23. King, A.D.J. and C.R. Coan, Solubility of Water in Compressed Carbon Dioxide, Nitrous Oxide and Ethane. Evidence for Hydration of Carbon Dioxide and Nitrous Oxide in the Gas Phase. J. Am. Chem. Soc., 1971. 93(8): p. 1857-1862.

24. Weibe, R. and V. Gaddy, The Solubility of Carbon Dioxide in Water at Various Temperatures from 12° to 40° and at Pressures to 500 Atmospheres, Critical Phenomena. J. Amer. Chem. Soc., 1940. 62 p. 815-817.

25. Lahann, R., et al., Influence of CO2 on New Albany Shale composition and pore structure. International Journal of Coal Geology, 2011(In Press): p. DOI: 10.1016/j.coal.2011.05.004.

26. Kumar, H., et al., Permeability Evolution of Shale and Coal Under Differential Sorption of He, CH4 And CO2. Presented at the 2010 Fall Meeting of the American Geophysical Union. 2010.

27. Mitra, A., S. Harpalani, and S. Liu, Laboratory measurement and modeling of coal permeability with continued methane production: Part 1 – Laboratory results. Fuel, 2012. 94(0): p. 110-116.

28. Fitzgerald, J.E., et al., Modeling the adsorption of pure gases on coals with the SLD model. Carbon, 2003. 41(12): p. 2203-2216.

29. Mohammad, S.A., et al., Generalized Simplified Local-Density/Peng-Robinson Model for Adsorption of Pure and Mixed Gases on Coals. Energy & Fuels, 2009. 23(12): p. 6259-6271.

30. Fitzgerald, J.E., R.L. Robinson, and K.A.M. Gasem, Modeling High-Pressure Adsorption of Gas Mixtures on Activated Carbon and Coal Using a Simplified Local-Density Model. Langmuir, 2006. 22(23): p. 9610-9618.

31. Rangarajan, B., C.T. Lira, and R. Subramanian, Simplified local-density model for adsorption over large pressure ranges. AIChE Journal, 1995. 41(4): p. 838-845.

32. Chen, J.H., et al., Adsorption and desorption of carbon dioxide onto and from activated carbon at high pressures. Industrial & Engineering Chemistry Research, 1997. 36(7): p. 2808-2815.

33. Puziy, A.M., et al., Modeling of high-pressure adsorption using the bender equation of state. Langmuir, 2003. 19(2): p. 314-320.

34. Soule, A.D., et al., Adsorption modeling with the ESD equation of state. Langmuir, 2001. 17(10): p. 2950-2957.

35. Yang, X. and C.T. Lira, Theoretical study of adsorption on activated carbon from a supercritical fluid by the SLD-ESD approach. Journal of Supercritical Fluids, 2006. 37(2): p. 191-200.

36. Fitzgerald, J.E., Adsorption of Pure and Multi-Component Gases of Importance to Enhanced Coalbed Methane Recovery: Measurements and Simplified Local-Density Modeling. 2005, Oklahoma State University: Stillwater, Oklahoma

37. Peng, D.-Y. and D.B. Robinson, A New Two-Constant Equation of State. Ind. Eng. Chem. Fund., 1976. 15(1): p. 59-64.

38. Gasem, K.A.M., et al., A Modified Temperature Dependence for the Peng-Robinson Equation of State. Fluid Phase Equilibria, 2001. 181(1-2): p. 113-125.

39. Lee, L.L., Molecular Thermodynamics of Non-ideal Fluids. 1988, Stoneham, MA Butterworth.

40. Steele, W.A., The Interaction of Gases with Solid Surfaces. 1974, Oxford: Pergamon Press.

41. Subramanian, R., H. Pyada, and C.T. Lira, Engineering model for adsorption of gases onto flat surfaces and clustering in supercritical fluids. Industrial & Engineering Chemistry Research, 1995. 34(11): p. 3830.

42. Reid, R.C., J.M. Prausnitz, and B.E. Poling, The Properties of Gases and Liquids. 1987, New York: McGraw-Hill

43. Mohammad, S.A., et al., High-Pressure Adsorption of Pure Gases on Coals and Activated Carbon: Measurements and Modeling. Energy & Fuels, 2011. 26(1): p. 536-548.

44. Lu, X.-C., F.-C. Li, and A.T. Watson, Adsorption Measurements in Devonian Shales. Fuel, 1995. 74(4): p. 599-603.

45. Lu, X., F.C. Li, and A.T. Watson. Adsorption Measurements in Devonian Shales. in Presented at the SCA Conference, Paper Number 9302. 1993.

46. Mohammad, S.A., et al., Experimental Uncertainties in Volumetric Methods for Measuring Equilibrium Adsorption. Energy & Fuels, 2009. 23(5): p. 2810-2820.

47. Mohammad, S.A., Adsorption modeling of coalbed gases and the effects of water on their adsorption behavior. 2009, Oklahoma State University.

48. Humayun, R. and D. Tomasko, High-resolution adsorption isotherms of supercritical carbon dioxide on activated carbon. AIChE Journal, 2000. 46(10): p. 2065-2075.

49. Lemmon, E.W., M.O. McLinden, and D.G. Friend, Thermophysical Properties of Fluid Systems in NIST Chemistry WebBook, NIST Standard Reference Database Number 69,

P.J. Linstrom and W.G. Mallard, Editors. 2012, National Institute of Standards and Technology,Gaithersburg MD, 20899, http://webbook.nist.gov (retrieved October 5, 2011).

CHAPTER IV

HIGH-PRESSURE ADSORPTION OF GASES ON WOODFORD AND CANEY SHALES FROM OKLAHOMA

4.1 Introduction

The rapid increase in natural gas consumption in the U.S. has stimulated the recovery of natural gas from unconventional resources such as coals and shales. Due to the recent technique of horizontal drilling in conjunction with hydraulic fracturing, the recovery of natural gas from shale reservoirs has increased significantly in the past few years [1]. Among shale reservoirs in the U.S., shales in Oklahoma (primarily Woodford and Caney shales) contain significant amounts of technically recoverable natural gas [2]. A recent study released by the U.S. Energy Information and Administration (EIA) reported that the Woodford shale is ranked among the top five U.S shale plays that produce natural gas commercially [3].

In addition to natural gas interests, numerous studies have evaluated the potential of shale reservoirs for possible use as CO_2 geological sinks. Nuttall et al. [4] estimated the CO_2 sequestration capacity in Devonian black shales and Big Sandy gas field in Kentucky and showed that a large volume of CO_2 can be stored in these shale plays. Kang et al. [5] provided mass-transport paths and mechanisms of CO_2 uptake in shales and identified that some micropores in organic matter acted as molecular sieves that allowed only linear molecular geometry such as CO_2 to access. Recently, Tao and Clarens [6] used a commutated method based on the kinetics of mass transport to estimate CO_2 sequestration capacity and time required to fill up the Marcellus shale reservoir with CO_2.

The results obtained from their computational work reveal that fractured shales may store a large amount of CO_2. Further, Tao and coworkers noted that despite having low permeability, the fractured shale can sequester CO_2 approximately five times faster than the time that the reservoir would require for completion of the methane recovery process.

As outlined above, shale reservoirs have attracted increased attention as a result of their abundant natural gas and their potential for CO_2 sequestration. Since a significant fraction of the gas in shale reservoirs is in an adsorbed state, the modeling of gas adsorption behavior is needed for developing gas-in-place estimates and conducting feasibility studies for CO_2 sequestration in shale-gas reservoirs. Two important elements for modeling gas adsorption behavior are (1) adsorption data measured at reservoir operating temperatures and pressures, and (2) a reliable model capable of describing accurately the adsorption behavior.

4.1.1 Previous Experimental Studies

Recently, several publications [7-12] have provided adsorption databases for shales. These publications focus mostly on adsorption of methane and studies of shale composition (i.e., types of organic carbon kerogen, types of mineral matter, etc.), maturity of the shale and shale pore structure that control the adsorption capacity of methane. Beaton et al. [7] measured methane adsorption isotherms on several shale samples from the Duvernay, Muskwa, Banff and Exshaw formations. Zhang et al. [8] investigated effects of organic-matter type and thermal maturity on methane adsorption on diverse shales. Wang et al. [9] measured methane adsorption capacity on Paleozoic shales from the Sichuan basin, China and investigated the effect of TOC and clay mineral content on adsorption capacity of methane. Rexer et al. [10] measured high-pressure adsorption of methane and pore characteristics on oil-window immature and gas-window mature samples from the Posidonia shale formation. Rexer and coworkers also found that apart from primary adsorption on organic carbon, methane adsorption on mineral content was significant on relatively dry shales.

Gasparik et al. [11] investigated constituents in Paleozoic and Mesozoic shales that control methane storage in these organic-rich shales. Hu et al. [12] studied the effect of thermal maturity induced by hydrous pyrolysis on methane adsorption on Woodford shale. Tan et al. [13] evaluated the gas potential of a shale formation from Yangtze platform in China by measuring adsorption capacities of methane on shales extracted from the platform.

To date, few publications have provided adsorption capacity of CO_2 on shales. Nuttall et al. [4] reported methane and carbon dioxide adsorption isotherms on the New Albany shales and Ohio shales extracted from various depths below the surface. Busch et al. [14] investigated CO_2 storage potential on Muderong shale. Weniger et al. [15] investigated the high-pressure adsorption behavior of methane and carbon dioxide on several coal and shale samples from the Paraná Basin, Brazil. Chareonsuppanimit et al. [16] measured high-pressure adsorption of methane, nitrogen and CO_2 on the New Albany shale. Khosrokhavar et al. [17] measured adsorption of methane and CO_2 on a carboniferous shale from Belgium.

4.1.2 Previous Models for Adsorption

Adsorption information is crucial for the modeling of gas production/storage processes in shale reservoirs. Several adsorption models have been used with varying success by authors for modeling gas adsorption on shales. These models include the Modified-Langmuir model [8, 10-13, 15], Ideal-Adsorption-Solution (IAS) Theory, Dubinin-Radushkevich (D-R) adsorption model and Two-Dimensional EOS model [18]. Among these adsorption models, the Simplified Local-Density model has been successful in describing gas adsorption on activated carbons, coals [31, 32] and shales [16]. Further, the SLD model parameters were generalized successfully based solely on surface characterization information [31]. The attributes possessed by the model and the desire to continue our prior development of the model [16] led to the selection of the SLD model for the present study.

Accordingly, the specific objectives of this work are to (1) enrich the adsorption database for shale, specifically for CO_2 adsorption at high pressures, (2) investigate the relation between adsorption behavior and shale compositional analyses such as TOC content, ash content, etc., (3) continue testing the viability of the SLD model for describing adsorption behavior with the new shale data, and (4) investigate the relation between the SLD model parameters and the shale composition.

To achieve our objectives, we investigated the high-pressure adsorption behavior of methane, nitrogen and CO_2 on Woodford shales from Payne and Hancock counties and Caney shale at 328.2 K and pressures up to 12.4 MPa. Data were obtained using our existing apparatus [16, 19], which utilizes a volumetric method of measuring adsorption. Then, the newly acquired data were described using the SLD model.

Details of this chapter are presented as follows: Section 4.2 provides the experimental procedures used in this study; Section 4.3 describes the SLD model and the modeling methodology; and Section 4.4 presents the experimental and modeling results.

4.2 Experimental Methods and Procedures

4.2.1. Adsorption Measurements

The experimental method used in this study employs the volumetric method of measuring adsorption isotherms. The volumetric method is based on the mass balance principle and requires precise measurements of pressure, volume and temperature. The experimental apparatus, shown schematically in Figure 4.1, has been used successfully in previous measurements [16, 19-21].

Briefly, the entire apparatus is maintained in a constant temperature air bath. The equilibrium cell (Figure 4.1) is filled with the adsorbent to be studied, and the cell is placed under vacuum prior to gas injection. The void volume, V_{void}, in the equilibrium cell is then determined by injecting a known quantity of helium from a calibrated injection pump (Ruska). Since helium adsorption is

considered negligible at these conditions, the void volume can be determined from measured values of the temperature, pressure and amount of helium injected into the cell.

The mass balance equation is:

$$V_{void} = \frac{\left(\frac{P\Delta V}{ZT}\right)_{pump}}{\left(\frac{P_2}{Z_2 T} - \frac{P_1}{Z_1 T}\right)_{cell}} \tag{4.1}$$

where ΔV is the volume of the gas injected from the pump, Z is the compressibility factor of helium, T is the temperature, P is the pressure, subscripts "cell" and "pump" refer to conditions in the cell and pump sections of the apparatus, respectively, and "1" and "2" refer to conditions in the cell before and after injection of gas from the pump, respectively. The helium void volume measurements were performed at the same temperature as the gas adsorption isotherms (328.2 K) and over a range of pressures from atmospheric to about 12.4 MPa (1800 psia) in intervals of 1.4 MPa (200 psia).

Generally, the void volume calculated from sequential injections varied less than 0.3 cm^3 from the average value of approximately 60 cm^3 for the measurements in this study. The helium void volume includes all the volume of the cell section exclusive of the adsorbent volume that is impenetrable to helium gas. The constancy of the calculated void volume from the incremental injections over a range of pressures confirmed our assumption that adsorption of helium is negligible at the conditions of the measurements.

The excess adsorption can be calculated directly from experimentally measured quantities. For pure-gas adsorption measurements, a known quantity, n_{inj}, of gas (e.g., methane) is injected from the pump section into the cell section. Some of the injected gas will be adsorbed, and the remainder,

n^{Ex}_{unads}, will exist in the equilibrium bulk gas phase in the cell. A material balance is used to calculate the amount adsorbed, n^{Ex}_{ads}, as

$$n^{Ex}_{ads} = n_{inj} - n^{Ex}_{unads} \tag{4.2}$$

The amount injected can be determined from pressure, temperature and volume measurements of the pump section

$$n_{inj} = \left(\frac{P\Delta V}{ZRT}\right)_{Pump} \tag{4.3}$$

The amount of unadsorbed gas is calculated from conditions at equilibrium in the cell

$$n^{Ex}_{unads} = \left(\frac{P V_{void}}{ZRT}\right)_{Cell} \tag{4.4}$$

where the pressure P is the equilibrium pressure, and Z is the compressibility factor of the gas. The cell pressure was recorded periodically and equilibrium was indicated by the constancy of the recorded pressure (usually within 6 to 12 hours). Further, prior to measuring adsorption isotherms, the apparatus was checked for pressure leaks. The adsorption isotherms were measured only when no leaks were observed in the system over a period of 24 hours.

The above steps are repeated at sequentially higher pressures to measure a complete adsorption isotherm. The amount adsorbed is presented as mmol/g of shale on a mass basis (1 mmol/g = 759 SCF/ton). Equations 4.2-4.4 show that the amount adsorbed may be calculated in a straightforward manner from the experimental measurements of pressures, temperatures and volumes, coupled with independent knowledge of the gas compressibility factors, Z, from an accurate equation of state.

Frequent instrument calibrations were conducted during the course of the experiments. The thermocouples and RTDs were calibrated against a Minco platinum reference RTD. Super TJE

pressure transducers (range: 0 – 13.8 MPa) were calibrated using helium as the working fluid against a Ruska deadweight tester with a calibration traceable to the National Institute of Standards and Technology. Detailed information on calibration is available elsewhere [22]. The uncertainties in the experimentally measured quantities after calibrations were estimated as follows: temperature, 0.1 K; pressure, 6.9 kPa; and injected gas volume, 0.02 cm^3.

4.2.2 Gas Compressibility Factors

As evident from the above equations, compressibility factors are required for the pure gases for proper data analysis. The compressibility factors for the pure gases were calculated from highly accurate equations of state [23-25]. For void volume determination, the helium compressibility factor was calculated with an expression based on experimental data from the National Bureau of Standards Technical Note 631 for helium [26].

4.2.3 Materials

The pure gases used in this study were obtained from Airgas with reported purities of 99.99% and were used as-received. The shale samples were provided by Dr. James Puckette from the School of Geology, Oklahoma State University, U.S.A. The Woodford shale from Payne county was retrieved at 4250 feet below the surface, the Woodford shale from Hancock county was retrieved at about 17730 feet below the surface, and the Caney shale was retrieved at 7366-7377 feet below the surface. The samples were pulverized and were stored in an inert environment to avoid possible oxidation until their use for measuring the adsorption isotherms. The gas adsorption isotherms were measured on the "as-received" sample without any drying of the sample. Table 4.1 presents the compositional analysis of the shale samples in this study. The analysis was conducted by Huffman Laboratory, Colorado, U.S.A. The Woodford shale from Payne county contains about 8.5% total organic carbon (TOC), 1% moisture and 84% ash content, the Woodford shale from Hancock

county contains about 6.4% TOC, 0.8% moisture and 86% ash and the Caney shale contains about 2% TOC, 1.7% moisture and 92% ash.

4.2.4 Gas Solubility in Water

In previous studies at Oklahoma State University (OSU) on wet/moist adsorbents [19, 20], we included a term in Equation (4.2) to account for the amount of gas, n_{sol}, dissolved in the water (rather than adsorbed on the coal surface).

$$n_{ads}^{Ex} = n_{inj} - n_{unads}^{Ex} - n_{sol} \tag{4.5}$$

To calculate the gas solubility in water as a function of pressure, an empirical equation was used for temperatures around 318 K.

$$x_{gas} = \frac{P}{a + bP + cP^2} \tag{4.6}$$

Since the solubilities of methane and nitrogen in water are small; the same equation and parameter values were used at other temperatures (e.g., 328.2 K in this study). Table 4.2 lists the values of parameters in Equation (4.6).

In comparison to nitrogen and methane, the solubility of CO_2 is significant at temperatures near 318 K. To calculate the gas dissolved in water for use in Equation (4.5), literature data [27-29] were used to construct an empirical relationship for CO_2/water solubility at temperatures from 313.2 K to 348.2 K. In the 0-15 MPa range, the empirical function represents their data with an average absolute deviation of 1.5%. Thus, the mole fraction of CO_2 present in water at temperature T (in K) and pressure P (in MPa) is given as:

$$x_{CO2} = \frac{P}{a + (b_1 + b_0 T)P + (c_1 + c_0 T)P^2} \tag{4.7}$$

The amount of CO2 dissolved in water can be given as

$$n_{sol} = \frac{x_{co_2} n_{water}}{(1 - x_{co_2})} \tag{4.8}$$

The denominator in Equation (4.8) is close to unity and therefore, the amount of gas dissolved in water was taken (approximately) as the product of mole fraction of CO_2 and the amount of water in moles in the system. Thus, the amount of CO_2 dissolved in water per unit mass of coal is expressed as

$$n_{sol} \approx \frac{x_{co_2} n_{water}}{m_{coal}} \tag{4.9}$$

where n_{water} is the amount of water in moles and m_{coal} is the mass of coal in the system.

The solubility of CO_2 in water calculated with Equation (4.7) is a monotonic increasing function of pressure at a given temperature. Thus, the maximum solubility of CO_2 in water was observed at 12.4 MPa and was about 2 mole percent. Table 4.3 lists the values of parameters in Equation (4.7).

As evident from the above discussion (Equation 4.5), accounting for the solubility of gas in water-rich adsorbed phase lowers the calculated excess adsorption values. In the above discussion, we have assumed that all the water present in the system is adsorbed and, therefore, the amount of gas dissolved in water was estimated based on all the water present in the system. In other words, all the water present in the adsorbent was considered to be accessible to the gas. Further, we assumed that the bulk gas-phase was water-free.

Due to the low levels of moisture present in the Woodford shale samples, the correction for gas solubility in water was quite small. The difference in amounts of gas adsorbed (with and without solubility correction) ranged from 2-6% of the gas adsorbed. Thus, the correction was not significant when compared with the experimental uncertainties of the isotherms. However, the

moisture content present in the Caney shale was higher than the Woodford shales. The higher presence of moisture does affect the dissolution of CO_2 in water. The difference in calculated amounts of gas adsorbed ranged from 10-15%. Thus, the correction for gas dissolved in water may be significant in samples that have higher moisture content.

4.3 Adsorption Model

4.3.1 Simplified Local-Density (SLD) Model

The SLD model envisions the adsorbent to be composed of rectangular-shaped slits and the adsorbate molecules reside within these two-surface slits. A molecule within a slit has interactions with both walls of the adsorbent slit. The SLD model accounts for both fluid-fluid and fluid-solid interactions in the slit-shaped pore. The model was first developed by Rangarajan et al. [30], who used the van der Waals equation of state (EOS) to account for the fluid-fluid interactions. Following our earlier work [31, 32], the Peng-Robinson EOS is used in this work. The following paragraphs provide the essential details of the SLD model as used in this work.

At equilibrium, the chemical potential of the fluid, μ, is expressed as the sum of the fluid-fluid and fluid-solid potentials at a position, "z", between the slit surfaces, as follows:

$$\mu(z) = \mu_{ff}(z) + \mu_{fs}(z) = \mu_{bulk} \tag{4.10}$$

where subscript "bulk" refers to the bulk fluid and "ff" and "fs" refer to the fluid-fluid and fluid-solid interactions, respectively. The equation shows how the chemical potential of the adsorbed fluid reflects the proximity of the fluid to the molecular wall of the adsorbent. Thus, the SLD model considers the inhomogeneity of the adsorbed phase in describing the molecular interactions of the adsorbed fluid with the adsorbent. The chemical potential of the bulk fluid can be expressed in terms of fugacity as

$$\mu_{bulk} = \mu_0(T) + RT \ln \frac{f_{bulk}}{f_0} \tag{4.11}$$

where subscript "0" designates an arbitrary reference state and "f" refers to fugacity. Similarly, the chemical potential from fluid-fluid interactions is given as

$$\mu_{ff}(z) = \mu_0(T) + RT \ln \frac{f_{ff}(z)}{f_0} \tag{4.12}$$

where "$f_{ff}(z)$" is fluid fugacity at position z and "f_0" refers to the same arbitrary reference state as in Equation (4.10).

The fluid-solid interactions in the model are accounted for through a potential energy function. In particular, the fluid-solid potential is given as

$$\mu_{fs}(z) = N_A\left[\Psi^{fs}(z) + \Psi^{fs}(L - z)\right] \tag{4.13}$$

where "N_A" is Avogadro's number, "$\Psi(z)$" and "$\Psi(L-z)$" are the fluid-solid interactions for the two surfaces of a slit of length L.

Substituting Equations (4.11), (4.12) and (4.13) into Equation (4.10) provides the equilibrium relationship for adsorption within the slit:

$$f_{ff}(z) = f_{bulk}\exp\left(-\frac{\Psi^{fs}(z) + \Psi^{fs}(L - z)}{kT}\right) \tag{4.14}$$

where k is the Boltzmann's constant.

Applying the SLD model, the excess adsorption (n^{Ex}) is given as

$$n^{Ex} = \frac{SA}{2}\int_{\text{Left Side of Slit}}^{\text{Right Side of Slit}} (\rho(z) - \rho_{bulk})\, dz \tag{4.15}$$

where n^{Ex} is the excess adsorption of adsorbate in number of moles per unit mass of adsorbent, and "SA" is the surface area of the adsorbate on a particular solid. The lower limit in Equation (4.15) is $3/8\ \sigma_{ff}$, which is 3/8 of the diameter of an adsorbed molecule touching the left plane surface. The upper limit is $L-3/8\sigma_{ff}$, the location of an adsorbed molecule touching the right plane

surface. The local density is assumed to be zero for the distances less than $3/8\sigma_{ff}$ away from the wall. The left and right sides of the slit each comprise half of the total surface area, SA/2.

The fluid-solid interaction, $\Psi^{fs}(z)$, was represented by Lee's partially-integrated 10-4 potential [33], which is a truncated form of Steele's 10-4-3 potential [34]

$$\Psi^{fs}(z) = 4\pi\rho_{atoms}\varepsilon_{fs}\sigma_{fs}^2\left(\frac{\sigma_{fs}^{10}}{5(z')^{10}} - \frac{1}{2}\sum_{i=1}^{4}\frac{\sigma_{fs}^4}{(z'+(i-1)-\sigma_{ss})^4}\right) \tag{4.16}$$

$$\varepsilon_{fs} = \sqrt{\varepsilon_{ff} \times \varepsilon_{ss}} \tag{4.17}$$

where ε_{fs} and ε_{ss} are the fluid-solid and solid-solid interaction energy parameters, respectively, and ρ_{atoms} = 0.382 atoms/Å^2. The parameters σ_{ff} and σ_{ss} signify, respectively, the molecular diameter of the adsorbate and the carbon interplanar distances. The carbon interplanar distance was taken to be the value for graphite, 0.335 nm [35] and values of σ_{ff} and ε_{ff} were taken from Reid et al. [36]. The fluid-solid molecular diameter, σ_{fs} and dummy coordinate z' used in numerical integration of Equation (4.16) are defined as:

$$\sigma_{fs} = \frac{\sigma_{ff} + \sigma_{ss}}{2} \tag{4.18}$$

$$z' = z + \frac{\sigma_{ss}}{2} \tag{4.19}$$

4.3.2 Modeling Methodology

For describing the pure-gas adsorption of three gases (i.e. methane, nitrogen and CO_2), the SLD model requires five parameters. They include the three surface areas, A_i, (one for each gas), solid-solid interaction energy, ε_{ss}/k, and the slit length, L. Thus, there is only one *gas-specific* parameter (A_i) for each gas. In particular, the accessible surface area, A_i, is specific to the adsorbing gas species whereas the other two parameters (solid-solid interaction energy and slit length) are the

same for all gases on a specific adsorbent. Thus, only five parameters are required for simultaneous representation of pure-gas adsorption of *three* gases.

The objective function (OF) used in the model regressions was the weighted root-mean-squared (WRMS) expressed as:

$$OF = \sqrt{\frac{\sum_{i=1}^{NPTS} \left(\frac{n_{cal} - n_{exp}}{\sigma_{exp}}\right)_i^2}{NPTS}} \tag{4.20}$$

where, n_{cal} is the calculated excess adsorption, n_{exp} is experimental excess adsorption, σ_{exp} is estimated experimental uncertainties in the adsorption data and NPTS is number of data points.

Additional statistics for SLD model representations are also provided:

Percent average absolute deviation:

$$\%AAD = \frac{\sum_{i=1}^{NPTS} \left|\frac{n_{cal} - n_{exp}}{n_{exp}}\right|_i}{NPTS} \times 100\% \tag{4.21}$$

Root-mean-squared error:

$$RMSE = \sqrt{\frac{\sum_{i=1}^{NPTS} (n_{cal} - n_{exp})_i^2}{NPTS}} \tag{4.22}$$

Weighted average absolute deviation:

$$WAAD = \frac{\sum_{i=1}^{NPTS} \left|\frac{n_{cal} - n_{exp}}{\sigma_{exp}}\right|_i}{NPTS} \tag{4.23}$$

4.4 Results and Discussion

4.4.1. Methane, Nitrogen and CO_2 Adsorption Isotherms

Adsorption of gases on the Woodford shales from Payne and Hancock counties and the Caney shale were measured using the high pressure adsorption apparatus illustrated in Figure 4.1. (In the following discussion the "Woodford Payne" refers to the Woodford shale from Payne county and the "Woodford Hancock" refers to the Woodford shale from Hancock county.) Tables 4.4(a)-(c) provide the newly acquired data for the adsorption of methane, nitrogen and CO_2 at 328.2 K and pressures up to 12.4 MPa on these shales. The tables list pressure, excess adsorption and expected experimental uncertainty for each datum. These uncertainties were calculated using propagation of errors [16]. The absolute errors are probably more meaningful than percentage errors for interpretation of gas adsorption data on shales due to their low adsorption nature [16]. The average expected experimental uncertainties for methane, nitrogen and CO_2 adsorption are, respectively, 0.0067, 0.0058 and 0.0260 on the Woodford Payne, 0.0062, 0.0051 and 0.0241 on the Woodford Hancock and 0.0069, 0.0057 and 0.0268 on the Caney shale.

Figures 4.2(a)-(c) present the adsorption isotherms for methane, nitrogen and CO_2 on the Woodford Payne, the Woodford Hancock and the Caney shales respectively. Error bars on each datum are the expected experimental uncertainty. The solid lines in these figures are SLD model representations, which are described in Section 4.4.4. As shown in these figures, the methane and nitrogen adsorption isotherms exhibited a Langmuir-type curve whereas the CO_2 isotherms exhibited a cusp-like curve which had a maximum adsorption at a pressure of about 9.7 MPa.

4.4.2 Effect of Organic Carbon on Gas Adsorption

To compare the excess adsorption of the three gases, the adsorption ratios at about 7 MPa were determined for each shale. The $N_2/CH_4/CO_2$ ratios were 1/2.9/6.1 on the Woodford Payne, 1/3.0/12.8 on the Woodford Hancock and 1/3.5/30.1 on the Caney shale. These ratios indicate that CO_2 was adsorbed on these shales more than other gases. This may be attributed to (1) hydrogen bond formed between organic functional groups (i.e., hydroxyl and carboxylic groups) and CO_2

[37], and (2) porous organic matter in shales that acted as a molecular sieve which allowed only a linear molecular structures such as CO_2 to access [5] the pores. Further, the CH_4/CO_2 ratio on these samples (ranged from about 1/2.1 to 1/8.6) were higher than the CH_4/CO_2 ratios observed in other carbon-based adsorbents such as activated carbon and coals [31, 32]. The higher CH_4/CO_2 adsorption ratio in shales is also seen in prior studies [15, 16]. Thus, these experimental results strongly support the point that a strong preference of shale samples for adsorbing CO_2 compared to other gases may indicate possible CO_2 storage potential.

Figures 4.3(a)-(c) provide comparison of adsorption on the three shales for methane, nitrogen and CO_2 respectively. As shown in these figures, the Woodford Payne has the highest adsorption capacity and the Caney shale has the lowest adsorption capacity for each adsorbed gas. Among these shale samples, the Woodford Payne also has the highest total organic carbon (TOC) content and the Caney shale has the lowest TOC content (see Table 4.1). Since the adsorption process occurs primarily on active sites containing organic carbon [4], shales that have a higher TOC content should have a larger adsorption capacity, which was consistent with the experimental results provided herein.

To quantify the relation between TOC content and adsorption capacity, the excess adsorption at about 9.7 MPa was chosen to represent the adsorption capacity of each sample for a particular gas from Tables 4.4(a)-(c). In this analysis, we considered only shales extracted from Oklahoma since our prior study [16] has shown that the correlation between TOC content and maximum excess adsorption were quite scattered, specifically when shales extracted from different locations (States or Countries). Using weighted linear regression where the assigned weights were the experimental uncertainties in the adsorption data, the obtained linear correlations for these gases are expressed below.

$$CH_4\ ADS_{9.7MPa} = 0.0076 \times TOC \tag{4.24}$$

$$N_2\ ADS_{9.7MPa} = 0.0029 \times TOC \quad (4.25)$$

$$CO_2\ ADS_{9.7MPa} = 0.0070 \times TOC + 0.1030 \quad (4.26)$$

where, $ADS_{9.7MPa}$ denotes adsorption capacity in mmol/g at 9.7 MPa and TOC is percentage total organic carbon content in as-received basis. As seen in the correlations above, the maximum adsorption capacities of methane, nitrogen and CO_2 increase linearly as a function of TOC content. For illustration purposes, Figure 4.4 provides the linear correlations of maximum adsorption capacities as a function of TOC content for the three shales.

4.4.3 Effect of Ash Content on Gas Adsorption

As seen in Figures 4.3(a)-(c), the Caney shale that had the highest ash content had the lowest gas adsorption capacities and vice versa for the Woodford Payne. This trend was expected since ash and TOC contents present in these shales vary inversely, as listed in Table 4.1. In fact, our previous study [16] indicated that carbon-based adsorbents that have higher ash content appeared to have less gas adsorption capacity as seen from the much lower adsorbed amounts in shales when compared to coals.

Typically, ash content contains mineral matter which is a hydrophilic adsorption site [13]. However, recent publications have reported adsorption of non-polar gases such as methane [38] and CO_2 [14] on mineral-matter-rich rocks. Since mineral matter is a major component in ash content, effect of ash content (or mineral matter) on gas adsorption behavior merits further study; specifically, whether methane or CO_2 is more preferred to be adsorbed on mineral matter.

Table 4.5 presents the adsorption ratios of CH_4/CO_2 on mineral-matter-rich rocks (Kaolinite and Illite) obtained at about 7 MPa. In Table 4.5, the adsorption of methane was obtained from Ji and Zhang [38] and the adsorption of CO_2 was obtained from Busch and Alles [14]. The CH_4/CO_2 ratio from the two sources was determined based on two assumptions: (1) the effect of minor temperature

difference (5 K difference) between the two sources on gas adsorption can be neglected, and (2) the rock samples from Busch and Alles [14] were assumed to contain only pure Illite and Kaolinite. The methane adsorption on samples from Ji and Zhang [38] (95 wt.% Kaolinite and 99 wt.% Illite rock samples) was normalized by the percentage weight of mineral matter (i.e. mmol/g of Kaolinite and mmol/g of Illite basis). As seen from Table 4.5, the adsorption ratio ranged from about 1/2.4 to 1/8.7 indicating that CO_2 was adsorbed preferentially on mineral matter relative to methane. Such preference of mineral matter for adsorbing CO_2 may be explained by the polarity of the CO_2 quadrupole as it interacts with the polar surface of mineral matter. As a result, CO_2 was adsorbed more than methane on mineral matter as seen in Table 4.5.

Table 4.6 provides ash content and CH_4/CO_2 adsorption ratio at 7 MPa. The ratios of the adsorption in Table 4.6 were obtained from shale samples 114, 117/118 and 181 [15] and from shale data in this study. The shales from these two sources were derived from different locations (Brazil and U.S.) where types of mineral matter in ash content may be different and may affect the adsorbed amount of methane and CO_2. Therefore, the adsorption ratios obtained from Weniger's samples and shales in this work were compared separately. As shown in the table, the CO_2 side in the CH_4/CO_2 ratio increased as ash content increased. This trend may be explained by a combination of two factors: (1) since CO_2 adsorbs more than methane on mineral matter, the corresponding reduction in CO_2 adsorption with increasing ash content is lower than that of methane, and (2) since methane adsorbs primarily on organic carbon, the adsorption capacity of methane decreases as ash content increases; this, in turn, inflates the CO_2 side in CH_4/CO_2 ratio. Since shales are typically rich in ash content (approximately 60-90 % of the total weight), utilization of CO_2 for enhancing methane recovery can be promising in ash-rich shales as evident from the preference of shale for adsorbing CO_2 that became stronger as ash content increases.

4.4.4 SLD Model Representations of Gas Adsorption on Shales

The ability of the SLD model to represent the adsorption data on shales in this study was evaluated. Five parameters in the SLD model were regressed, namely: surface area, A_i (one for each gas), solid-solid interaction energy, ε_{ss}/k, and slit length, L. Table 4.7 lists the regressed values of the SLD model parameters. In the table, the differences in the surface areas of the gases reflects the different accessibilities of the coal surface to the three gases. For each shale, the accessible surface area for CO_2 was the largest among the three gases and nitrogen had the smallest surface area in the SLD regressions. Thus, these surface areas were consistent with the adsorption capacities on shales where CO_2 adsorption was the highest and nitrogen the lowest adsorption capacity.

Table 4.8 presents the statistics for these shale adsorption systems, including the weighted average absolute deviation (WAAD), the root-mean-squared error (RMSE) and the percentage average-absolute deviation (%AAD). As evident from the table, the SLD model was capable of describing the adsorption data of the three gases on these shale samples within the experimental uncertainties. In particular, the overall %AADs for Woodford Payne, Woodford Hancock and Caney shales were 6.6%, 8.3% and 6.8%, respectively. The representations of the data for N_2 adsorption on Woodford Hancock and Caney shales at 2.9 MPa yield anomalously high percentage errors due to extremely low adsorbed amounts. As a result, these data were removed from the modeling analysis and are not included in the statistics reported in Table 4.8. For illustration purposes, Figures 4.2(a)-(c) present the SLD model representations for methane, nitrogen and CO_2 adsorption on the three shales.

Figures 4.5(a)-(c) present the percentage deviations for all the adsorbed data in this study. For adsorption on the three samples, about 88% of the data for methane, 74% of the data for nitrogen and 83% of the data for CO_2 were represented within 10% deviation. Overall, 81% of the total data points were represented within 10% deviation. Therefore, the SLD model was found capable of representing the adsorption data on these shales with satisfactory accuracy.

Figures 4.6(a)-(b) show the relationship between SLD model parameters and TOC content. In particular, Figure 4.6(a) presents the correlation between the surface area of gases and TOC content and Figure 4.6(b) presents the correlation between ε_{ss}/k and TOC content. As shown in Figure 4.6(a), the surface area for each gas was positively correlated with TOC. Since the surface area in the SLD model represents the adsorption capacity on shales, the results in Figure 4.6(a) are consistent with the relation between adsorption capacities and TOC illustrated in the figures. Figure 4.6(b), shows that ε_{ss}/k is positively correlated with TOC. In the SLD model, the ε_{fs}/k (or the fluid-solid energy parameter) is a geometric mean of $\varepsilon_{ss}/_{k}$ and ε_{ff}/k. Since the fluid-fluid energy parameter is fixed for each gas independent of the adsorbent, the higher values of ε_{ss}/k signify stronger *fluid-solid* interactions. As a result, shales that have higher TOC content have larger ε_{ss}/k.

The results shown in Figures 4.6(a)-(b) illustrate general trends in the SLD model parameters as a function of shale properties such as TOC content. These figures offer encouragement that the parameter may be generalized in terms of these shale properties. However, establishing reliable correlations will require additional adsorption data and concomitant shale characterizations in future measurements.

4.5 Conclusions

Adsorption of methane, nitrogen and CO_2 was measured on the Woodford shales from Payne and Hancock counties and the Caney shale. For each shale, CO_2 had the highest adsorption capacity and nitrogen the lowest. The CH_4/CO_2 ratios for these shales were higher than the CH_4/CO_2 ratios observed in other carbon-based adsorbents such as activated carbons and coals.

The relation between adsorption capacity and TOC was evident in this study. Linear correlation of maximum adsorption capacity and total organic carbon content was observed for each gas. The effect of ash content on gas adsorption was also observed. As ash content increased, the adsorption

ratio of CO_2/CH_4 increased. This points to the potential for utilizing shale reservoirs as CO_2 geological storage as well as utilizing CO_2 for enhancing methane recovery in shale reservoirs.

The SLD model was used to describe adsorption data on these shales. The SLD model appears capable of describing the adsorption data on these shale sample within the uncertainty of the data. Two of the SLD model parameters, i.e., surface areas and $\varepsilon_{ss/k}$ were positively correlated with TOC content which were consistent with the relation between TOC content and gas adsorption observed in this study. This highlights the importance of shale characterization, which may provide the basis for SLD model parameter generalization in future work.

Table 4.1. Compositional Analyses of Shale Samples from Oklahoma

Analyses	Woodford Payne Shale	Woodford Hancock Shale	Caney Shale
Ultimate	**Dry-ash-free basis**		
Carbon %	56.0	56.0	32.1
Hydrogen %	7.3	5.5	9.8
Oxygen %	0.6	10.9	31.8
Sulfur %	34.3	25.3	22.5
Proximate	**As-received basis**		
Moisture %	0.98	0.84	1.67
TOC %	8.49	6.38	2.23
Volatile Matter %	11.9	11.6	6.6
Ash %	83.57	85.72	91.74

Table 4.2. Parameters for Methane and Nitrogen Solubility in Water at Temperatures Near 318 K

Constant	Units of Constant	Methane	Nitrogen
a	MPa	5302.07	10204.24
b	-	150.4	127.3
c	1/MPa	-0.78	-0.09

Table 4.3. Parameters for CO_2 Solubility in Water at Multiple Temperatures

Constant	Value	Units of Constant
a	272.21	MPa
b_1	-332.637	-
b_0	1.06683	1/K
c_1	19.18	1/MPa
c_0	-0.05609	1/(MPa K)

Table 4.4(a). Excess Adsorption of Methane, Nitrogen and CO_2 on Woodford Shale from Payne County at 328.2 K

CH_4			N_2			CO_2		
Pressure (MPa)	**Excess Adsorption (mmol/g)**	**σ Excess Adsorption* (mmol/g)**	**Pressure (MPa)**	**Excess Adsorption (mmol/g)**	**σ Excess Adsorption* (mmol/g)**	**Pressure (MPa)**	**Excess Adsorption (mmol/g)**	**σ Excess Adsorption* (mmol/g)**
2.77	0.0382	0.0046	2.82	0.0078	0.0039	2.72	0.0932	0.0246
4.57	0.0545	0.0051	4.24	0.0139	0.0042	4.16	0.1169	0.0242
5.57	0.0603	0.0054	5.60	0.0181	0.0047	5.56	0.1337	0.0239
6.92	0.0676	0.0060	7.04	0.0234	0.0053	6.94	0.1437	0.0237
8.36	0.0716	0.0067	8.48	0.0265	0.0059	8.29	0.1546	0.0239
9.72	0.0737	0.0075	9.73	0.0286	0.0065	9.66	0.1616	0.0251
11.07	0.0751	0.0086	11.07	0.0297	0.0071	10.70	0.1565	0.0276
12.43	0.0771	0.0094	12.43	0.0306	0.0085	11.84	0.1490	0.0350

*Estimated absolute uncertainty in excess adsorption

Table 4.4(b). Excess Adsorption of Methane, Nitrogen and CO_2 on Woodford Shale from Hancock County at 328.2 K

CH_4			N_2			CO_2		
Pressure (MPa)	**Excess Adsorption (mmol/g)**	**σ Excess Adsorption (mmol/g)**	**Pressure (MPa)**	**Excess Adsorption (mmol/g)**	**σ Excess Adsorption (mmol/g)**	**Pressure (MPa)**	**Excess Adsorption (mmol/g)**	**σ Excess Adsorption (mmol/g)**
2.90	0.0128	0.0045	2.79	0.0010	0.0035	2.87	0.0607	0.0224
4.37	0.0198	0.0048	4.19	0.0037	0.0038	4.23	0.0838	0.0221
5.75	0.0256	0.0052	5.56	0.0060	0.0042	5.61	0.1054	0.0218
6.97	0.0291	0.0057	7.06	0.0097	0.0048	7.04	0.1232	0.0217
8.39	0.0328	0.0063	8.32	0.0111	0.0053	8.47	0.1390	0.0219
9.70	0.0377	0.0069	9.73	0.0134	0.0059	9.80	0.1487	0.0230
11.19	0.0379	0.0077	11.08	0.0142	0.0064	10.92	0.1452	0.0254
12.41	0.0397	0.0084	12.48	0.0150	0.0071	12.34	0.1371	0.0348

Table 4.4(c). Excess Adsorption of Methane, Nitrogen and CO_2 on Caney Shale at 328.2 K

CH_4			N_2			CO_2		
Pressure (MPa)	**Excess Adsorption (mmol/g)**	**σ Excess Adsorption (mmol/g)**	**Pressure (MPa)**	**Excess Adsorption (mmol/g)**	**σ Excess Adsorption (mmol/g)**	**Pressure (MPa)**	**Excess Adsorption (mmol/g)**	**σ Excess Adsorption (mmol/g)**
2.86	0.0028	0.0050	2.86	0.0003	0.0039	2.88	0.0434	0.0255
4.25	0.0060	0.0053	4.20	0.0013	0.0043	4.22	0.0621	0.0251
5.67	0.0090	0.0058	5.59	0.0023	0.0047	5.60	0.0773	0.0248
6.99	0.0107	0.0063	6.97	0.0030	0.0052	6.95	0.0918	0.0246
8.38	0.0119	0.0070	8.34	0.0035	0.0058	8.32	0.1036	0.0247
9.74	0.0128	0.0077	9.72	0.0041	0.0065	9.72	0.1182	0.0259
11.10	0.0137	0.0084	11.10	0.0043	0.0071	10.65	0.1130	0.0280
12.48	0.0138	0.0094	12.48	0.0044	0.0078	11.61	0.1073	0.0357

Table 4.5. Excess Adsorption Ratio of Methane and CO_2 on Illite and Kaolinite

Adsorbate	**Temperature (K)**	**Excess Adsorption at about 7 MPa on Mineral Matter (mmol/g Mineral)**		**Reference**
		Illite	**Kaolinite**	
CH_4	323.5	0.044	0.063	[38]
CO_2	318.2	0.388	0.149	[14]
CH_4/CO_2 Ratio		1:8.8	1:2.4	

Table 4.6. Excess Adsorption Ratio of Methane and CO_2 on Brazilian, Woodford and Caney Shales

Sample	Temperature (K)	Characterization		Adsorption at about 7 MPa			Reference
		TOC (%)	Ash (%)	CH_4	CO_2	CH_4/CO_2	
117/118*	318.2	21.1	67.2	0.2231	0.3359	1/1.5	Weniger, et al. [15]
181*		11.1	81.7	0.0999	0.2863	1/2.9	
114*		1.7	93.1	0.0461	0.2412	1/5.2	
Woodford Payne	328.2	8.5	83.6	0.0676	0.1437	1/2.1	Current Work
Woodford Hancock		6.4	85.7	0.0291	0.1232	1/4.2	
Caney		2.2	91.7	0.0107	0.0918	1/8.6	

*These samples are shales from Rio Bonito formation, Brazil

Table 4.7. SLD Model Parameters for Methane, Nitrogen and CO_2 Excess Adsorption on Woodford Shales from Payne and Hancock Counties and Caney Shale

Parameter	Woodford Payne	Woodford Hancock	Caney
CH_4 Surface Area (m^2/g)	16.8	7.9	3.3
N_2 Surface Area (m^2/g)	8.7	4.2	1.6
CO_2 Surface Area (m^2/g)	20.0	16.4	15.1
$\varepsilon_{ss/k}$ (K)	5.1	3.4	2.6
Slit Length (nm)	1.04	1.32	1.33

Table 4.8. SLD Model Statistics for Methane, Nitrogen and CO_2 Excess Adsorption on Woodford Shales from Payne and Hancock Counties and Caney Shale

Adsorbate	Woodford Payne			Woodford Hancock			Caney		
	%AAD*	RMSE*	WAAD*	%AAD	RMSE	WAAD	%AAD	RMSE	WAAD
CH_4	4.6	0.0032	0.4	2.7	0.0010	0.1	4.8	0.0008	0.1
N_2	6.9	0.0013	0.2	18.5	0.0018	0.4	10.7	0.0004	0.1
CO_2	8.3	0.0136	0.4	5.1	0.0071	0.2	5.2	0.0047	0.2
Overall	**6.6**	**0.0081**	**0.4**	**8.3**	**0.0043**	**0.2**	**6.8**	**0.0028**	**0.1**

%AAD is percentage absolute average deviation in excess adsorption, RMSE is root-mean-squared error presented in mmol/g, and WAAD is weighted absolute average deviation in excess adsorption where the assign weights were experimental uncertainties in adsorption data.

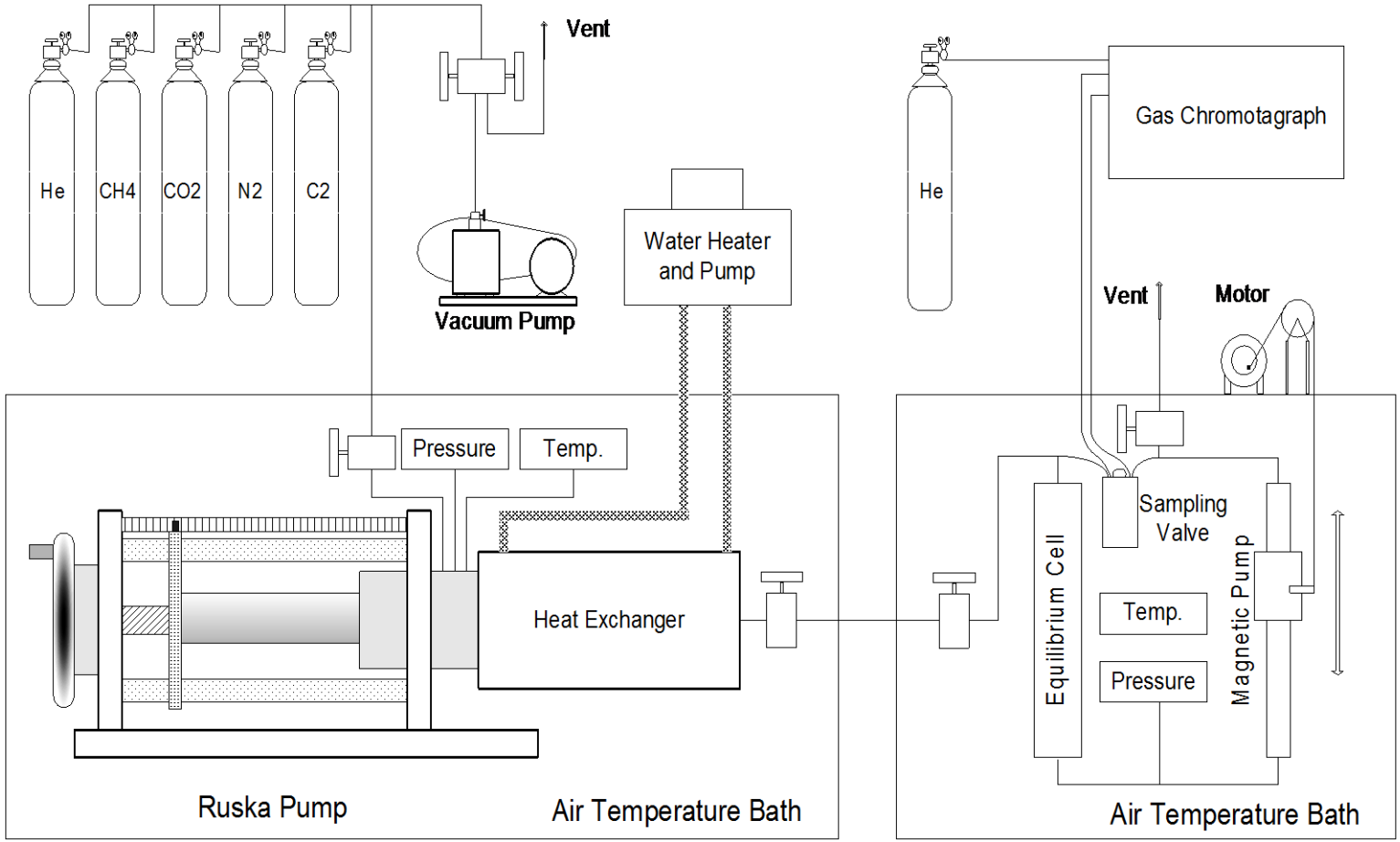

Figure 4.1. Schematic Diagram of the Experimental Apparatus

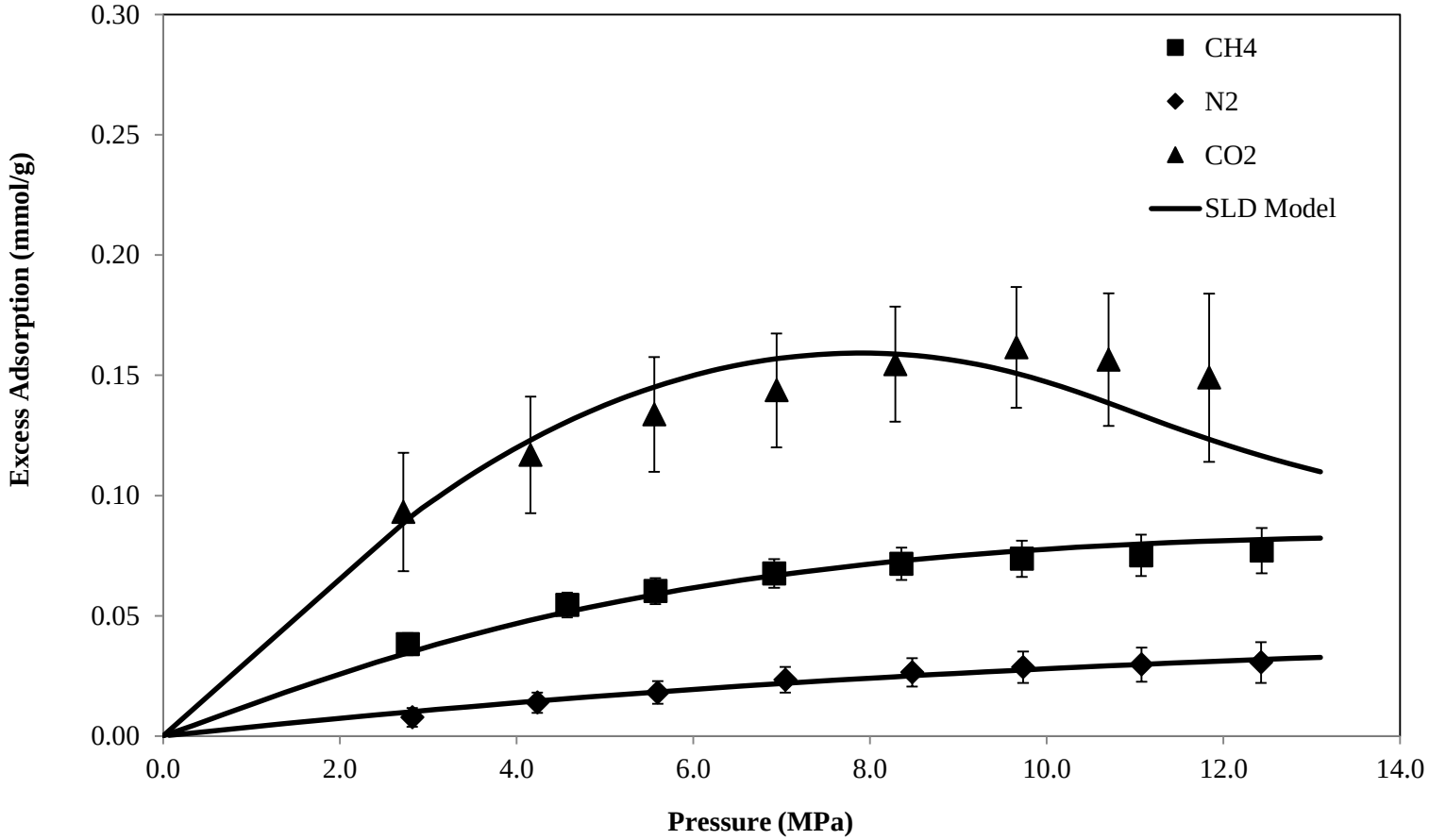

Figure 4.2(a). Adsorption of Methane, Nitrogen and CO_2 on Woodford Shale from Payne County at 328.2 K

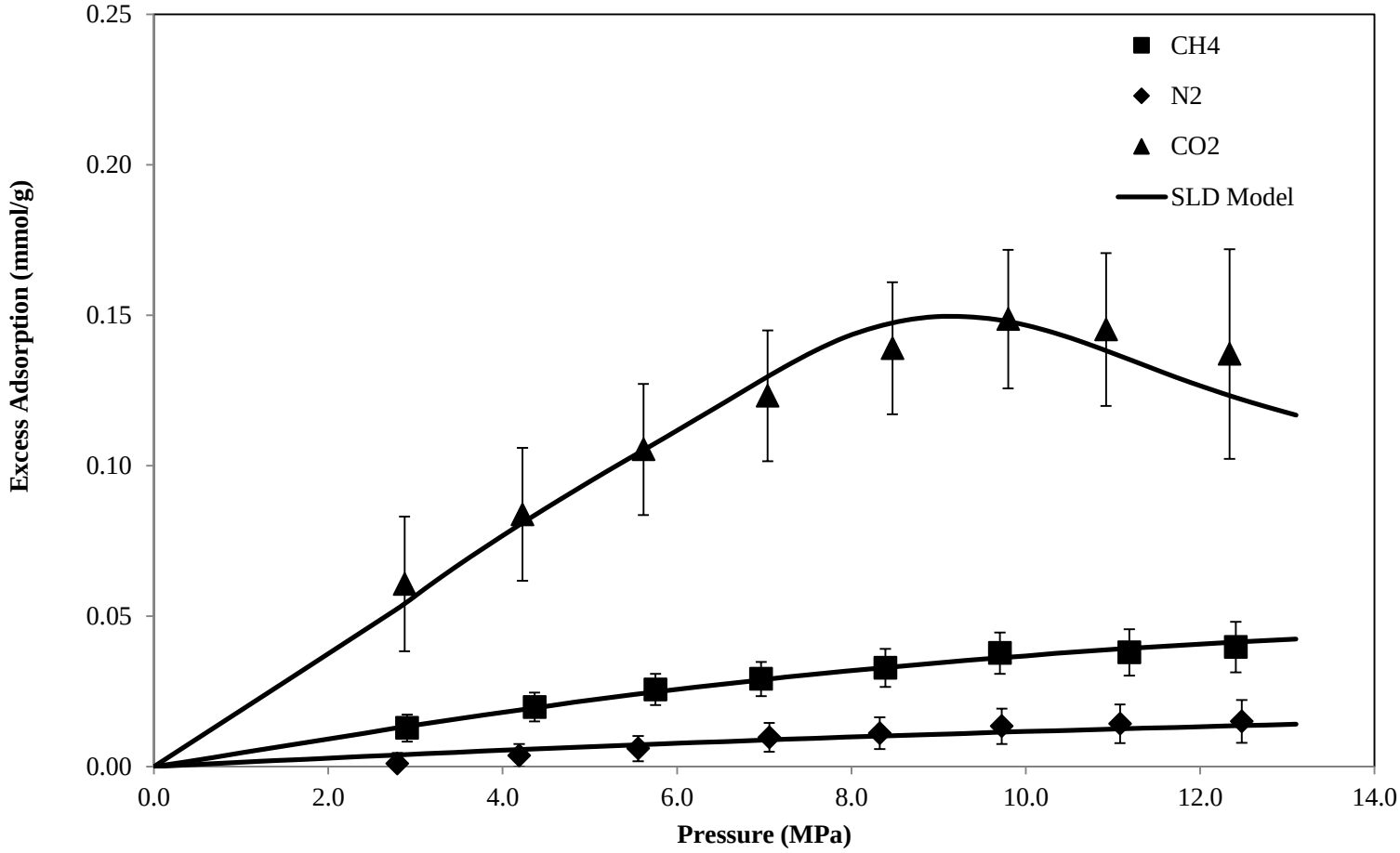

Figure 4.2(b). Adsorption of Methane, Nitrogen and CO_2 on Woodford Shale from Hancock County at 328.2 K

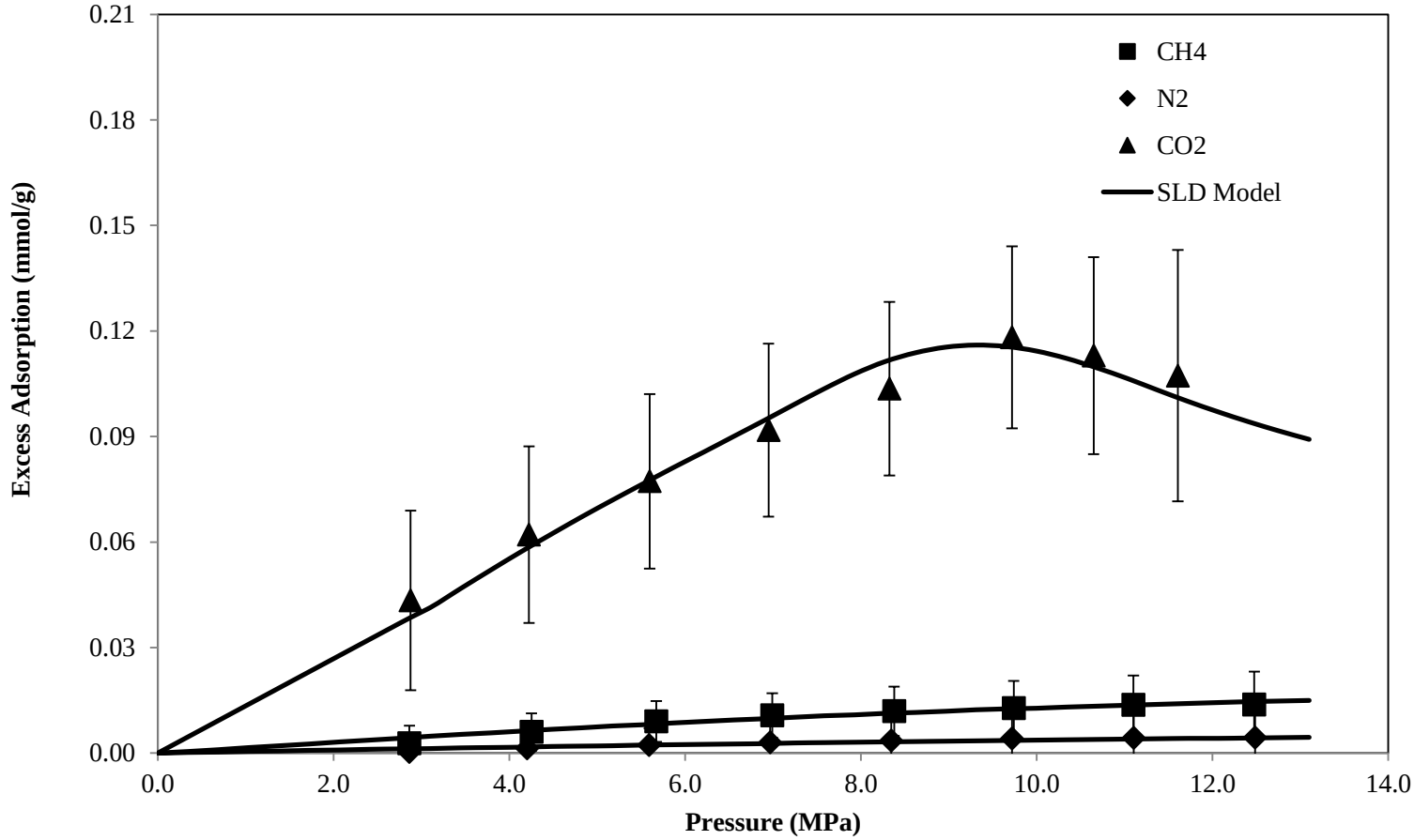

Figure 4.2(c). Adsorption of Methane, Nitrogen and CO_2 on Caney Shale at 328.2 K

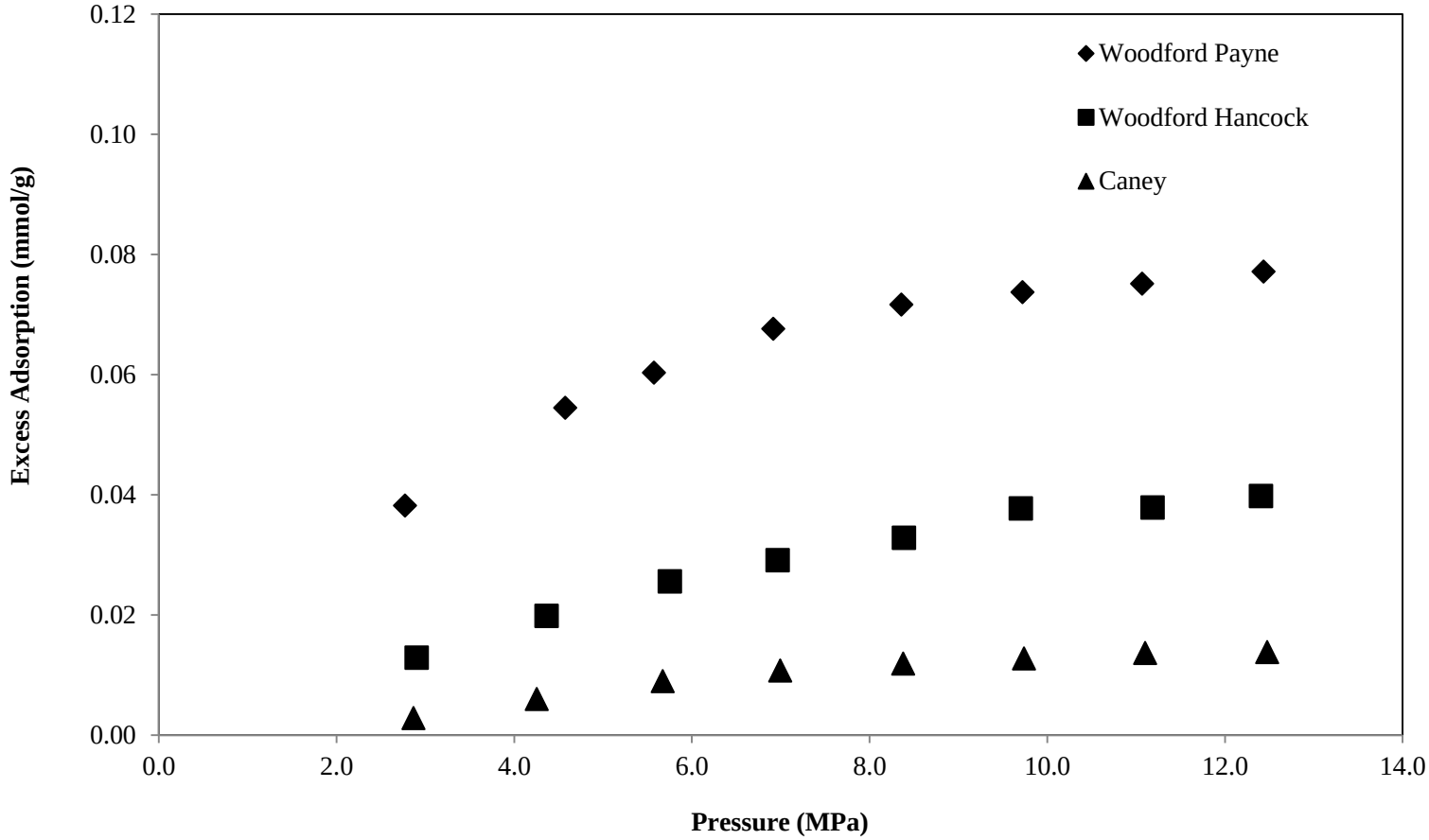

Figure 4.3(a). Comparison of Methane Adsorption on Woodford Shales from Payne and Hancock Counties and Caney Shale at 328.2 K

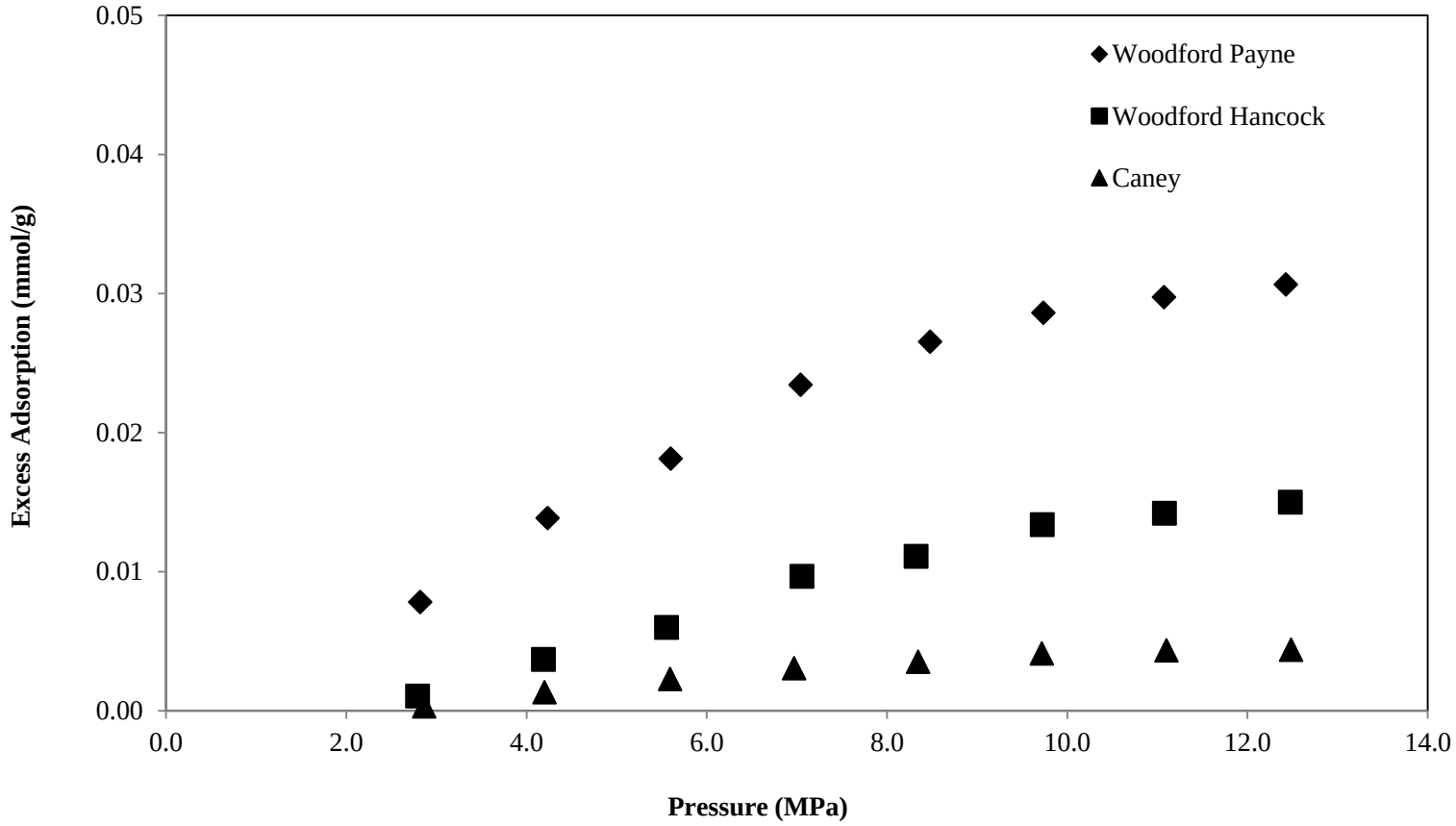

Figure 4.3(b). Comparison of Nitrogen Adsorption on Woodford Shales from Payne and Hancock Counties and Caney Shale at 328.2 K

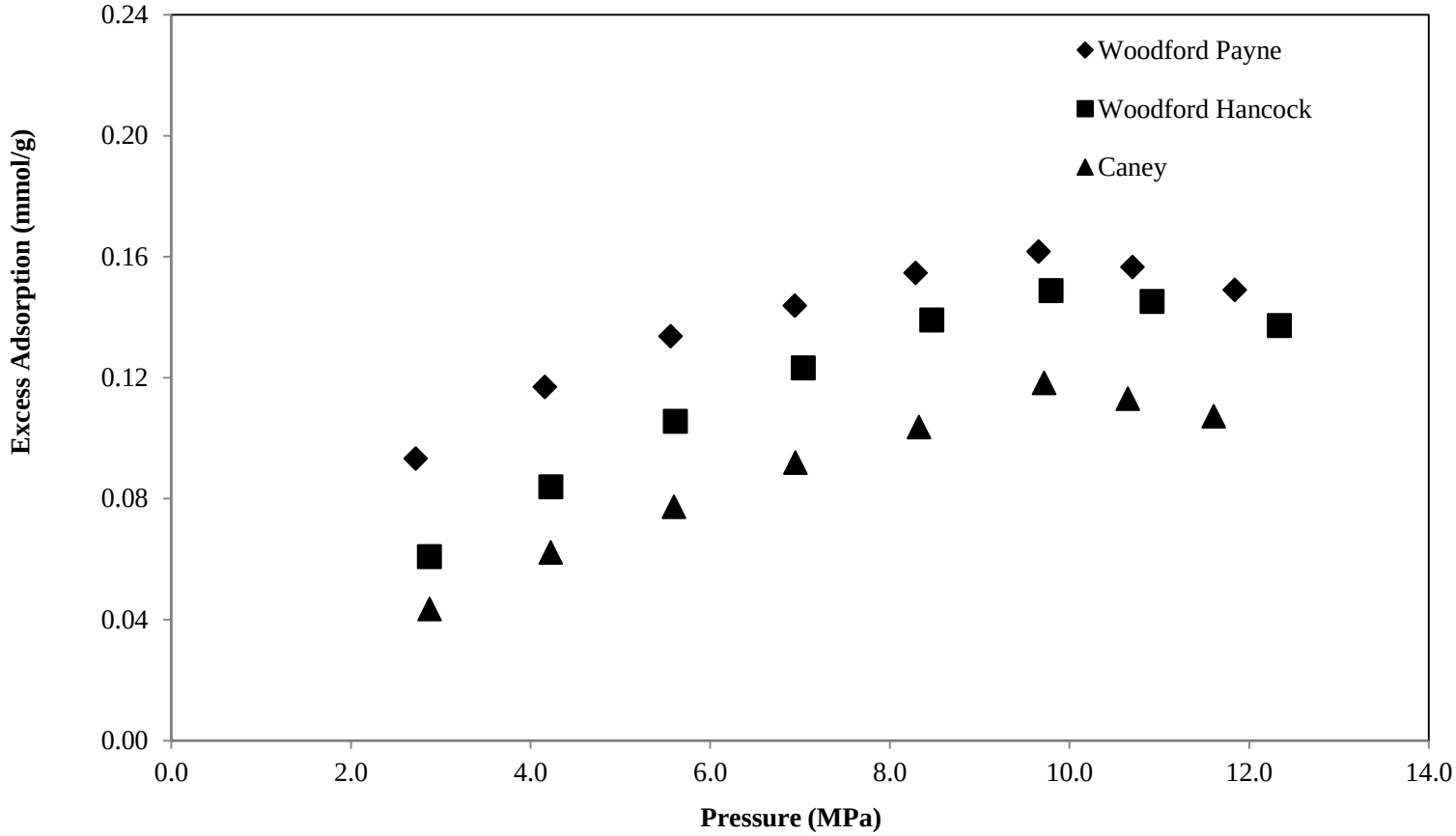

Figure 4.3(c). Comparison of CO_2 Adsorption on Woodford Shales from Payne and Hancock Counties and Caney Shale at 328.2 K

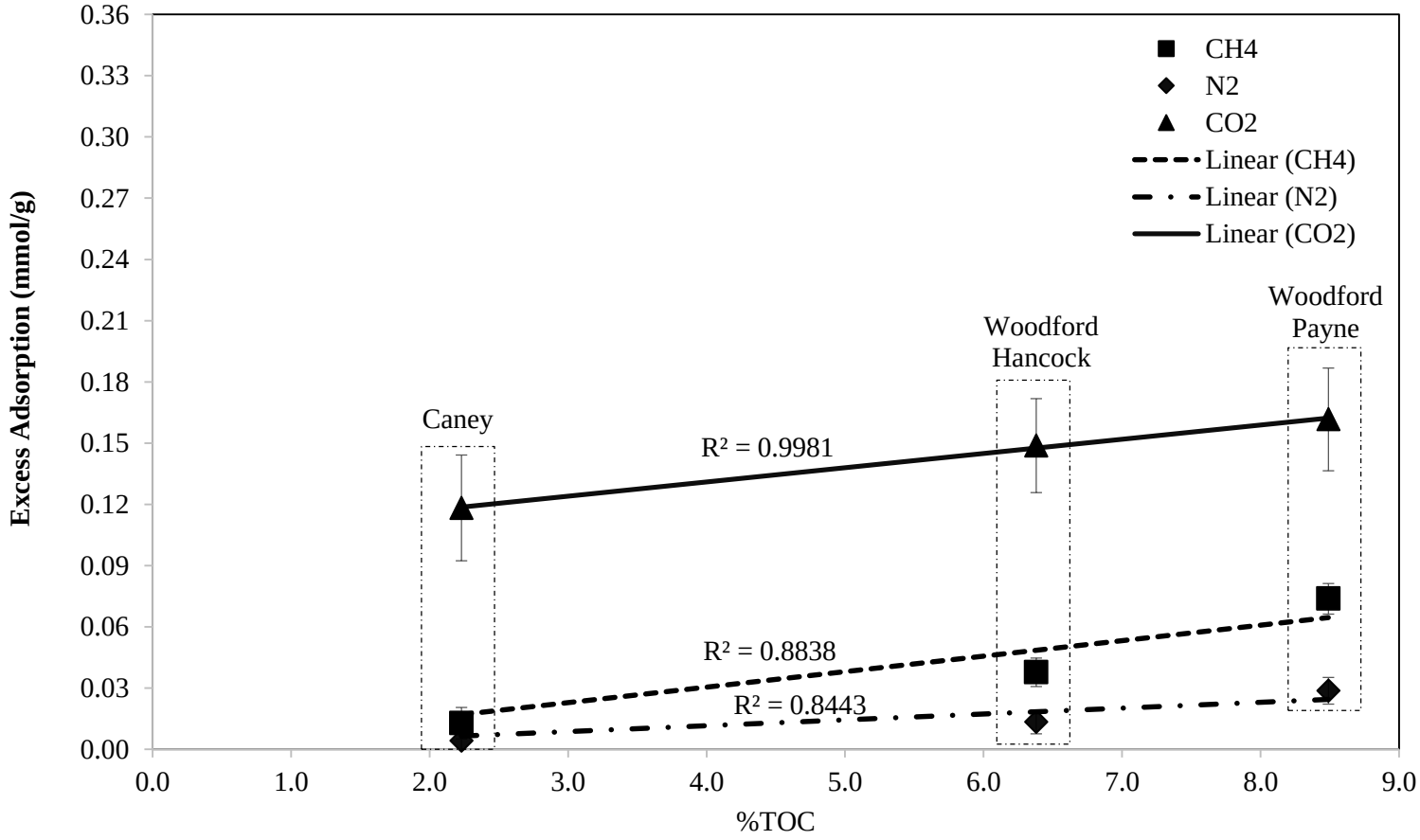

Figure 4.4. Excess Adsorption Capacity at 9.7 MPa as a function of TOC for Methane, Nitrogen and CO_2 at 328.2 K

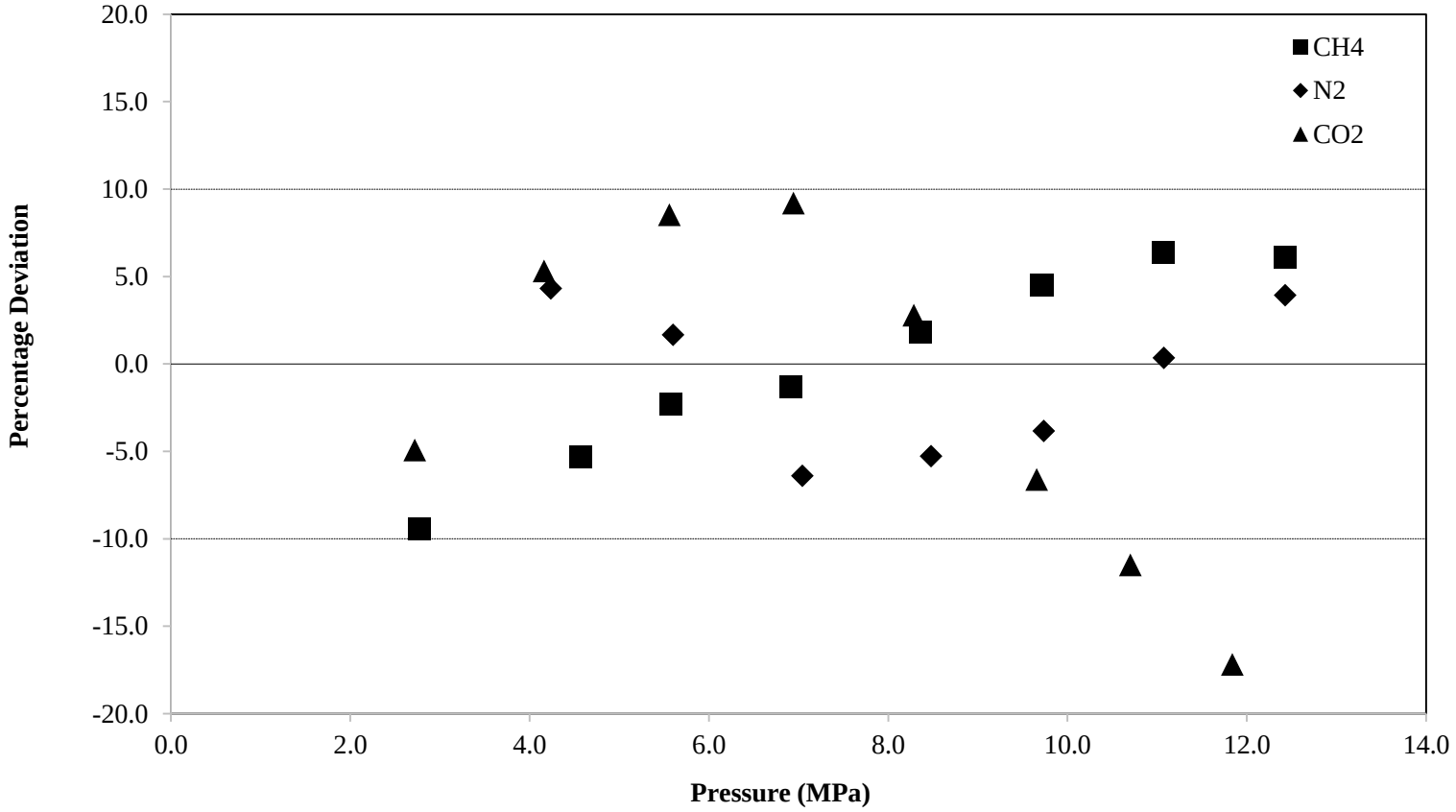

Figure 4.5(a). Percentage Deviation of SLD Model Representations for Methane, Nitrogen and CO_2Adsorption at 328.2 K on Woodford Shale from Payne County

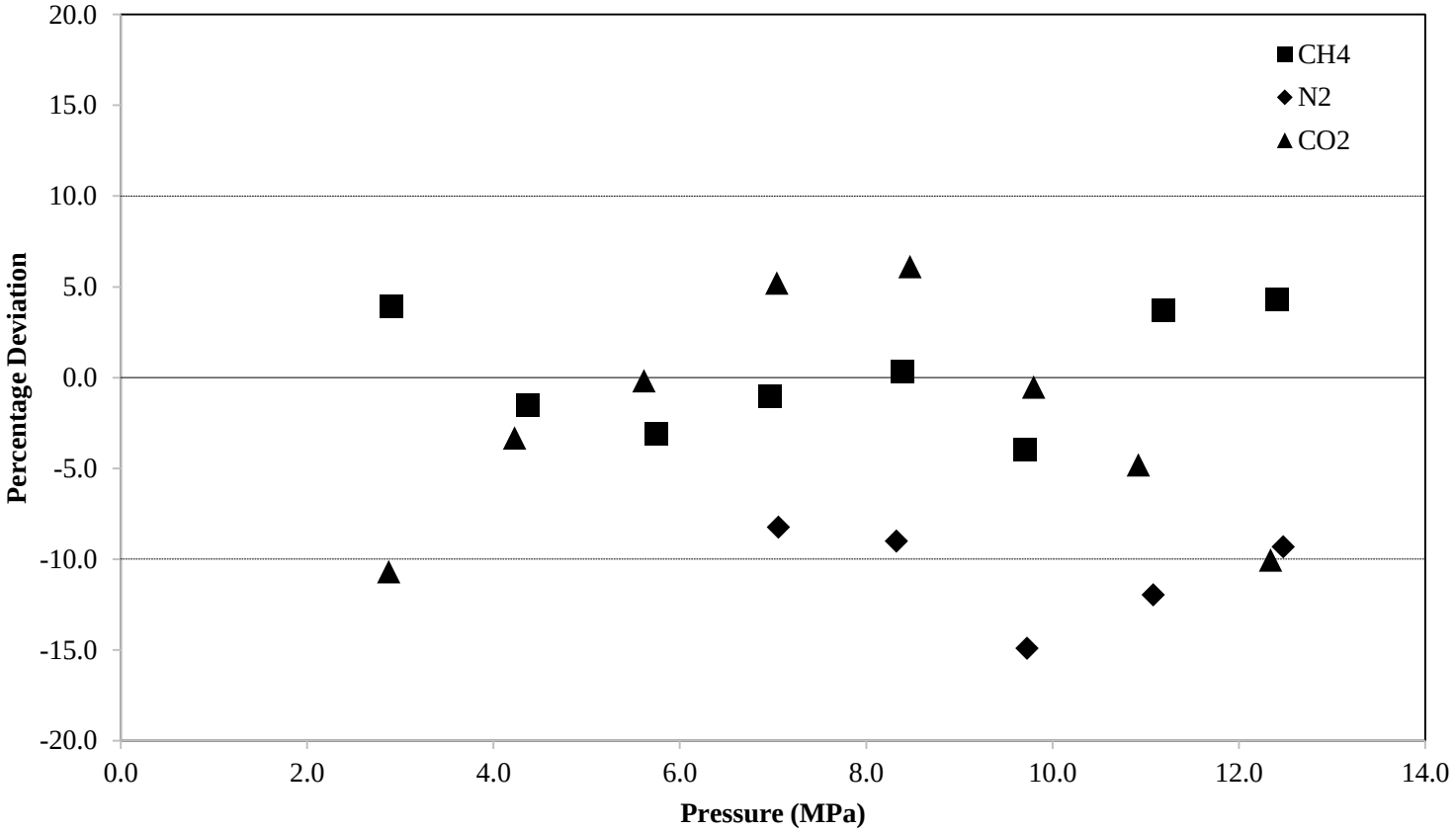

Figure 4.5(b). Percentage Deviation of SLD Model Representations for Methane, Nitrogen and CO_2 Adsorption at 328.2 K on Woodford Shale from Hancock County

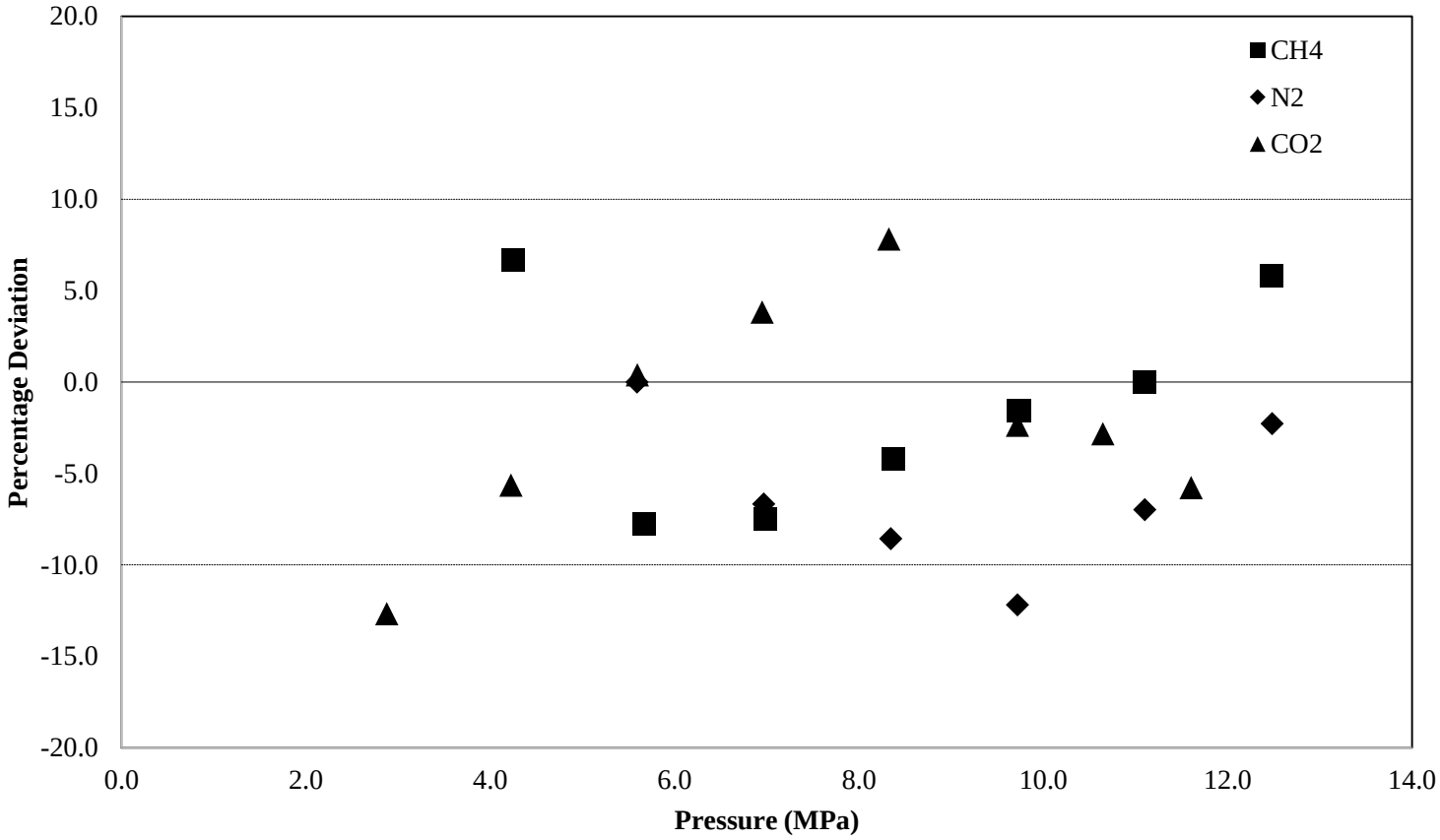

Figure 4.5(c). Percentage Deviation of SLD Model Representations for Methane, Nitrogen and CO_2 Adsorption at 328.2 K on Caney Shale

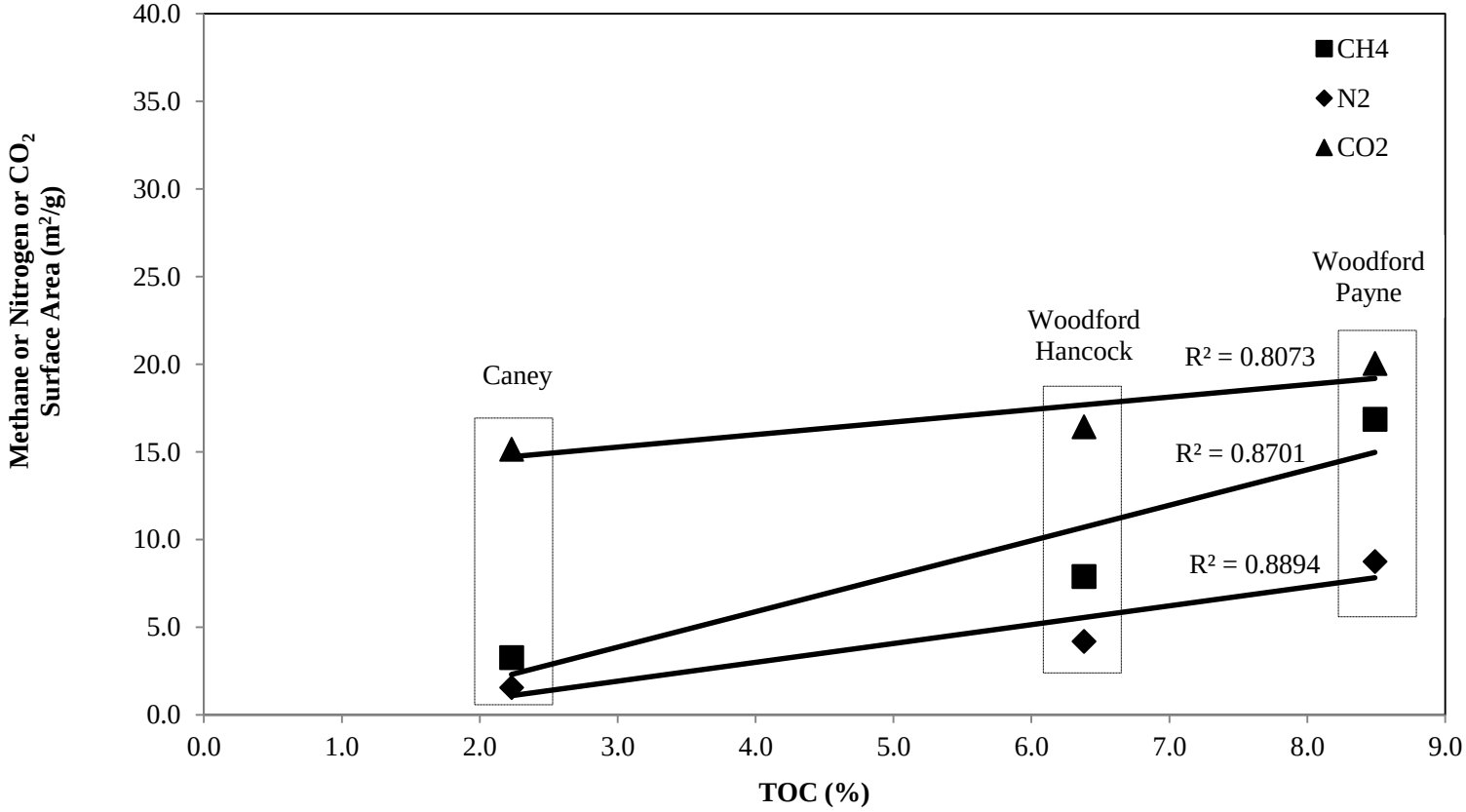

Figure 4.6(a). Correlations of Regressed Surface Area as a Function of TOC Content for Methane, Nitrogen and CO_2

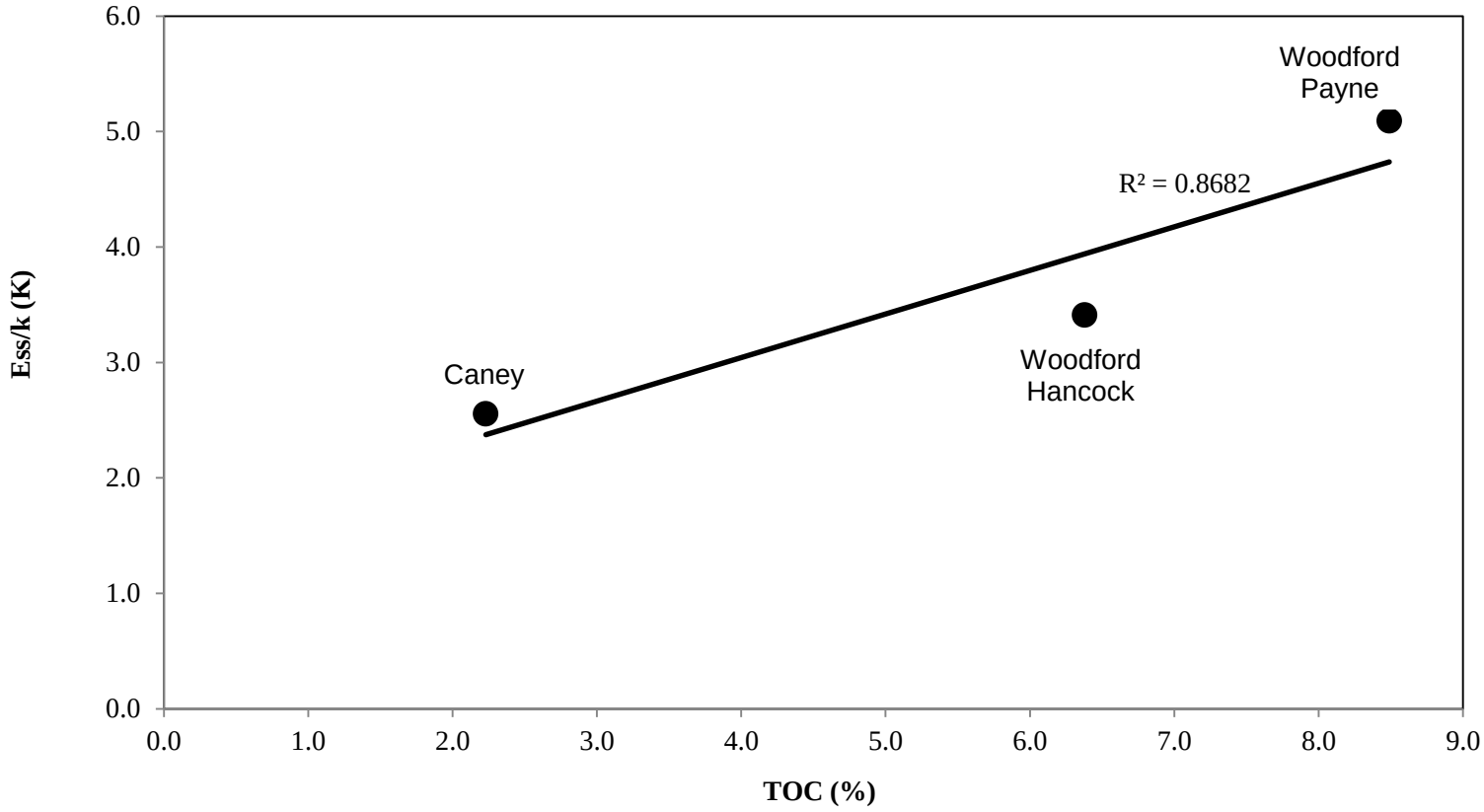

Figure 4.6(b). Correlation of Regressed Solid-Solid Interaction Energy ($\varepsilon_{ss/k}$) as a Function of TOC Content

REFERENCES

1. EIA, Natural Gas Gross Withdrawals and Production, U.S. Energy Information Administration. http://www.eia.gov/dnav/ng/ng_prod_sum_dcu_NUS_m.htm. Released October 2014. 2014.

2. Cardott, B.J., Woodford Shale: From Hydrocarbon Source Rock to Reservoir. AAPG Woodford Shale Forum. 2013.

3. EIA, Outlook for U.S. shale oil and gas. http://www.eia.gov/pressroom/presentations/sieminski_01042014.pdf. 2014.

4. Nuttall, B.C., et al., Analysis of Devonian Black shales in Kentucky for potential carbon dioxide sequestration and enhanced natural gas production, in Kentucky Geological Survey. 2005, University of Kentucky: Lexington, Kentucky.

5. Kang, S.M., et al., Carbon Dioxide Storage Capacity of Organic-Rich Shales. 2011.

6. Tao, Z. and A. Clarens, Estimating the Carbon Sequestration Capacity of Shale Formations Using Methane Production Rates. Environmental Science & Technology, 2013. 47(19): p. 11318-11325.

7. Beaton, A.P., et al., Total organic carbon and adsorption isotherms of the Duvernay and Muskwa formations in Alberta: shale gas data release. 2010, Energy Resources Conservation Board, ERCB/AGS: Edmonton, Alberta. p. 33.

8. Zhang, T., et al., Effect of organic-matter type and thermal maturity on methane adsorption in shale-gas systems. Organic Geochemistry, 2012. 47(0): p. 120-131.

9. Wang, S., et al., The methane sorption capacity of Paleozoic shales from the Sichuan Basin, China. Marine and Petroleum Geology, 2013. 44(0): p. 112-119.

10. Rexer, T.F., et al., High-Pressure Methane Adsorption and Characterization of Pores in Posidonia Shales and Isolated Kerogens. Energy & Fuels, 2014. 28(5): p. 2886-2901.

11. Gasparik, M., et al., Geological controls on the methane storage capacity in organic-rich shales. International Journal of Coal Geology, 2014. 123(0): p. 34-

12. Hu, H., et al., Experimental investigation of changes in methane adsorption of bitumen-free Woodford Shale with thermal maturation induced by hydrous pyrolysis. Marine and Petroleum Geology, 2014. 59(0): p. 114-128.

13. Tan, J., et al., Shale gas potential of the major marine shale formations in the Upper Yangtze Platform, South China, Part II: Methane sorption capacity. Fuel, 2014. 129(0): p. 204-218.

14. Busch, A., et al., Carbon dioxide storage potential of shales. International Journal of Greenhouse Gas Control, 2008. 2(3): p. 297-308.

15. Weniger, P., et al., High-pressure methane and carbon dioxide sorption on coal and shale samples from the Paraná Basin, Brazil. International Journal of Coal Geology, 2010. 84(3–4): p. 190-205.

16. Chareonsuppanimit, P., et al., High-pressure adsorption of gases on shales: Measurements and modeling. International Journal of Coal Geology, 2012. 95(0): p. 34-46.

17. Khosrokhavar, R., K.-H. Wolf, and H. Bruining, Sorption of CH4 and CO2 on a carboniferous shale from Belgium using a manometric setup. International Journal of Coal Geology, 2014. 128–129(0): p. 153-161.

18. Clarkson, C.R. and B. Haghshenas, Modeling of Supercritical Fluid Adsorption on Organic-Rich Shales and Coal. 2013, Society of Petroleum Engineers.

19. Mohammad, S.A., et al., Adsorption of Pure Carbon Dioxide on Wet Argonne Coals at 328.2 K and Pressures up to 13.8 MPa. Energy & Fuels, 2009. 23(2): p. 1107-1117.

20. Hall, F., et al., Adsorption of Pure Methane, Nitrogen, and Carbon Dioxide and Their Binary Mixtures on Wet Fruitland Coal, in SPE Eastern Regional Conference & Exhibition, SPE Paper 29194. 1994: Charleston, S.C.

21. Sudibandriyo, M., et al., Adsorption of Methane, Nitrogen, Carbon Dioxide, and Their Binary Mixtures on Dry Activated Carbon at 318.2 K and Pressures up to 13.6 MPa. Langmuir, 2003. 19(13): p. 5323-5331.

22. Hall, F.E., Adsorption of Pure and Multicomponent Gases on Wet Fruitland Coal, in Chemical Engineering. 1993, Oklahoma State University: Stillwater.

23. Angus, S., B. Armstrong, and K.M. de Reuck, International Thermodynamic Tables of the Fluid State-5: Methane. IUPAC Chemical Data Series No.16. 1978, New York: Pergamon Press.

24. Angus, S., K.M. de Reuck, and B. Armstrong, International Thermodynamic Tables of the Fluid State-6: Nitrogen. IUPAC Chemical Data Series No.20. 1979, New York: Pergamon Press.

25. Span, R. and W. Wagner, A New Equation of State for Carbon Dioxide Covering the Fluid Region from the Triple Point Temperature to 1100 K at Pressures up to 800 MPa. J. Phys. Chem. Ref. Data, 1996. 25: p. 1509-1590.

26. McCarty, R.D., Thermophysical Properties of Helium-4 from 2 to 1500 K with Pressures to 1000 Atmospheres. 1972, U.S. Dept. of Commerce

27. Dhima, A., J. de Hemptinne, and J. Jose, Solubility of Hydrocarbons and CO2 Mixtures in Water under High Pressure. Ind. & Eng. Chem. Res., 1999. 38(8): p. 3144-3161

28. King, A.D.J. and C.R. Coan, Solubility of Water in Compressed Carbon Dioxide, Nitrous Oxide and Ethane. Evidence for Hydration of Carbon Dioxide and Nitrous Oxide in the Gas Phase. J. Am. Chem. Soc., 1971. 93(8): p. 1857-1862.

29. Weibe, R. and V. Gaddy, The Solubility of Carbon Dioxide in Water at Various Temperatures from 12° to 40° and at Pressures to 500 Atmospheres, Critical Phenomena. J. Amer. Chem. Soc., 1940. 62 p. 815-817.

30. Rangarajan, B., C.T. Lira, and R. Subramanian, Simplified local-density model for adsorption over large pressure ranges. AIChE Journal, 1995. 41(4): p. 838-845.

31. Mohammad, S.A., et al., Generalized Simplified Local-Density/Peng−Robinson Model for Adsorption of Pure and Mixed Gases on Coals. Energy & Fuels, 2009. 23(12): p. 6259-6271.

32. Fitzgerald, J.E., R.L. Robinson, and K.A.M. Gasem, Modeling High-Pressure Adsorption of Gas Mixtures on Activated Carbon and Coal Using a Simplified Local-Density Model. Langmuir, 2006. 22(23): p. 9610-9618.

33. Lee, L.L., Molecular Thermodynamics of Non-ideal Fluids. 1988, Stoneham, MA Butterworth.

34. Steele, W.A., The Interaction of Gases with Solid Surfaces. 1974, Oxford: Pergamon Press.

35. Subramanian, R., H. Pyada, and C.T. Lira, Engineering model for adsorption of gases onto flat surfaces and clustering in supercritical fluids. Industrial & Engineering Chemistry Research, 1995. 34(11): p. 3830.

36. Reid, R.C., J.M. Prausnitz, and B.E. Poling, The Properties of Gases and Liquids. 1987, New York: McGraw-Hill

37. Huang, X., et al., Investigation of oxygen-containing group promotion effect on CO2–coal interaction by density functional theory. Applied Surface Science, 2014. 299(0): p. 162-169.

38. Ji, L., et al., Experimental investigation of main controls to methane adsorption in clay-rich rocks. Applied Geochemistry, 2012. 27(12): p. 2533-2545.

39. NIST, Thermophysical Properties of Fluid Systems. the U.S. Secretary of Commerce on behalf of the United States of America. 2011.

CHAPTER V

MODELING GAS-ADSORPTION-INDUCED SWELLING AND PERMEABILITY CHANGES IN COALS

The content in this chapter has been published in the International Journal of Coal and Geology*.

5.1 Introduction

The significant increase in greenhouse gas emissions has stimulated research efforts on CO_2 capture and subsequent storage of CO_2 in underground reservoirs such as depleted oil and gas fields, unmineable coalbeds and saline aquifers. The geological storage or sequestration of CO_2 into deep, unmineable coal seams offers a particularly attractive method since the sequestration also provides another benefit - additional recovery of coalbed methane or natural gas. However, modeling these processes requires detailed knowledge regarding gas adsorption and transport within the reservoir, among other factors. Although significant efforts have been made to investigate gas adsorption in coals, the adsorption-induced swelling of coals has received limited theoretical treatment thus far. CO_2 sequestration capability can be affected significantly by the adsorption-induced expansion of coal - more commonly referred to as *coal swelling*. This phenomenon can reduce the cleat permeability by constricting the porous cleat networks, as illustrated in Figure 1(a), thereby causing decreased injectivity of CO_2 into the reservoir. Therefore, gas adsorption-induced swelling of coals is an important factor for the optimal design of CO_2 sequestration processes in coalbed reservoirs.

* Charoensuppanimit, P., et al., Modeling gas-adsorption-induced swelling and permeability changes in coals. International Journal of Coal Geology, 2014. 121(0): p. 98-109.

The relationship between gas adsorption and coal swelling has been studied by several authors. Reucroft and Patel [1] measured CO_2-induced coal swelling by recording the change in length of coal samples. They found that CO_2 could swell coals ranging from about 0.36% to 1.31% volumetrically, whereas a non-adsorbed gas such as helium produced negligible dimension changes to the coal samples. Levine [2] measured the swelling of coals by methane and CO_2 and showed that CO_2 caused about three-fold larger swelling than methane at the same bulk pressure. Similarly, Pini et al. [3] measured the swelling of coal due to adsorption of nitrogen and CO_2. The authors observed that the swelling of coal due to CO_2 was significantly larger than swelling from nitrogen adsorption. CO_2 is the most strongly adsorbed gas and nitrogen is least adsorbed, while methane adsorption is intermediate to these gases. Pan and Connell [4] also measured coal swelling caused by methane, nitrogen and CO_2 adsorption. The authors observed that the coal swelling caused by *different* gases was very similar when compared at the *same* molar adsorption amounts (viz. at different pressures). In other words, they observed that the coal swelling is dependent on adsorption *amounts*, and equal adsorbed amounts of different gases produced similar levels of swelling in coals. This observation is tested in Section 5.4.3.

The reversibility of gas adsorption-induced swelling of coals on release of gas pressure was also studied by several authors [2, 3, 5, 6]. These authors found that the dimensional changes in coals were negligible after evacuation of the adsorbates from their experimental apparatus and, thus, swelling appeared to be largely reversible under laboratory conditions.

Several attempts have been made to quantify the relationship between gas adsorption and the swelling of coals. Levine [2] observed that swelling vs. pressure profile measured in terms of the linear strain were Langmuir-like. The author used an empirical expression similar to the well-known Langmuir adsorption equation to model coal swelling. Cui and Bustin [7] observed a linear relation between the volumetric strain and the adsorbed amount in the pressure range of 0-6 MPa.

Recently, Pan and Connell [4] and Day et al. [5] showed that the relation between adsorbed amount and coal swelling was not necessarily linear, especially at the higher pressures.

Coal swelling and its effect on data reduction from adsorption experiments has also been studied. Several authors have included empirical corrections for coal swelling in adsorption isotherm data reduction calculations. For example, corrections for swelling that have been introduced include the Langmuir model [8] and Dubinin-Radushkevich model [9]. Although these empirical corrections can describe adsorption data on specific systems, they do not possess predictive capabilities due to their inherently empirical nature. In contrast, theoretically rigorous models would offer a distinct advantage in modeling of gas adsorption as well as coal swelling.

Recently, Pan and Connell [10] developed a theoretical model for describing coal swelling by considering the changes in surface potential energy due to gas adsorption. Clarkson [11] integrated Pan and Connell (PC) coal swelling model with the Ideal Adsorbed Solution (IAS) model and the Two-Dimensional Equation of state (2-D EOS) model to describe coal swelling in binary mixture of CO_2 and methane. The results showed that at low pressure Extended Langmuir (EL) model, the IAS and the 2-D EOS predicted similar coal swelling strains. At higher pressures the IAS and 2-D EOS produced comparable results and fit the swelling data better than the EL model. The advantage of using IAS and 2-D EOS appearing in Clarkson's work is that both adsorption models were used to extend the available adsorption isotherms of pure gas and predict mixture adsorptions. Then, the surface potentials were estimated to predict the swelling strain. However, we do not include the coal swelling in binary mixture [12] used in Clarkson's work because our current focus is only for coal swelling in pure gas. The coal swelling in binary mixture will be developed in our future work.

In case that adsorption isotherms are absent completely such as the coal swelling data from Robertson and Christiansen [13], the PC model requires the adsorption model capable of predicting the missing adsorption isotherms. This leads to a distinct advantage of the SLD model over the IAS and the 2-D EOS. The SLD model accounts for molecular interactions between *the carbon surface*

and the adsorbed molecules whereas the IAS and 2-D EOS treats the carbon surface to be thermodynamically inert. The adsorbent characteristics i.e. Proximate and Ultimate analyses are utilized in order for generating the SLD parameters. Our previous work [14] has showed that the SLD model is capable of providing *generalized* predictions of gas adsorption based solely on coal characterization information. As such, this predictive capability is also utilized in the current study in cases where no adsorption data are reported with the corresponding coal swelling data.

The current study differs from earlier work [4, 10, 11] in several aspects. In this study, the (1) SLD-PC approach has been shown to provide *theoretically consistent* estimates for adsorption surface potential that leads to the improved representations of coal swelling especially for CO_2, (2) non-linear relation observed between adsorption surface potential and linear strain is accounted for in the SLD-PC model and (3) generalized SLD model is used to provide *a priori* predictions of adsorption data where experimental isotherm data are lacking.

The ultimate goal for modeling of adsorption-induced coal swelling is estimation of permeability changes in the coal matrix based on the knowledge of adsorption and swelling behaviors. During adsorption, stress develops in coal as the matrix swells. To account for these changes, a stress-strain relationship for poroelastic media [15] was used by several authors [4, 16, 17] to estimate changes in stress from information on strain in coals. In this study, a theory-based permeability model developed originally by Pan and Connell [4] was selected due to its capability to represent both isotropic and anisotropic coal swelling. As will be shown later, the SLD-PC approach combined with a permeability model appears capable of representing the permeability data for the coal samples studied. The remainder of this paper is organized as follows: Section 5.2 describes the SLD-PC swelling and permeability models, Section 5.3 presents the literature database compiled and employed and Section 5.4 presents the modeling results obtained in this study.

5.2 Adsorption, Swelling and Permeability Model

5.2.1 Simplified Local-Density (SLD) Adsorption Model

The simplified local-density (SLD) model was used to describe the adsorption behavior of pure gases on several coals. The detailed theoretical background of the SLD model has appeared in our previous studies [14, 18] and, therefore, these details are not repeated here. In this section, we briefly outline the essential details of the SLD model.

Lira and Coworkers [19, 20] originally developed the SLD model by applying the mean field approximation and superimposing the fluid-solid potential on a fluid equation of state. The SLD model assumes the adsorbent to be composed of rectangular-shaped slit pores, where the adsorbate molecules reside within this two-surface slit. The distance between the slit surfaces is L representing the *effective* pore width of the adsorbent. The position of a molecule within the slit, z, is measured orthogonal to the one of the coal solid surfaces formed by carbon atoms. Further, a molecule within the slit has interactions with both walls of the adsorbent slit at distances z and L-z.

The SLD model partitions the interactions in the adsorbed phase into fluid-fluid and fluid-solid contributions. Using the criterion of equality of chemical potentials of the bulk and adsorbed fluids and expressing the chemical potentials in terms of fugacities, the following equilibrium relation for describing adsorption is derived

$$f_{ads}(z) = f_{bulk}\exp\left(-\frac{\Psi^{fs}(z) + \Psi^{fs}(L-z)}{kT}\right) \qquad (5.1)$$

where $f_{ads}(z)$ is the fugacity of the adsorbate due to fluid-fluid interactions in the slit, f_{bulk} is the fugacity of bulk fluid and Ψ^{fs} is the fluid-solid potential function. In Equation (5.1), $f_{ads}(z)$ denotes that the fluid fugacity is modified to account for the proximity of the adsorbed molecule to the slit or adsorbent surface. The fluid-solid interaction, $\Psi^{fs}(z)$, is represented by Lee's partially-integrated 10-4 potential [21], which is a truncated form of Steele's 10-4-3 potential [22]

$$\Psi^{fs}(z) = 4\pi\rho_{atoms}\varepsilon_{fs}\sigma_{fs}^2\left(\frac{\sigma_{fs}^{10}}{5(z')^{10}} - \frac{1}{2}\sum_{i=1}^{4}\frac{\sigma_{fs}^4}{(z'+(i-1)\cdot\sigma_{ss})^4}\right) \tag{5.2}$$

$$\varepsilon_{fs} = \sqrt{\varepsilon_{ff} \times \varepsilon_{ss}} \tag{5.3}$$

where ε_{fs} and ε_{ss} are the fluid-solid and solid-solid interaction energy parameters, respectively, σ_{ff} and σ_{ss} are the molecular diameter of the adsorbate and the carbon interplanar distances, respectively and ρ_{atoms} = 0.382 atoms/Å^2.

The excess adsorption (n^{Ex}) in the SLD model is given as

$$n^{Ex} = \frac{A}{2}\int_{\text{Left Side of Slit}}^{\text{Right Side of Slit}}(\rho(z)-\rho_{bulk})dz \tag{5.4}$$

where n^{Ex} is the excess adsorption of pure gas and A is the accessible surface area of the adsorbate on a particular adsorbent.

Absolute adsorption (n_{ads}^{Abs}) can be determined readily from the regressed SLD model parameters [23]. The relation between the excess adsorption and the absolute adsorption is expressed as

$$n_{ads}^{Abs} = n^{Ex} + \frac{A}{2}\rho_{bulk}(L - \frac{3}{4}\sigma_{ff}) \tag{5.5}$$

where ρ_{bulk} is the bulk gas density determined from the Peng-Robinson equation of state. Combining Equation (5.5) with Equation (5.4) yields

$$n_{ads}^{Abs} = \frac{A}{2}\int_{\text{Left side of slit}}^{\text{Right side of slit}}(\rho(z)-\rho_{bulk})dz + \frac{A}{2}\rho_{bulk}(L-\frac{3}{4}\sigma_{ff}) = V_{Ads}\rho_{Ads} \tag{5.6}$$

where V_{Ads} is adsorbed-phase volume per gram of adsorbent, ρ_{Ads} is adsorbed-phase density estimated by the averaged local adsorbed density across the slit. The use of n_{ads}^{Abs} and V_{Ads} appears later in Section 5.2.3 where the modeling of coal swelling is outlined.

5.2.2 Modifying the SLD Model to Account for Coal Swelling

In this study, additional modifications were implemented in the SLD model to facilitate the *simultaneous* modeling of gas adsorption and swelling in coals. The slit length parameter L in the SLD model represents the effective pore width of the microporous coal structure. The swelling of coals could result in altering the pore width in coals and thus, the SLD model was modified to account for these changes.

Typically, measurement of adsorption on coal is undertaken based on the assumption of constancy of void volume. In practice, the void volume can be measured using helium to estimate the total unoccupied space that excludes volume of solid material in an adsorption system. Such unoccupied space includes micropores residing in coal matrix and remaining empty volume (i.e. dead space in adsorption cell or in tubing from the reference cell to the adsorption cell). Figure 5.1(b) depicts the assumption used in this work for coal swelling such that the total expansion of micropores is identical to the total enlargement of the bulk coal matrix. By using this assumption, the total unoccupied space remains unchanged since the increase in bulk volume of coal is compensated by the increased in pore volume as depicted in Figure 5.1(c). To model this aspect, the slit length in the SLD model was considered to be a function of bulk pressure. Our analysis indicated that the following expression is useful in describing possible changes in pore width

$$L = (L_{max} - L_{min})(1 - e^{-\alpha P}) + L_{min} \tag{5.7}$$

where L_{max} and L_{min} are the maximum and minimum slit lengths and α is an exponent that allows for flexible and continuous variation of slit length as a function of pressure. Specifically, different values of α provide different curvatures of the changes in slit length with pressure. Values of α in the range of 10^{-6} to 10^{-5} yield an essentially linear relation, while α in the range of 10^{-4} to 10^{-3} yields a curvature similar to a typical Langmuir adsorption isotherm. Further, a value of zero for α reduces the model to using a constant slit length with pressure. These variations are illustrated in Figure 5.2.

5.2.3 SLD-PC Coal Swelling Model

Adsorption of gases, especially CO_2, can result in appreciable swelling of coals resulting in significant changes in the normalized permeability of a coalbed reservoir during CO_2-enhanced gas recovery processes. Such permeability changes can lead to problems related to CO_2 injectivity. The limited studies available on this behavior have indicated that permeability is related to coal mechanical properties and changes to permeability can be estimated based on strain measurements on coals. Pan and Connell [10] presented a theoretical model to investigate adsorption-induced swelling of coals. In the present study, we integrated the simplified local-density (SLD) adsorption model into the Pan and Connell (PC) swelling model. The resultant, internally-consistent SLD-PC model was used to investigate gas adsorption and swelling behavior for methane, nitrogen and CO_2 on several coals.

Pan and Connell [10] observed that the swelling measured in terms of linear strain in coals is related to the surface potential energy during gas adsorption. The adsorption of gas lowers the potential energy of the coal surface and this change can be related to the observed swelling in coals. Accordingly, by following the development outlined elsewhere [24], Pan and Connell [10] presented the following relation to describe the surface potential energy during gas adsorption

$$\Phi = \int_0^P V_{ads} dP - RT \int_0^P n_{ads}^{abs} d\ln f_{ads} \tag{5.8}$$

where Φ is surface potential energy, V_{ads} is adsorbed phase volume, n_{ads}^{abs} is absolute adsorption, f_{ads} is fugacity of the adsorbed fluid, P is pressure, and T is temperature.

The surface potential, Φ is defined and expressed as [24]

$$\Phi = \mu_{ads}^{solid} - \mu_{clean}^{solid} \tag{5.9}$$

where μ_{ads}^{solid} is the chemical potential of the coal solid with gas adsorbed on the surface and μ_{clean}^{solid} is the reference chemical potential of the clean surface without the adsorbed gas. The degrees of freedom obtained from Gibbs phase rule for adsorption of a pure component is two and the natural variables for differential functions such as the μ_{ads}^{solid} are temperature and adsorbed amount [24]. Thus, when the solid surface becomes saturated with an adsorbate, the μ_{ads}^{solid} remains unchanged at constant temperature and adsorbed amount.

Equation (5.8) facilitates the calculation of surface potential by relating it to gas adsorption, i.e., V_{ads} and n_{ads}^{abs}. When a pressure derivative is considered for Equation (5.1), the following equation is obtained

$$d \ln f_{Ads} = d \ln f_{bulk} \tag{5.10}$$

Substituting $d \ln f_{Ads}$ for $d \ln f_{bulk}$ into Equation (5.8) yields

$$\Phi = \int_0^P V_{ads} dP - RT \int_0^P n_{ads} d \ln f_{bulk} \tag{5.11}$$

As such, the SLD model can yield the surface potential Φ since both V_{ads} and n_{ads} are readily predicted by the model.

Pan and Connell [10] suggested that the surface potential can be related to linear strain in coals by the expression

$$\varepsilon = k_1 P + k_2 \Phi \tag{5.12}$$

where ε is the linear strain in coals, k_1 is $-\frac{1}{E_s}(1-2\nu_s)$ and k_2 is $-\frac{\rho_s}{E_s} f(x, \nu_s)$. These k_1 and k_2 are model constants obtained by regression of swelling data on coals. Our analysis, however,

indicates that the relation between surface potential energy and strain is non-linear especially at elevated pressures. Therefore, we adopted a three-parameter expression for the strain given as

$$\varepsilon = k_1 P + k_2 \Phi + k_3 \Phi^2 \tag{5.13}$$

where k_1, k_2 and k_3 are model constants obtained by regression of swelling data on coals. While the strain constants (k_1-k_3) may be related to mechanical properties of the solid such as the Young's modulus and Poisson's ratio [10], the parameters were regressed from available coal swelling data in the present study.

5.2.4 Permeability Model

Pan and Connell [4] studied the impact of anisotropic swelling of coal on evolution of permeability and derived stress-strain relation expressed as

$$\Delta\sigma = \frac{E_x}{E_z}\frac{(\nu_{zx} + \nu_{xy}\nu_{zy})}{1 - \nu_{xy}^2}(-(P - P_0)) + \frac{E_x(\varepsilon_x - \varepsilon_{x0})}{(1 - \nu_{xy})} \tag{5.14}$$

where, $\Delta\sigma$ is change in effective stress, E is the Young's modulus, ν is the Poisson's ratio, P is pore pressure and ε is linear strain. The subscripts "x" and "y" denote parallel directions and subscript "z" denotes perpendicular direction to the coal's bedding plane. The subscript "0" refers to the reference state measured at pressure P_0.

If isotropic swelling of coal is assumed, Equation (5.14) reduces to Shi and Durucan stress change equation.

$$\Delta\sigma = \frac{\nu}{1 - \nu}(-(P - P_0)) + \frac{E(\varepsilon - \varepsilon_0)}{(1 - \nu)} \tag{5.15}$$

Further, Seidle [25] provided the following expression to quantify the normalized permeability change in terms of the change in effective stress as

$$\frac{k}{k_0} = e^{-3C_f\Delta\sigma} \tag{5.16}$$

where k is coal permeability and C_f is cleat compressibility. To model permeability changes, we employ the three-parameter SLD-PC model (Equation 5.13) to provide values of linear strain, which is then used as an input to the permeability model described above.

Typically, there are two types of permeability model, the stress-permeability model (such as Shi and Durucan model (SD) and the porosity-permeability model (such as Palmer and Mansoori model (PM). Pan and Connell used the stress-permeability model (Equation 5.16) since stress has directional attribute used to account for anisotropic permeability change. Thus, in this work we followed Pan and Connell and chose the stress-permeability model. Clarkson [11] integrated the PC model with PM model and tested the combined model with the permeability change obtained from Fruitland coal fairway well data. His work shows that the PC-PM permeability model matched the permeability data accurately. However, our current work includes only permeability data obtained from laboratory due to, (i) the permeability data are measured in the more controlled environment that the laboratory can provide and (ii) the permeability data are reported with their corresponding swelling data or adsorption data or both of them.

5.3 Database Employed for Gas Adsorption and Coal Swelling

Coal swelling is generally measured in terms of a change in length relative to an initial length known as linear strain or $\Delta L/L_0$, where L_0 is an initial length of bulk coal sample. To measure the linear strain, either physical method or optical methods are generally utilized. In the physical method, the linear strain is measured directly by a strain gauge whereas the optical method uses an image processor and/or microscope to interpret the relative change in the length of coal sample. Table 1 presents the sources, gas adsorbates, temperature and pressure ranges for the data used in the current study. The table also lists the availability of adsorption isotherm, swelling and coal characterization data from the original authors. A brief analysis of these data is provided below.

Chen et al. [26] used a high-sensitivity linear variable differential transformer (LVDT) displacement transducer to measure linear strain in coal samples. The authors reported swelling data for methane and CO_2. However, at pressures higher than 9 MPa, the measured excess adsorption of methane was reported to be significantly greater than that of CO_2. Figure 5.3(a) and (b) present comparisons of their adsorption isotherms on both excess and absolute bases, respectively. The adsorbed-phase density used to convert the excess adsorption to the absolute adsorption for methane was assumed to be equal to the liquid density at normal boiling point [27], and the CO_2 the adsorbed-phase density was estimated from the graphical method. Figure 5.3(b) displays an absolute adsorption of methane that is *larger* for methane than for CO_2. Due to this anomalous behavior, the methane adsorption data from the authors were excluded from our model analysis. Pan and Connell [4] measured the anisotropic coal swelling of Hunter Valley coal using strain gauge. In their work, linear strain was measured in two orthogonal directions- parallel and perpendicular to the bedding plane. Their results showed that the strain in the perpendicular direction was larger than in the parallel direction at any given pressure. This anisotropic swelling behavior was also observed by Levine [2] and Day et al. [5]. Pan and Connell [4] reported the ratio of linear strains for methane, nitrogen and CO_2 to be about 1: 0.4: 2 in both parallel and perpendicular directions at about 10 MPa.

Pini et al. [3] and Ottiger et al. [6] used a disk-shaped coal sample to measure linear strain in the radial direction using an optical method. The authors reported volumetric or three-dimensional strain by assuming isotropic swelling of coal. The expression used to convert the radial strain into the volumetric strain was also provided by the authors. The volumetric strain data was restored to the radial strain because the SLD-PC swelling model is expressed in terms of linear strain.

Day et al. [5] used an optical method to measure linear strain in coal samples in both perpendicular and parallel directions. They observed that the calculated amount adsorbed at higher pressures could increase by 30% when a swelling correction is included in the adsorption data reduction

calculations. Robertson and Christiansen [13] measured linear strain in coal samples from Anderson and Gilson coal seams. Since the authors did not report the corresponding adsorption isotherm data on these coal samples, the linear strain data cannot be used directly to generate surface potential values in the SLD-PC model. To include these swelling data in our analysis, we employed our previously developed generalized SLD model [14] to predict the adsorption isotherms for methane, nitrogen and CO_2 based on the available coal characterization i.e. proximate and ultimate analyses. Our experience is that the generalized model can be expected to predict gas adsorption data based on coal characterization with an accuracy of about 15%. Additional discussion of this capability and the results obtained are provided in Section 5.4.4.

5.4 Results and Discussion

5.4.1 SLD Model Representations for Gas Adsorption Data on Coals

The SLD model was used to represent gas adsorption data on several coals from the literature. Table 5.2 lists the overall percentage average absolute deviation (%AAD) obtained in representing gas adsorption on these coals. Two cases were considered in these model regressions. Specifically, Case 1 utilized a variable slit length as a function of pressure appearing in Equation (5.7) to account for the changes in pore width, whereas Case 2 utilized a constant slit length independent of pressure. Since the expected experimental uncertainties in gas adsorption are not available for these data from the literature, the objective function used in the model regressions was the average absolute percentage deviation. As evident from Table 5.2, using a variable slit length provides improved representations of the adsorption data on these coals. Since gas species swell coals by different amounts as a function of pressure, a different α appearing in Equation (5.7) was utilized for each gas. In this manner, the effect of swelling in coals can be accounted for in the SLD-PC model.

Table 5.3 presents the SLD-PC regressed model parameters for gas adsorption data on the datasets used in this study. The table lists the parameters obtained for both Cases 1 and 2. For a meaningful

comparison, the surface areas for each adsorbate and the solid-solid interaction energy were constrained to be the same in both cases. Thus, the only difference between Cases 1 and 2 is the functionality of slit length. A comparison of slit lengths reveals that the constant slit length values from Case 2 were within the values of L_{min} and L_{max} obtained under Case 1. Further, the values of α are the highest for CO_2, intermediate for methane and lowest for nitrogen. Since the slit pore expands during adsorption-induced swelling process and the calculated slit length for each gas is proportional to a size of α at constant pressure, CO_2 causes the largest swelling at a given pressure among these gases because of its largest α value. Figure 5.4 illustrates the slit length profiles as a function of pressure for nitrogen and CO_2. The figure shows that CO_2 causes a large change in effective pore width as a function of pressure. In contrast, the effect caused by nitrogen is negligible.

In fact, before the pressure-dependent slit length expressed in Equation (5.7) was finalized, we tested the variation of the slit length as a linear function of pressure i.e. $L = \alpha P + L_{min}$. By implementing this linear function into representation of CO_2 excess adsorption, the predicted absolute adsorption is not Langmuir-like at high pressures for CO_2. Figure 5.5 illustrates the comparison of predicted absolute adsorptions when (i) the linear-pressure-dependent function is used and (ii) Equation (5.7) is used. Thus, we used Equation (5.7) since it introduces flexibility to the slit-length variation that does not result in inconsistency in absolute adsorption values. Figures 5.6(a)-(d) present the SLD-PC model representations for adsorption on coals from the literature. As evident from the figures, the model is capable of precise representations for supercritical adsorption of these gases on coals, including the near-critical region for CO_2.

5.4.2 SLD-PC Model Representations of Coal Swelling

Using the model parameters obtained from the gas adsorption data listed in Table 5.3, the SLD-PC model was used to investigate the swelling behavior of coals. For comparison, the well-known

Langmuir model, combined with the Pan and Connell swelling model (Langmuir-PC, Equation (5.24) in Pan and Connell [10]), was also tested. Table 5.4 presents the results obtained from the Langmuir-PC, the two-parameter SLD-PC and the three-parameter SLD-PC models. Overall, the three parameter SLD-PC model provided about half the error of the Langmuir-PC model. Table 5.5 lists the parameters obtained from the SLD-PC model for use in Equation (5.13) for each system.

An important difference between the SLD-PC and the Langmuir-PC models is that the SLD-PC model uses gas fugacities to determine the surface potential shown in Equation (5.11), whereas the Langmuir-PC model utilizes the ideal gas assumption and uses gas pressure instead of fugacities. Typical curvatures for the surface potential obtained from the SLD-PC and the Langmuir-PC models are depicted in Figure 5.7, which indicates that the curvature for surface potential obtained from the SLD-PC model is asymptotic at higher pressures. This asymptotic behavior is similar to the observed curvature of experimental linear strain in coals. When the coal surface is saturated with adsorbed gas, the surface potential becomes almost constant for higher pressures. Further, as shown in Figure 5.7, the SLD-PC model gives the correct curvature for surface potential in the high pressure region whereas the surface potential profile for the Langmuir-PC model increases almost linearly up to much higher pressures. In fact, the Langmuir-PC model yields a logarithm expression for surface potential [10] that does not provide the correct asymptotic behavior. Thus, using gas fugacities is more appropriate in calculating adsorption surface potential.

To confirm the important role of gas fugacity in determining the surface potential profile, illustrative calculations were made with the SLD-PC model using either the gas pressure or fugacity. Figure 5.8 presents the results obtained for these scenarios, showing clearly that the use of fugacity in the integration for surface potential is a significant factor. Since the SLD model readily calculates the bulk gas fugacities as part of adsorption equilibrium calculations, using the fugacities instead of the pressure in the SLD-PC model is quite straightforward. Further, the SLD model utilizes slit shaped pore geometry that facilitates estimating the adsorbed-phase volume

required in the first term of Equation (5.11). This term can be significant at high pressures and has been accounted for explicitly by the SLD-PC model.

Figure 5.9 presents a comparison between the surface potential obtained by the SLD-PC and the Langmuir-PC models. Since fugacity is approximately equal to pressure for lighter gases such as nitrogen and methane at the pressures of interest, the surface potential estimated by both models is similar for these gases. However, a large difference in surface potential is observed in CO_2, which is attributed to the non-ideality of high-pressure CO_2 gas as evident in Figure 5.10. The figure shows that pure CO_2 deviates by approximately 40% from ideal gas behavior at the highest pressures, while nitrogen is almost ideal and methane deviates by no more than about 10%. As such, this figure suggests that replacing fugacity with pressure in calculating surface potential is not appropriate for CO_2 but is fairly appropriate for methane and nitrogen.

Further, for the fair comparison between SLD-PC and Langmuir-PC models, the bulk fugacities have been utilized in the Langmuir-PC model. Figure 5.11 depicts the comparison between the SLD-PC and Langmuir-PC when the bulk fugacities are used in surface potential calculations. The figure shows that for lighter gases both models produce comparable surface potential values while significant difference is observed for the surface potential of CO_2. In the SLD adsorption calculation the absolute adsorption is internally consistent and corresponds with bulk phase fugacity since these values satisfy the adsorption equilibrium appearing in Equation (5.1). Given that the Langmuir model does not have the equilibrium criterion, the absolute adsorptions and the bulk fugacities do not relate and correspond to each other. As such, using a rigorous adsorption model such as the SLD model offers a distinct advantage over simpler, empirical adsorption models.

Figure 5.12 presents the relation observed between the calculated surface potentials and the linear strains in coals [3]. Note that the “best” curve that fits these data is constrained to pass though the

zero coordinates since strain is identically zero when surface potential is zero. As seen from the figure, the relation is non-linear at the higher pressures and this is accounted for in the SLD-PC model by including a quadratic term as shown in Equation (5.13). Note that the uncertainties shown in Figure 5.12 were provided by the authors. Figures 5.13(a) and (b) present the SLD-PC results for representing linear strain in coals. Both the two- and three-parameter SLD-PC models as well as the Langmuir-PC model are shown in these figures. The SLD-PC model provides improved representations, especially for CO_2-induced strain in coals. Figure 5.14 presents the deviations in linear strain in coals obtained with the SLD-PC model (Case 1) for each gas. Most of the data are represented within a deviation of 0.02 in linear strain, which is also close to the RMSE given in Table 5.4.

As mentioned previously, absolute adsorption is required in the integral appearing in Equation (5.11) for calculating the surface potential. For empirical adsorption models such as the Langmuir model, an important aspect of determining absolute gas adsorption is the estimation of the adsorbed-phase density, which is not measureable experimentally. Typical estimates used for coals are the liquid density values at the normal boiling point [27] or triple-point density for CO_2. The adsorbed-phase density values are used to estimate absolute adsorption from experimentally measured excess adsorption data. Figure 5.15(a) presents absolute adsorption of CO_2 based on two different estimates of adsorbed-phase densities. The two estimates were 1 g/cc, which has been used in previous studies [28] and 1.25 g/cc obtained from the graphical method [29], as illustrated in Figure 5.15(b). Figure 5.15(a) indicates that the density estimate obtained from the graphical method appears more suitable for this system. Note that the SLD model provided an estimate of 1.22 g/cc, which is in good agreement with the graphical estimate. This further confirms the assertion that the SLD model can provide reliable estimates for adsorbed phase densities and absolute adsorption based solely on the excess adsorption data.

5.4.3 Effect of Different Adsorbates on Coal Swelling

In this study, we also tested the hypothesis [10] that the swelling of a specific coal is related more strongly to the *amount* of gas adsorbed rather than the *particular gas* adsorbed. In other words, when different gases are compared at the *same* adsorption level, the observed strains in the coal appear to be similar. Table 5.6 presents a comparison of absolute adsorption amounts of three gases and their corresponding strains observed for several different coals. The results indicate that the coals undergo comparable swelling (columns 5 and 6) when the amount of absolute adsorption (column 2) of the different gases is the same. Note that in Table 5.6, there is up to a 16% difference in strain values induced by CO_2 and methane adsorption reported in one of the datasets. However, these strains [6] are within the reported experimental uncertainties and, as such, this difference may not be significant. As such, the results indicate that similar amounts of strain are produced in coals for equal levels of adsorption of any of the three gases studied in this work. This observation lends credence to the hypothesis proposed by Pan and Connell [10].

5.4.4 SLD-PC Model Representation of Coal Swelling in Absence of Experimental Adsorption Data

Robertson and Christiansen [13] reported the linear strain in two coal samples from the Gilson and Anderson seams of the Black Warrior basin. However, the authors did not report corresponding adsorption data on these coals, which is required for a complete analysis of swelling data using the SLD-PC model. Therefore, we used our previously developed generalized adsorption model to obtain *a priori* predictions of adsorption for these two coals. Our previous work [14] has shown that the generalized SLD model is capable of providing useful predictions for adsorption based solely on the ultimate and proximate analyses of coals. In particular, the generalized model was tested in our earlier study on several coal samples with widely varying coal rank and the adsorption predictions were within about 12%, on average.

Using the coal characterization from the Gilson and Anderson seams, adsorption isotherms were predicted from the generalized SLD model. Then, the SLD-PC model was used to represent the swelling behavior of these coals. Table 5.7 presents the results obtained for linear strain in these coals. The strain data for the Gilson and Anderson seam coals were represented with about 7 and 11 %AAD and RMSE of about 0.02 in linear strain, which is also the overall RMSE for all other systems we studied. Thus, the method adopted to predict adsorption data from coal characterization and its subsequent use for estimating surface potential and strain in coals appears useful in cases where experimental adsorption data are unavailable.

To further test this prediction method, we performed a similar calculation where the experimental adsorption data were, in fact, available. We utilized coal characterization data from Pan and Connell [4] and predicted the adsorption isotherms for methane, nitrogen and CO_2 from the generalized SLD model developed earlier. The model predictions yielded AADs of 7, 13 and 10% for adsorption of methane, nitrogen and CO_2 when compared with the experimental data. Thus, the generalized model appears capable of providing gas adsorption predictions with reasonable accuracy. Using the predicted adsorption data, the SLD-PC model yielded overall results of about AAD of 6% and RMSE of 0.008 in linear strain for representing the linear strain induced in coal by adsorption of methane, nitrogen and CO_2. The results and the model parameters obtained for these systems are summarized in Table 5.7.

Although this prediction method has provided promising results for these three systems, additional testing of this approach is required. Unfortunately, none of the other systems in Table 5.1 contained the ultimate and proximate analyses of the coal samples, which precluded additional testing of this predictive approach. We encourage those performing future experiments on adsorption and/or swelling to report the corresponding coal characterization information. This will facilitate additional analysis of different approaches and models used to describe the relation between coal properties, gas adsorption and swelling behavior.

5.4.5 Adsorption-Induced Strain and Normalized Permeability Changes in Coal

The SLD-PC approach and the permeability model discussed previously were used to represent the changes in coal permeability resulting from gas adsorption. Table 5.8 presents the model parameters obtained and the corresponding statistics for two systems. In these permeability representations, Equation (5.15) was used since the authors assumed isotropic swelling in coals. The regressed parameters given in Table 5.8 for Sulcis and Anderson coals i.e. Poisson's ratio, ν, Young's modulus, E and cleat compressibility, C_f are within the expected range reported in literature [30-32]. Typical values for these parameters are about 0.2 to 0.5 for Poisson's ratio, 0.8 to 3.4 GPa for Young's modulus and 0.044 to 0.363 MPa^{-1} for Cleat compressibility. Although the Poisson's ratios in Table 5.8 appeared to be higher than the typical value of 0.35 [11, 25], the ratios are within the range reported in literature for the same rank of coal. For example, Sulcis coal is ranked bituminous coal that the Poisson ratio range is reported about 0.2-0.5 for a bituminous coal in Gentzis et al. (2007). Figures 5.16(a) and (b) present the model representations of normalized permeability changes in coal due to CO_2 adsorption. As evident from these figures, the permeability model combined with the SLD-PC approach provides useful representations of the normalized permeability profiles for these coals. Further testing of this approach is recommended when additional data encompassing gas adsorption, swelling and permeability measurements become available.

Historically, studies on gas adsorption on coals have treated the effect of swelling superficially or ignored it completely. The approach presented here combines a theoretical adsorption model with a swelling model to provide a self-consistent approach to investigate coal swelling behavior and permeability changes in coal affected by gas adsorption.

5.5 Conclusion

A modeling study was conducted to investigate the gas-adsorption-induced swelling and permeability changes in coals. The SLD model was extended to account for the effect of coal swelling on adsorption predictions. Further, the SLD model was integrated with the PC swelling model to relate linear strain in coals to adsorption and tested using data for methane, nitrogen and CO2 adsorption. The resultant SLD-PC model provided useful representations of both supercritical gas adsorption and swelling behavior on diverse coals. Further, a simple non-linear model was found capable of describing the relation between strain and surface potential for these systems.

Results indicate that the SLD-PC model yields lower errors than the commonly employed Langmuir model. Further, the SLD model provided generalized predictions of adsorption based solely on adsorbent characterization, which is a unique capability of the SLD model as of this writing. This approach was demonstrated by testing this capability on three representative systems. The results indicate that the model appears capable of providing useful predictions in cases where adsorption data on coals are not reported with the corresponding swelling data.

An important application of the adsorption-induced coal swelling modeling is predicting changes in coal permeability based on the knowledge of swelling behavior. Our results indicate that the SLD-PC approach is capable of providing representations of gas adsorption and linear strain and, when combined with the permeability model, the approach highlighted herein can provide useful capability in the form of a unified modeling framework for describing the interrelations among adsorption, strain and permeability of coals.

The SLD-PC model represents the strain data well at high pressure specifically near the critical pressure of CO2. This indicates that the SLD-PC model is suitable for ECBM application where CO_2 is injected at pressure significantly higher than the initial reservoir pressure. However, for the system that the operating pressure is low to moderate such as the primary depletion of coalbed gas, using either the SLD-PC or a simpler model such as Langmuir-PC model should produce comparable results.

Table 5.1. Gas Adsorption and Swelling Data Used in this Study

Data Source	Coal Sample	Method Used	Gas Adsorbates	Temperature (K)	Pressure Range (MPa)	Adsorption Isotherm	Characterization Data	Linear Strain Data	Permeability Data
Chen et al.[26]	Chinese coal	Physical LVDT	CO_2	318	0-18	X	-	X	-
Pan and Connell [4]	Hunter Valley Coal	Strain gauge	CH_4, N_2, CO_2	308	0-12	X	X	X	-
Pini et al. [3]	Sulcis Coal*	Optical	N_2, CO_2	318	0-13	X	-	X	X
Ottiger et al. [6]	Sulcis Coal**	Optical	CH_4, CO_2	318	0-13	X	-	X	-
Day et al. [5]	-	Optical	CO_2	313	0-12	X	-	X	-
Robertson and Christiansen [13]	Anderson and Gilson Coal	Optical	CH_4, N_2, CO_2	300	0-7	-	X	X	X

*Sample was extracted in 2004; **Sample was extracted in 2006; X indicates that information is available.

Table 5.2. Model Representations of Gas Adsorption Data from the Literature

Data Source	Coal Sample	%AAD in Adsorption	
		Case 1*	Case 2**
Chen et al. [26]	Chinese coal	2.9	4.6
Pan and Connell [4]	Hunter Valley Coal	1.3	6.9
Pini et al. [3]	Sulcis Coal	1.7	4.2
Ottiger et al. [6]	Sulcis Coal	1.4	4.7
Day et al. [5]	-	8.5	9.8
Overall		**3.2**	**6.0**

*Case 1 - variable slit length; **Case 2 - constant slit length

Table 5.3. SLD-PC Model Parameters for Gas Adsorption on Coals

Parameters	Data Source									
	Chen et al. [26]		**Pan and Connell [4]**		**Pini et al. (2009)**		**Ottiger et al. [6]**		**Day et al. [5]**	
	Case 1	**Case 2**	**Case 1**	**Case 2**	**Case 1**	**Case 2**	**Case 1**	**Case 2**	**Case 1**	**Case 2**
CH_4 surface area (m^2/g)	-	-	73.6	73.6	-	-	102.0	102.0	-	-
N_2 surface area (m^2/g)	-	-	58.0	58.0	78.8	78.8	-	-	-	-
CO_2 surface area (m^2/g)	154.7	154.7	91.6	91.6	115.7	115.7	124.8	124.8	200.2	200.2
ε_{ss}/k (K)	24.7	24.7	25.5	25.5	41.5	41.5	35.0	35.0	16.8	16.8
L_{min} (nm)	0.59	1.12	0.69	0.97	0.84	1.19	0.79	1.13	0.83	0.90
L_{max} (nm)	1.13		1.10		1.21		1.17		0.91	
α_{CH4} (1/psia)	-	-	1.74E-03	-	-	-	6.50E-04	-	-	-
α_{N2} (1/psia)	-	-	9.56E-04	-	1.58E-04	-	-	-	-	-
α_{CO2} (1/psia)	3.98E-03	-	2.08E-03	-	3.80E-03	-	3.73E-03	-	1.74E-03	-

Table 5.4. Model Statistics for Coal Swelling: Errors in Linear Strain Predictions

Database	Langmuir-PC			Two Parameter SLD-PC			Three Parameter SLD-PC		
	%AAD	RMSE	WAAD	%AAD	RMSE	WAAD	%AAD	RMSE	WAAD
Chen et al. [26]	3.7	0.018	NA*	2.7	0.013	NA	1.3	0.007	NA
Pan and Connell [4]	9.0	0.034	1.8	6.5	0.015	1.3	4.0	0.008	0.8
Pini et al. [3]	9.7	0.054	0.5	10.2	0.049	0.5	7.8	0.036	0.3
Ottiger et al. [6]	7.4	0.052	0.5	8.0	0.067	0.7	4.2	0.035	0.3
Day et al. [5]	6.9	0.025	NA	4.2	0.018	NA	1.7	0.009	NA
Overall	9.7	0.040	-	6.5	0.037	-	4.1	0.022	-

%AAD is the average absolute percentage deviation, RMSE is root-mean-squared error in linear strain and WAAD is weighted average absolute deviation in linear strain. NA refers to unavailability of experimental uncertainties from the original authors. *Note: All SLD-PC statistics are based on Case 1(Equation 5.7).*

Table 5.5. SLD-PC Model Parameters (Equation 5.13) for Linear Strain in Coals

Data Source	Direction	k_1 (MPa^{-1})	k_2 (J/g)	k_3 $(J/g)^{-2}$
Chen et al. [26]	NS	-7.30E-03	-4.43E-02	8.79E-04
Pan and Connell [4]	Perpendicular	2.04E-03	-7.55E-02	1.33E-03
	Parallel	-1.03E-03	-3.98E-02	1.52E-03
Pini et al. [3]	NS	-4.97E-03	-5.07E-02	1.90E-03
Ottiger et al. [6]	NS	5.23E-03	-5.27E-02	1.88E-03
Day et al. [5]	Perpendicular	-5.59E-04	-3.73E-02	3.46E-03
	Parallel	-3.16E-03	-3.80E-02	1.17E-03

*NS refers to not specified by the author

Table 5.6. Adsorption and Linear Strain: Comparison of Different Adsorbates at Same Adsorbed Amount

Source	Absolute Adsorption (mmol/g)	Adsorbate	Pressure (MPa)	Percentage Linear Strain	
				Perpendicular	Parallel
Pan and Connell [4]	0.60	CH_4	2.2	0.21	0.11
		N_2	9.7	0.19	0.09
		CO_2	0.3	0.19	0.10
	0.50	CH_4	1.4	0.16	0.08
		N_2	6.6	0.15	0.07
		CO_2	0.2	0.14	0.07
	0.40	CH_4	0.8	0.11	0.06
		N_2	4.3	0.11	0.05
		CO_2	0.1	0.09	0.05
Pini et al. [3]	0.75	N_2	5.8	0.148	
		CO_2	0.2	0.180	
	0.50	N_2	2.3	0.082	
		CO_2	0.1	0.087	
	0.25	N_2	0.8	0.034	
		CO_2	0.02	0.031	
Ottiger et al. [6]	1.50	CH_4	11.7	0.658	
		CO_2	1.4	0.567	
	1.00	CH_4	2.8	0.324	
		CO_2	0.4	0.287	
	0.50	CH_4	0.5	0.099	
		CO_2	0.1	0.085	

Table 5.7. Summary Model Statistics for SLD-PC Model Representations of Coal Swelling in Absence of Adsorption Data

Data Source	Coal Sample	Adsorbates	%AAD	RMSE	Direction	SLD-PC Parameters		
						k_1 (MPa^{-1})	k_2 (J/g)	k_3 $(J/g)^{-2}$
Robertson and Christiansen [13]	Anderson	CH_4, N_2, CO_2	7.2	0.020	NS	-1.09E-02	-1.10E-01	8.24E-03
Robertson and Christiansen [13]	Gilson	CH_4, N_2, CO_2	11.2	0.022	NS	-3.34E-03	-9.44E-02	3.47E-03
Pan and Connell [4]	Hunter Valley	CH_4, N_2, CO_2	6.3	0.008	Perpendicular	-2.10E-03	-1.07E-01	-5.45E-04
					Parallel	-3.63E-03	-5.84E-02	5.25E-04

*NS refers to not specified by the author

Table 5.8. Summary Model Statistics for Permeability Model Representations of Normalized permeability Changes Due to CO_2 Adsorption: Data from [3, 31]

Model Parameter	Sulcis Coal	Anderson Coal
Young's Modulus, E (GPa)	2.41	1.09
Poisson's ration, ν	0.48	0.45
Cleat compressibility, C_f (1/MPa)	0.225	0.228
Statistics for Normalized permeability	**Sulcis Coal**	**Anderson Coal**
%AAD	2.2	3.7
RMSE	0.06	0.03

Figure 5.1(a). Adsorption and Swelling of Coal Matrix

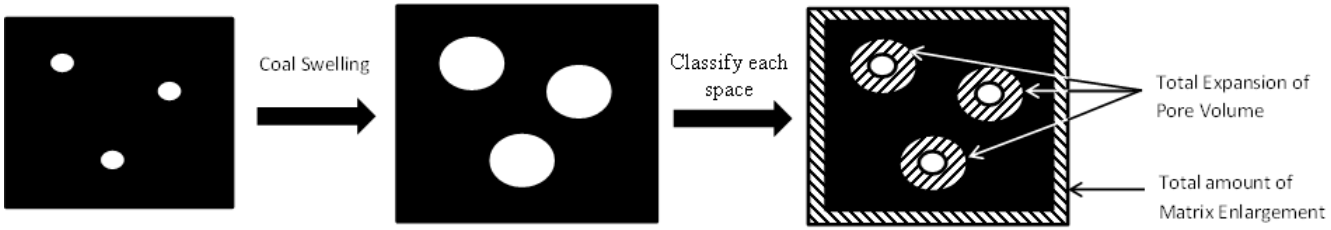

Figure 5.1(b) Equality of Total Expansion of Pore Volume and Total amount of Matrix Enlargement

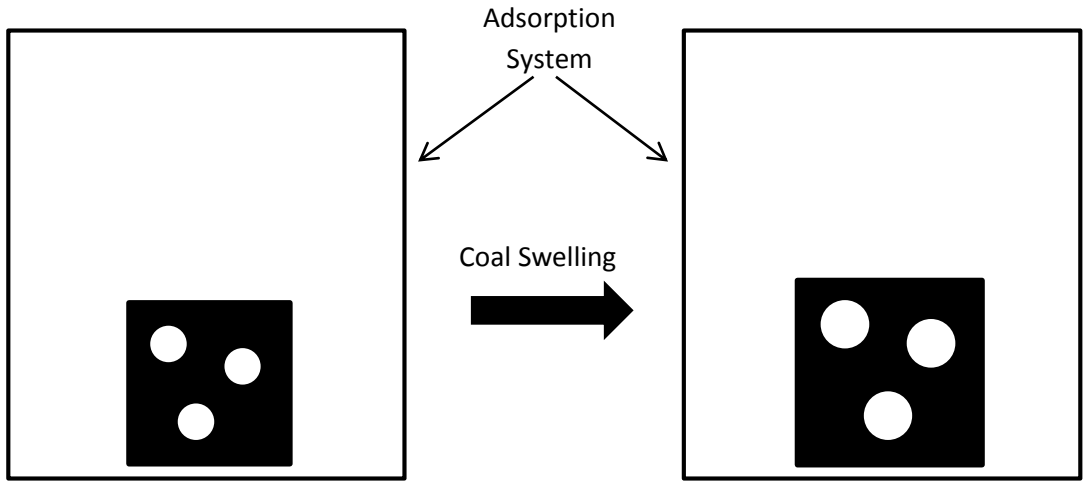

Figure 5.1(c) Constant Empty Space in an Adsorption System: White Area Represents Void Space and Black Area Represents Coal Solid in Adsorption System

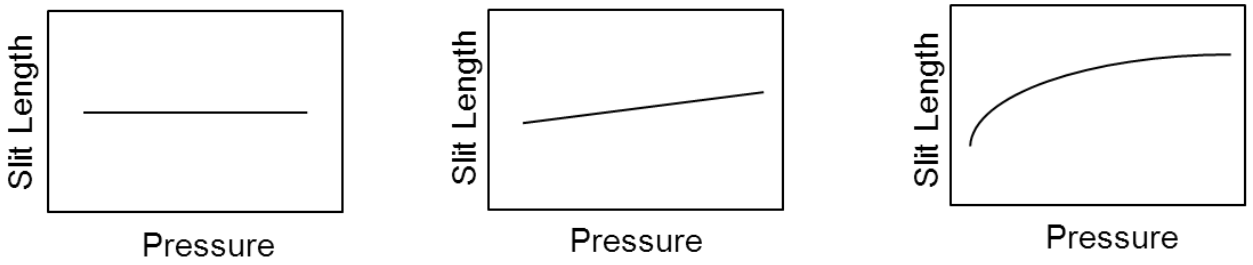

Figure 5.2. Effect of increasing swelling exponent α (from left to right) on the curvature of slit length profile

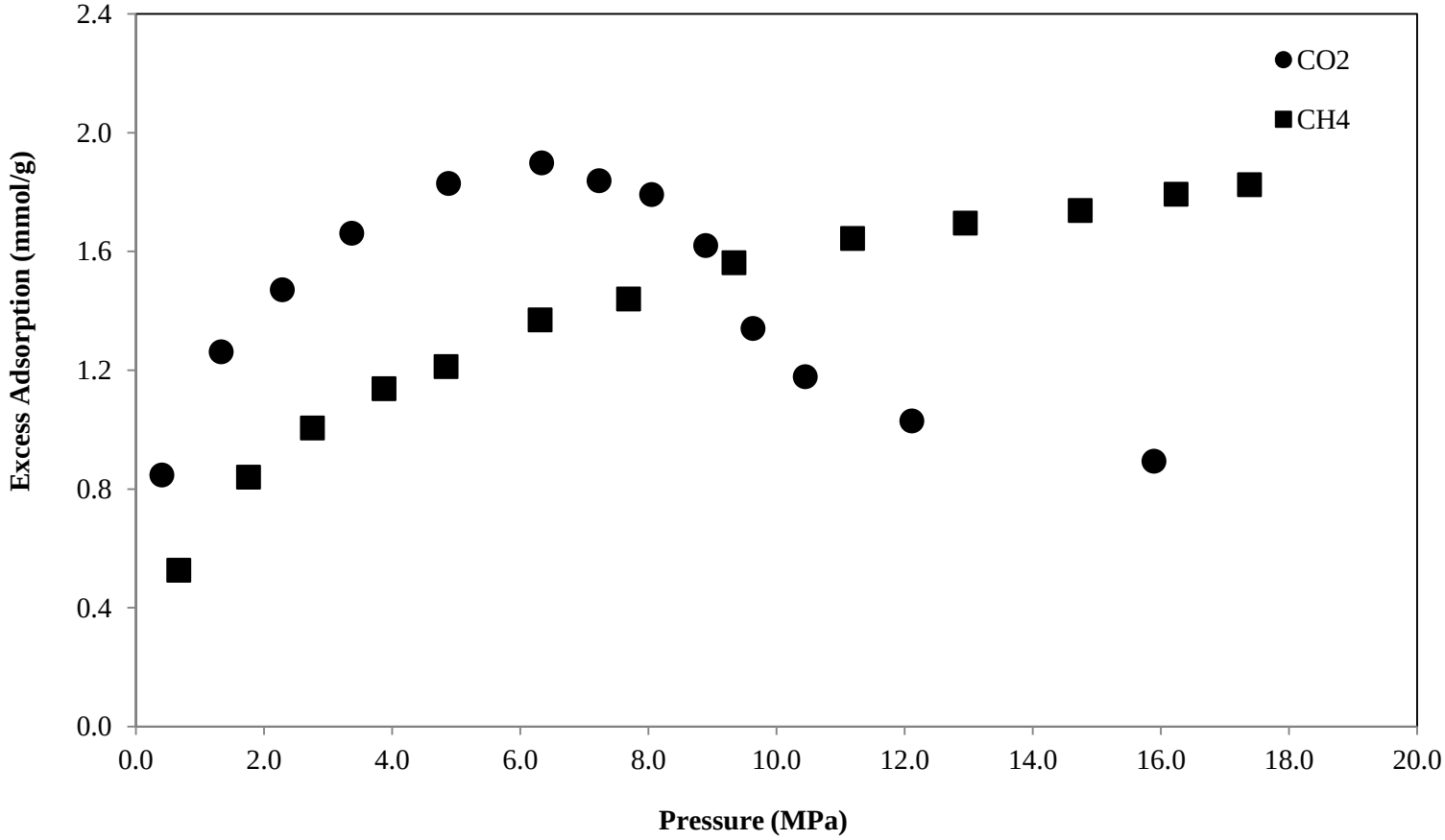

Figure 5.3(a). Comparison of Excess Adsorption of Methane and CO_2 (Points are data from [26])

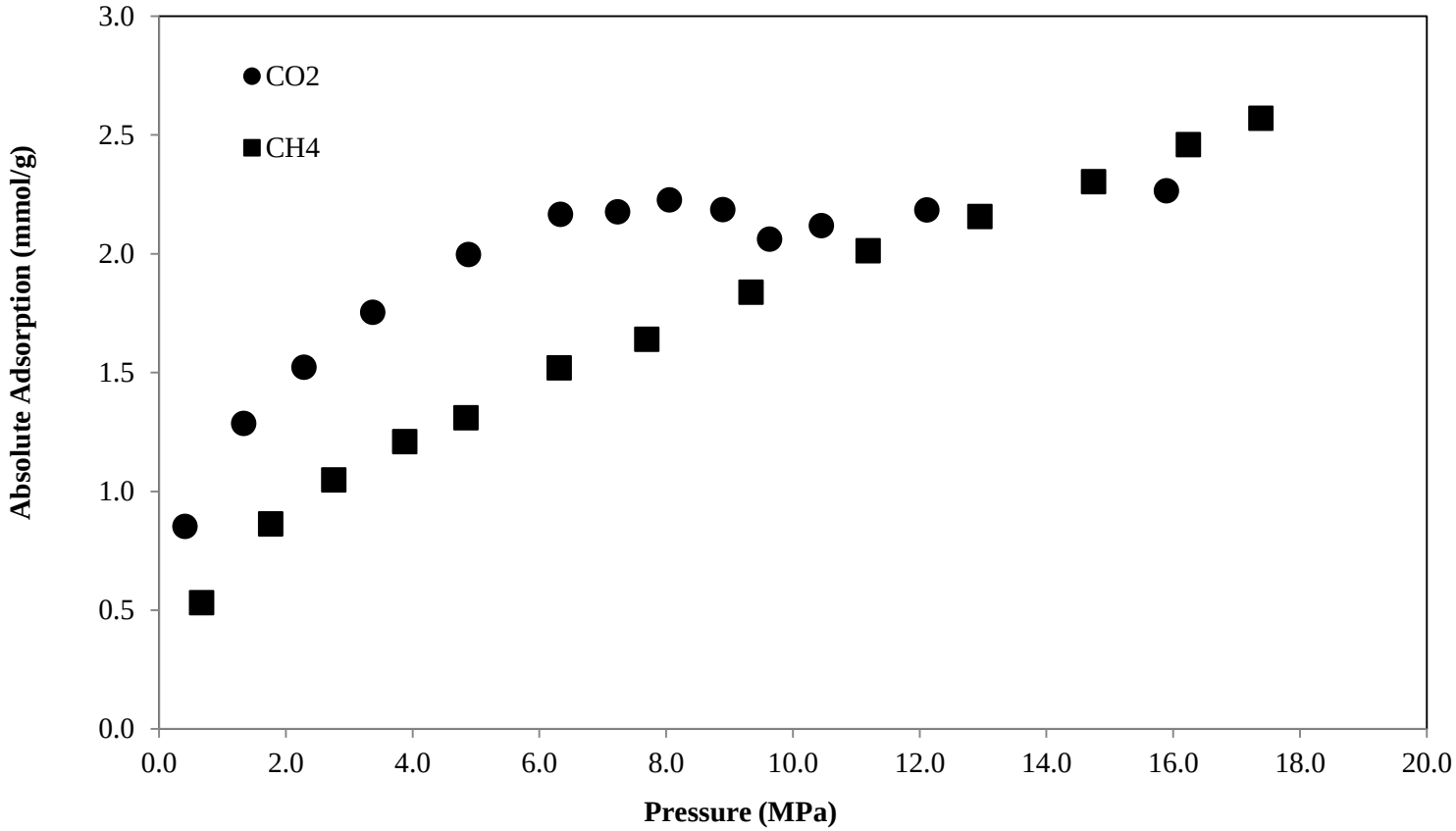

Figure 5.3(b). Comparison of Absolute Adsorption of Methane and CO_2 (Points are data from [26])

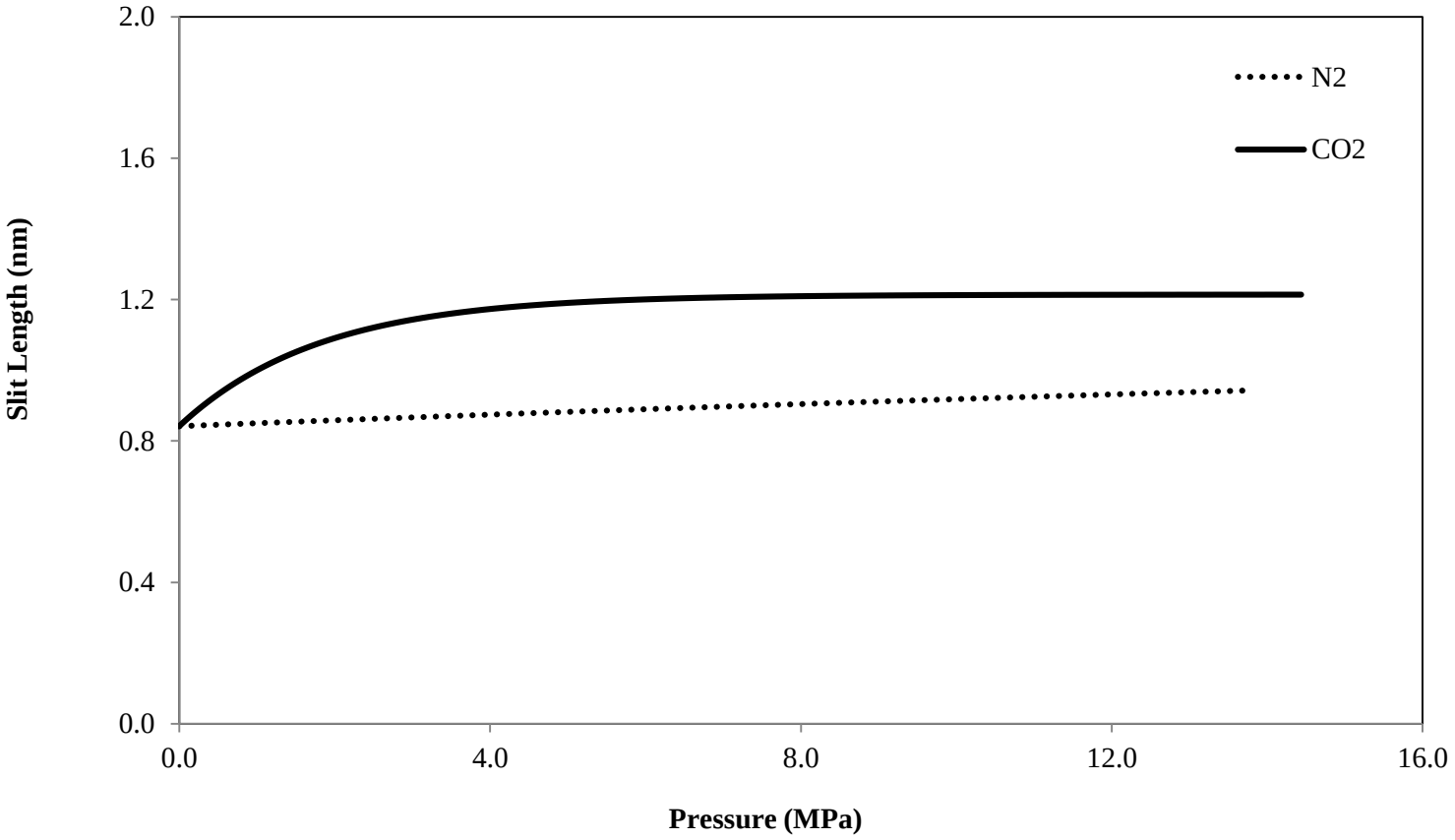

Figure 5.4. Slit length profiles as a function of equilibrium pressure (fits to data from [3])

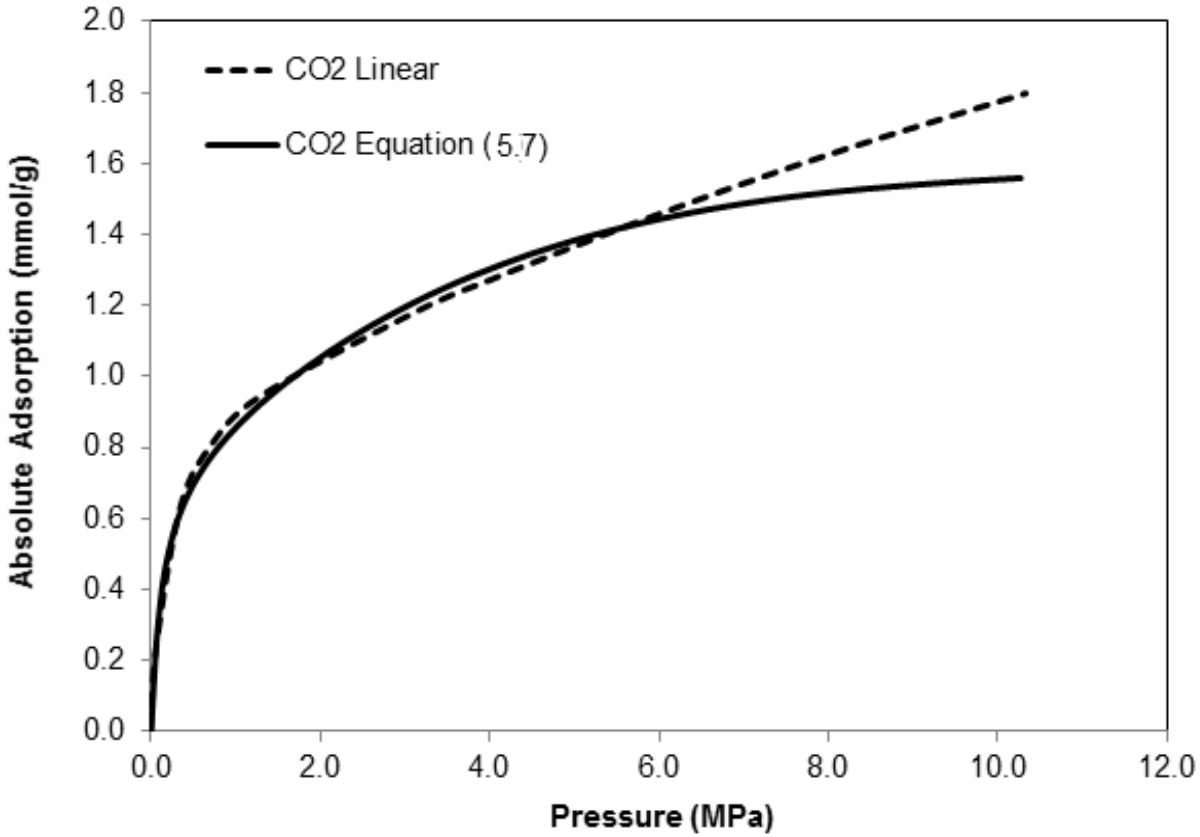

Figure 5.5. Absolute Adsorption Profile: Comparison between the Linear-Pressure-Dependent Slit Length and the Pressure-Dependent Slit Length in Equation (5.7) based on Fit to Adsorption Data from [4]

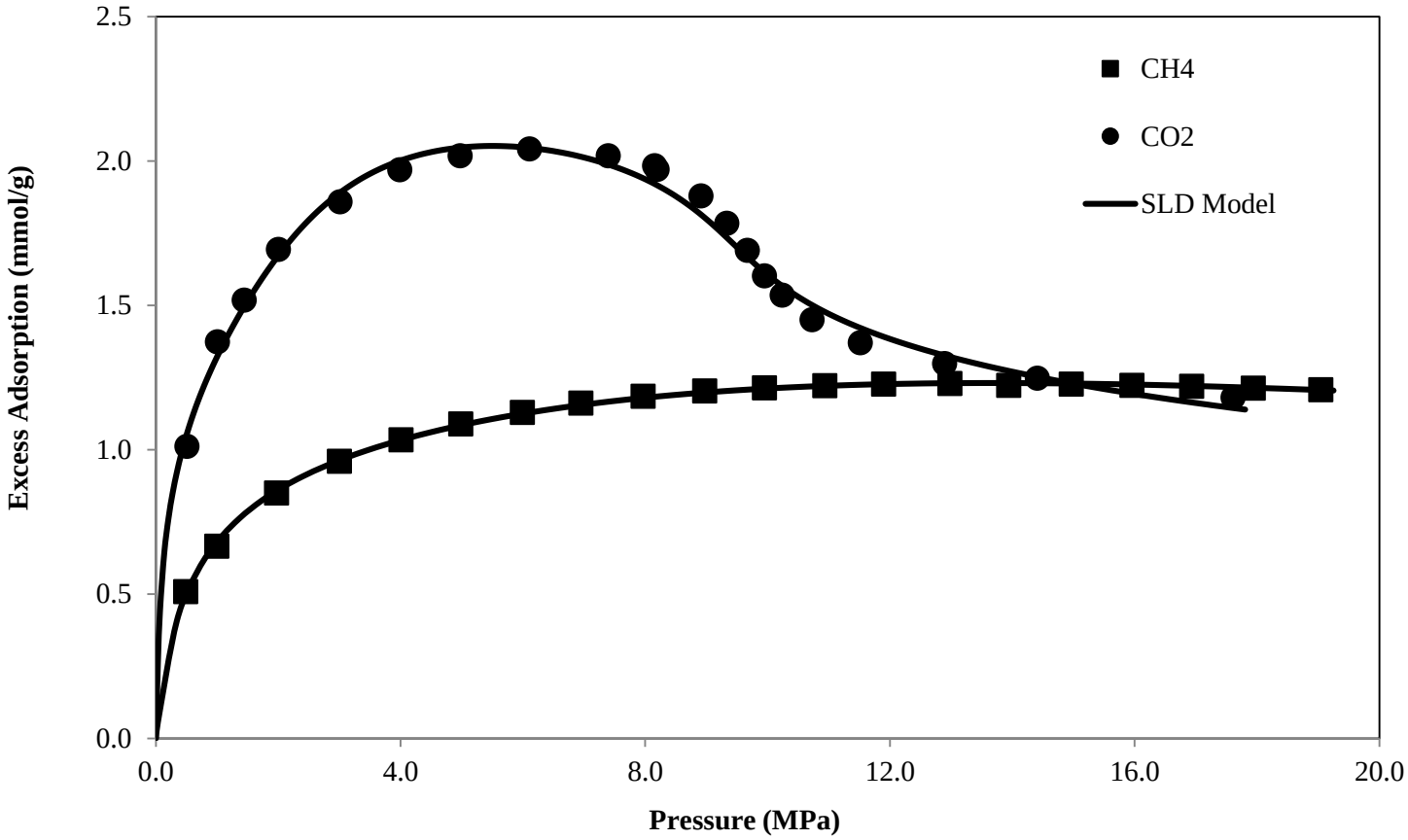

Figure 5.6(a). SLD Model Representation for Gas Adsorption
(Points are data from [6])

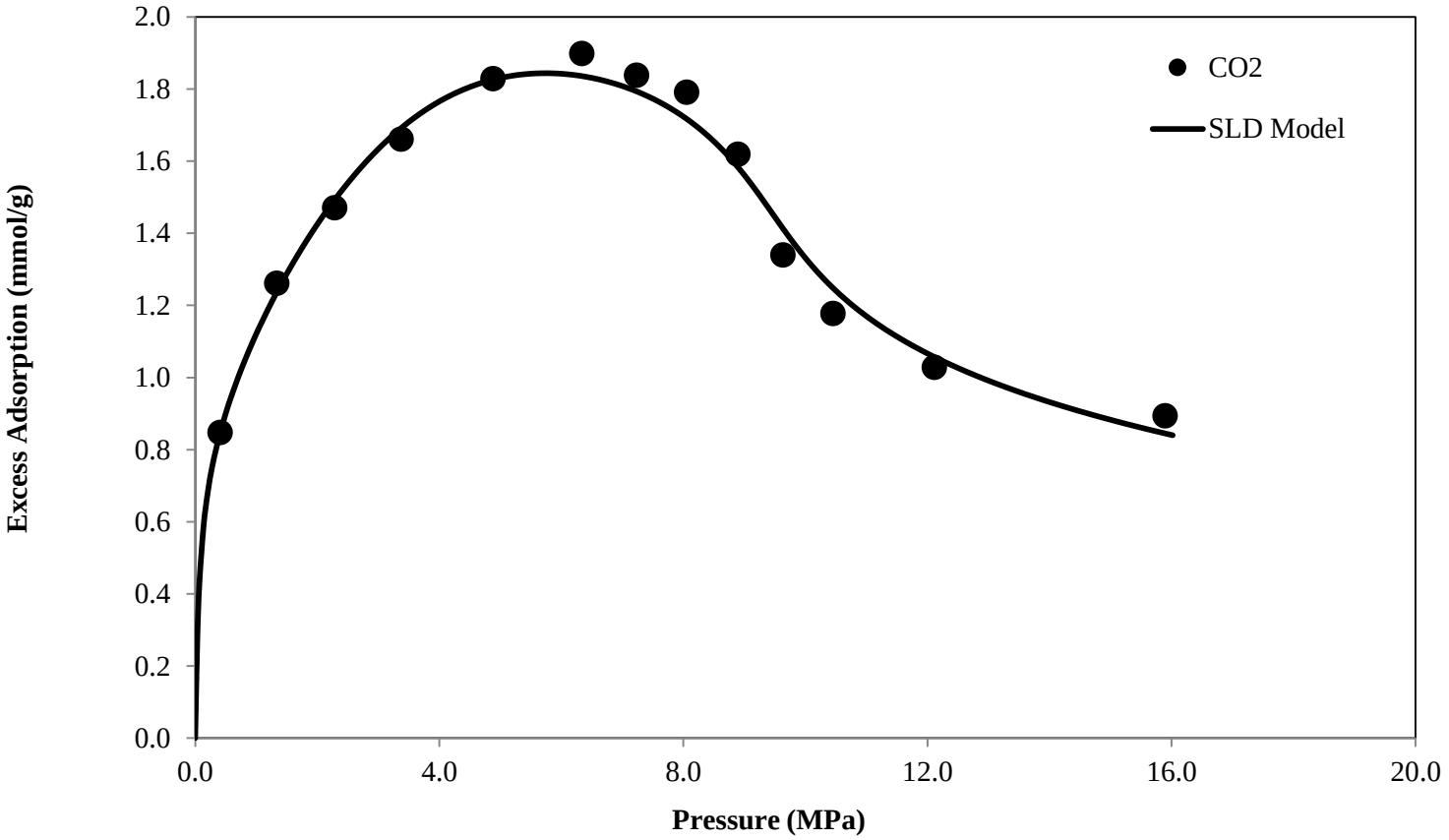

Figure 5.6(b): SLD Model Representation for Gas Adsorption
(Points are data from [26])

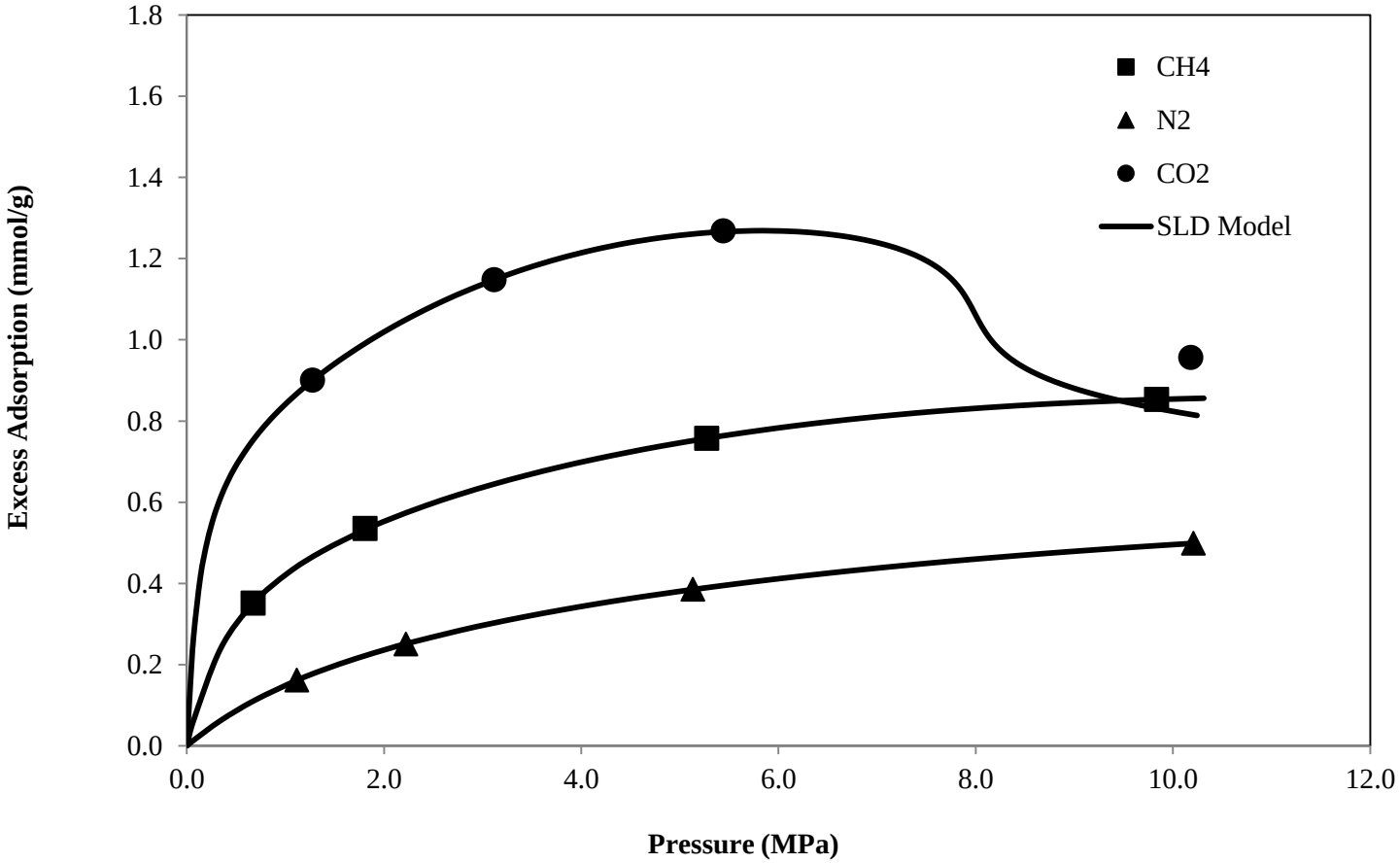

Figure 5.6(c). SLD Model Representation for Gas Adsorption (Points are data from [4])

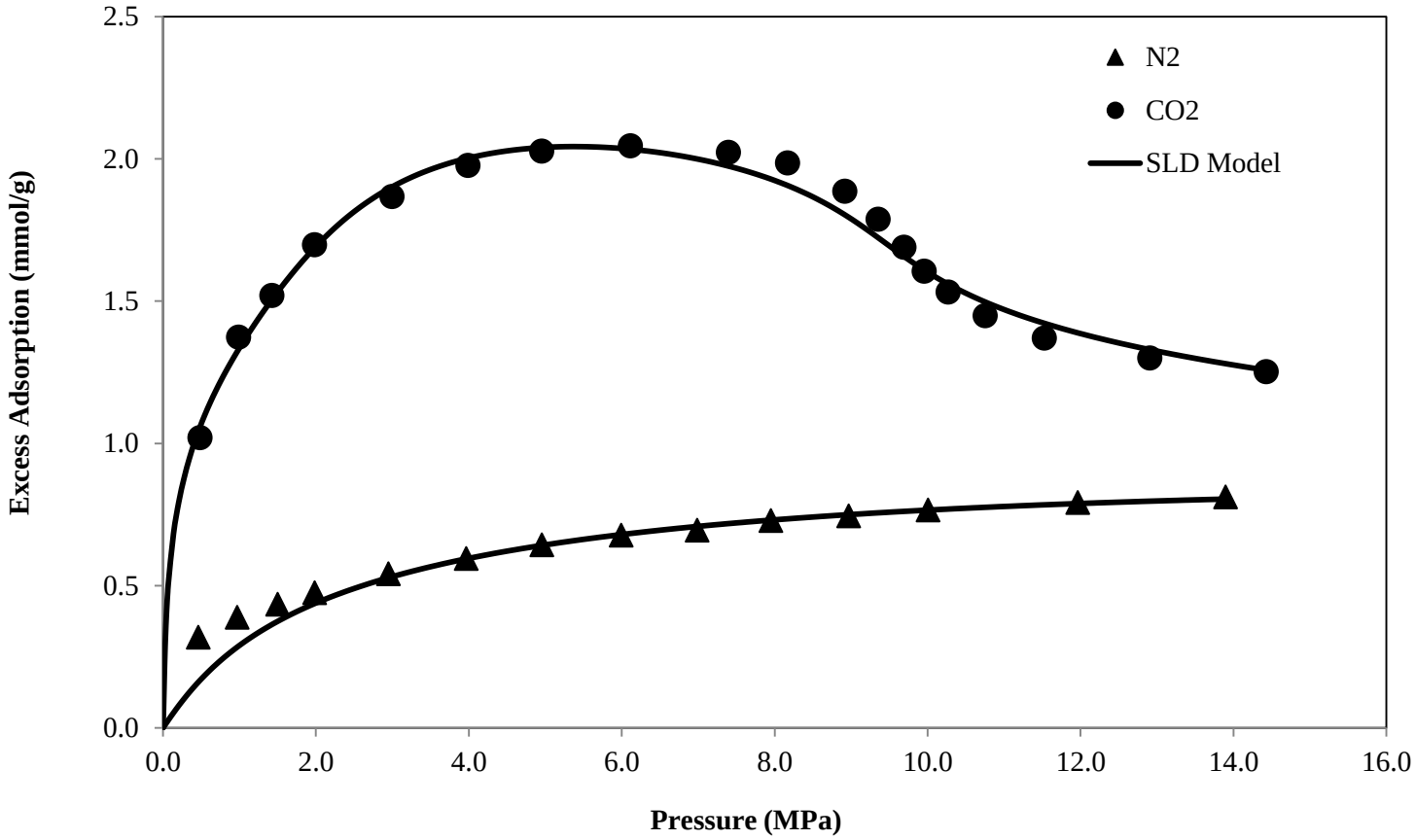

Figure 5.6(d). SLD Model Representation for Gas Adsorption
(Points are data from [3])

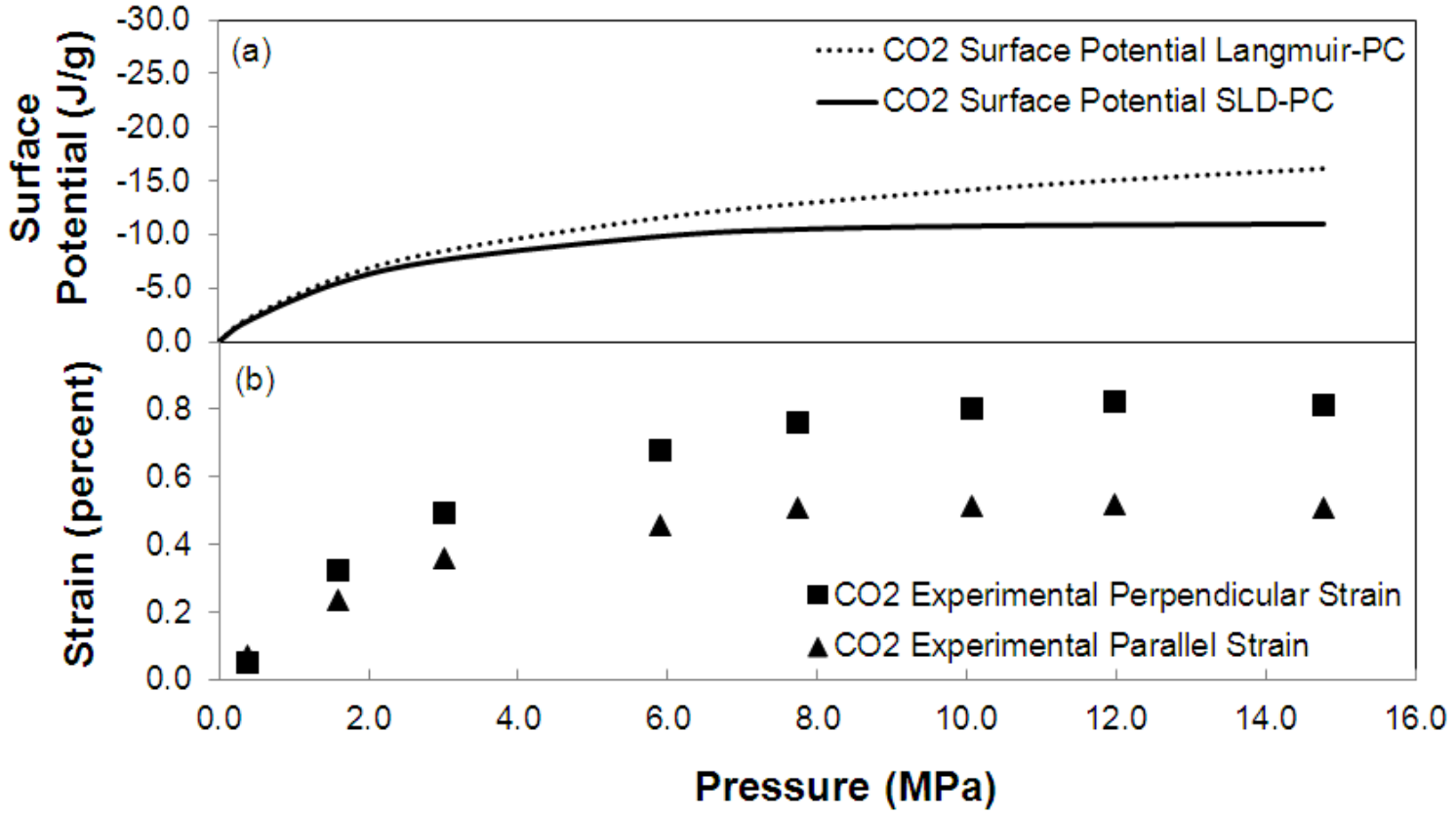

Figure 5.7. Comparison of Surface Potential Profiles and Experimental Strain (Data from [5]): (a) Surface Potential Profiles from SLD-PC and Langmuir-PC models and (b) Experimental Strain

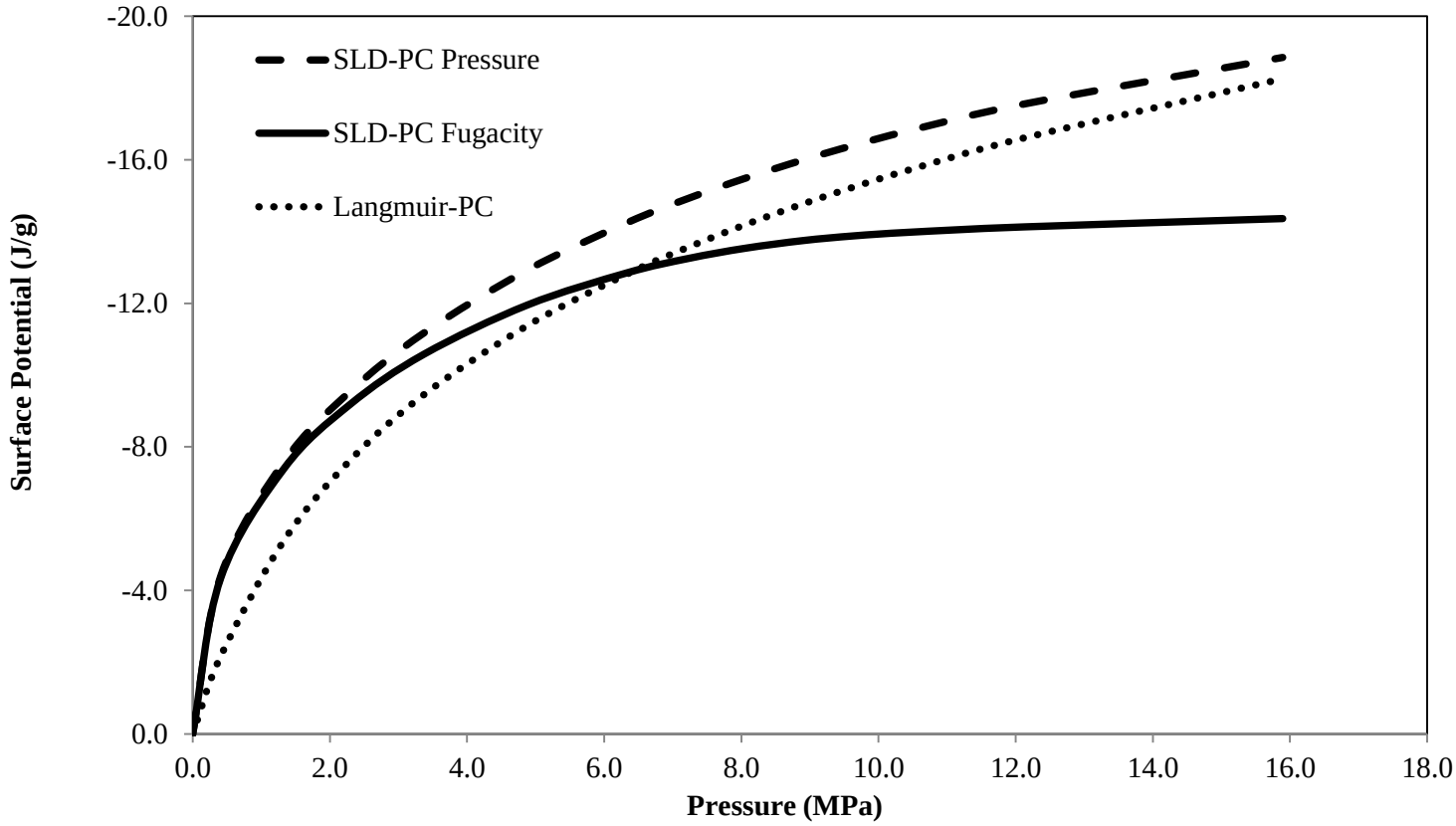

Figure 5.8. Surface potential profiles using fugacity or pressure based on fits to CO_2 data from [26]

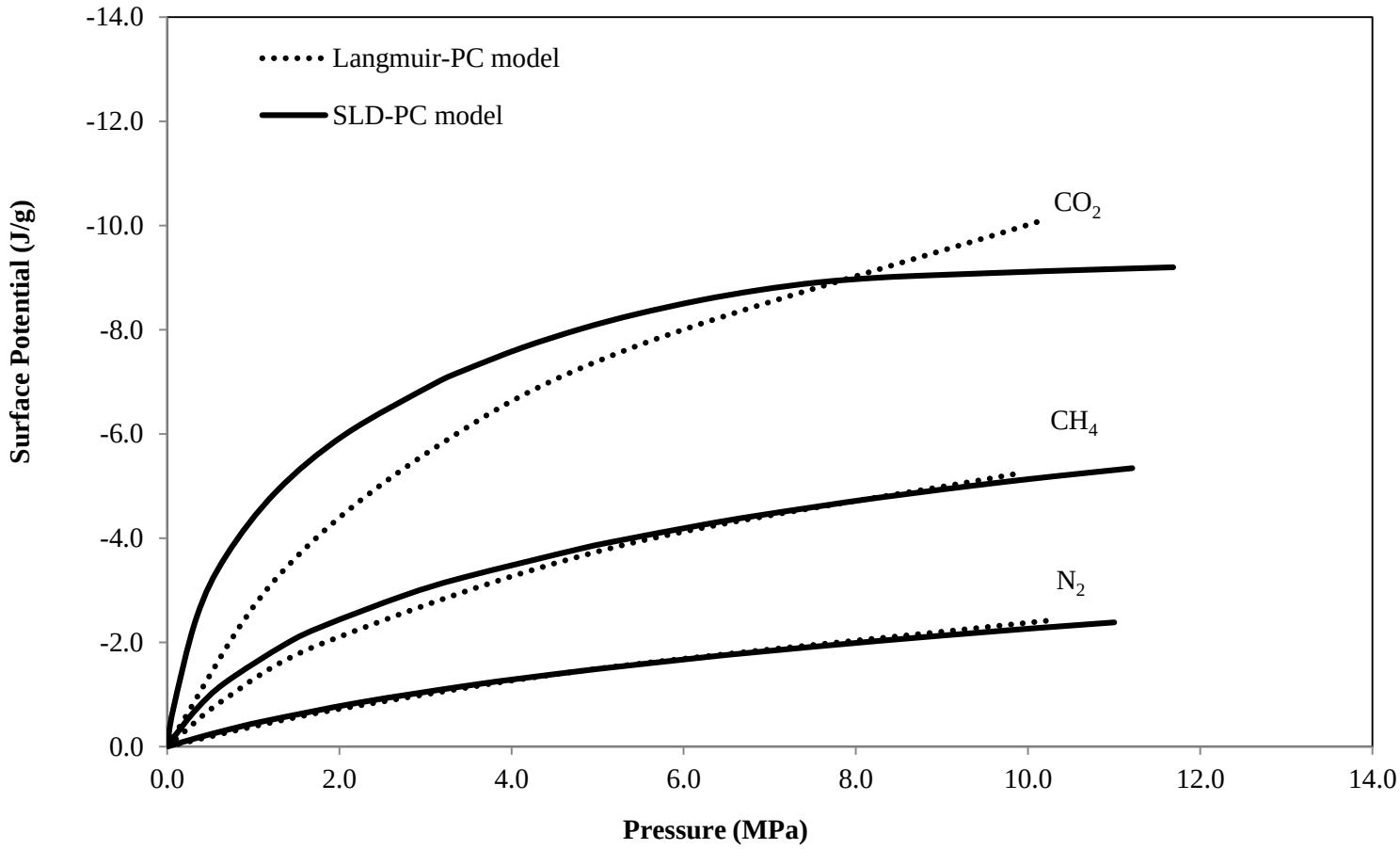

Figure 5.9. Surface Potential Profiles: Comparison between SLD-PC and Langmuir-PC Models based on fits to data from [4]

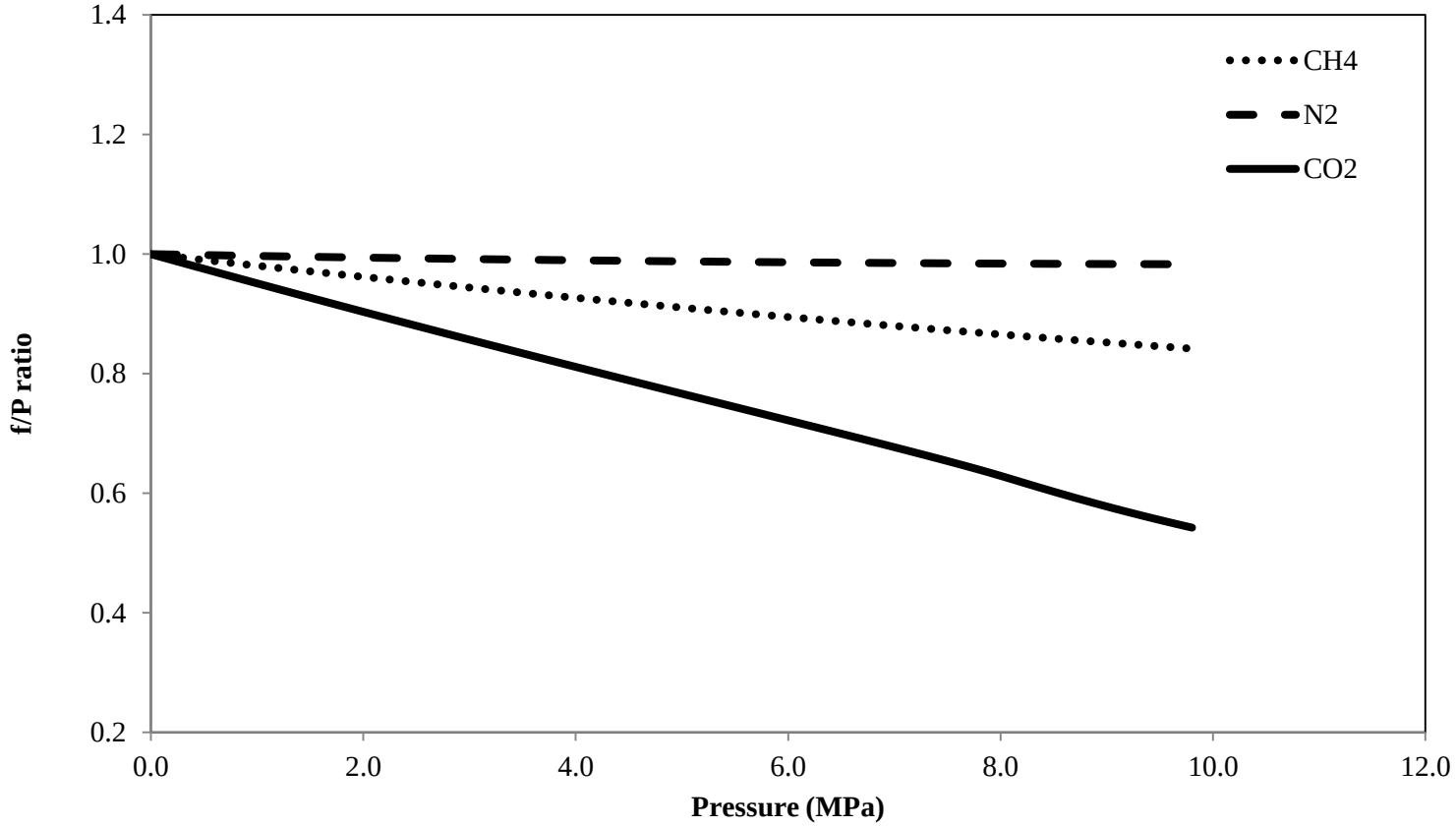

Figure 5.10. Fugacity-Pressure Ratio Profile: Fugacity is obtained from Peng-Robinson Equation of State at 308 K

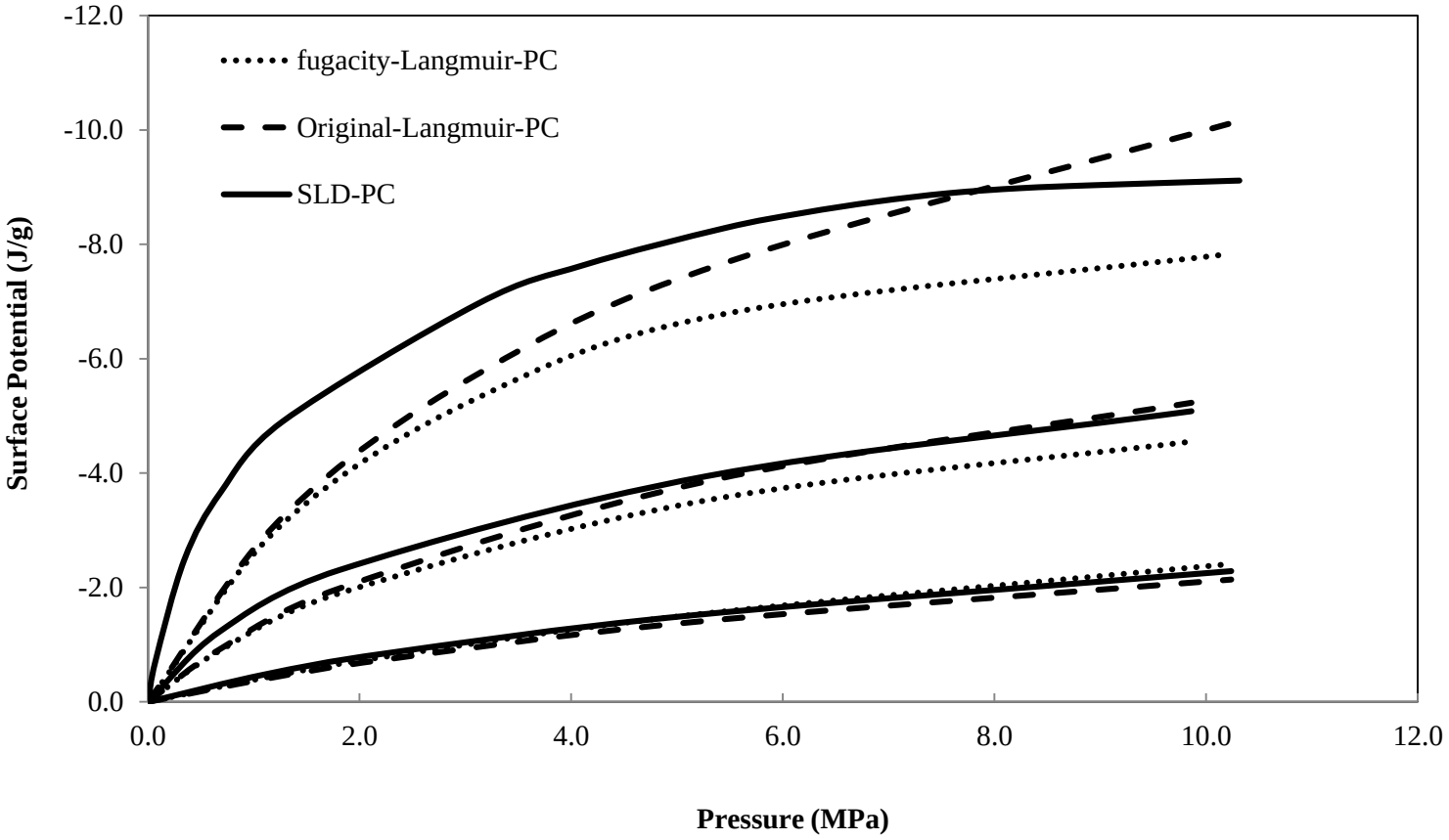

Figure 5.11. Surface Potential Profile: Comparison between the SLD-PC, the Original Langmuir-PC and the Fugacity Langmuir-PC based on Fit to the data from [4]

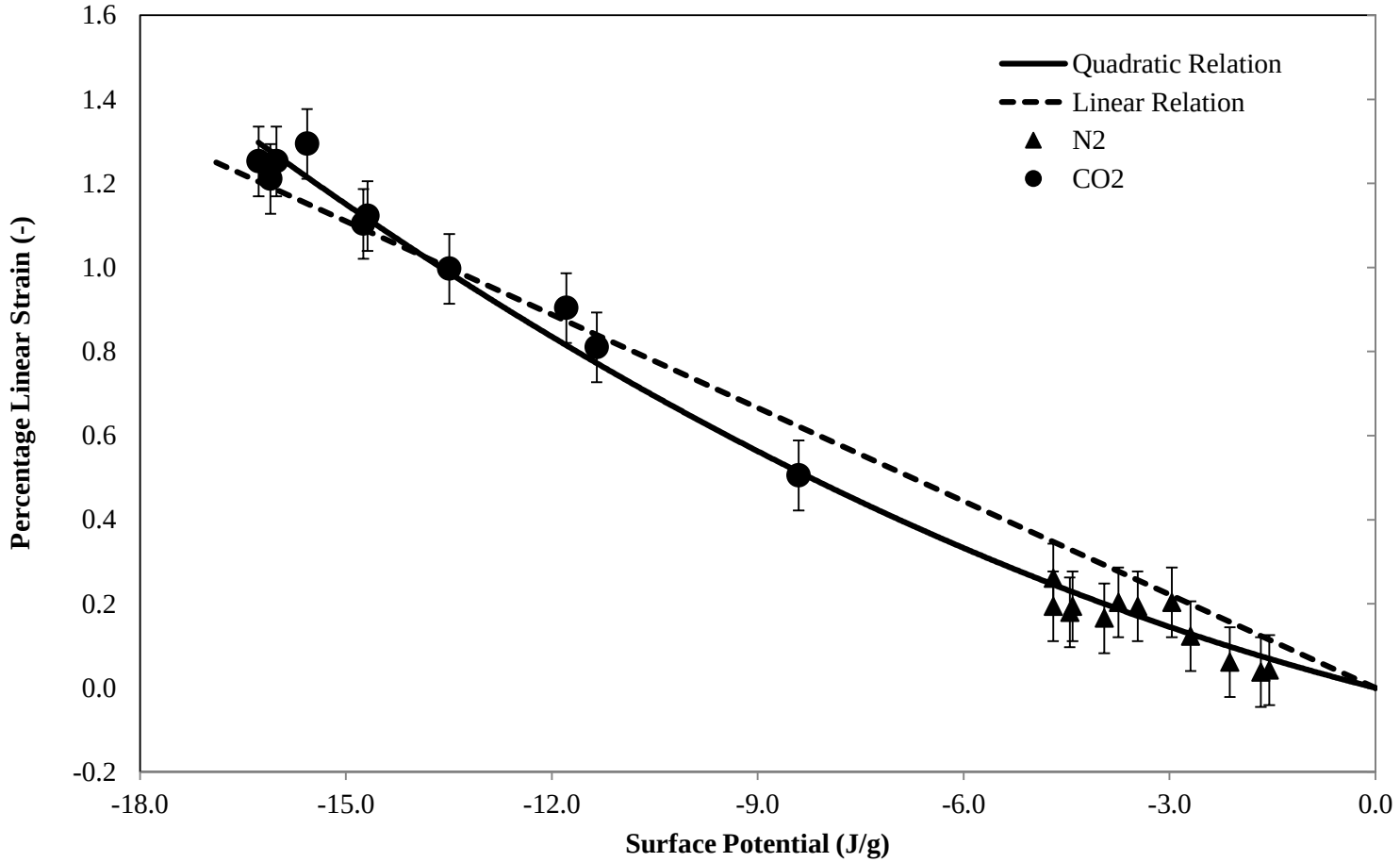

Figure 5.12. Non-linear relation between surface potential and strain (Points are data from [3])

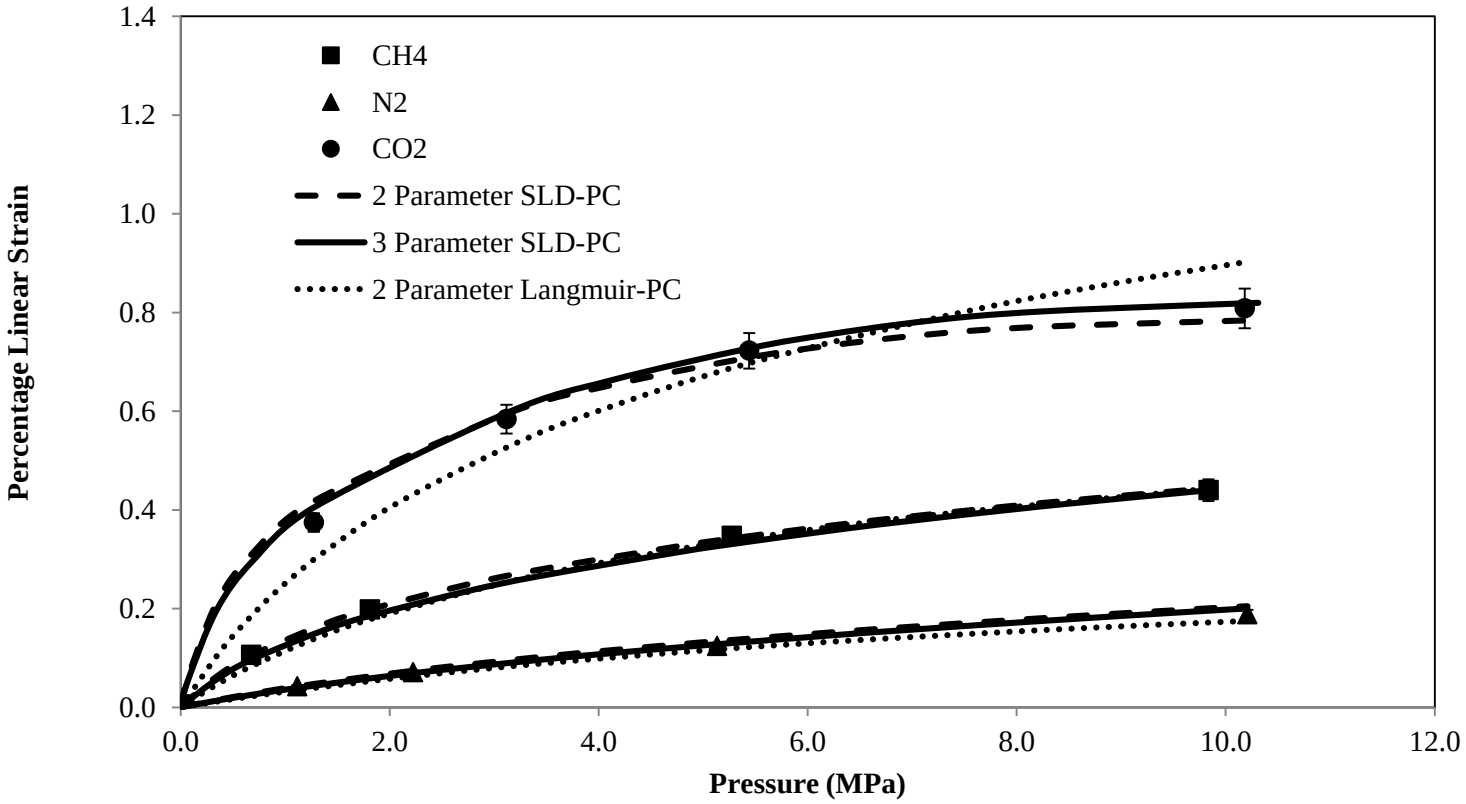

Figure 5.13(a). Strain in Perpendicular Direction to the Bedding Plane of Coal: Comparison between SLD-PC and Langmuir-PC Models (Points are data from [4])

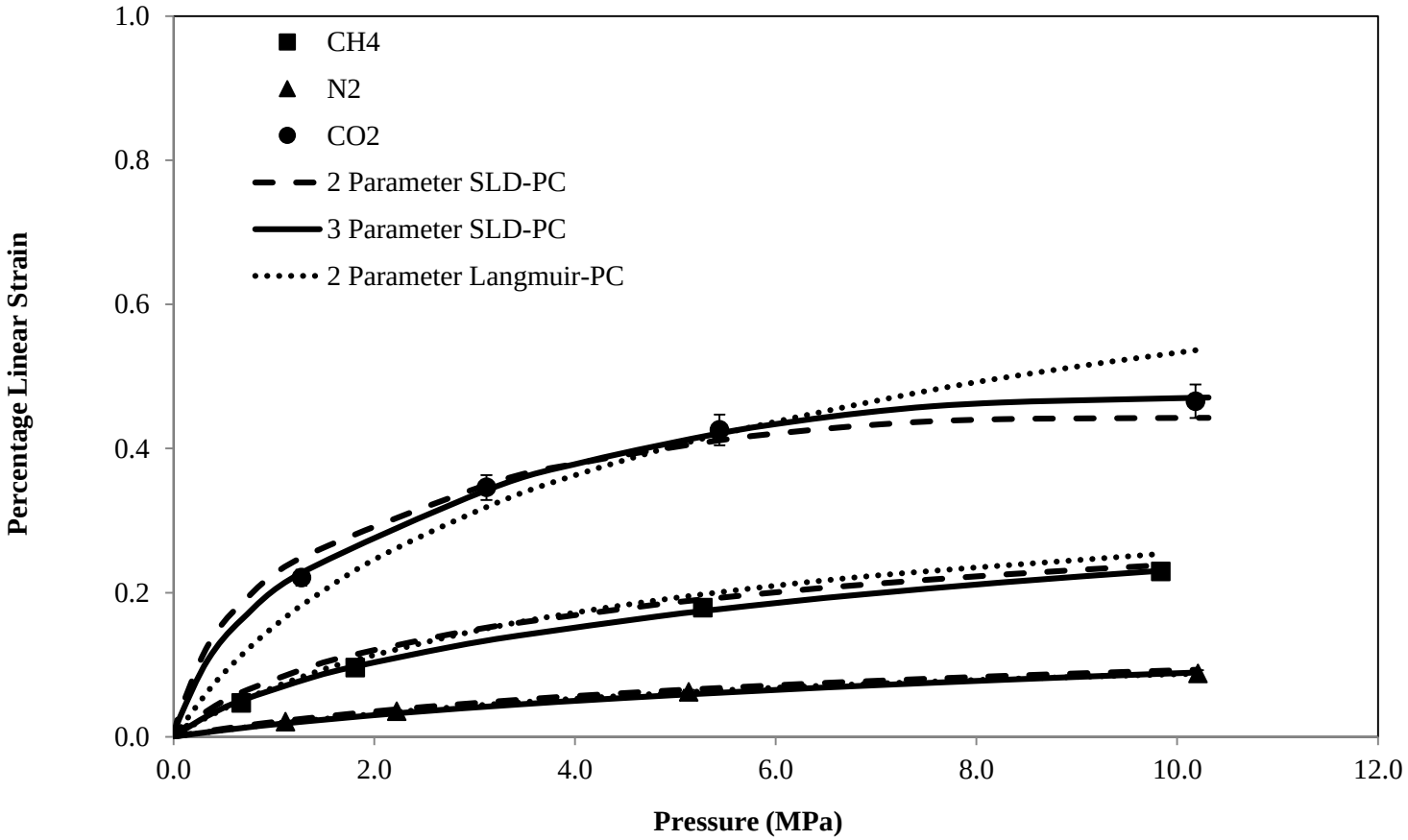

Figure 5.13(b). Strain in Parallel Direction to the Bedding Plane of Coal: Comparison between SLD-PC and Langmuir-PC Models (Points are data from [4])

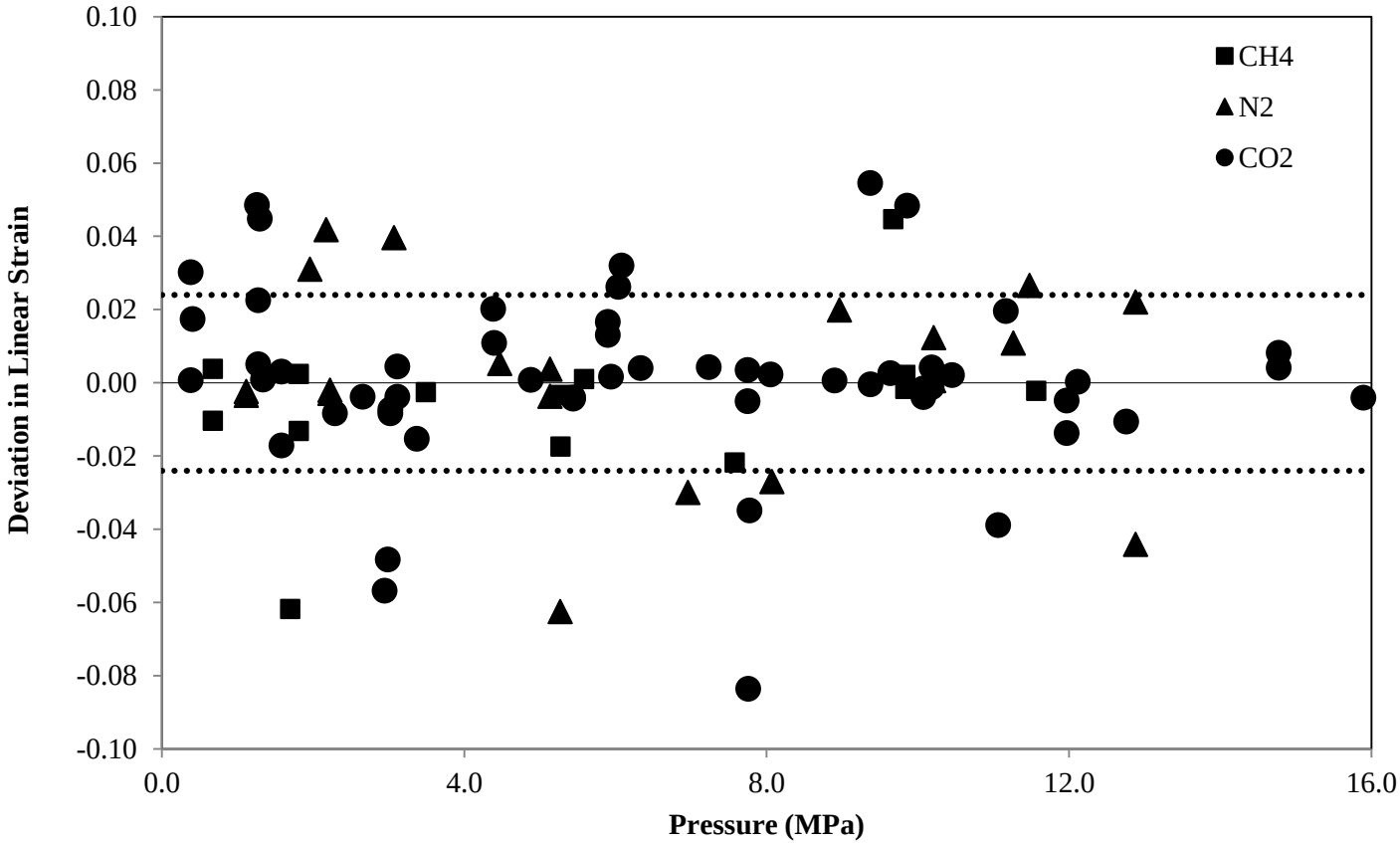

Figure 5.14. Deviations in linear strain predictions obtained from the SLD-PC model (Case 1)

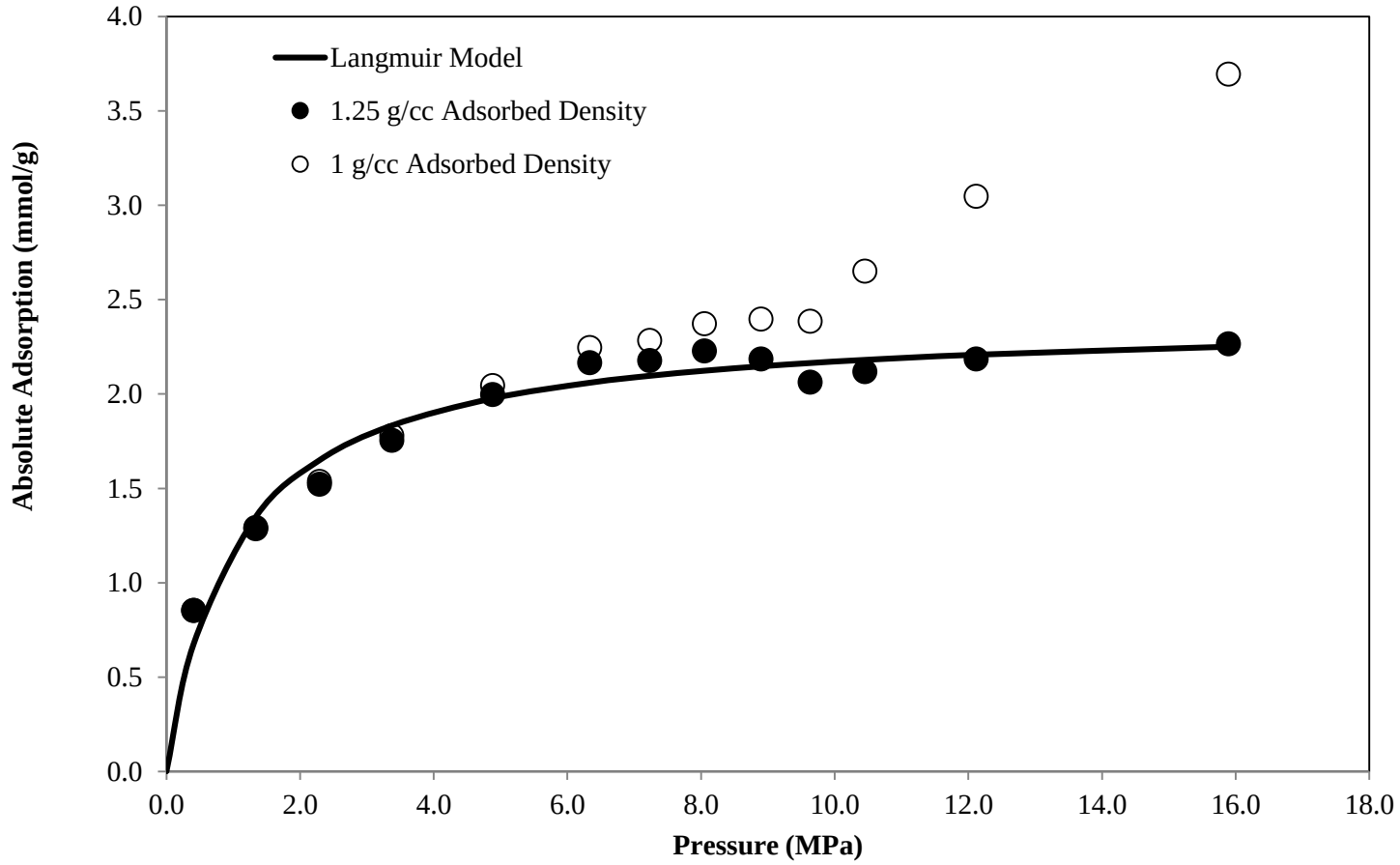

Figure 5.15(a). Comparison between the absolute adsorption using different values of the CO_2 adsorbed phase density, based on data from [26]

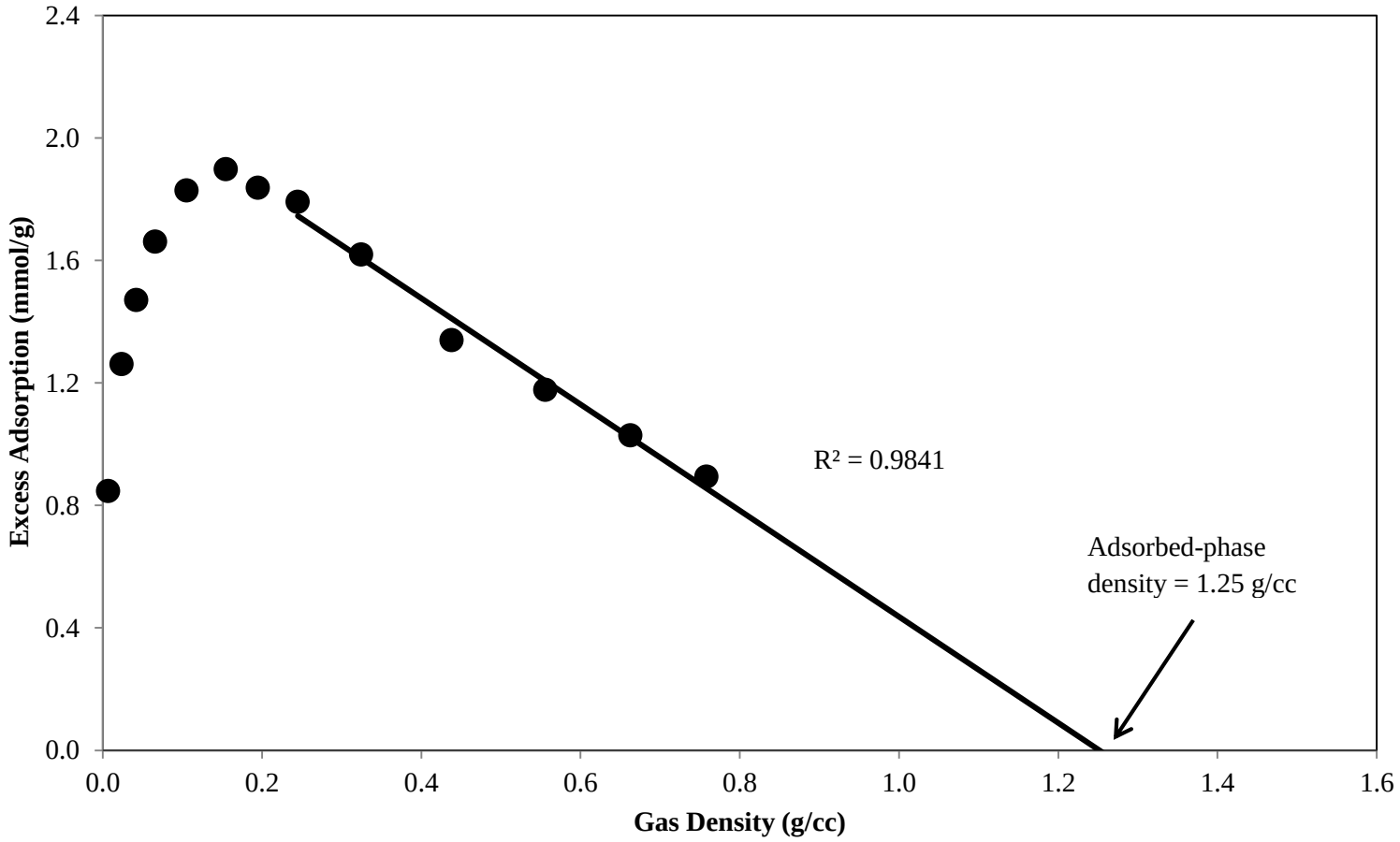

Figure 5.15(b). Graphical method for the adsorbed phase density estimation, based on data from [26]

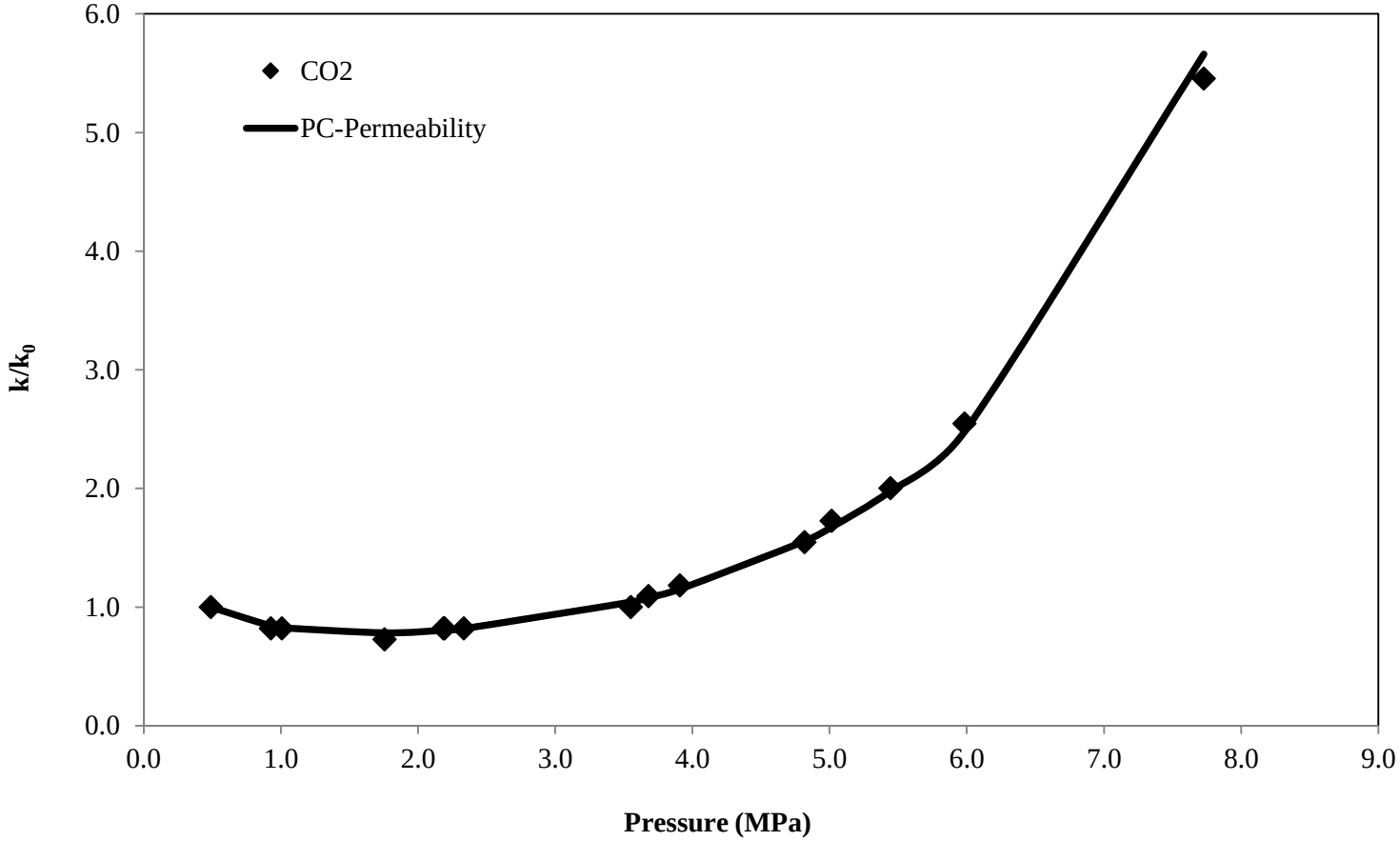

Figure 5.16(a). Representation of Normalized permeability Changes in Coal (Points are data from [3])

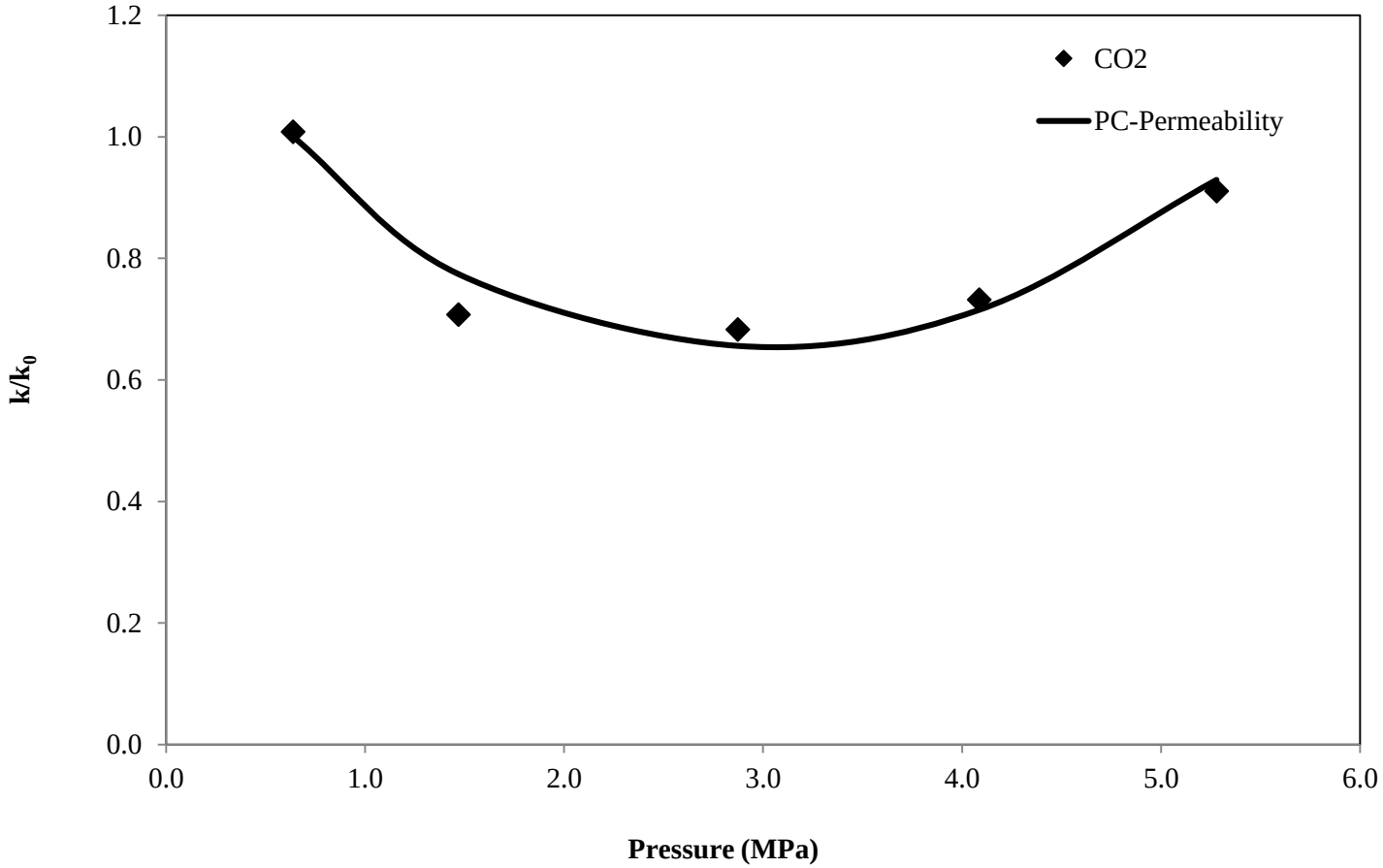

Figure 5.16(b). Representation of Normalized permeability Changes in Coal (Points are data from [31])

REFERENCES

1. Reucroft, P.J. and H. Patel, Gas-induced swelling in coal. Fuel, 1986. 65(6): p. 816-820.
2. Levine, J.R., Model study of the influence of matrix shrinkage on absolute permeability of coal bed reservoirs. Coalbed methane and Coal Geology, 1996. 109: p. 197-212.
3. Pini, R., et al., Role of adsorption and swelling on the dynamics of gas injection in coal. J. Geophys. Res., 2009. 114(B4): p. B04203.
4. Pan, Z. and L.D. Connell, Modelling of anisotropic coal swelling and its impact on permeability behaviour for primary and enhanced coalbed methane recovery. International Journal of Coal Geology, 2011. 85(3–4): p. 257-267.
5. Day, S., R. Fry, and R. Sakurovs, Swelling of Australian coals in supercritical CO2. International Journal of Coal Geology, 2008. 74(1): p. 41-52.
6. Ottiger, S., et al., Competitive adsorption equilibria of CO2 and CH4 on a dry coal. Adsorption, 2008. 14(4-5): p. 539-556.
7. Cui, X., R.M. Bustin, and L. Chikatamarla, Adsorption-induced coal swelling and stress: Implications for methane production and acid gas sequestration into coal seams. Journal of Geophysical Research: Solid Earth, 2007. 112(B10): p. B10202.
8. Ozdemir, E., B.I. Morsi, and K. Schroeder, Importance of Volume Effects to Adsorption Isotherms of Carbon Dioxide on Coals. Langmuir, 2003. 19(23): p. 9764-9773
9. Sakurovs, R., et al., Application of a Modified Dubinin−Radushkevich Equation to Adsorption of Gases by Coals under Supercritical Conditions. Energy & Fuels, 2007. 21(2): p. 992-997.

10. Pan, Z. and L.D. Connell, A theoretical model for gas adsorption-induced coal swelling. International Journal of Coal Geology, 2007. 69(4): p. 243-252.
11. Clarkson, Z.P., Ian D. Palmer, Satya Harpalani, Predicting Sorption-Induced Strain and Permeability Increase With Depletion for Coalbed-Methane Reservoirs. Society of Petroleum Engineering, 2010. 15: p. 152-159.
12. A. Mitra, S.H., Modeling Incremental Swelling of Coal Matrix with CO2 Injection in Coalbed Methane Reservoirs. Society of Petroleum Engineering, 2007.
13. Robertson, E.P. and R.L. Christiansen. Measurement of Sorption-Induced Strain. in 2005 International Coalbed Methane Symposium. 2005.
14. Mohammad, S.A., et al., Generalized Simplified Local-Density/Peng−Robinson Model for Adsorption of Pure and Mixed Gases on Coals. Energy & Fuels, 2009. 23(12): p. 6259-6271.
15. Jaeger, J.C., N.G.W. Cook, and R.W. Zimmerman, Fundamentals of Rock Mechanics (4th Edition). 1969, John Wiley & Sons.
16. Shi, J.Q. and S. Durucan, Drawdown Induced Changes in Permeability of Coalbeds: A New Interpretation of the Reservoir Response to Primary Recovery. Transport in Porous Media, 2004. 56(1): p. 1-16.
17. Cui, X. and R.M. Bustin, Volumetric strain associated with methane desorption and its impact on coalbed gas production from deep coal seams. AAPG Bulletin, 2005. 89(9): p. 1181-1202.
18. Chareonsuppanimit, P., et al., High-pressure adsorption of gases on shales: Measurements and modeling. International Journal of Coal Geology, 2012. 95(0): p. 34-46.
19. Rangarajan, B., C.T. Lira, and R. Subramanian, Simplified local-density model for adsorption over large pressure ranges. AIChE Journal, 1995. 41(4): p. 838-845.

20. Chen, J.H., et al., Adsorption and desorption of carbon dioxide onto and from activated carbon at high pressures. Industrial & Engineering Chemistry Research, 1997. 36(7): p. 2808-2815.

21. Lee, L.L., Molecular Thermodynamics of Non-Ideal Fluids. 1988, Stoneham: Butterworths.

22. Steele, W.A., The Interaction of Gases with Solid Surfaces. 1974: Pergamon Press, Oxford.

23. Fitzgerald, J.E., et al., Modeling the adsorption of pure gases on coals with the SLD model. Carbon, 2003. 41(12): p. 2203-2216.

24. Myers, A.L., Thermodynamics of adsorption in porous materials. AIChE Journal, 2002. 48(1): p. 145-160.

25. Seidle, J.P., Jeansonne, M.W., Erickson, D.J., Application of Matchstick Geometry To Stress Dependent Permeability in Coals. Society of Petroleum Engineering, 1992.

26. Chen, G., J. Yang, and Z. Liu, Method for Simultaneous Measure of Sorption and Swelling of the Block Coal under High Gas Pressure. Energy & Fuels, 2012. 26(7): p. 4583-4589.

27. Arri, L.E. and D. Yee. Modeling Coalbed Methane production with binary gas sorption, SPE paper 24363. in SPE Rocky Mountain regional meeting. 1992. Casper, WY.

28. Sudibandriyo, M., et al., Adsorption of Methane, Nitrogen, Carbon Dioxide, and Their Binary Mixtures on Dry Activated Carbon at 318.2 K and Pressures up to 13.6 MPa. Langmuir, 2003. 19(13): p. 5323-5331.

29. Humayun, R. and D.L. Tomasko, High-resolution adsorption isotherms of supercritical carbon dioxide on activated carbon. AIChE Journal, 2000. 46(10): p. 2065-2075.

30. Gentzis, T., N. Deisman, and R.J. Chalaturnyk, Geomechanical properties and permeability of coals from the Foothills and Mountain regions of western Canada. International Journal of Coal Geology, 2007. 69(3): p. 153-164.

31. Robertson, E.P., Measurement and Modeling of Sorption Induced Strain and Permeability Changes in Coal. 2005, Idaho National Laboratory.

32. Seidle, J., Fundamentals of Coalbed Methane Reservoir Engineering. 2011: PennWell.

CHAPTER VI

CONCLUSIONS AND RECOMMENDATIONS

The conclusions and recommendations of the present study are presented below.

6.1 Modeling the Temperature Dependence of Supercritical Gas Adsorption on Activated Carbons, Coals and Shales

The objective was to extend the predictive capability of the SLD model to represent the temperature dependence of supercritical gas adsorption over significant temperature ranges based on adsorption data on activated carbons, coals and shales. The conclusions and recommendations of this part of the study are as follows.

Conclusions

- The SLD model was modified successfully by including a temperature-dependent expression for the adsorbed-phase volume, which provided improved representations of gas adsorption on activated carbons over wider ranges of temperature.
- The model for the thermal expansion coefficient was generalized in terms of molecular properties of adsorbates and adsorbents. Results obtained from the generalized model were comparable to the results obtained from direct regressions.

- The generalized model was used to obtain predictions at multiple temperatures based on available adsorption isotherm at a single isotherm.
- The modified model was utilized to describe supercritical gas adsorption on coals and shales at multiple temperatures. The model was found capable of providing accurate descriptions of adsorption at multiple temperatures on these adsorbents.

Recommendations

- The generalized model presented in this work should be further tested, once additional data on coals and shales at wider ranges of temperatures becomes available.
- The information of adsorbent characterization such as proximate and ultimate analyses should be provided in adsorption databases since the information is crucial for generalization of model parameters.
- Temperature-dependent properties of an adsorbent such as thermal expansion of the adsorbent should be made available for developing the generalized expression for δ; currently, however, these temperature-dependent properties of adsorbent are lacking.
- The experimental uncertainties of gas adsorption should be provided in adsorption databases since they quantify the quality of data which is important for data selection.

6.2 High-Pressure Adsorption of Gases on the New Albany Shale

The objectives of this part of the study were to (1) measure adsorption isotherms of methane, nitrogen and CO_2 on the New Albany Shale and (2) extend the SLD model for describing the adsorption of gases on the newly acquired shale data and the shale data from the literature. Following are the conclusions and recommendations of this specific study.

Conclusions

- High-pressure adsorption isotherms of methane, nitrogen and CO_2 were measured successfully on a New Albany shale sample using the existing adsorption apparatus in OSU adsorption laboratory.
- Since the adsorbed amount in shales is relatively smaller than in coals and activated carbons, the adsorption apparatus was re-optimized by minimizing the dead volume in the adsorption system which reduced the experimental uncertainties by about 50%.
- The SLD model was capable of describing the adsorption on the New Albany shale data as well as the shale data from literature.

Recommendations

- The generalized SLD model for predicting adsorption on shales should be developed further if shale data become more available in literature.
- The proximate and ultimate analyses should be provided in adsorption databases since they are useful for developing a generalized adsorption model.
- The experimental uncertainties of gas adsorption should be provided since they quantify the quality of data which is important for data selection.

6.3 High-Pressure Adsorption of Gases on the Shale from Oklahoma

The objectives of this part of the study were to (1) measure adsorption isotherms of methane, nitrogen and CO_2 on shales from Oklahoma including the Woodford and the Caney shales and (2) enlarge the OSU shale database, which will be useful for SLD model generalization applied for shales. Following are the conclusions and recommendations of this specific study.

Conclusions

- High-pressure adsorption isotherms of methane, nitrogen and CO_2 were measured successfully on shales from Oklahoma using the existing adsorption apparatus in OSU adsorption laboratory.
- The maximum adsorption capacity was positively correlated with the TOC content of shales in this study.
- The preference of shales for adsorbing CO_2 increased as ash content increased.
- Two of the SLD model parameters, i.e., surface areas and ε_{ss}/k were positively correlated with TOC content, which was consistent with the relation between TOC content and gas adsorption observed in this study.

Recommendations

- General trends in the SLD model parameters (i.e. surface areas and ε_{ss}/k) as a function of shale properties such as TOC content have been shown in this work. However, further testing should be undertaken, which will require additional adsorption data and shale characterization.
- Since shales contain large amount of mineral matter (or ash content), information on shale mineralogy should be determined to develop the SLD model parameters in terms of shale properties.

6.4 Modeling Gas-Adsorption-Induced Swelling and Permeability Changes in Coals

The objectives of this part of the study were to (1) incorporate the SLD adsorption model with the theory-based swelling model by Pan and Connell (PC) to produce internally-consistent SLD-PC model and (2) utilize the results obtained from the SLD-PC model for describing the permeability changes in coals. Following are the conclusions and recommendations of this specific study.

Conclusions

- The SLD model was extended to account for the effect of coal swelling by integrating the SLD model with the PC coal swelling model. The resultant SLD-PC model provided useful representations of both supercritical gas adsorption and swelling behavior on diverse coals.
- A simple non-linear model (quadratic expression) was found capable of describing the relation between strain and surface potential for these systems.
- The SLD model provided generalized predictions of adsorption based solely on adsorbent characterization which appeared capable of providing useful predictions in cases where adsorption data on coals are not reported with the corresponding swelling data.
- The SLD-PC approach is capable of providing representations of gas adsorption and linear strain and, when combined with the permeability model, this approach can provide useful capability in the form of a unified modeling framework for describing the interrelations among adsorption, strain and permeability of coals.

Recommendations

- Availability of a complete dataset (i.e., from adsorption, swelling to permeability changes data) is limited. Thus, more data should be assembled to test the SLD-PC model.
- Surface characterization information and solid mechanical properties should be provided and assembled in order to develop the generalized SLD-PC model.

VITA

Pongtorn Charoensuppanimit

Candidate for the Degree of

Doctor of Philosophy

Thesis: DEVELOPMENT OF AN INTEGRATED APPROACH FOR MODELING GAS ADSORPTION AND COAL SWELLING

Major Field: Chemical Engineering

Biographical:

Education:

Completed the requirements for the Doctor of Philosophy in Chemical Engineering at Oklahoma State University, Stillwater, Oklahoma in May, 2015.

Completed the requirements for the Bachelor of Science in Chemical Engineering at Chulalongkorn University, Bangkok, Thailand in 2007.

Experience:

- Research Assistant, Oklahoma State University, Stillwater, Oklahoma, June 2010 – May 2015
- Teaching Assistant in Senior Chemical Engineering Plant Design, Oklahoma State University, Stillwater, Oklahoma, August 2009 – December 2009

Professional Memberships:

American Institute of Chemical Engineers (AIChE), 2010-Present